CANADIAN THESES

THÈSES CANADIENNES

NOTICE

The quality of this microfiche is heavily dependent upon the quality of the original thesis submitted for microfilming. Every effort has been made to ensure the highest quality of reproduction possible.

If pages are missing, contact the university which granted the degree.

Some pages may have indistinct print especially if the original pages were typed with a poor typewriter ribbon or if the university sent us an inferior photocopy.

Previously copyrighted materials (journal articles, published tests, etc.) are not filmed.

Reproduction in full or in part of this film is governed by the Canadian Copyright Act, R.S.C. 1970, c. C-30.

AVIS

La qualité de cette microfiche dépend grandement de la qualité de la thèse soumise au microfilmage. Nous avons tout fait pour assurer une qualité supérieure de reproduction.

S'il manque des pages, veuillez communiquer avec l'université qui a conféré le grade.

La qualité d'impression de certaines pages peut laisser à désirer, surtout si les pages originales ont été dactylographiées à l'aide d'un ruban usé ou si l'université nous a fait parvenir une photocopie de qualité inférieure.

Les documents qui font déjà l'objet d'un droit d'auteur (articles de revue, examens publiés, etc.) ne sont pas microfilmés.

La reproduction, même partielle, de ce microfilm est soumise à la Loi canadienne sur le droit d'auteur, SRC 1970, c. C-30.

THIS DISSERTATION
HAS BEEN MICROFILMED
EXACTLY AS RECEIVED

LA THÈSE A ÉTÉ
MICROFILMÉE TELLE QUE
NOUS L'AVONS REÇUE

Canada

An Analytical and Experimental Study
on
Diesel Injectors Design

Hiep Cong To

A Thesis

in

The Department

of

Mechanical Engineering

Presented in Partial Fulfillment of the Requirements
for the Degree of Master of Engineering at
Concordia University
Montréal, Québec, Canada

March 1986

ABSTRACT

An Analytical and Experimental Study on Diesel Injectors Design

Hiep Cong To

The objective of this thesis is to elaborate the methods to improve the design and operation of multi-hole fuel injectors for high speed diesel engines. Optimization of such injectors involves two contradictory requirements. The first, is to minimize the fuel injection time period at maximum engine power without excessively increasing the injection pressure. The second, is to obtain a good atomization of fuel injected at idling and at starting engine speeds without reducing the injector orifices diameter which has been sized for high power conditions.

The first step was to develop an improved mathematical model for the fuel injection system, and to calculate the fuel discharge characteristics. Then, the simulation results were compared with those obtained experimentally. The good agreement between calculated and experimental results allowed to use this mathematical model for further investigations.

In optimization of the diesel injectors at maximum power, a procedure was applied involving the use of a computerized data acquisition system. This procedure was found to have some advantages in saving of computing time and in increasing the accuracy of calculations.

When studying the performance of diesel injectors at low engine speed, the seat pressure factor which contributes significantly to the injector dynamic response, was introduced into the calculations. Several tests were made to measure the seat pressure which allowed to determine the flow coefficients at the nozzle seat chamber and at the orifices which were required for calculations.

In order to evaluate the injector's behaviour, factors affecting the dynamic response of the injector and the injector's stability were studied. This allowed to draw conclusions concerning the criteria toward an improvement in fuel atomization at low engine speeds.

Finally, a summary was made, and recommendations were drawn toward implementation of the conclusions into the diesel engine technology.

ACKNOWLEDGEMENTS

TABLE OF CONTENTS

LIST OF FIGURES

LIST OF TABLES

NOMENCLATURE

s = sound velocity in fluid [m/s]

D = pipe diameter [m]

D_{dv} = diameter of delivery valve [m]

D_{si} = nozzle seat inner diameter [m]

D_{so} = nozzle seat outer diameter [m]

D_o = diameter of injector orifice [m]

e = pipe wall thickness [m]

E = fluid modulus of elasticity [Pa]

ES = effective stroke of pump plunger [m]

EV = empty volume [m^3]

f = fluid friction factor in injection pipe

F = cross-sectional area [m^2]

F_{dv} = cross-sectional area of delivery valve [m^2]

F_{fdv} = flow area of delivery valve [m^2]

F_{fo} = flow area of injector orifice [m^2]

F_i = cross-sectional area of injector needle [m^2]

F_p = cross-sectional area of pump plunger [m^2]

F_r = cross-sectional area of injector needle rod [m^2]

F_{fse} = flow area at nozzle seat exit section [m^2]

F_{fsi} = flow area at nozzle seat inlet section [m^2]

F_{si} = cross-sectional area corresponding to nozzle seat inner diameter [m^2]

F_{so} = cross-sectional area corresponding to nozzle seat outer diameter [m^2]

F_{sp} = flow area of barrel spill port $[m^2]$

F_I = cross-sectional area of injection pipe at control surface I-I $[m^2]$

F_{II} = cross-sectional area of injection pipe at control surface II-II $[m^2]$

g = gravity acceleration $[m/s^2]$

G_p = Young's modulus of elasticity for injection pipe material $[Pa]$

G_r = Young's modulus of elasticity for injector needle rod material $[Pa]$

h_{dv} = displacement of delivery valve $[m]$

h_i = displacement of injector needle $[m]$

h_{imax} = maximum displacement of injector needle $[m]$

h_p = displacement of pump plunger $[m]$

I = number of injector orifices

k_{dv} = delivery valve spring constant $[N/m]$

k_{is} = injector spring constant $[N/m]$

L = length of injection pipe $[m]$

L_r = length of injector needle rod $[m]$

$\dot{m}$ = mass flow rate $[kg/s]$

m_{dv} = mass of delivery valve $[kg]$

m_{ds} = mass of delivery valve spring $[kg]$

m_{in} = mass of injector needle $[kg]$

m_{is} = mass of injector spring $[kg]$

m_r = mass of injector needle rod $[kg]$

N = pump speed $[RPM]$

p = fluid pressure $[Pa]$

P_a — atmospheric pressure [Pa]

P_b — pressure in bag chamber [Pa]

P_c — pressure in combustion chamber [Pa]

P_{cl} — injector closing pressure [Pa]

P_d — pressure in delivery chamber [Pa]

P_{db} — amplitude of backward propagating pressure wave at control surface I-I [Pa]

P_{df} — amplitude of forward propagating pressure wave at control surface I-I [Pa]

P_{do} — residual pressure at control surface I-I [Pa]

P_f — pressure in pump feeding chamber [Pa]

P_i — pressure in injector chamber [Pa]

P_{ib} — amplitude of backward propagating pressure wave at control surface II-II [Pa]

P_{if} — amplitude of forward propagating pressure wave at control surface II-II [Pa]

P_{io} — residual pressure at control surface II-II [Pa]

P_o — fluid pressure at the beginning of motion [Pa]

P_{op} — injector opening pressure [Pa]

P_p — pressure in pumping chamber [Pa]

P_s — pressure in nozzle seat chamber [Pa]

P — total pressure force acting on injector needle [N]

P_b — bag pressure force [N]

P_{ds} — preload on delivery valve spring [N]

P_i — injector pressure force [N]

P_{is} — preload on injector spring [N]

P_s — seat pressure force [N]

P_{sp} = injector spring force [N]

q = volumetric flow rate [m^3/s]

q_{fo} = volumetric flow rate through injector orifices [m^3/s]

q_{fse} = volumetric flow rate through nozzle seat exit area [m^3/s]

q_{fsi} = volumetric flow rate through nozzle seat inlet area [m^3/s]

Q = injected fuel dose [m^3]

r_{sp} = radius of barrel spill port [m]

R_d = mechanical friction acting on delivery valve [N]

R_i = mechanical friction acting on injector needle [N]

S_r = retraction stroke of delivery valve [m]

t = instant time [s]

v = fluid velocity [m/s]

v_{bI} = amplitude of backward propagating velocity wave at control surface I-I [m/s]

v_{bII} = amplitude of backward propagating velocity wave at control surface II-II [m/s]

v_{dv} = velocity of delivery valve [m/s]

v_{fI} = amplitude of forward propagating velocity wave at control surface I-I [m/s]

v_{fII} = amplitude of forward propagating velocity wave at control surface II-II [m/s]

v_i = velocity of injector needle [m/s]

v_o = fluid velocity at the beginning of motion [m/s]

v_p = velocity of pump plunger [m/s]

v_I = total fluid velocity at control surface I-I [m/s]

v_{II} — total fluid velocity at control surface II-II [m/s]

V — volume [m³]

V_a — volume of accumulator chamber [m³]

V_b — volume of bag chamber [m³]

V_d — volume of delivery chamber [m³]

V_{exp} — expansion volume of compressed fuel [m³]

V_i — volume of injector chamber [m³]

V_p — volume of pumping chamber [m³]

V_r — retraction volume of delivery valve [m³]

V_{sys} — total volume of injection system [m³]

x — space coordinate [m]

Greek Letters

α — half of nozzle seat angle [degree]

α_{dv} — half of delivery valve seat angle [degree]

α_{spl} — lower helix angle of pump plunger [degree]

α_{spu} — upper helix angle of pump plunger [degree]

β — half of injector needle tip cone angle [degree]

δ_d — damping coefficient acting on delivery valve [kg/s]

δ_i — damping coefficient acting on injector needle [kg/s]

Δh_i — elastic deflection of injector needle rod [m]

Δt_{inj} — injection time duration [s]

$\Delta \varphi_{\text{inj}}$ — pump cam rotation angle during injection [degree]

γ — half of differential angle between injector needle tip and nozzle seat cones [degree]

μ_d — flow coefficient at delivery valve

μ_o = flow coefficient at injector orifices

μ_{se} = flow coefficient at nozzle seat exit section

μ_{si} = flow coefficient at nozzle seat inlet section

μ_{sp} = flow coefficient at spill port

ρ = fluid density $[kg/m^3]$

θ = angle between pipe center line and horizontal [degree]

Φ = function of argument $(t - x/\bar{a})$

Ψ = function of argument $(t + x/\bar{a})$

φ = pump cam rotation angle [degree]

Chapter 1

INTRODUCTION

1.1. General

Presently, the high speed direct injection diesel engines are faced with new requirements.

1. The diesel engines with direct injection are being developed for higher speeds, also for car propulsion. This is made mainly for improvement in specific fuel consumption.

2. The diesel engines are becoming higher rated, usually supercharged (turbocharged), mainly to increase the specific power.

3. The diesel engines are required to run at lower idle-speed with less noise, vibrations, and pollution emission. They are also required to start easier, particularly at lower temperatures.

4. The diesel engines are required to run longer without service intervention and overhaul.

5. The diesel engines might be required to be converted for alternative fuels such as alcohols, propane, natural gas, etc.

In a diesel engine, the fuel injectors play a most important role, because they have to inject and distribute a precisely metered and atomized quantity of fuel to the proper region of the combustion chamber at the right time and during a short time period. The injection period and the atomization of the injected fuel are dependent on the ability of the injector to open and to close fast. Therefore, the diesel injectors should be better designed to avoid following undesired

phenomena:

1. Too long fuel injection period at maximum power in high-rated (turbocharged) engines with high injection pressure.

2. Too poor fuel atomization at idle-speed and at starting conditions in those engines.

3. Excessive wear of fuel injectors resulting in frequent service interventions, excessive fuel consumption, and air pollution.

1.2. Thesis Outlines

To deal with the undesired phenomena in high speed direct injection diesel engines, as specified in section 1.1, following research has been proposed:

1. The fuel injection process will be analyzed through mathematical model and computer simulation. This should allow to obtain the calculated fuel injection process which will be proved to give the results very close to those obtained experimentally. There is sufficient literature content describing several fuel injection calculation methods. However, the attempts of application of the published methods showed that the deviations between calculated and experimental results can be substantial. It was also found that there is a lack of correct coefficients required for calculations and that some phenomena important for the injection process computing are not well explained or are not even taken into account. Furthermore, the model for the particular injection system operation required to be calculated for purposes of this thesis could not be found in the literature.

Therefore, it was concluded that a critical analysis of the published calculation methods should be made including particular improvements to be proposed and implemented.

2. Evaluation of the diesel injector dynamic response should be made using, if possible, simplified calculation and test methods. Such methods could be used not only for the assessment of the dynamic properties of the diesel injectors, but also for the evaluation of the quality of the nozzles being manufactured or being worn after a period of time in the service. A model for a test set-up for diesel

injectors should be proposed and described mathematically with emphasis given particularly to the differential angle between the injector needle tip and nozzle seat cones which seems to contribute significantly to the dynamic response of the injector. Based on mathematical simulation, a relation should be developed between the maximum lift of the injector needle, as the dynamic response measure, and the design and operational parameters of the injector. This will serve to develop the optimization graphs which should help in designing of an injector with the best dynamic response, as well as in creating of the criteria for evaluation of the quality of the injector nozzles in the service.

3. Optimization of the diesel injector design for low engine speed conditions should be based on results derived from investigation of dynamic response of an injector at very low fuel flow rate. There is almost no publication in the literature concerning the required behaviour of the diesel injectors at idling and starting engine conditions. This, however, is one of the most difficult areas where the compromise must be reached concerning the nozzle orifices flow area for the maximum power and for the idling and starting speed of a diesel engine. In the hole-type nozzles, the same orifices are used for atomization of fuel when injected at very high flow rate at maximum power, and at very low flow rate at idling speed. Consequently, the nozzle orifices which provide optimum engine performance at maximum power are usually too large for the idling speed conditions resulting in poor atomization of injected fuel. The conventional answer to this problem was the use of an unstable injector which remains open only when the pressure inside the injector is high enough. Such injector,

however, is handicapped by the presence of the nozzle seat configuration which throttles the flow and reduces the differential pressure across the orifices. Trying to include that factor into calculation of the fuel discharge process, it was decided to introduce the seat pressure into the calculations, particularly at low engine speed where the fuel flow throttling in the nozzle seat has its biggest impact.

The requirement for calculation of the coefficients for the flow in and out of the seat chamber should be experimentally realized by measurement of the seat pressure under the injector needle.

4. Optimization of the diesel injector design should be performed to obtain the required fuel discharge characteristic at full engine load and speed. Based on the available computer-controlled hardware, the proposed optimization method should allow a fast and accurate evaluation of the impact of the design parameters of a diesel injector on the fuel discharge characteristic.

A good opportunity arises here to use the computerized data acquisition system to record the pressure wave produced by the fuel injection pump equipped with a specially made long injection pipe. That pressure wave will be next used to calculate the fuel injection process in the injector. This procedure would have following advantages:

a/ It would avoid collecting data from the fuel injection pump and making calculation of the pumping process.

b/ It would provide the digitized pressure wave produced by the injection pump as the input data to the computer to continue calculation of the fuel injection process in the injector.

c/ It would save time and increase the accuracy of fuel discharge process calculation

The use of a long injection pipe would protect the forward pressure wave produced by the pump against deformation caused by the reflected wave arriving from the injector, which would superimpose on the forward pressure wave.

5. Evaluation of the factors affecting diesel injector stability should allow to predict the behaviour of an injector supplied with a particular fuel flow rate. A mathematical derivation of the injector stability criteria will be made. From these criteria, a critical fuel flow rate at which the diesel injector, being a differential pressure valve, changes from an unstable behaviour to a stable one, will be determined. Then, the effects of the injector design and operational parameters on the injector stability will be studied.

The proposed research should lead to a significant contribution toward the clarification of the knowledge in the area of diesel injectors and their use for specific engine applications. In this thesis, the procedure will be formulated leading towards an optimum configuration of a diesel injector regarding the improvement of the fuel injection process, as discussed at the beginning of this chapter.

Finally, it has to be mentioned that while a great progress in the application of micro-processor based control is radically changing fuel injection pattern in spark ignition engines, there is almost no impact of it in the present applications for diesel engines. It seems that the recently advertized new developments in diesel injectors using solenoids and unit-injectors are paving the way for future radical changes in the design of diesel fuel system. However, it will take quite long time to overcome some serious difficulties hampering their implementation into the production. Until then, and also long time later, the present conventional design of injectors will be still overwhemingly used, allowing only for minor modifications of the current well developed pattern of diesel injectors.

In the view of this prediction, the investigations made for this thesis should have a certain value in the current diesel engines technology.

Chapter 2
LITERATURE REVIEW AND COMMENTS

The literature review has been divided into several sections to discuss specific topics related to the thesis.

2.1. Literature Review on
Fuel Injection System Improvement for
High Speed Direct Injection Diesel Engines

Improvement in the fuel injection process for high speed direct injection diesel engines has been the subject of several investigations. The study of these works has led to following analysis:

In a technical paper written by Neitz and D'Alfonso [1] describing the research at M.A.N., Nürnberg, Germany, a specially developed pintle nozzle has been used in a high speed direct injection engine. This nozzle has a single hole with a variable geometry pintle inserted into the orifice. This is producing a variable flow area which is a function of the position of the needle. The aim of this exercise was to adjust the injector flow area according to the fuel flow rate passing through the orifice. M.A.N. tested the pintle nozzle on the engine using the regular injector holder but with the maximum needle lift limited. The results were excellent only at low load and at idling speed in respect to unburnt Hydrocarbons. However, at high load the flow area of the orifice was too small for large fuel injection rate. This led to too long injection time duration and to too high injection pressures. On the other hand, when the maximum needle lift was readjusted to provide higher flow area for full load conditions, the small fuel dose required for idling speed was injected through too

large flow area, and poor fuel atomization resulted from low flow rate.

To overcome this controversy, M.A.N. used two-spring injector, as shown in figure 2.1. The first spring was set for the opening pressure of the valve. After a small lift, the needle moved against the stop which was preloaded by a second spring. Then, the orifice flow area increased only if the pressure in the injector rised high enough to overcome the preload of the second spring. Therefore, the discharge area could be controlled by the injector pressure which was dependent on engine speed and load, to obtain the desired fuel injection rate characteristics for all engine operational conditions.

It has to be added that the proposed pintle nozzle design, although satisfied some requirements, required more complicated nozzle holder. Also, the effect of fuel atomization from a pintle nozzle is inferior to that from a multi-hole nozzle.

A multi-hole variable orifice plunger valve nozzle was another design proposed by Hulsing [2] to overcome the deficiences of a hole-type nozzle. Figure 2.2 describes the design of the proposed nozzle in which the flow area of orifices made in a plunger was controlled by the sharp edge of the barrel from which the plunger was protruding. The plunger was spring loaded, therefore, the flow area increased or decreased as engine speed and fuel flow rate changed. For example, as the engine speed increased, the pressure in the injector was built-up, the plunger went down and, hence, the flow area increased. According to the author, the variable orifice plunger valve design was capable of maintaining almost any required level of injection pressure across the orifices for proper atomization and

Second Spring

First Spring
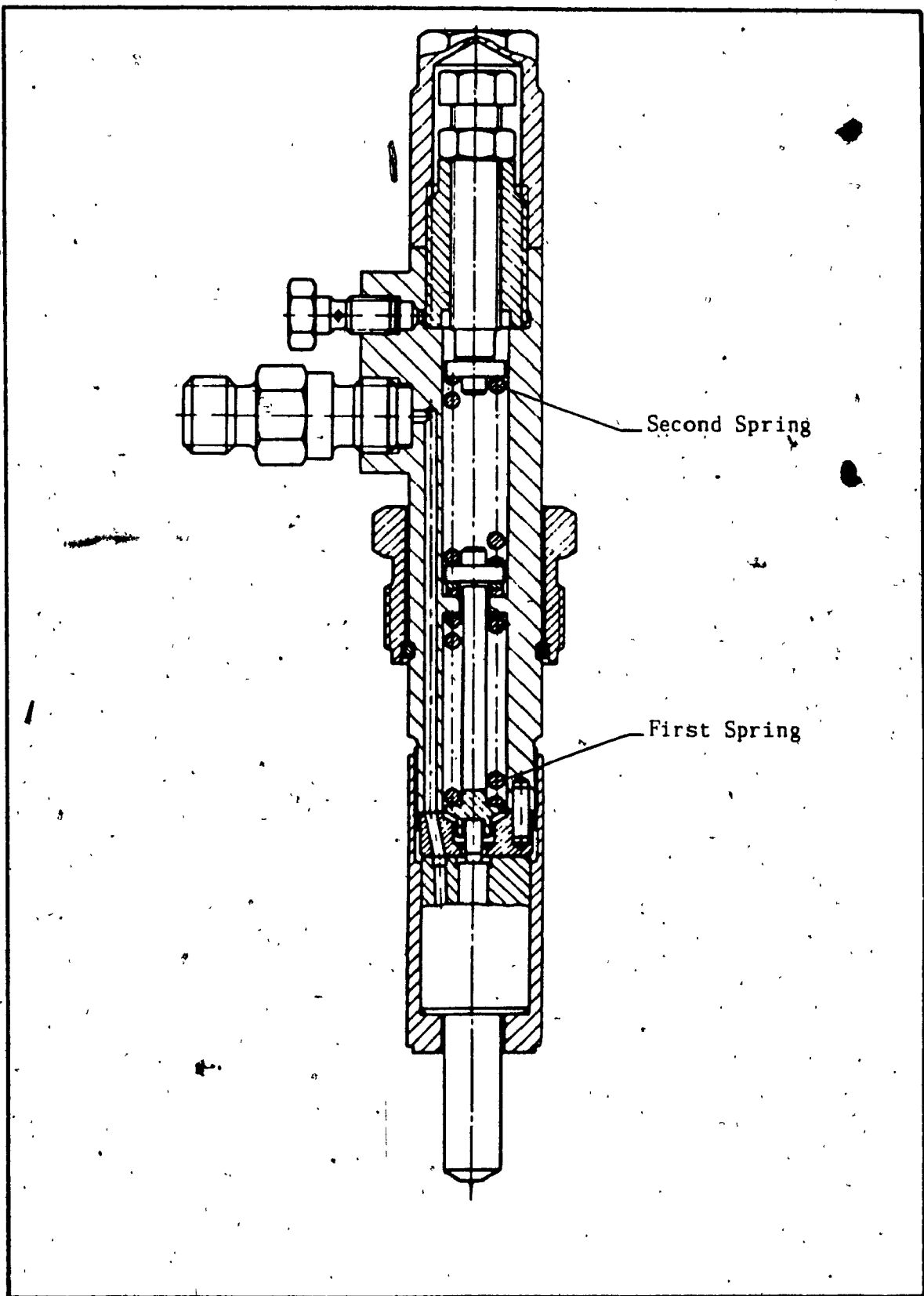
Fig.2.1. Drawing of Two-Spring Injector (Ref.[1])

Valve Body

Plunger Valve

Lapped Fit

Fuel Spray
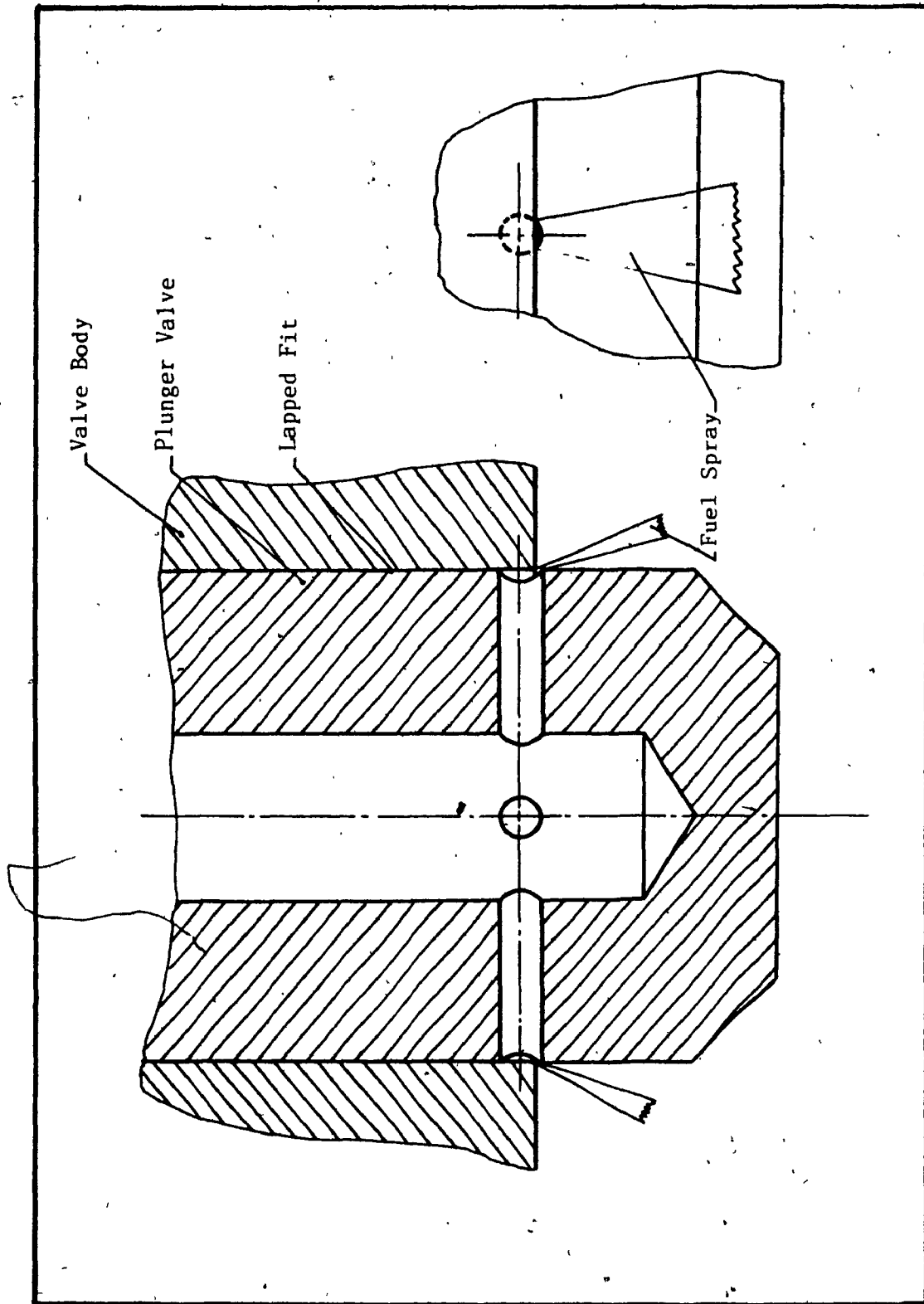
Fig.2.2 Multi-hole Variable Orifice Plunger Valve Nozzle (Ref.[2])

penetration of fuel.

A comment must be made that this idea was never proved experimentally. If the proposed nozzle was tested, it would show that it is not possible to keep the precisely machined plunger inside the combustion chamber without contamination, deformation, and seizure.

From these examples, it can be seen that the problem of diesel injector orifices flow area for successful operation at both high power and low speed conditions is not yet solved. Several attempts have been made to satisfy this requirement of contemporary high speed diesel engines.

2.2. Literature Review on Methods of Calculation of Fuel Injection System

Not long ago, before the computer era, studies of the fuel injection system were limited by the need of lengthy mathematical computations. Therefore, the application of theoretical simulation to improve the design of a fuel injection system could be performed only after making some simplifying assumptions.

After reviewing previous works, it was found that some investigators paid their attention to include different factors into the calculation which could become important for particular types of injection systems or for particular working conditions. The other gave more attention to the calculation methods to obtain the agreement between calculated and experimental results.

Davis and Giffen [3], in England, were among the earliest investigators who contributed significantly to the study of fuel injection system. In their work, many of significant variables, such as: fluid compressibility, elastic deformation of components, pressure propagation, fluid friction, pump and nozzle characteristics, and secondary injection, were discussed.

Pischinger [4] and Blaum [5], in Germany, introduced a different approach to the calculation of the fuel discharge rate in a diesel injection system. Pischinger proposed a specially elaborated graphical method reducing significantly the injection process calculation time. Blaum included the throttling effect of the partly opened inlet and outlet ports of the barrel on the pressure built up at the beginning and at the end of the pump discharge process.

Knight [6], in England, was the first investigator who used a digital computer to simulate a fuel injection system model with viscous friction and cavitation in the injection pipe.

Krepec [7], in Poland, included in the calculation the effect of the fuel leakage between the plunger and the barrel of the fuel injection pump. Kijewski [8], also in Poland, took into consideration the impact of elastic deformation of the pump camshaft on the velocity decrease of the pump plunger.

Becchi [9], in Italy, derived a mathematical model for the fuel injection system in more detailed form. In his model, the fluid continuity and momentum equations for the injection pipe were simplified by neglecting the convective terms and the friction term. From those simplified equations, the author used the "small amplitude wave theory" to calculate the pressure waves in the injection pipe.

Wylie, Bold, and El-Erian [10], in USA, developed and improved the theoretical model for digital simulation of a conventional diesel fuel injection system. They solved the partial differential equations describing the continuity and motion of fluid in the injection pipe by the method of characteristics. In their mathematical model, the pressure wave propagation phenomena, pipe friction, and cavitation were taken into account. The authors also discussed the accuracy of the simulation model affected by the fuel bulk modulus and wave speed variations, the residual pressure in the system, and the discharge coefficient at orifices.

Kumar, Gaur, Garg, and Babu [11], in India, made a comparison between several methods used in solving the continuity and momentum equations for a fuel injection system. They placed the differential equations in a finite difference scheme comprising of two-step Lax-Wendroff and Leap-Frog techniques. To draw the conclusions on the methods used, the authors carried out several tests, and the predicted and experimental results were compared. According to the authors, the comparison showed that their model could be used to predict the performance of the injection system.

It has to be mentioned that none of these investigators fully discussed two important phenomena of the injection process:

1. The initial period of the pumping process leading to the beginning of the fuel compression in the injection pump.

2. The throttling effect of the needle seat in the nozzle having a considerable effect on the needle lift, particularly at low engine speed.

2.3. Literature Review on Investigations of
Diesel Injector Behaviour on a Test-Rig

The investigations of the diesel injector quality on a test-rig have a long history. They started with the introduction of forced hydraulic injection systems for the diesel engines sixty years ago. Specialized injector test-rigs for the evaluation of injector's quality have been produced by several manufacturers of diesel injector equipment [12]. These test-rigs are simple, however, well qualified operators are required to be able to draw the right conclusions regarding the factors affecting the quality of tested injectors. Therefore, the evaluation methods being used have to be considered as highly subjective, and a great deal of efforts has been sacrificed by various investigators, including the injector manufacturers, to make the evaluation methods less dependent on the test-rig operators and to enable drawing of more objective conclusions from the behaviour of injectors on the test-rigs.

The first important attempt was made by Woodward [13], who acknowledged the effect of several factors on the behaviour of the injectors on the test-rigs. However, he did not produce any analytical relationship between particular injector parameters and its behaviour. His conclusions had rather qualitative character, and his main contribution was in showing the important effect of the needle seat geometry on the injector "chatter", a workshop expression related to the injector needle oscillation and to the noise produced, during the fuel injection on the test-rig.

Next attempt was made by Höfken [14], who was able to simulate the behaviour of an injector, using mathematical approach, and to draw conclusions regarding the effect of the various design and operational parameters on the "chatter" of an injector on a test-rig, as well as the injector's stability. His main fault was in neglecting the importance of the needle seat geometry by assuming a common combined critical flow area through both the seat and the orifices of the nozzle.

Further attempt was made by Krepec [15], who created the conditions at which the dynamic response of a diesel injector could be exactly evaluated by a device and not by a subjective feeling of the operator. He proposed to measure the maximum lift of the injector needle as the measure of its dynamic response to an exactly determined pressure signal. He also proposed a device with which the pressure signal could be varied adapting the testing conditions to the particular type of the injector.

All these investigators did not establish, however, a fully valid mathematical model for the injector tested on the test-rig, which could lead to the full evaluation of the injector's quality and to the conclusions regarding the quantitative effect of the design and operational parameters on the dynamic response of a diesel injector.

Chapter 3
FUEL INJECTION SYSTEM MODELLING
AND COMPUTER SIMULATION

3.1. Introduction

The purpose of this chapter is to develop an improved mathematical model for the fuel injection system of a diesel engine.

This topic has already been the subject of several publications. However, it was found that none of them was specific enough to provide the investigator with the tool for successful calculation of the injection process at all operational conditions of a diesel engine, and particularly at low engine speed and power. Therefore, it is necessary to develop an improved model which takes into consideration two important phenomena of the injection process:

1. The preliminary filling up of the injection system at the beginning of pumping eliminating the empty spaces which were created by the retraction action of the delivery valve of the pump at the end of a preceding injection process; this allows to find the beginning of fuel compression in the injection pump.

2. The specific impact of the pressure developed in the nozzle seat on the opening and closing processes of the injector, and also on the injector closing pressure which decides about the residual pressure inside the injection system.

It has to be mentioned that the use of numerical computing methods for this complex injection system is a big challenge, and that the computing program has to be first developed and carefully tested to perform the full and accurate calculation of the fuel discharge process.

3.2. Analytical Model of the Fuel Injection System

A schematic representation of the fuel injection system is shown in figure 3.1. It consists of three major components: the fuel injection pump, the injection pipe, and the fuel injector. These three components are distinguished by two control surfaces I-I and II-II as indicated in figure 3.1. Within the pumping chamber of the pump, fuel is metered for a particular dose, and it is compressed as the pump plunger moves up. At a certain pressure, the delivery valve which separates the pumping and the delivery chambers, is lifted off its seat and allows the fuel to flow through the valve into the delivery chamber. The fuel, then, is delivered through the injection pipe to the injector by means of pressure wave propagation. At the injector end, if the amplitude of the pressure is smaller than the injector opening pressure, the injector nozzle remains closed. Then, the pressure wave is reflected from the injector towards the pump superimposing itself on the next coming pressure wave. When the fuel pressure in the injector chamber overcomes the nozzle opening pressure, the injector needle is lifted off its seat. The fuel, then, flows through the seat chamber into the bag chamber where the fuel is injected into the engine cylinder through the orifices. If the fuel pressure in the injector increases rapidly, the injector needle will move fast until it reaches the stop at the injector body. If the fuel pressure, however, does not increase high enough, the needle will float at some level below the stop until the pressure drops to the injector closing pressure. At this moment, the nozzle valve is closed by the spring force, and the fuel flow through the valve is cut.
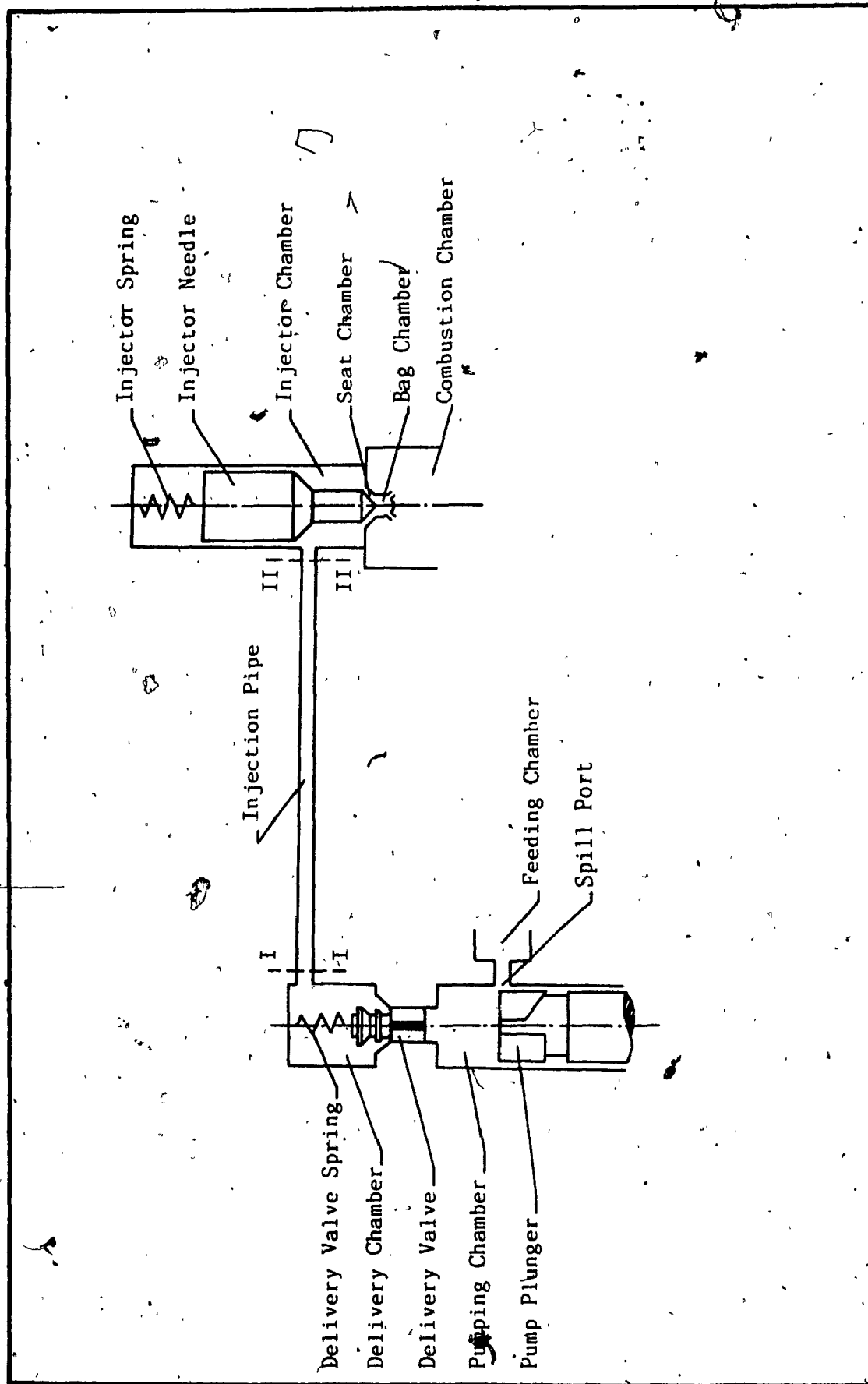
Fig.3.1. Schematic of a Fuel Injection System

Calculation of fuel discharge rate in a diesel injection system has to take into consideration several factors affecting this very fast and high pressure hydraulic process spreading from the injection pump to the injector through the injection pipe. Two of main factors are the fuel compressibility and the propagation of pressure waves. Fuel compressibility has to be taken into account when dealing with pressures in the range of 500 bars in the fuel injection systems for high speed diesel engines with direct injection combustion chamber. The modulus of elasticity E, which represents the fuel compressibility increases significantly with the pressure increase, as shown in figure 3.2, and decreases with the temperature increase, as shown in figure 3.3, [12]. Since the fuel temperature is usually kept in the range of $30^\circ C$ to $40^\circ C$ ($86^\circ F$ to $104^\circ F$) during the system calibration as well as during the service, the modulus change due to temperature variations does not need to be taken into account during calculation. However, the modulus variations due to the fuel pressure changes cannot be neglected, and there are two approaches:

1. The average value of the modulus of elasticity of fuel can be used as a constant value corresponding to the average fuel pressure created inside the injection system.

2. The modulus of elasticity can be substituted for every pressure value in subsequent calculation steps using a formula or a table.

The propagation of the pressure waves has to be taken into account in calculations of fuel discharge process for the injection systems used on diesel engines with the speed over 500 RPM if they are fitted with a longer injection pipe. As fuel is compressed in the
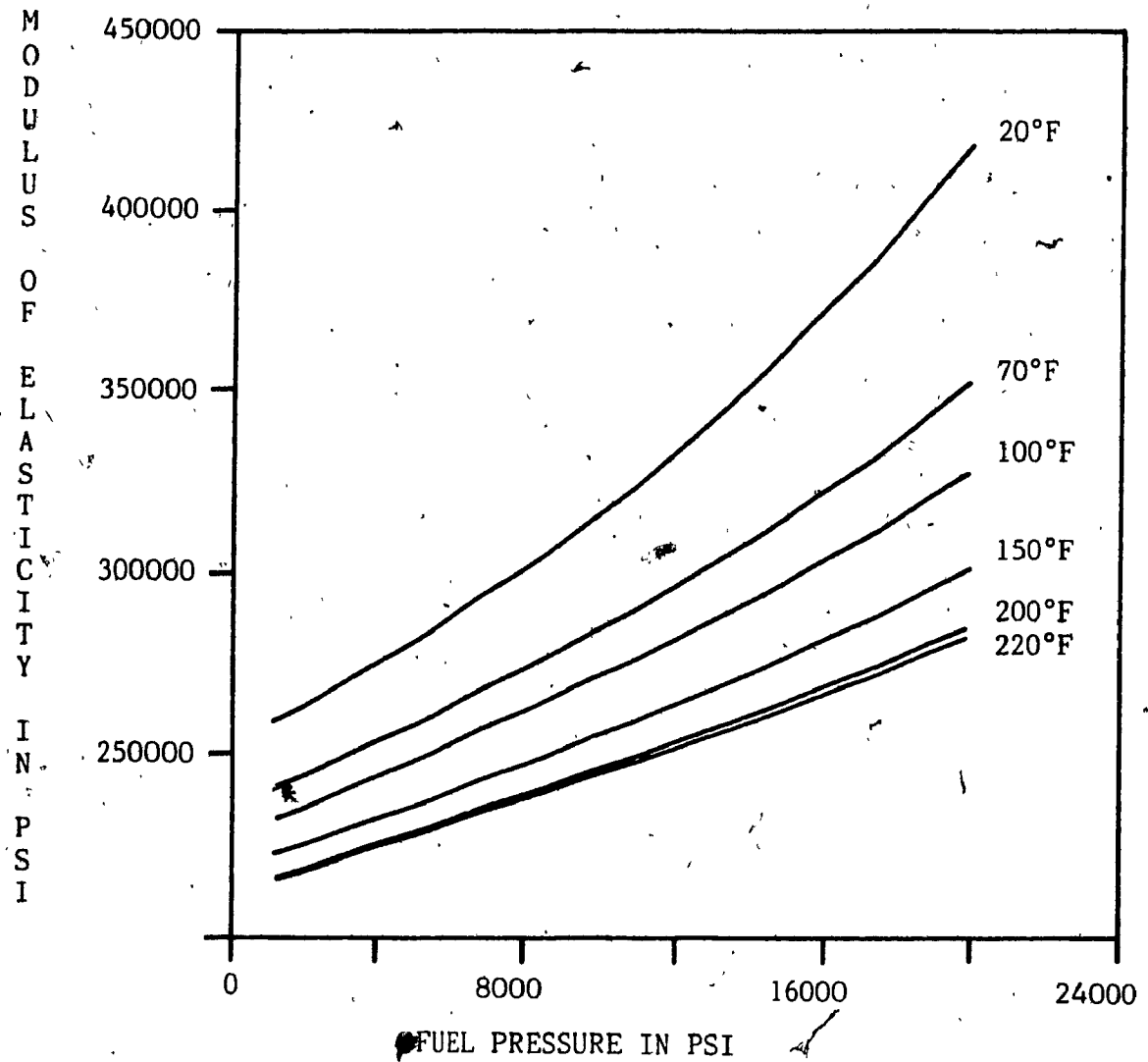
Fig.3.2. Fuel Modulus of Elasticity versus Pressure
(Reproduced from Ref.[12])
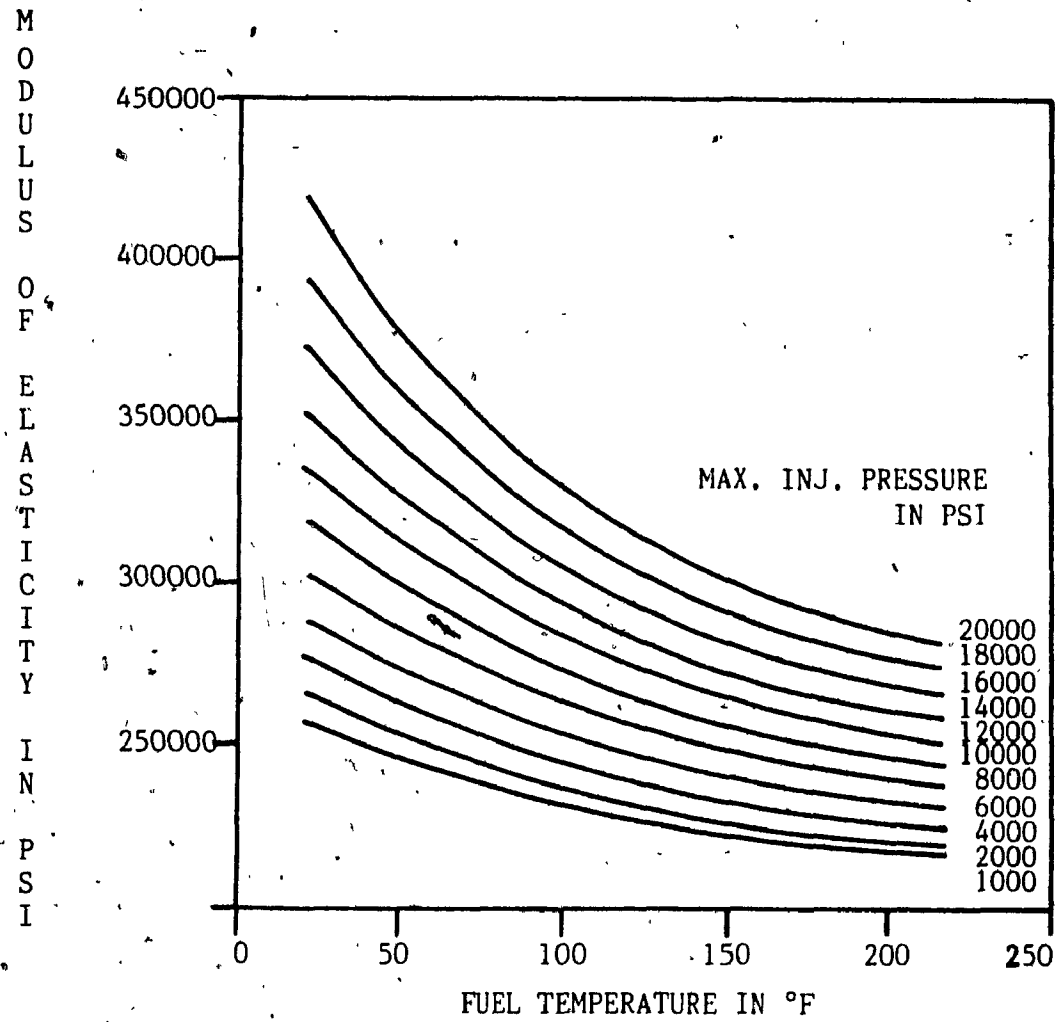
Fig.3.3 Fuel Modulus of Elasticity versus Temperature
(Reproduced from Ref.[12])

fuel injection pump, a pressure wave initiated by the pump plunger movement is propagated through the injection pipe at the speed of sound in the fuel. This wave does not only travel from the pump to the injector nozzle, but it is also reflected back towards the pump from the injector. The presence of pressure waves alters the fuel discharge rate of the injection pump so that complex theoretical methods of analysis and computing have been developed to simulate this process.

Taking into account all calculation methods already developed and published, an attempt is made in this thesis to include the needle seat chamber pressure into the calculation of the fuel discharge process in a diesel engine. The value of that pressure is of great significance to the evaluation of the injector's opening and closing processes because it produces an additional force acting on the injector needle. In the existing calculation procedures, the seat pressure was assumed to be equal either to the injector chamber pressure or to the bag chamber pressure. In fact, this seat pressure actually changes from the bag chamber pressure to the injector chamber pressure, following the movement of the injector needle during the opening process.

In some cases, such as at maximum engine power conditions, the injector opening process is so fast that the specific impact of the seat pressure can be neglected because of the very fast pressure increase in the injector due to the high amplitude pressure wave produced by the pump. However, at low engine speed, particularly at idling and starting conditions, the pressure wave amplitude is low and the

pressure in the injector drops very fast after the injector's opening. For that reason, the contribution of the seat pressure to the needle lifting force during the opening process of the injector is much greater and cannot be neglected. Also, during the injector closing process, the seat pressure can have a great impact on the injector closing pressure, and hence on the injector's tendency to open again due to the pressure wave peaks, i.e. to produce the post-injection phenomenon. Finally, since the seat chamber is connected to the bag chamber of the injector, the higher value of the seat pressure can prevent the possibility of the combustion gases penetration through the injector orifices, what causes corrosion, overheating and carbon deposits inside the nozzle.

The proposed seat pressure approach in calculation of the fuel discharge rate in a diesel injection system is considered as one of the main topics of this work. The importance of this approach will be proved in the next chapters of this thesis.

3.3. Derivation of Continuity and Motion Equations

3.3.1. Continuity and Motion Equations for Injection Pipe

Two partial differential equations representing the continuity and motion derived in reference [16] will be employed for the compressible fuel flow through a cylindrical tube with pressure waves. These two partial differential equations are:

1. Equation of Continuity:

$$\frac{\partial p}{\partial t} + v\frac{\partial p}{\partial x} + \rho \bar{a}^2 \frac{\partial v}{\partial x} = 0 \qquad (3.1)$$

The sound velocity in fluid is given by:

$$\bar{a}^2 = \frac{E/\rho}{1 + \dfrac{E\,D}{G_p\,e}} \qquad (3.2)$$

2. Equation of motion:

$$\frac{1}{\rho}\frac{\partial p}{\partial x} + v\frac{\partial v}{\partial x} + \frac{\partial v}{\partial t} + g\sin\theta + f\frac{|v|v}{2D} = 0 \qquad (3.3)$$

In water hammer applications, the terms $v\frac{\partial p}{\partial x}$ and $v\frac{\partial v}{\partial x}$, in equations (3.1) and (3.3), are much smaller than the terms $\frac{\partial p}{\partial t}$ and $\frac{\partial v}{\partial t}$, respectively. Therefore, if the friction is also neglected and the pipe is horizontal, i.e. $\theta = 0$, the above continuity and motion equations become:

1. Simplified Equation of Continuity:

$$\frac{\partial v}{\partial x} = -\frac{1}{\rho \bar{a}^2}\frac{\partial p}{\partial t} \tag{3.4}$$

2. Simplified Equation of-Motion:

$$\frac{\partial v}{\partial t} = -\frac{1}{\rho}\frac{\partial p}{\partial x} \tag{3.5}$$

Both equations can be solved in the form of two-solution equations, as given in appendix A, and the solutions are:

$$p = p_0 + g\rho\left[\Phi(t - \frac{x}{a}) - \Psi(t + \frac{x}{a})\right] \tag{3.6}$$

$$v = v_0 + \frac{g}{a}\left[\Phi(t - \frac{x}{a}) + \Psi(t + \frac{x}{a})\right] \tag{3.7}$$

The solutions (3.6) and (3.7) of equations (3.4) and (3.5) are found under condition that the sound velocity in the fluid does not change. This is not true. However, if the average pressure and temperature of fluid are correctly determined, the average constant sound velocity $\bar{a}$ does not cause significant differences in calculation results and can be accepted.

The forms of the arguments in equations (3.6) and (3.7) tell that the values of amplitudes for the functions Φ and Ψ are moving with the sound velocity in the positive or in the negative x direction. Also, from equations (3.6) and (3.7), one can see that the pressure and the velocity of fuel consist of three terms. They can be identified as the initial values p_0 and v_0, the forward moving values p_f and v_f, and the backward moving values p_b and v_b.

Then, equations (3.6) and (3.7) can be written as:

$$p = p_o + p_f + p_b \tag{3.8}$$

$$v = v_o + v_f + v_b \tag{3.9}$$

where,

$$p_f = \rho g \Phi \left(t - \frac{x}{a} \right) \tag{3.10}$$

$$p_b = - \rho g \Psi \left(t + \frac{x}{a} \right) \tag{3.11}$$

$$v_f = \frac{g}{a} \Phi \left(t - \frac{x}{a} \right) \tag{3.12}$$

$$v_b = \frac{g}{a} \Psi \left(t + \frac{x}{a} \right) \tag{3.13}$$

Creating a constant:

$$K = \frac{1}{\rho \bar{a}} \tag{3.14}$$

Then, comparing equations from (3.10) to (3.13) and using equation (3.14), one obtains:

$$p_f = \frac{1}{K} v_f \tag{3.15}$$

and

$$p_b = - \frac{1}{K} v_b \tag{3.16}$$

Substituting equations (3.15) and (3.16) into equations (3.8) and (3.9) yields:

$$p = p_o + \frac{1}{K} v_f - \frac{1}{K} v_b \tag{3.17}$$

$$v = v_o + v_f + v_b \tag{3.18}$$

In these equations, the pressure and the velocity are expressed by the residual pressure and by two amplitude-values of the velocity waves. The magnitudes v_f and v_b are still the discretional functions which can be determined by establishment of the boundary conditions at the pump and at the injector.

3.3.2. Continuity and Motion Equations at Pump

To derive the equations for the two conditions of continuity and force equilibrium, the pump is divided into two chambers: pumping chamber and delivery chamber. These two chambers are separated by a delivery valve. A schematic representation of the pumping chamber and delivery chamber is given in figure 3.4.

3.3.2.1. Continuity Equation for Pumping Chamber

Applying the conservation of mass law which states that the time rate of the net mass inflow into a control volume is equal to the time rate of increase of mass within the control volume, i.e.

$$\sum \dot{m}_{in} - \sum \dot{m}_{out} = \frac{d}{dt}(m_{cv})$$

(3.19)

If the fuel density ρ is constant, then equation (3.19) can be written as:

$$\sum q_{in} = \sum q_{out} + q_{cv}$$

(3.20)

where q is the volumetric flow rate and

$$q_{cv} = \frac{dV}{dt}$$

(3.21)

with V being the volume inside the control volume.

The definition of fluid modulus of elasticity can be expressed by:

$$E = \frac{dp}{\dfrac{dV}{V}}$$

or,

Control Surface I-I

DELIVERY PRESSURE p_d

SPRING FORCE
$P_{ds} + k_{dv}h_{dv}$

PRESSURE FORCE P_d

INERTIA FORCE
$m_p \dfrac{dv_{dv}}{dt}$

DAMPING FORCE $\delta_d v_{dv}$

FRICTION FORCE R_d

PRESSURE FORCE P_p

PUMPING
PRESSURE p_p

FEEDING
PRESSURE p_f
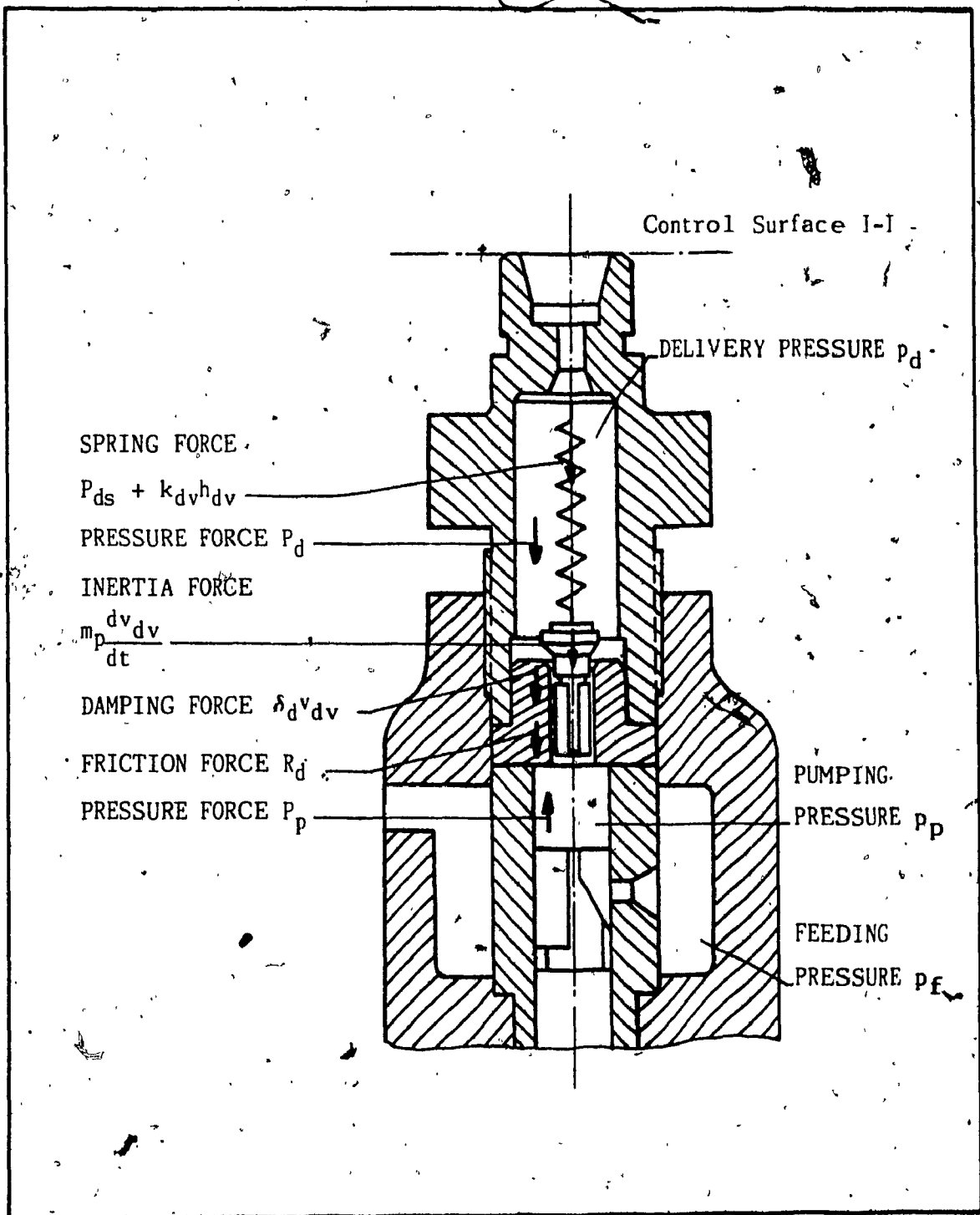
Fig.3.4. Schematic of an Injection Pump

$$dV = \frac{V}{E} dp$$

or,

$$\frac{dV}{dt} = \frac{V}{E} \frac{dp}{dt} \tag{3.22}$$

Using equation (3.22), equation (3.21) is rewritten as:

$$q_{cv} = \frac{V}{E} \frac{dp}{dt} \tag{3.23}$$

For the pumping chamber, the fuel inflow rate is:

$$q_{in} = F_p v_p$$

and this is due to the pump plunger movement.

The fuel outflow rate is:

$$q_{out} = \varsigma_{sp} \mu_{sp} F_{sp} \sqrt{\frac{2}{\rho}|P_p - P_f|} + F_{dv} v_{dv} + \varsigma_d \mu_d F_{fdv} \sqrt{\frac{2}{\rho}|P_p - P_d|}$$

where,

$$\varsigma_{sp} = 1 \quad \text{if } P_p > P_f$$

$$\varsigma_{sp} = -1 \quad \text{if } P_p < P_f$$

$$\varsigma_d = 1 \quad \text{if } P_p > P_d$$

$$\varsigma_d = -1 \quad \text{if } P_p < P_d$$

In this expression, the first term on the right side is the fuel flow from the pumping chamber through the spill port into the feeding chamber, the second term is due to the motion of the delivery valve, and the last one is the fuel flow through the delivery valve into the delivery chamber.

The fuel accumulation due to the elastic deformation of the fluid contained in the pumping chamber, caused by the variation of the pressure is:

$$q_{cv} = \frac{V_p - F_p h_p}{E} \frac{dp_p}{dt}$$

Here, it must be noted that the volume of the pumping chamber varies according to the plunger displacement. Therefore, the pumping chamber volume takes the form $(V_p - F_p h_p)$ as indicated above.

Thus, a first continuity equation combined from the above equations according to equation (3.20) is:

$$F_p v_p = \varsigma_{sp} \mu_{sp} F_{sp} \sqrt{\frac{2}{\rho} |P_p - P_f|} + \frac{V_p - F_p h_p}{E} \frac{dp_p}{dt} + F_{dv} v_{dv} +$$

$$+ \varsigma_d \mu_d F_{fdv} \sqrt{\frac{2}{\rho} |P_p - P_d|} \qquad (3.24)$$

In this equation, the flow areas through the spill port F_{sp} and through the delivery valve F_{fdv} are functions of the variables h_p and h_{dv}, as shown in figures 3.5 and 3.6, respectively. The formulae for those flow areas are:

1. Flow area through the spill port:

– If $0 \leq h_p \leq h_{p1}$:
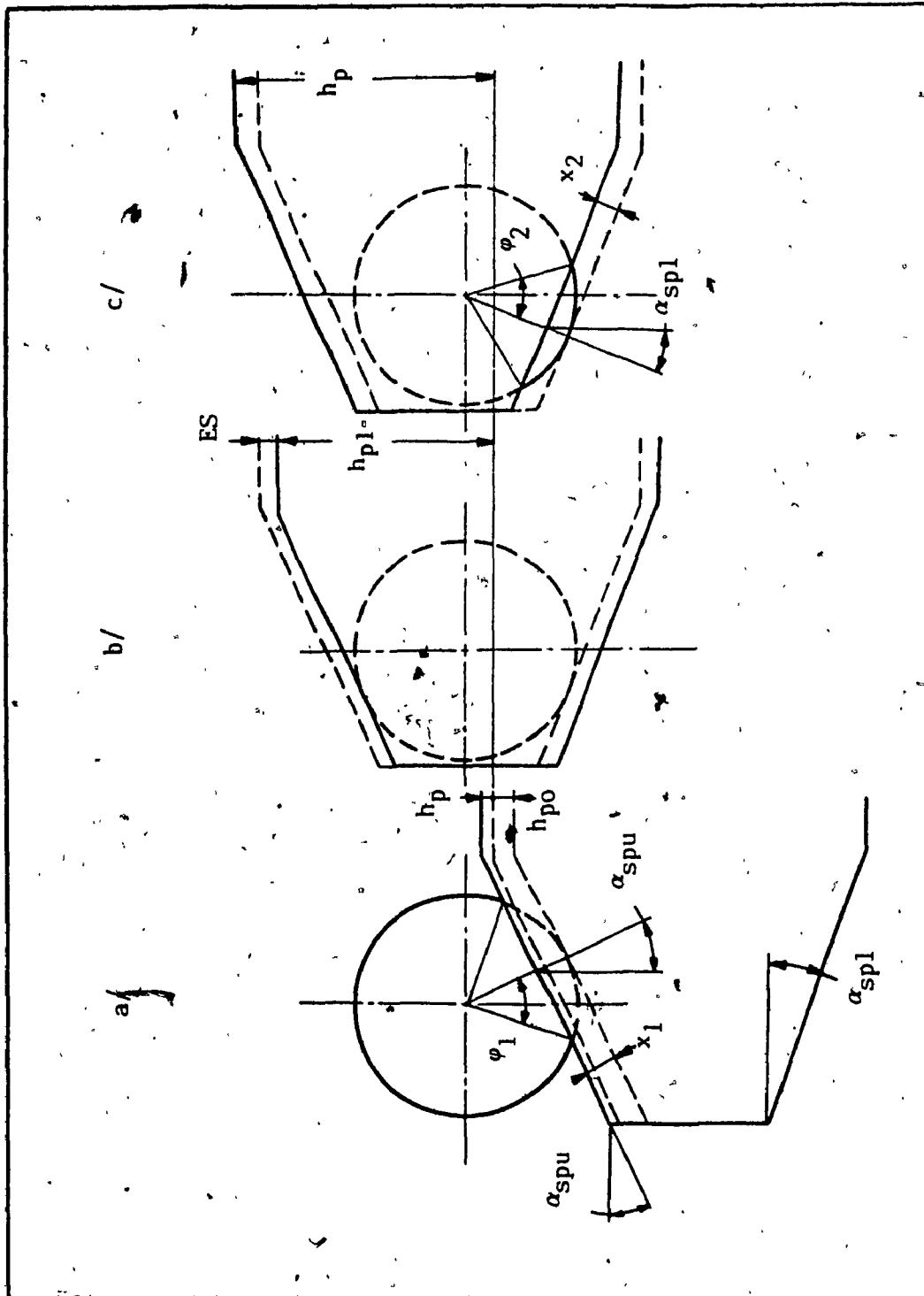
where,

Fig.3.5. Schematic of the Spill Port Opening Area
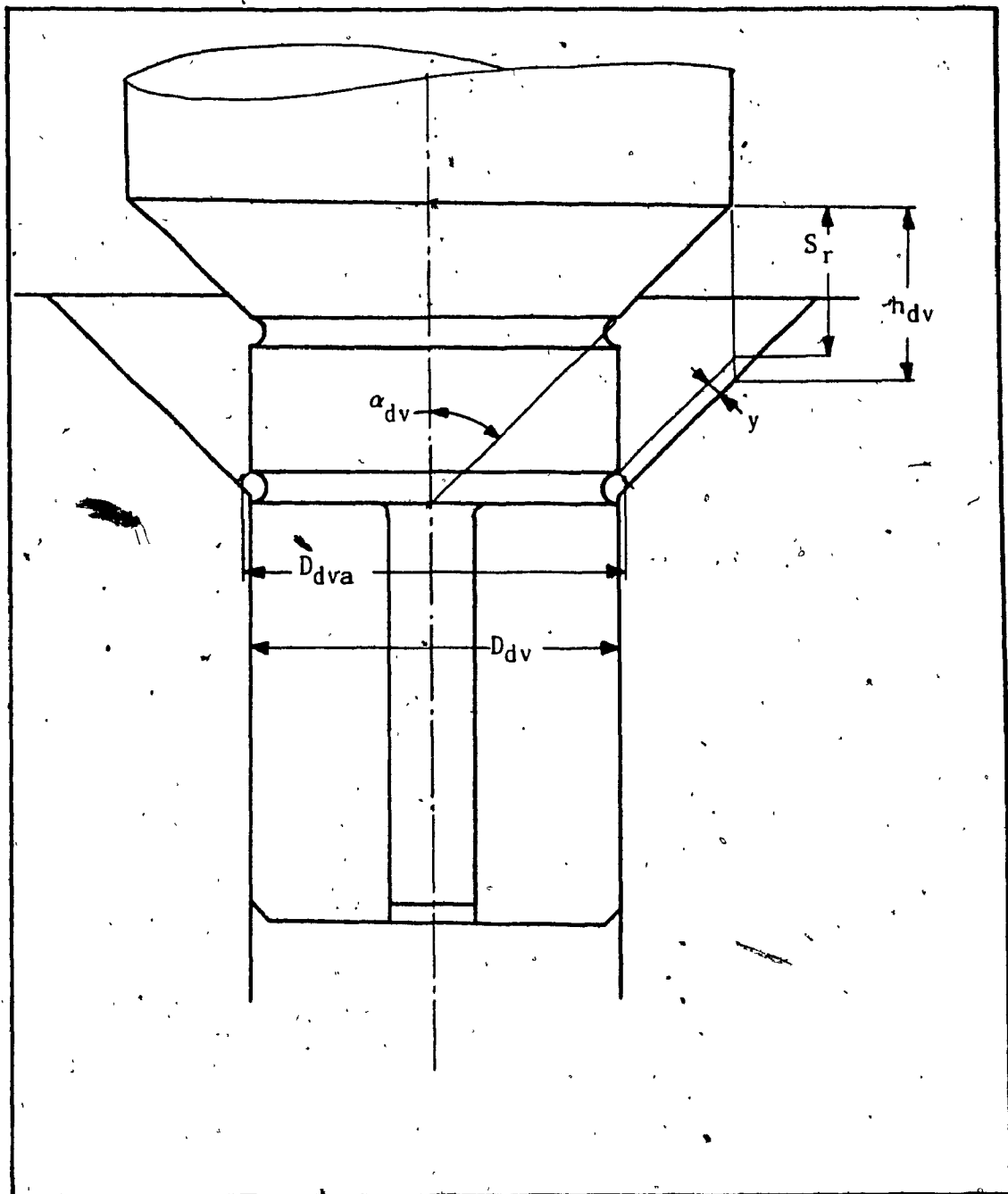
Fig.3.6. Schematic of Flow Area between Delivery Valve and Seat

$$h_{p1} = \frac{2r_{sp}}{\cos\alpha_{spu}} - h_{po} \qquad (3.25)$$

$$F_{sp} = \pi(r_{sp})^2 - \left[(r_{sp})^2\varphi_1 - (r_{sp} - x_1)r_{sp}\sin\varphi_1\right] \qquad (3.26)$$

where,

$$x_1 = (h_p + h_{po})\cos\alpha_{spu} \qquad (3.27)$$

$$\cos\varphi_1 = \frac{r_{sp} - x_1}{r_{sp}} \qquad (3.28)$$

$$\sin\varphi_1 = \frac{1}{r_{sp}}\sqrt{(r_{sp})^2 - (r_{sp} - x_1)^2} \qquad (3.29)$$

- If $h_{p1} < h_p \leq (h_{p1} + ES)$:

$$F_{sp} = 0 \qquad (3.30)$$

- If $h_p > (h_{p1} + ES)$:

$$F_{sp} = (r_{sp})^2\varphi_2 - (r_{sp} - x_2)r_{sp}\sin\varphi_2 \qquad (3.31)$$

where,

$$x_2 = \left[h_p - (h_{p1} + ES)\right]\cos\alpha_{spl} \qquad (3.32)$$

$$\cos\varphi_2 = \frac{r_{sp} - x_2}{r_{sp}} \qquad (3.33)$$

$$\sin\varphi_2 = \frac{1}{r_{sp}}\sqrt{(r_{sp})^2 - (r_{sp} - x_2)^2} \qquad (3.34)$$

2. Flow area through delivery valve:

$$F_{fdv} = \pi\left[D_{dv} + (h_{dv} - S_r)\sin\alpha_{dv}\cos\alpha_{dv}\right](h_{dv} - S_r)\sin\alpha_{dv} \qquad (3.35)$$

The detailed derivation of these two flow areas is presented in appendices B and C.

3.3.2.2. Continuity Equation for Delivery Chamber

The continuity equation for delivery chamber can be derived by comparing the fuel inflow into the delivery chamber:

$$q_{in} = \varsigma_d \mu_d F_{fdv} \sqrt{\frac{2}{\rho} |p_p - p_d|} + F_{dv} v_{dv}$$

to the fuel outflow and the fuel accumulation.

The fuel outflow is:

$$q_{out} = F_I v_I$$

where the fluid velocity v_I at control surface I-I is given by:

$$v_I = v_{fI} + v_{bI}$$

with v_{fI} and v_{bI} being the forward and backward fluid velocity wave amplitudes at control surface I-I respectively.

Based on equations (3.15) and (3.16) derived in the previous section, one can write:

$$v_I = K(p_{df} - p_{db})$$

where p_{df} and p_{db} are the forward and backward pressure wave amplitudes at control surface I-I respectively.

From equation (3.8):

$$p_{df} = p_d - p_{db} - p_{do}$$

Substituting, one gets:

$$v_I = K(p_d - 2p_{db} - p_{do})$$

The fuel accumulation:

$$q_{cv} = \frac{V_d - F_{dv}h_{dv}}{E} \frac{dp_d}{dt}$$

Thus, the continuity equation for the delivery chamber is:

$$\varsigma_d \mu_d F_{fdv} \sqrt{\frac{2}{\rho}|p_p - p_d|} + F_{dv}v_{dv} = \frac{V_d - F_{dv}h_{dv}}{E} \frac{dp_d}{dt} +$$
$$+ F_I K(p_d - 2p_{db} - p_{do}) \tag{3.36}$$

3.3.2.3. Motion Equation for Delivery Valve

The motion equation for delivery valve is derived by balancing the force exerted on the delivery valve by the pressure in the pumping chamber $p_p F_{dv}$ with the forces due to: pressure in the delivery chamber $p_d F_{dv}$, spring load $(P_{ds} + k_{dv} h_{dv})$, inertia $m_p \dfrac{dv_{dv}}{dt}$, and mechanical friction and damping $(\pm R_d + \delta_d v_{dv})$, i.e.

$$F_{dv} p_p = F_{dv} p_d + P_{ds} + k_{dv} h_{dv} + m_p \frac{dv_{dv}}{dt} \pm$$
$$\pm R_d + \delta_d v_{dv} \qquad\qquad (3.37)$$

with,

$$\frac{dh_{dv}}{dt} = v_{dv} \qquad\qquad (3.38)$$

In equation (3.37), m_p represents the mass of moving parts which are the delivery valve and the spring. This mass can be approximately given as:

$$m_p = m_{dv} + \frac{1}{3} m_{ds} \qquad\qquad (3.39)$$

3.3.3. Continuity and Motion Equations at Injector

A schematic representation of the injector is shown in figure 3.7. The injector is divided into three areas: injector chamber, seat chamber, and bag chamber. The continuity and motion equations are derived as follows: -

3.3.3.1. Continuity Equation for Injector Chamber

At the control surface II-II, as indicated in figure 3.7, the fuel enters the injector delivery chamber with a velocity v_{II}. The fuel inflow rate, thus, is:

$$q_{in} = F_{II} v_{II}$$

where the fluid velocity v_{II} at control surface II-II is:

$$v_{II} = v_{fII} + v_{bII}$$

with v_{fII} and v_{bII} being the forward and backward fluid velocity wave amplitudes at control surface II-II respectively.

From equations (3.15) and (3.16):

$$v_{II} = K(p_{if} - p_{ib})$$

where p_{if} and p_{ib} are the forward and backward /pressure wave amplitudes at control surface II-II respectively.

From equation (3.8):

SPRING FORCE

$P_{is} + k_{is}h_i$

INERTIA FORCE

$m_i\dfrac{dv_i}{dt}$

DAMPING FORCE

$\delta_i v_i$

FRICTION FORCE

R_i

PRESSURE FORCE

$P_i + P_s + P_b$

INJECTOR PRESSURE p_i

SEAT PRESSURE p_s

BAG PRESSURE p_b

F_i

Control Surface II-II

F_{so}

h_i

F_{si}

F_{fo}
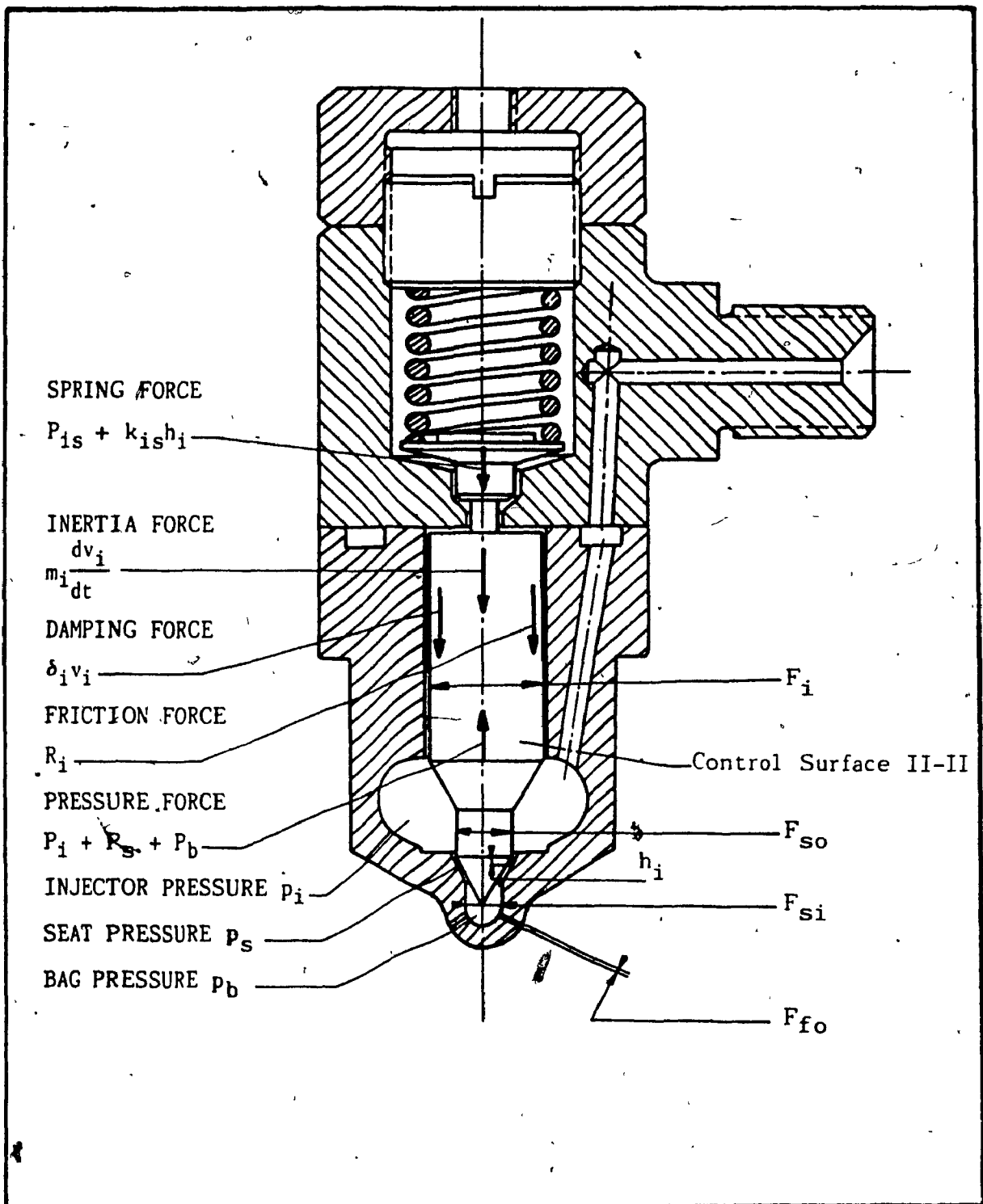
Fig.3.7. Schematic of a Diesel Injector

$$P_{1b} = (p_i - p_{if} - p_{io})$$

Substituting, one obtains:

$$q_{in} = F_{II}K(2p_{if} - p_i + p_{io})$$

The fuel outflow rate is :

$$q_{out} = \varsigma_{si}\mu_{si}F_{fsi}\sqrt{\frac{2}{\rho}|p_i - p_s|} + (F_i - F_{so})v_i$$

where,

$$\varsigma_{si} = 1 \quad \text{if } p_i > p_s$$

$$\varsigma_{si} = -1 \quad \text{if } p_i < p_s$$

In this expression, the first term on the right side is the fuel flow from the injector chamber into the seat chamber, and the second one is due to the motion of the injector needle.

The fuel accumulation is:

$$q_{cv} = \frac{V_i}{E}\frac{dp_i}{dt}$$

Thus, the continuity equation for the injector chamber is obtained as:
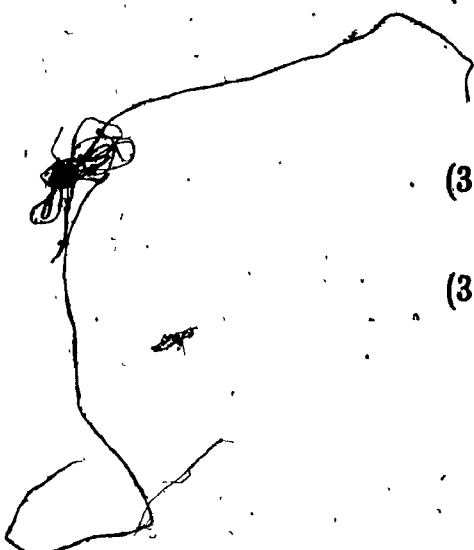
$$F_{II}K(2p_{if} - p_i + p_{io}) = \frac{V_i}{E}\frac{dp_i}{dt} + (F_i - F_{so})v_i +$$

$$+ \varsigma_{si}\mu_{si}F_{fsi}\sqrt{\frac{2}{\rho}|p_i - p_s|} \qquad (3.40)$$

The seat inlet flow area F_{fsi}, as indicated in figure 3.8, is derived in appendix D and has the form of:

$$F_{fsi} = A_{fsi}h_1^2 + B_{fsi}h_1 \qquad (3.41)$$

where,

$$A_{fsi} = \pi \left(\frac{\sin\alpha}{\cos\gamma}\right)^2 \cos\beta \qquad (3.42)$$

$$B_{fsi} = \pi D_{so} \frac{\sin\alpha}{\cos\gamma} \qquad (3.43)$$
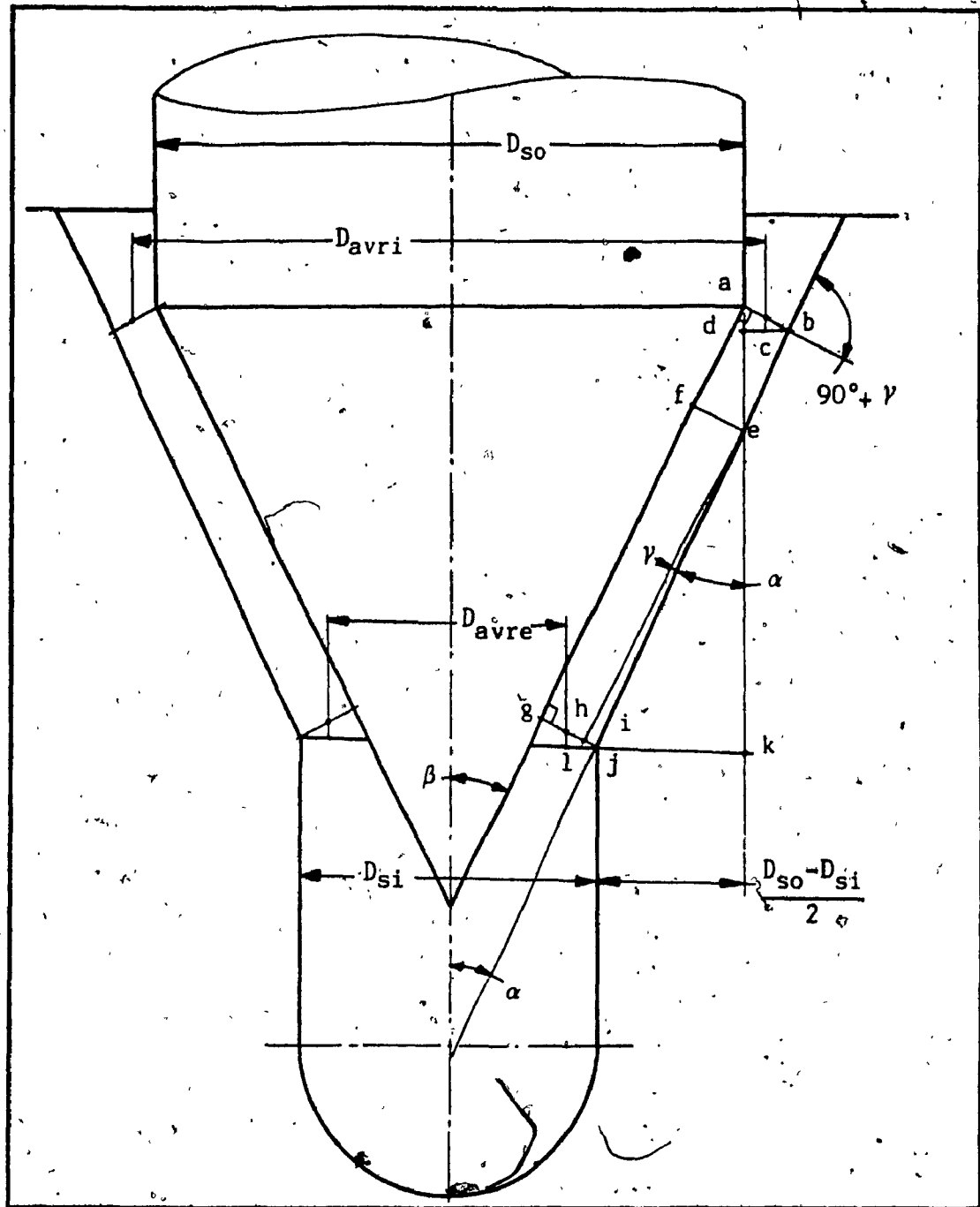
Fig. 3.8. Schematic of the Injector Needle Seat

3.3.3.2. Continuity Equation for Seat Chamber

Similar considerations to those for the injector chamber are made in derivation of continuity equation for the seat chamber.

The fuel inflow rate at the seat inlet section:

$$q_{in} = \varsigma_{si} \mu_{si} F_{fsi} \sqrt{\frac{2}{\rho} |p_i - p_s|}$$

must be equal to the fuel flow rate due to the motion of the injector needle:

$$(F_{so} - F_{si}) \dot{v}_i$$

and the fuel flow rate through the seat exit section into the bag chamber:

$$\varsigma_{se} \mu_{se} F_{fse} \sqrt{\frac{2}{\rho} |p_s - p_b|}$$

where,

$$\varsigma_{se} = 1 \quad \text{if } p_s > p_b$$

$$\varsigma_{se} = -1 \quad \text{if } p_s < p_b$$

Since the seat chamber volume is small, the fuel accumulation due to elastic deformation of the fluid contained in this chamber, caused by the variation of the seat pressure p_s is neglected.

Thus, the continuity equation for the seat chamber is:

$$\varsigma_{si}\mu_{si}F_{fsi}\sqrt{\frac{2}{\rho}|p_i - p_s|} = (F_{so} - F_{si})v_i +$$

$$+ \varsigma_{se}\mu_{se}F_{fse}\sqrt{\frac{2}{\rho}|p_s - p_b|} \qquad (3.44)$$

with the seat exit flow area F_{fse}, as indicated in figure 3.8, having the form of:

$$F_{fse} = A_{fse}h_i^2 + B_{fse}h_i + C_{fse} \qquad (3.45)$$

where,

$$A_{fse} = -\pi(\sin\beta)^2\cos\beta \qquad (3.46)$$

$$B_{fse} = \pi\left[D_{si} - (D_{so} - D_{si})\frac{\sin\gamma\cos\beta}{\sin\alpha}\right]\sin\beta \qquad (3.47)$$

$$C_{fse} = \pi(D_{so} - D_{si})\frac{\sin\gamma}{2\sin\alpha}\left[D_{si} - (D_{so} - D_{si})\frac{\sin\gamma\cos\beta}{2\sin\alpha}\right] \qquad (3.48)$$

The detailed derivation of this formula is given in appendix D.

3.3.3.3. Continuity Equation for Bag Chamber.

The continuity equation for the bag chamber is derived by equating the fuel flow into the bag chamber from the seat chamber:

$$q_{in} = \varsigma_{se}\mu_{se}F_{fse}\sqrt{\frac{2}{\rho}|p_s - p_b|}$$

to the fuel outflows due to the motion of the injector needle and to the fuel discharge from the bag chamber to the combustion chamber of a diesel engine:

$$q_{out} = F_{si}v_i + I\varsigma_o\mu_oF_{fo}\sqrt{\frac{2}{\rho}|p_b - p_c|}$$

where,

$$\varsigma_o = 1 \text{ if } p_b \gtrless p_c$$

$$\varsigma_o = 0 \text{ if } p_b < p_c$$

and the fuel accumulation:

$$q_{cv} = \frac{V_b}{E}\frac{dp_b}{dt}$$

Thus, the continuity equation for the bag chamber is:

$$\varsigma_{se}\mu_{se}F_{fse}\sqrt{\frac{2}{\rho}|p_s - p_b|} = \frac{V_b}{E}\frac{dp_b}{dt} + F_{si}v_i +$$

$$+ I\varsigma_o\mu_oF_{fo}\sqrt{\frac{2}{\rho}|p_b - p_c|} \tag{3.49}$$

3.3.3.4. Motion Equation for Injector Needle

The motion equation for the injector needle is derived by balancing the forces exerted on the needle by the pressures in the injector chamber, seat chamber, and bag chamber:

$$p_i(F_i - F_{so}) + p_s(F_{so} - F_{si}) + p_b F_{si}$$

with the forces due to the injector spring load $(P_{is} + k_{is} h_i)$, inertia $m_i \dfrac{dv_i}{dt}$, mechanical friction and damping $(\pm R_i + \delta_i v_i)$, i.e.

$$p_i(F_i - F_{so}) + p_s(F_{so} - F_{si}) + p_b F_{si} = P_{is} + k_{is} h_i +$$

$$+ m_i \frac{dv_i}{dt} \pm R_i + \delta_i v_i \qquad (3.50)$$

with,

$$\frac{dh_i}{dt} = v_i \qquad (3.51)$$

In equation (3.50):

$$m_i = m_{in} + m_r + \frac{1}{3} m_{is} \qquad (3.52)$$

3.4. Solving the Continuity and Motion Equations

In the system of differential equations describing the continuity and motion for the fuel injection system, which are derived in the previous section, the following parameters are to be determined for each instant in the calculation:

p_p : Pressure in the pumping chamber

p_d : Pressure in the delivery chamber

p_{df} : Forward pressure at section I-I

v_{dv} : Velocity of the delivery valve

h_{dv} : Displacement of the delivery valve

p_i : Pressure in the injector delivery chamber

p_{ib} : Backward pressure at section II-II

p_s : Pressure in the seat chamber

p_b : Pressure in the bag chamber

v_i : Velocity of the injector needle

h_i : Displacement of the injector needle

The calculation also includes:

The discharge flow rate:

$$q_{fo} = I\mu_a F_{fo} \sqrt{\frac{2}{\rho}(p_b - p_c)} \qquad (3.53)$$

The fuel dose:

$$Q = \int q_{fo} dt \qquad (3.54)$$

A computer program is written based on a four-step Runge Kutta approximation to solve the system of differential equations for the parameters listed above.

It is also possible to determine the variations of the above parameters versus the pump cam rotation angle, instead of time, by changing the time independent variable into cam rotation angle variable according to the following formula:

$$\varphi = \frac{360Nt}{60} = 6Nt \tag{3.55}$$

Taking derivatives of both sides of equation (3.55) with respect to t,

$$\frac{d\varphi}{dt} = 6N \tag{3.56}$$

or,

$$dt = \frac{d\varphi}{6N} \tag{3.57}$$

Substituting dt from equation (3.57) into equations (3.24), (3.36), (3.37), (3.38), (3.40), (3.44), (3.49), (3.50) and (3.51), and rearranging, one obtains:

1. <u>In the pump:</u>

− Pumping chamber continuity equation:

$$\frac{dp_p}{d\varphi} = \frac{E}{6N(V_p - F_p h_p)} \left(F_p v_p - \varsigma_{sp} \mu_{sp} F_{sp} \sqrt{\frac{2}{\rho}|p_p - p_f|} - \right.$$

$$\left. - F_{dv} v_{dv} - \varsigma_d \mu_d F_{fdv} \sqrt{\frac{2}{\rho}|p_p - p_d|} \right) \tag{3.58}$$

- Delivery chamber continuity equation:

$$\frac{dp_d}{d\varphi} = \frac{E}{6N(V_d - F_{dv}h_{dv})}\left[\varsigma_d\mu_d F_{fdv}\sqrt{\frac{2}{\rho}|p_p - p_d|} + \right.$$

$$\left. + F_{dv}v_{dv} - F_I K(p_d - 2p_{db} - p_{do})\right] \tag{3.59}$$

- Delivery valve motion equation:

$$\frac{dv_{dv}}{d\varphi} = \frac{1}{6Nm_p}\left(p_p F_{dv} - p_d F_{dv} - P_{ds} - k_{dv}h_{dv} \pm \right.$$

$$\left. \pm R_d - \delta_d v_{dv}\right) \tag{3.60}$$

with,

$$\frac{dh_{dv}}{d\varphi} = \frac{v_{dv}}{6N} \tag{3.61}$$

- Forward pressure wave amplitude at control surface I-I:

$$P_{df} = P_d - P_{db} - P_{do} \tag{3.62}$$

2. <u>In the injector:</u>

- Injector chamber continuity equation:

$$\frac{dp_i}{d\varphi} = \frac{E}{6NV_i}\left[F_{II}K(2p_{if} - p_i + p_{io}) - (F_i - F_{so})v_i - \right.$$

$$\left. - \varsigma_{si}\mu_{si}F_{fsi}\sqrt{\frac{2}{\rho}|p_i - p_s|}\right] \tag{3.63}$$

- Seat chamber continuity equation:

$$\varsigma_{si}\mu_{si}F_{fsi}\sqrt{\frac{2}{\rho}|p_i - p_s|} = \varsigma_{se}\mu_{se}F_{fse}\sqrt{\frac{2}{\rho}|p_s - p_b|} +$$

$$+ \left(F_{so} - F_{si}\right)v_i \qquad (3.64)$$

- Bag chamber continuity equation:

$$\frac{dp_b}{d\varphi} = \frac{E}{6NV_b}\left(\varsigma_{se}\mu_{se}F_{fse}\sqrt{\frac{2}{\rho}|p_s - p_b|} - F_{si}v_i - \right.$$

$$\left. - I\varsigma_o\mu_oF_{fo}\sqrt{\frac{2}{\rho}|p_b - p_c|}\right) \qquad (3.65)$$

- Injector needle motion equation:

$$\frac{dv_i}{d\varphi} = \frac{1}{6Nm_i}\left[p_i\left(F_i - F_{so}\right) + p_s\left(F_{so} - F_{si}\right) + p_bF_{si} - \right.$$

$$\left. - P_{is} - k_{is}h_i \pm R_i - \delta_iv_i\right] \qquad (3.66)$$

and,

$$\frac{dh_i}{d\varphi} = \frac{v_i}{6N} \qquad (3.67)$$

- Backward pressure wave amplitude at control surface II-II:

$$P_{ib} = P_i - P_{if} - P_{io} \qquad (3.68)$$

3.5. An Example of Fuel Injection System Simulation on a Digital Computer

In this section, a particular fuel injection system is simulated on a digital computer. Also, the computer programming used for calculation is discussed.

The work is based on the following specific data for each component of the fuel injection system.

3.5.1. Data for the Fuel Injection System

The pump used is of PE6A75B420LS59/1 type by R. Bosch, and it has the velocity-lift chart for the pump cam shown in figure 3.9. The injector used is of BKBL87S5299XS type by CAV with the hole-type nozzle BDLL150S6502.

The specific data for the injection pump, the injector, and the injection pipe are shown in tables 3.1, 3.2, and 3.3 respectively.

The fuel used in the system is calibration fluid SAE J967d and its properties are given in table 3.4.

3.5.2. Assumptions

The procedure of calculation is carried out for the system which is simplified by making some assumptions. These assumptions are:

— The sound propagation velocity $\bar{a}$, and the fuel density are not affected by the pressure variations, and are considered constant. However, they are taken as an average for the pressure range appearing in calculation.
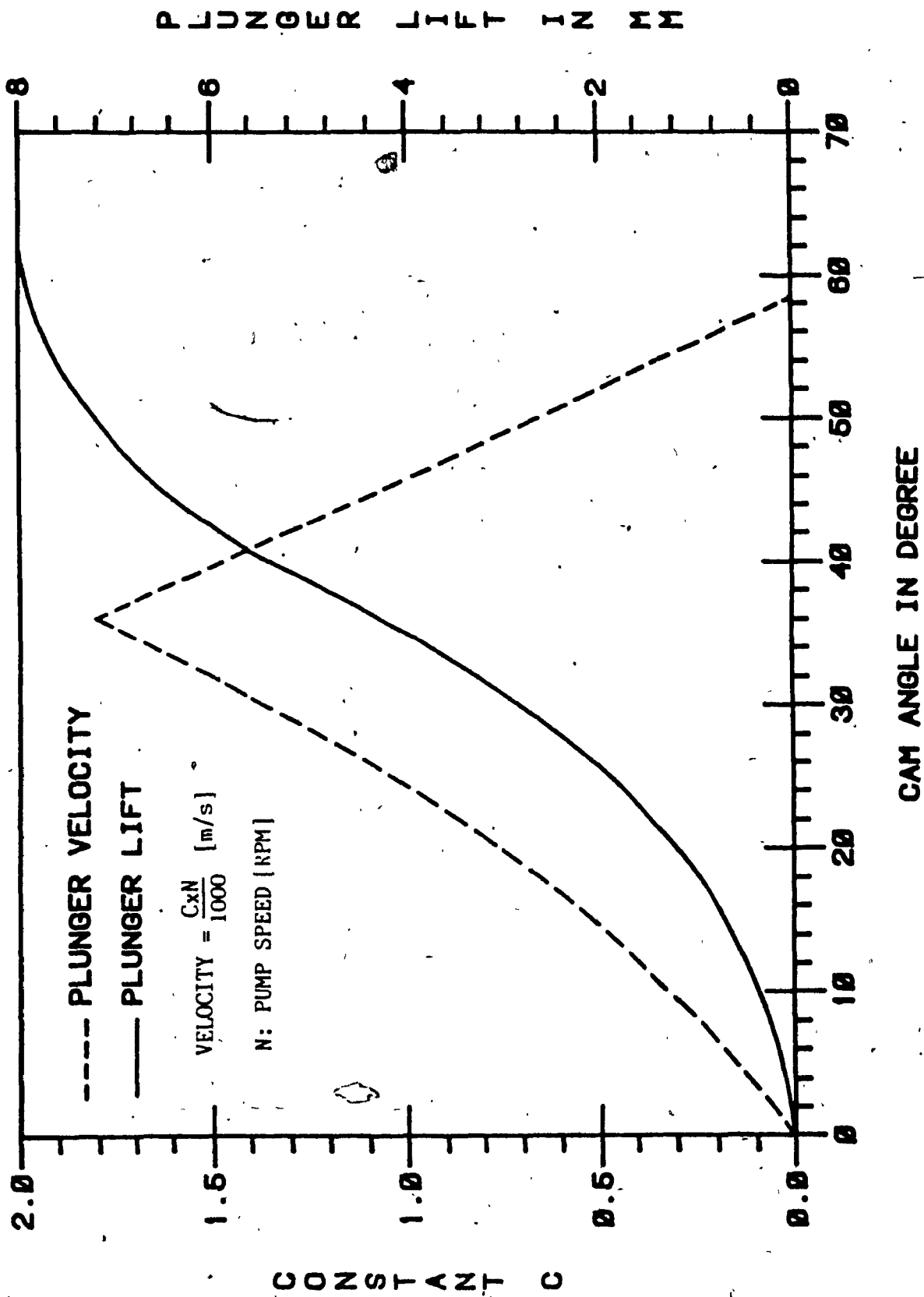
Fig.3.9. Velocity-Lift Chart for the Plunger of the Injection Pump

(Cam Form PPZ 34S-2)

– The sealing of mechanical components is considered perfect. Therefore, fuel leakages are not taken into account.

– The elastic deformation of solid parts of the system due to the force and pressure changes is neglected. Hence, the relationship between sound velocity $\bar{a}$ and fuel modulus of elasticity E given by equation (3.2) is simplified as:

$$\bar{a} = \sqrt{\frac{E}{\rho}}$$

– The feeding chamber of the fuel injection pump, which is a fuel supply source, has a large volume, and a constant fuel pressure.

– The fuel is discharged to the atmosphere, instead of into the engine cylinder.

– Mechanical friction for delivery valve and for injector needle are neglected due to the existing clearance.

– Damping force acting on delivery valve is neglected due to the large clearance in the valve.

Plunger diameter [mm]	7.5
The upper helix angle of plunger [degree]	0.
The lower helix angle of plunger [degree]	26.
Diameter of spill port [mm]	3.
Number of spill ports	1.
Diameter of delivery valve [mm]	6.
Mass of delivery valve [g]	3.1374
Mass of delivery valve spring [g]	3.2246
Delivery valve spring constant [N/mm]	6.65
Maximum displacement of delivery valve [mm]	No limit
Delivery valve spring preload [N]	40.54
Delivery valve opening pressure [bar]	14.34
Half of delivery valve seat angle [degree]	45.
Retraction volume of delivery valve [mm^3]	50.
Volume of pumping chamber [mm^3]	585.
Volume of delivery chamber [mm^3]	1850.
Fuel pressure in feeding chamber [bar]	1.

Table 3.1. Specific Data for Injection Pump

Diameter of injector needle [mm]	6.
Diameter of nozzle seat at inlet section [mm]	3.5
Diameter of nozzle seat at exit section [mm]	1.75
Diameter of injector orifice [mm]	0.32
Mass of injector needle [g]	9.027
Mass of injector needle rod [g]	11.067
Mass of injector spring [g]	22.388
Half of injector needle tip angle	$30°10'$
Half of injector nozzle seat angle	$30°$
Injector spring constant [N/mm]	200.
Injector spring preload [N]	317.
Injector openning pressure [bar]	170.
Damping coefficient acting on injector needle [kg/s]	40.
Maximum displacement of injector needle [mm]	0.35
Number of injector orifices	4
Volume of injector chamber [mm^3]	600.
Volume of bag chamber [mm^3]	4.

Table 3.2. Specific Data for Injector

Length of injection pipe [mm]	950.
Internal diameter of injection pipe [mm]	2.

Table 3.3. Specific Data for Injection Pipe

Fuel modulus of elasticity [bar]	14400.
Fuel density [kg/m^3]	820.
Fuel viscosity at 37.8°C [mm^2/s]	2.8

Table 3.4. Specific Data for SAE Calibration Fluid

3.5.2. Computing Flow Chart

The program for the fuel injection system simulation is compiled by using the mathematical model derived in sections 3.3 and 3.4 for application of the four-step Runge Kutta approximation.

The computing flow chart is shown in figure 3.10. In the flow chart, the following variables are used:

T : Instant time

ΔT : Time step

TP : Print time

ΔT : Print time step

T_{max} : Maximum time of calculation

EV : Empty volume

The other variables are given in the nomenclature.

The flow chart consists of two phases:

In the first phase, the data for each component of the fuel injection system, as well as the constants which are valid for the duration of the whole calculation, are calculated first.

The second phase is divided into two main branches by introducing the IF statement, $(F_{dv} h_{dv} \leq EV)$. When the displacement h_{dv} of delivery valve creating a volume, $F_{dv} h_{dv}$ during the pumping process is less than the empty volume EV, the pressure p_d in the delivery chamber is not generated, and remains as initial value. Thus, one needs to calculate only the variations of the pumping pressure p_p, displacement h_{dv} and velocity v_{dv} of the delivery valve,
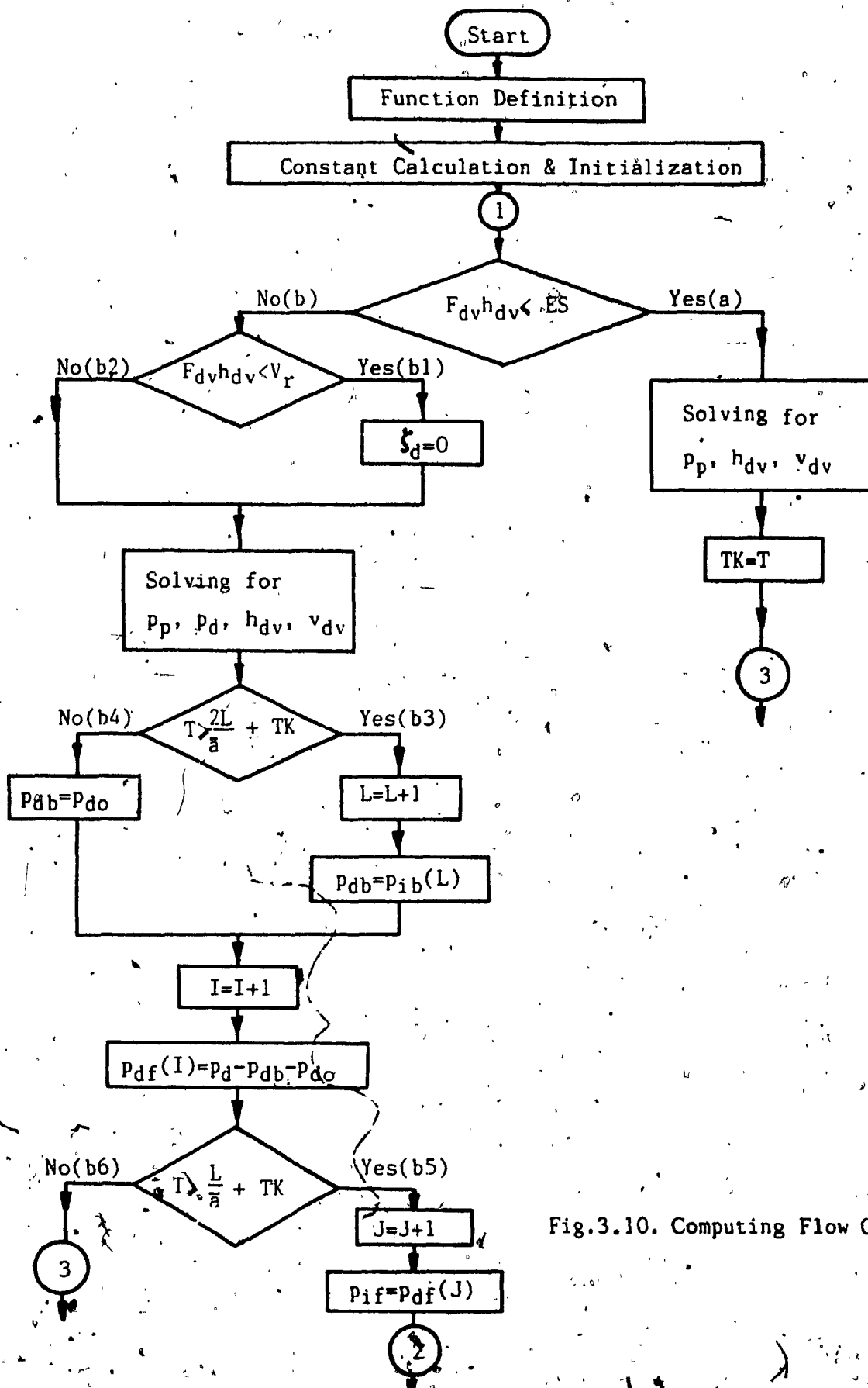
Fig.3.10. Computing Flow Chart.
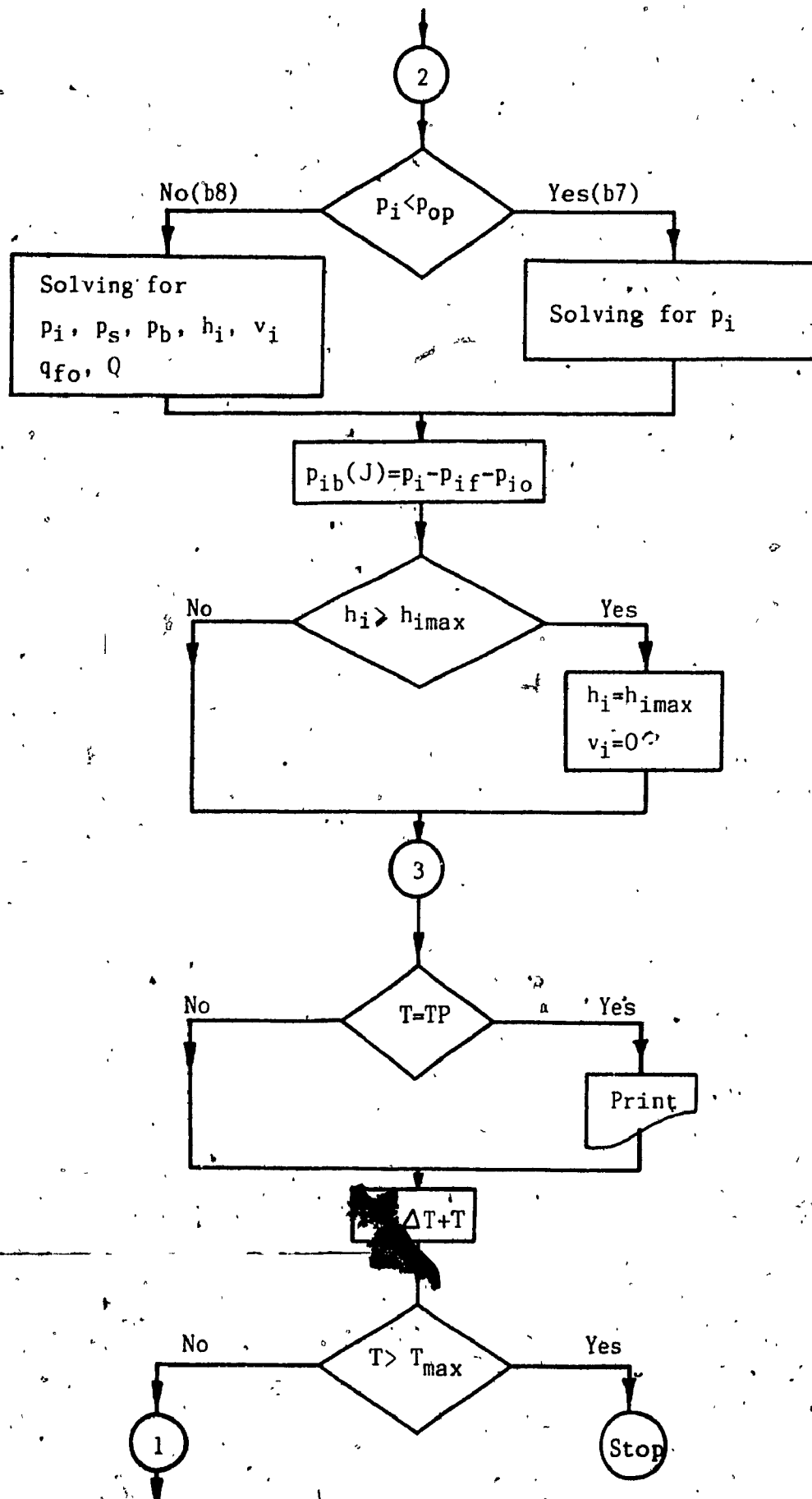
Fig.3.10.(Cont'd) Computing Flow Chart

as shown in branch (a) of figure 3.10.

Once the volume $F_{dv}h_{dv}$ is greater than the empty volume, computing will be performed in the branch (b). In the branch (b), if the volume $F_{dv}h_{dv}$ is less than the retraction volume V_r, the delivery valve is still closed but the fuel in the delivery chamber starts to be compressed. Then, the equations (3.24), (3.36), (3.37), and (3.38) are solved simultaneously for p_p, p_d, h_{dv}, v_{dv} but with $\varsigma_d = 0$ because there is no fuel flowing into the delivery chamber, as shown in the sub-branch (b1). If the volume $F_{dv}h_{dv}$ created by the delivery valve movement is greater than the retraction volume, the delivery valve is opened, and therefore $\varsigma_d \neq 0$, as shown in the sub-branch (b2).

At each step of calculation the values of the forward propagating pressure wave p_{df} at the pump are stored in the computer memories by introducing the statement, $(p_{df}(I)=p_d-p_{db}-p_{do})$, in the computing flow chart. Also, in the branch (b) the IF statement, $(T \geq \frac{2L}{a}+TK)$, is used to determine the values of the backward propagating pressure wave at the pump. At any instant $T < \frac{2L}{a}+TK$, the backward propagating pressure wave does not yet come to the pump. Therefore, the value of the backward propagating pressure wave p_{db} at any instant $T < \frac{2L}{a}+TK$ is equal to the residual pressure p_{do}. In contrast, at time $T > \frac{2L}{a}+TK$ the values of the backward propagating pressure wave are no longer equal to the residual pressure, as indicated in the sub-branch (b3).

In the sub-branch (b5), the variations of the pressures generated in the injector chamber, in the seat chamber, and in the bag chamber are calculated separately by the statement, $(p_i < p_{op})$, where p_{op} is the nozzle opening pressure, because as long as the injector nozzle remains closed, i.e. $p_i < p_{op}$, the pressures in the seat chamber p_s and in the bag chamber p_b are still constant and equal to the atmospheric pressure.

Once the amplitude values of the backward propagating pressure wave p_{ib} have been found, they should be stored in the computer memories for later use by using the equation $p_{ib}(J) = p_i - p_{if} - p_{io}$.

The computer program is written in Fortran language and is given in appendix F.

3.5.4. Transient Response of the Fuel Injection System

As the results of simulation, the transient response of the fuel injection system is shown in the following figures:

Figure 3.11 shows the pressure p_d in the delivery chamber versus time. At the injector side, figures 3.12, 3.13, and 3.14 are the plots of pressures versus time in the injector chamber, seat chamber, and bag chamber, respectively. Also, the injector needle displacement, the fuel flow rate through the orifices and injected fuel dose are presented in figures 3.15, 3.16 and 3.17, respectively.

Several tests have been conducted on a test bench to measure the pressures in the delivery chamber and in the injector chamber, as well as the injector needle lift. The results of experiments are shown together with the calculated results in figures 3.11, 3.12, and 3.15. The comparison of the results is showing that the calculated results are complying with those of the experiments.
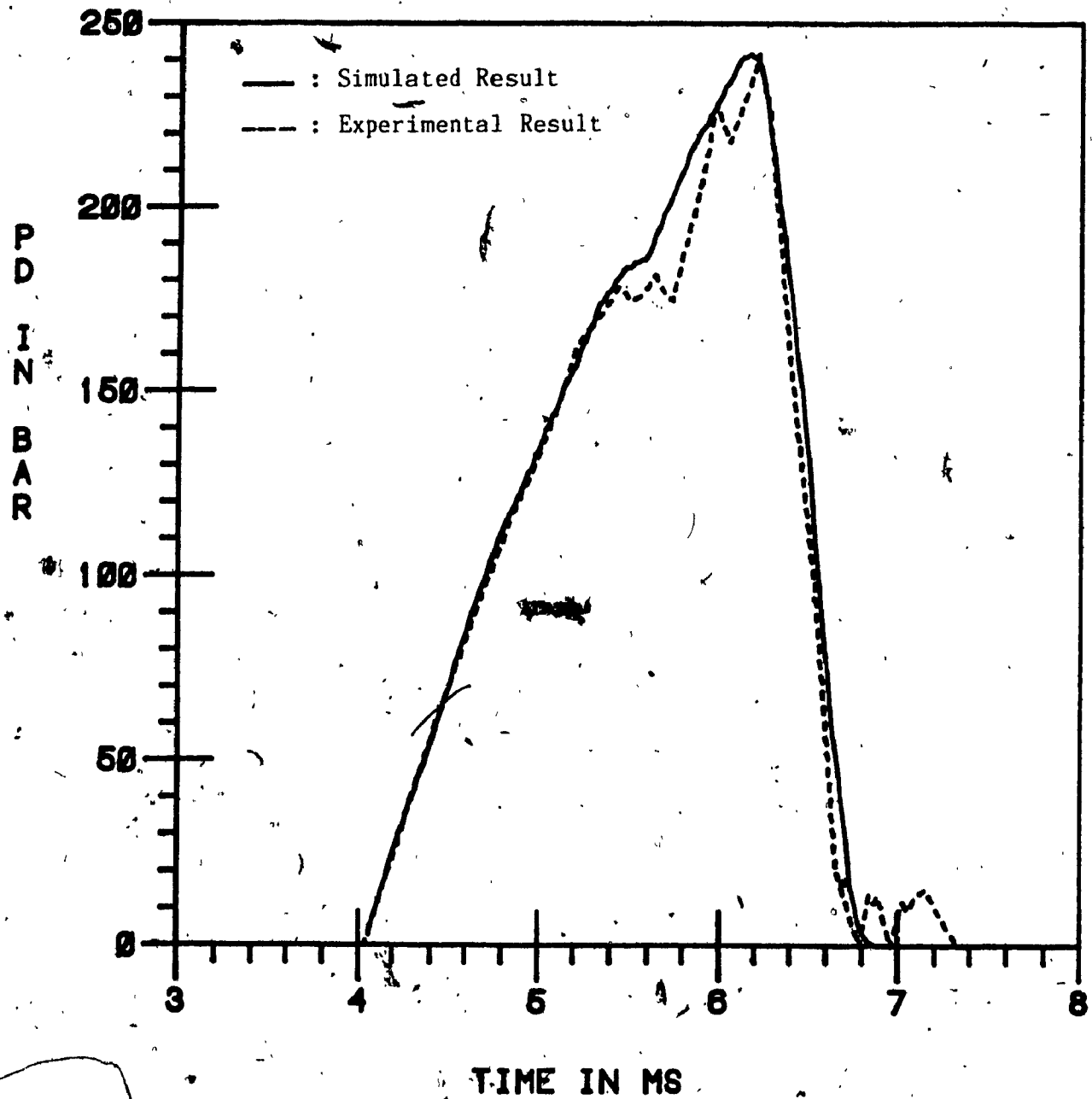
Fig.3.11. Pressure in Delivery Chamber p_d versus Time
at Pump Speed of 1000 RPM
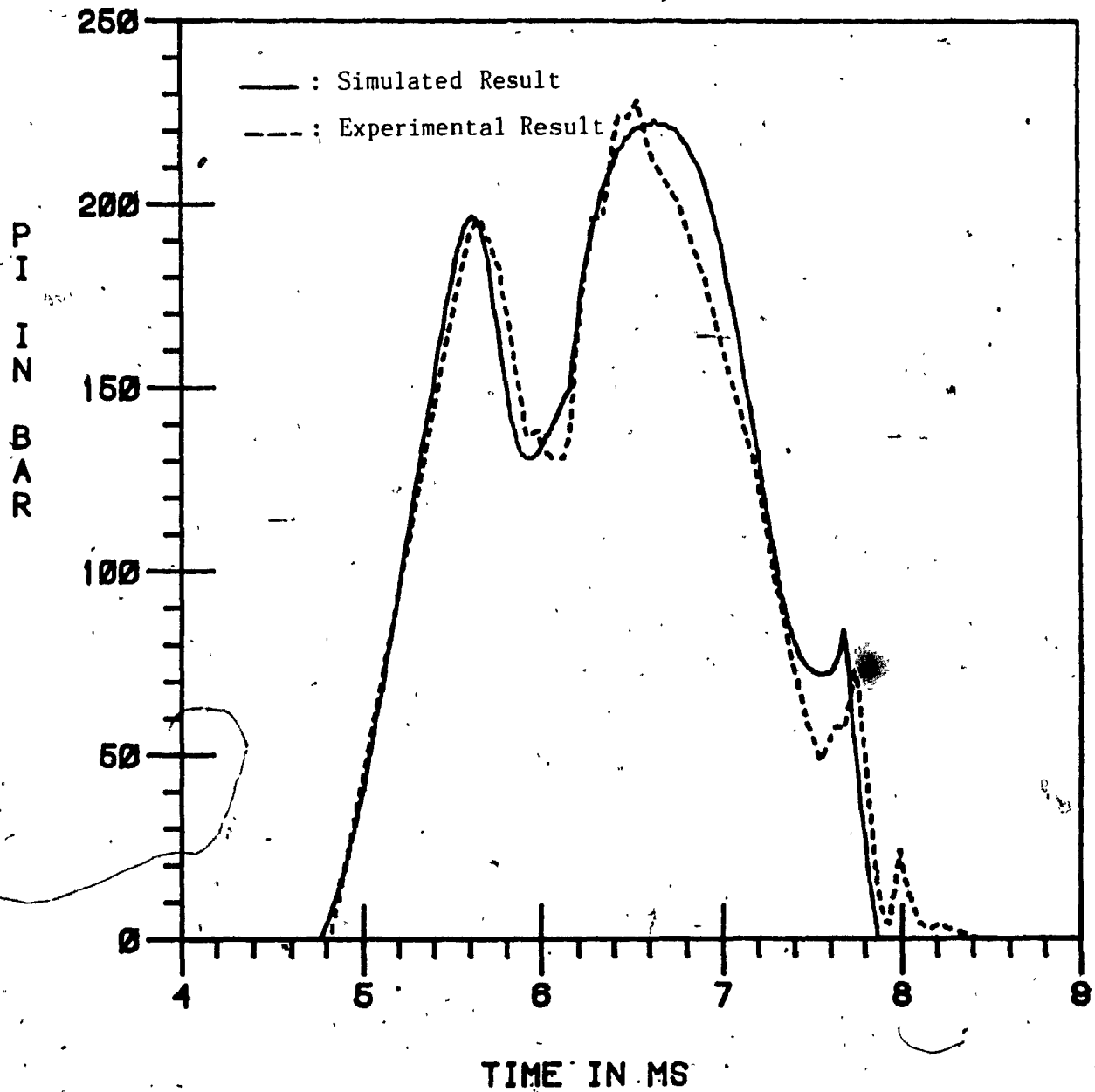
Fig.3.12. Pressure in Injector Chamber p_i versus Time at Pump Speed of 1000 RPM
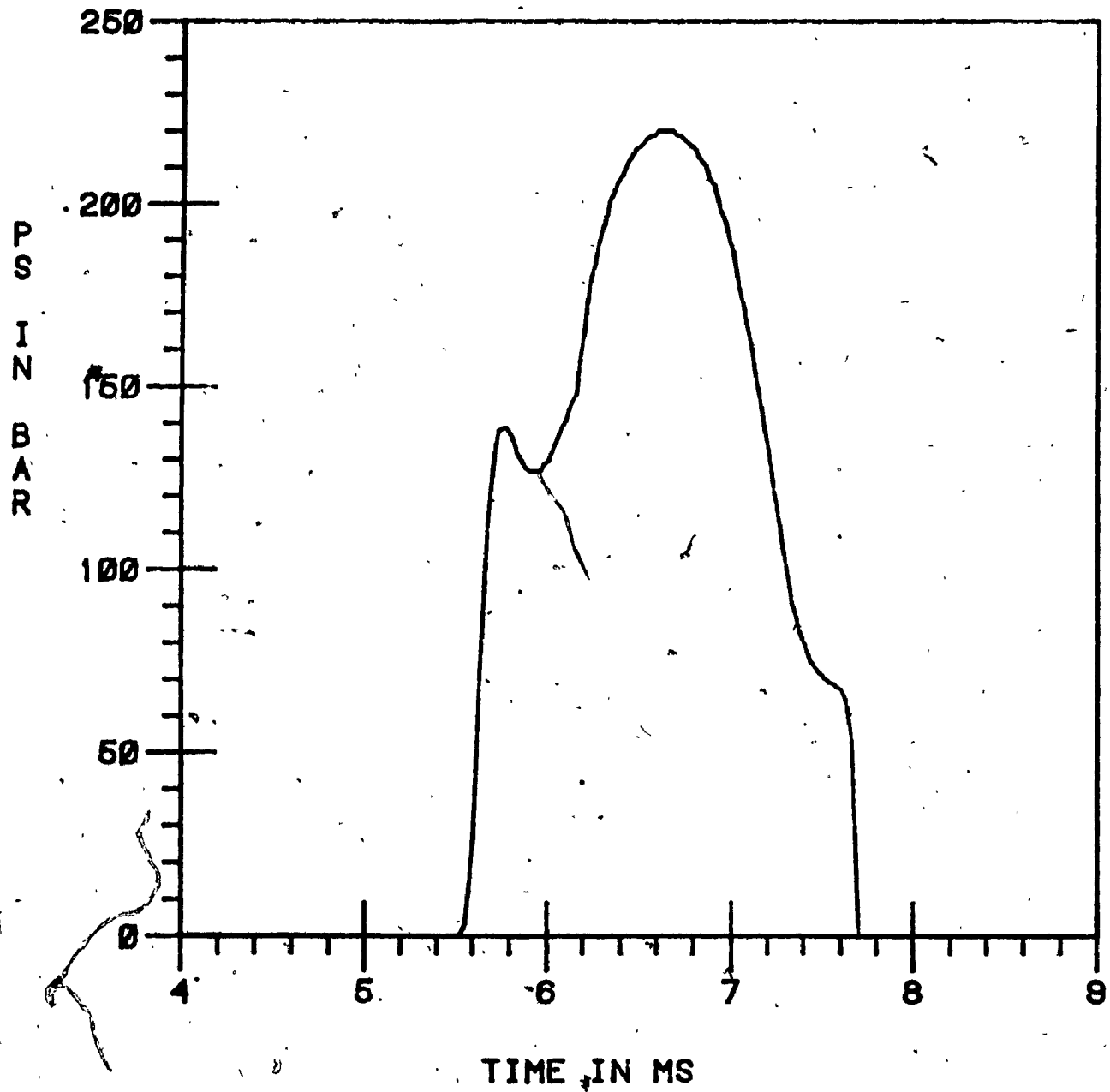
Fig.3.13. Pressure in Nozzle Seat Chamber p_s versus Time
at Pump Speed of 1000 RPM
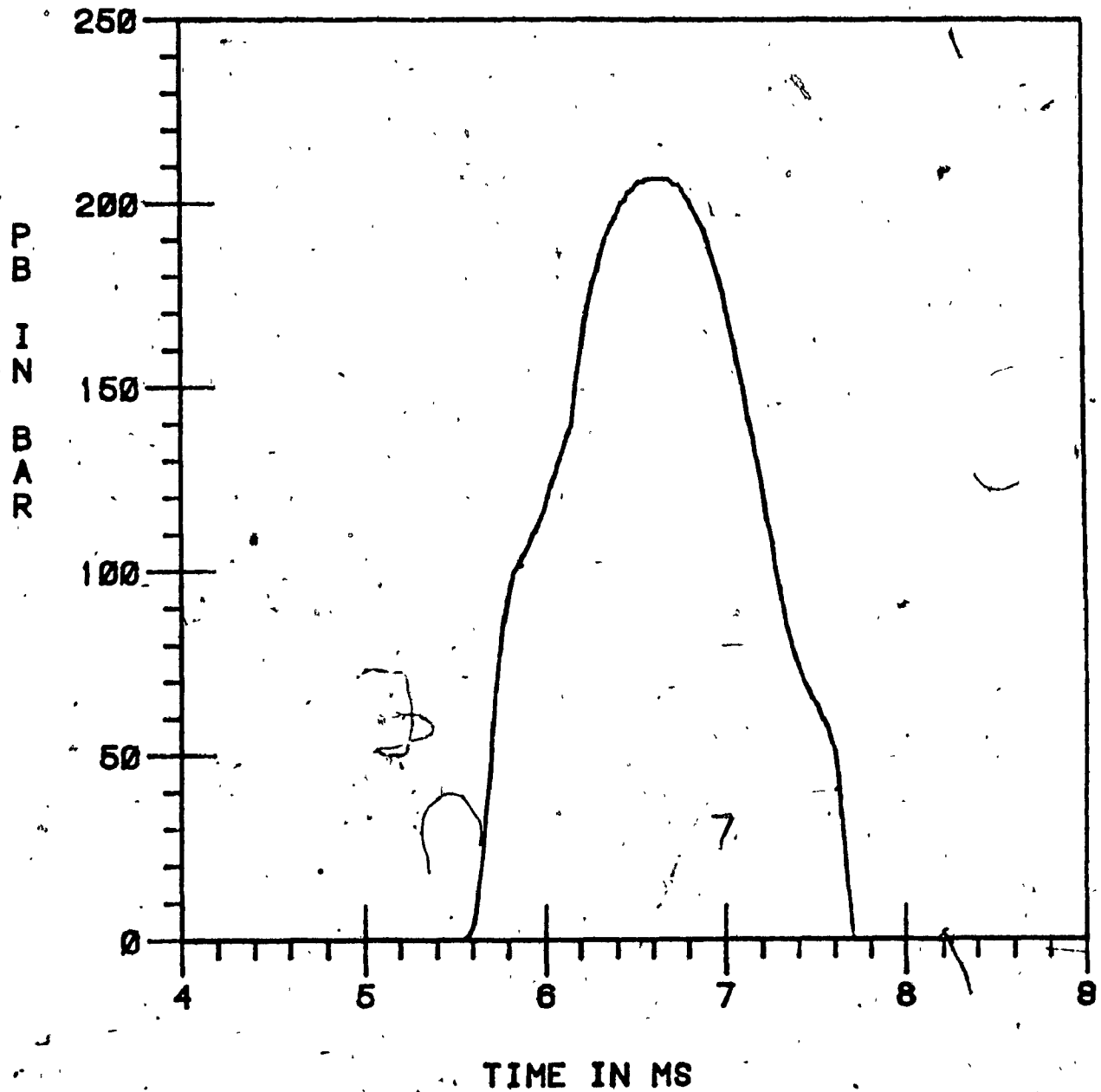
Fig.3.14. Pressure in Bag Chamber p_b versus Time
at Pump S   of 1000 RPM
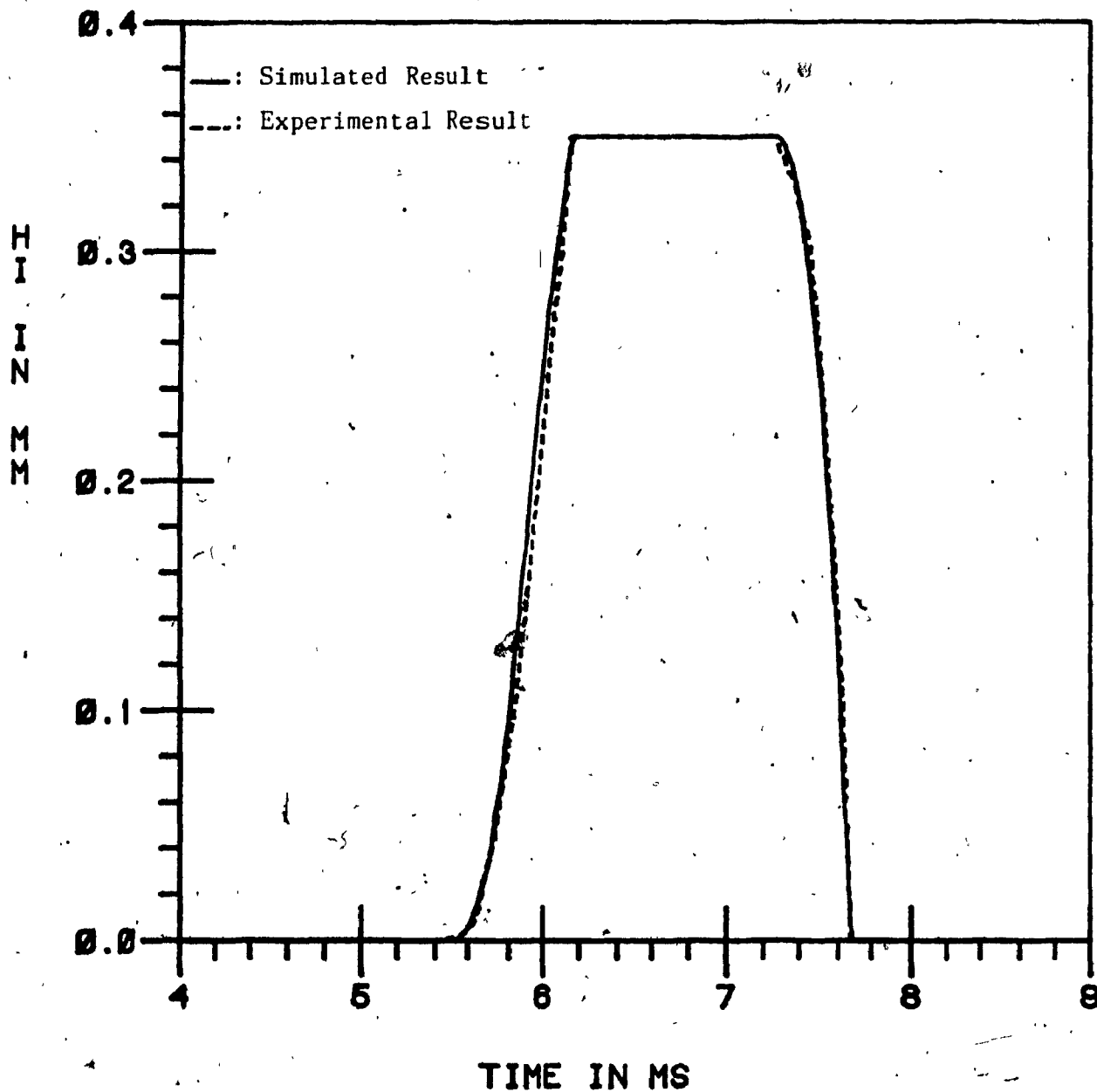
Fig.3.15. Injector Needle Lift h_i versus Time
at Pump Speed of 1000 RPM
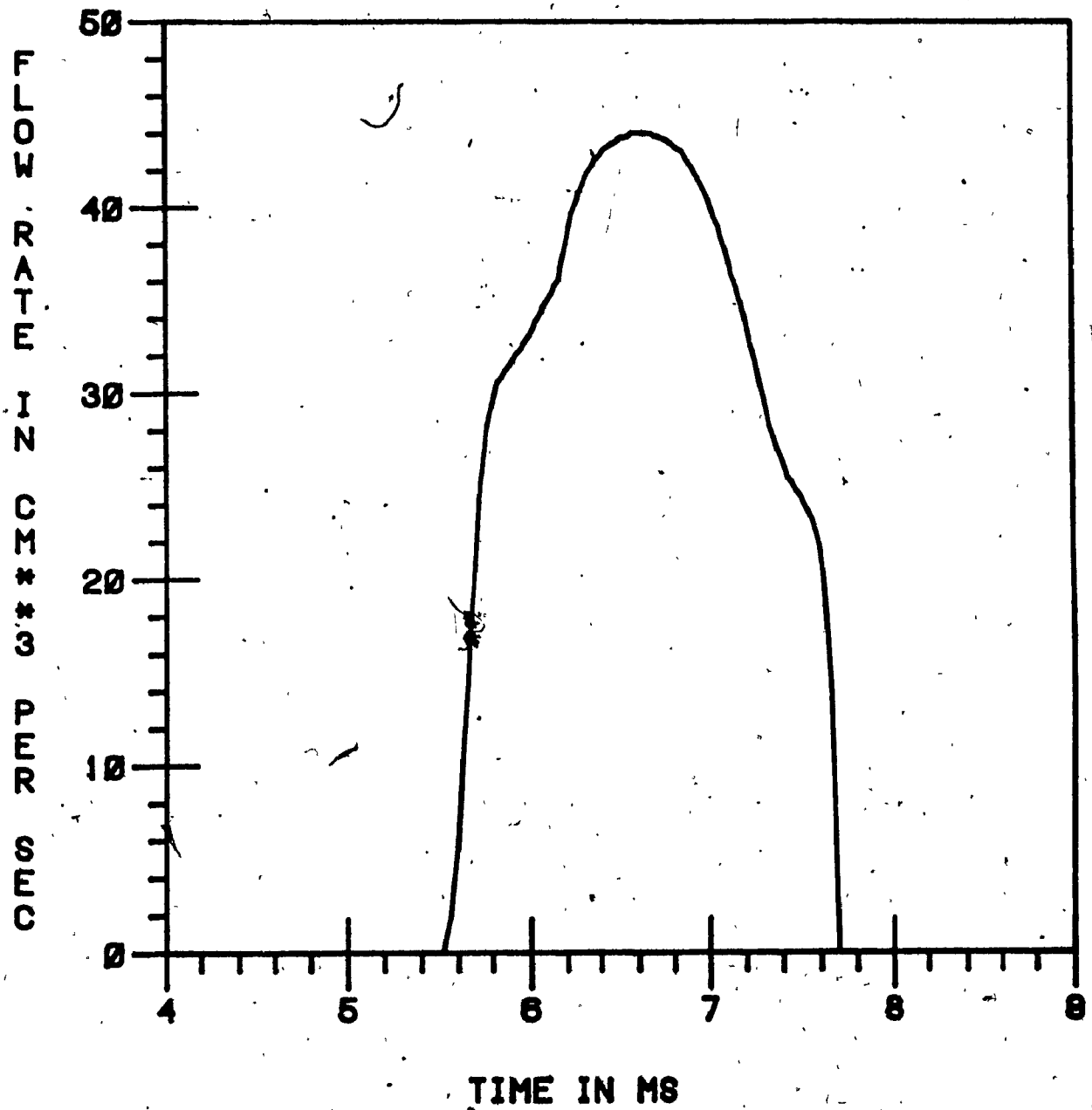
Fig.3.16. Fuel Flow Rate q_{fo} versus Time
at Pump Speed of 1000 RPM
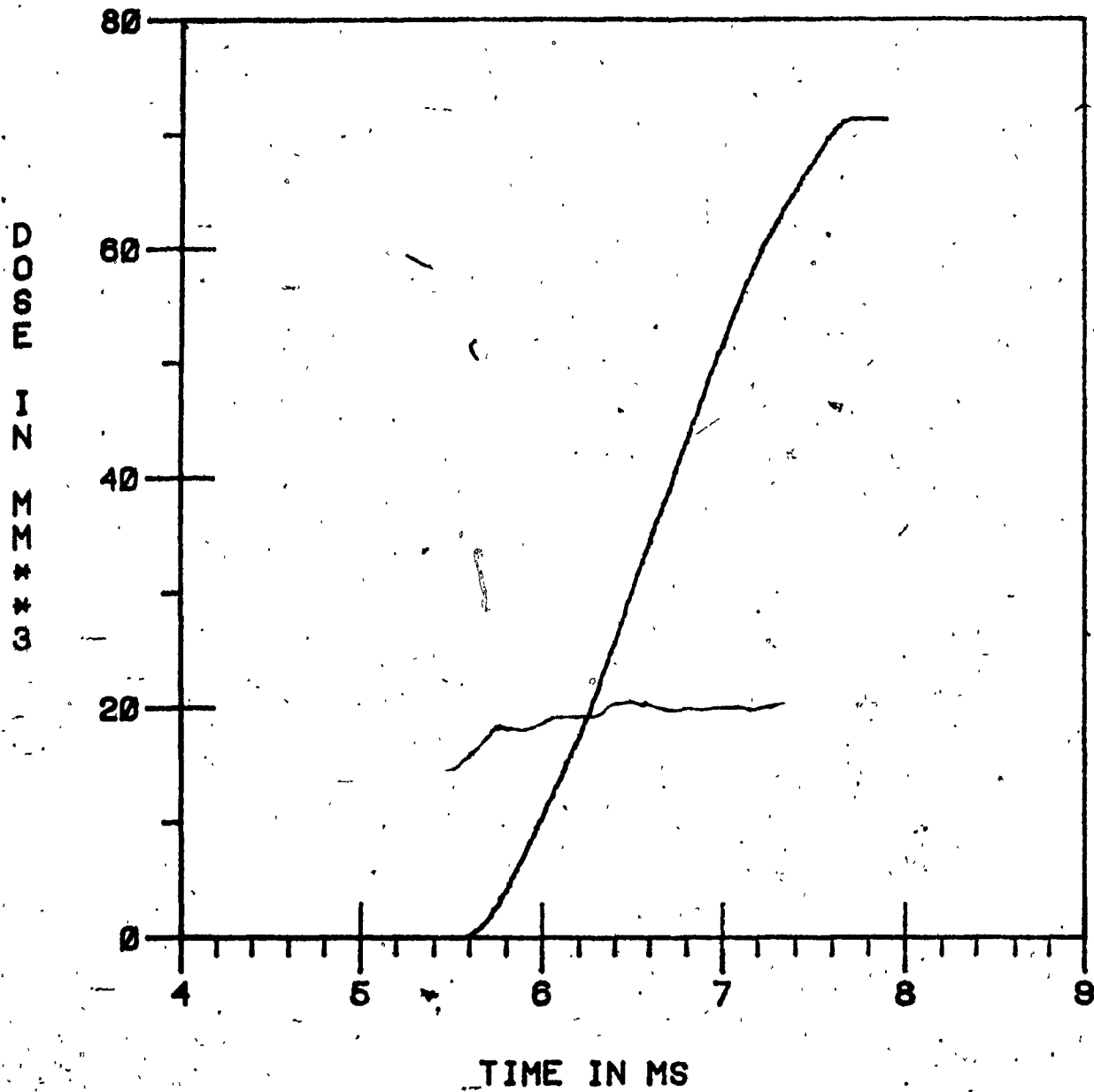
Fig.3.17. Injected Fuel Dose Q versus Time
at Pump Speed of 1000 RPM

3.6. Experimental Investigation

3.6.1. Introduction

The experimental investigation presented in this section has been made to confirm the developed mathematical model and the simulation results. Practically, it is impossible to measure all variables which were calculated. However, if a satisfactory agreement between the calculated and experimental results is achieved for several measured variables, a consensus can be acknowledged.

3.6.2. Test Set-up

A pictorial view of the test set-up of a diesel fuel injection system on the test bench is shown in figure 3.18. The schematic for the experiment is presented in figure 3.19. In this test set-up, a R. Bosch pump of PE6A75B420LS59/1 type with a plunger diameter of 7.5 mm was used. The pump is connected to a CAV injector BKBL67S5299XS type fitted with a hole-type nozzle BDLL150S6502 by an injection pipe of 2 mm internal diameter and the length of 950 mm. The effective stroke of the pump was adjusted for a particular dose of 75 mm^3/stroke corresponding to maximum engine power. This effective stroke was carefully measured by a special device fitted with a dial indicator.

The pump was installed and driven by a variable speed motor of the test bench, and the pump speed was adjusted at 1000 RPM. Fuel from a reservoir was supplied by a feed pump to the injection pump, and the pressure in the feeding chamber was kept at a constant value of 1 bar approximately. The fuel delivered by the injection pump was
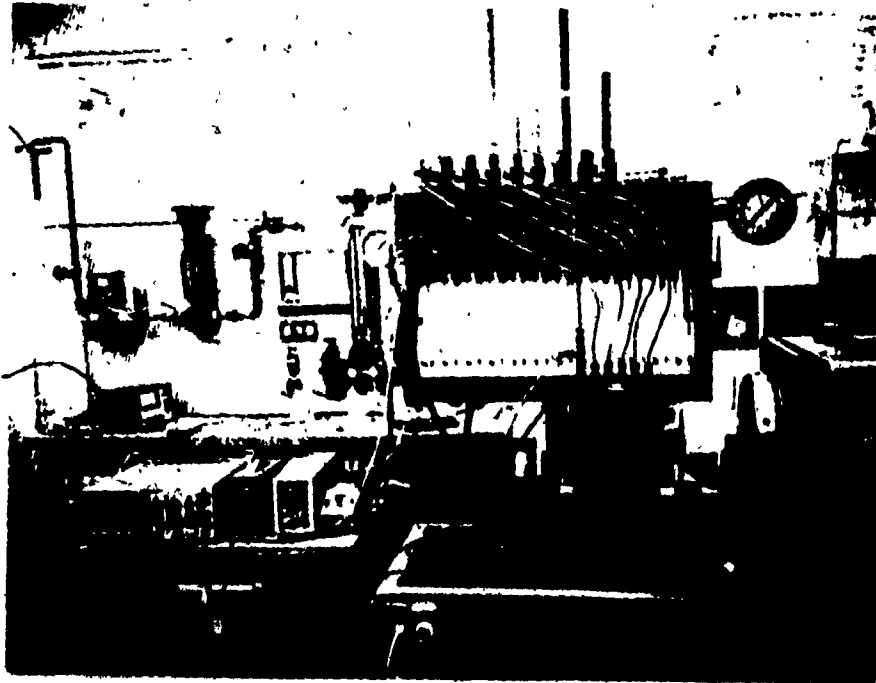
Fig.3.18, Pictorial View of the Test Set-up
on the Test Bench
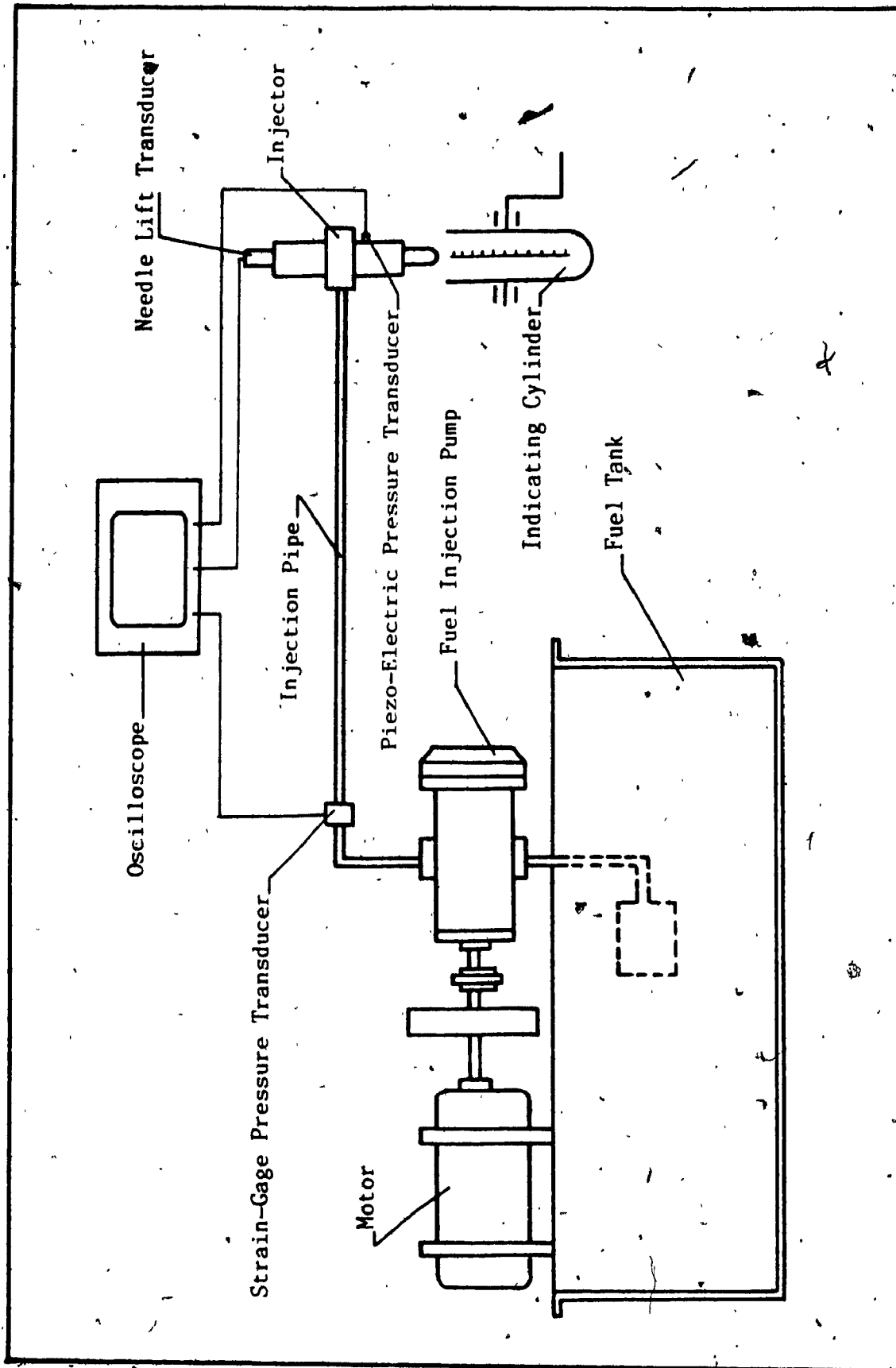
Fig. 3.19. Schematic of the Test Set-up

brought through the injection pipe to the injector where it was discharged to a measuring cylinder. To record the pressures in the pump delivery chamber and in the injector chamber, a strain-gage pressure transducer and a piezo-electric pressure transducer were used, respectively. These transducers were located as shown in figure 3.19. Another AVL nozzle needle lift transducer (LVDT) was installed in the injector holder to record the injector needle lift. The output from these transducers was displayed on a Tektronix dual beams oscilloscope. A polaroid camera was used to photograph the pressure and needle lift histories.

3.6.3. Experimental Results

The pressures recorded in the delivery chamber of the fuel injection pump and in the injector chamber as well as the injector needle lift are presented in figure 3.20. In figure 3.20.a, the pressure in the pump is shown. In figure 3.20.b, the upper line is the pressure in the injector chamber and the lower one is the injector needle lift.

The experimental data obtained were reproduced in the same scale as for simulation results, and they were placed in the same graph for comparison purposes, as seen in figures 3.11, 3.12 and 3.15.

Analysis of those graphs shows that a satisfactory agreement between the calculated and experimental results was obtained. It can be then concluded that the developed mathematical model for the injection system of a diesel engine could be used to predict the performance of the fuel injection system.
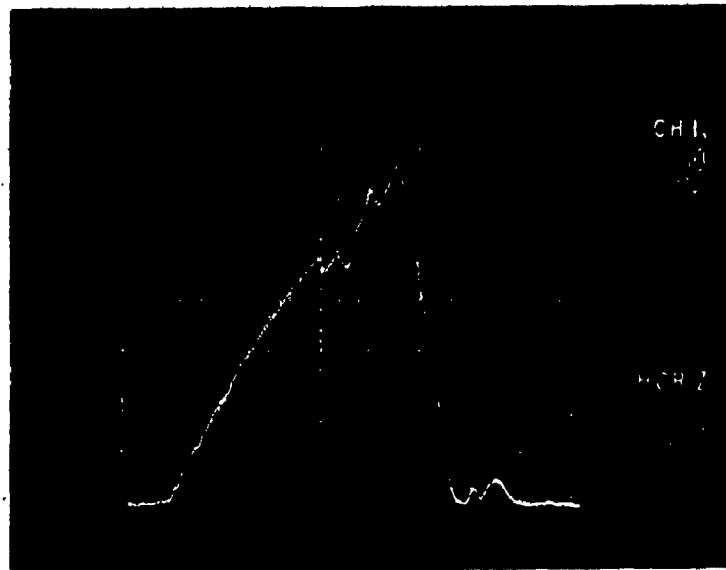
Fig.3.20.a. Pressure in Delivery Chamber

Injector
Pressure
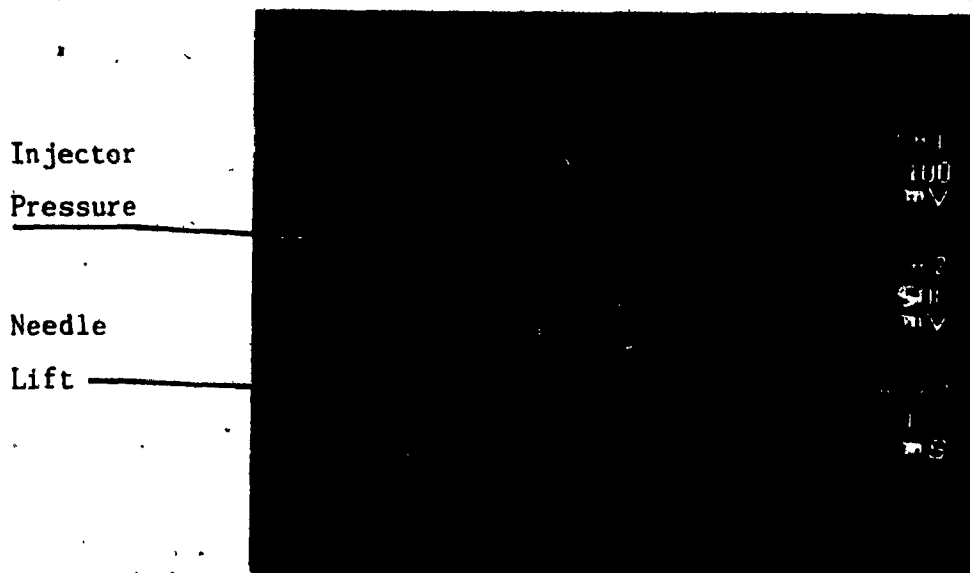
Needle
Lift

Fig.3.20.b. Pressure in Injector Chamber
and Injector Needle Lift

Fig.3.20. Experimental Results

Chapter 4

SEAT PRESSURE MEASUREMENT

4.1. Introduction

The main aim of this chapter is to introduce a method that can be used to measure the pressure in the nozzle seat chamber of the injector.

Until now, all calculations made by the researchers to determine the fuel discharge rate from the injector have been made with a simplifying assumption that the pressures in the seat and in the bag chambers of the injector nozzle are identical. However, there must be a pressure drop between these two chambers which maintains the fuel flow. This pressure difference should affect substantially the force acting on the needle.

To prove this fact, several experiments have been made which allowed not only to establish the seat chamber pressure but also the flow coefficients for the orifices, seat inlet and exit, as well as the Reynolds numbers for the flow through the seat gap. These values will be used for further calculations of the fuel discharge rate in the next chapters.

Some design problems such as modification of the injector holder to record the pressure and injector needle lift values, test set-up and facilities, as well as experimental results will also be discussed in this chapter.

4.2. Analysis of Fuel Flow Through the Nozzle Seat

The schematic representation of the nozzle seat is given in figure 3.8, where two critical flow areas can be distinguished: one at the outer seat diameter and the other at the inner seat diameter. These flow areas are functions of the injector needle displacement and their formulae are derived in appendix D. The plot of these two flow areas together with injector orifices area versus needle lift is shown in figure 4.1 for the injector with specific data given in table 3.2.

Referring to figure 4.1, at the beginning of the injector needle movement, the seat inlet flow area starts to open throttling the flow into the seat chamber. Since the seat exit flow area is larger than the seat inlet flow area, due to the difference in the angles of both conical surfaces on the needle and in the nozzle body, there is not much restriction of the flow at the inner seat diameter. Therefore, there is not high differential pressure between the seat chamber and the bag chamber of the injector. Due to the relatively larger flow area of the orifices, the pressure in the latter two chambers remains low and close to each other at the beginning of the injection.

When the needle reaches the lift of 0.02 mm approximately, the critical flow area switches from the outer to the inner diameter of the seat. This is causing the pressure in the seat chamber to be built-up faster and to affect positively the acceleration of the needle.

When the needle reaches the lift of 0.11 mm, i.e. one third of maximum needle lift, the critical flow area switches again to the orifices and the pressure under the full needle surface tends to be equal to the injector pressure. The particular effect of the seat
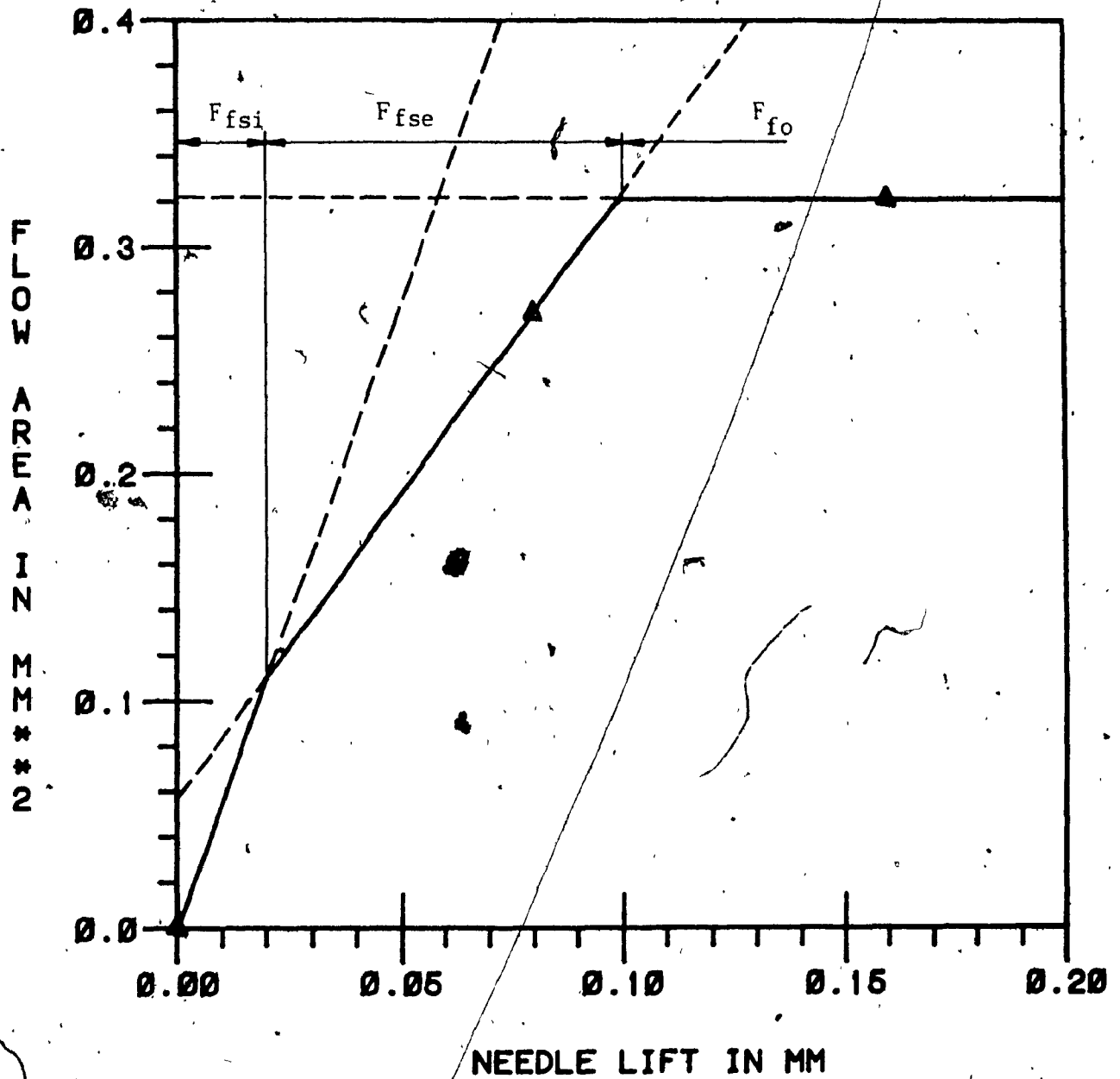
Fig.4.1. Flow Areas at Nozzle Seat Inlet, and Exit Sections
and at Orifices versus Needle Lift

pressure on the needle acceleration, therefore, disappears at higher needle position.

The flow areas of the seat inlet and exit, and of orifices change with the variations of the nozzle design parameters. Figures 4.2, 4.3, 4.4, and 4.5 are the plots of the seat inlet and exit, and orifices flow areas versus the injector needle lift for different values of conical surfaces differential angle γ, orifice diameter D_o, outer seat diameter D_{so}, and inner seat diameter D_{si}, respectively.

Two predictions could be made from this analysis:

1. In case if the differential angle between both conical surfaces of the seat would approach zero, the critical flow area through the inner seat circumference would also be zero when the needle is on its seat. Then the pressure in the seat would start to be built-up much earlier resulting in faster acceleration of the needle.

2. The space in the seat between seat inlet and exit areas could be considered as a chamber. Then, knowing the flow areas and assuming the correct flow coefficients, it would be possible to calculate the seat pressure for particular injector pressures and needle lifts.
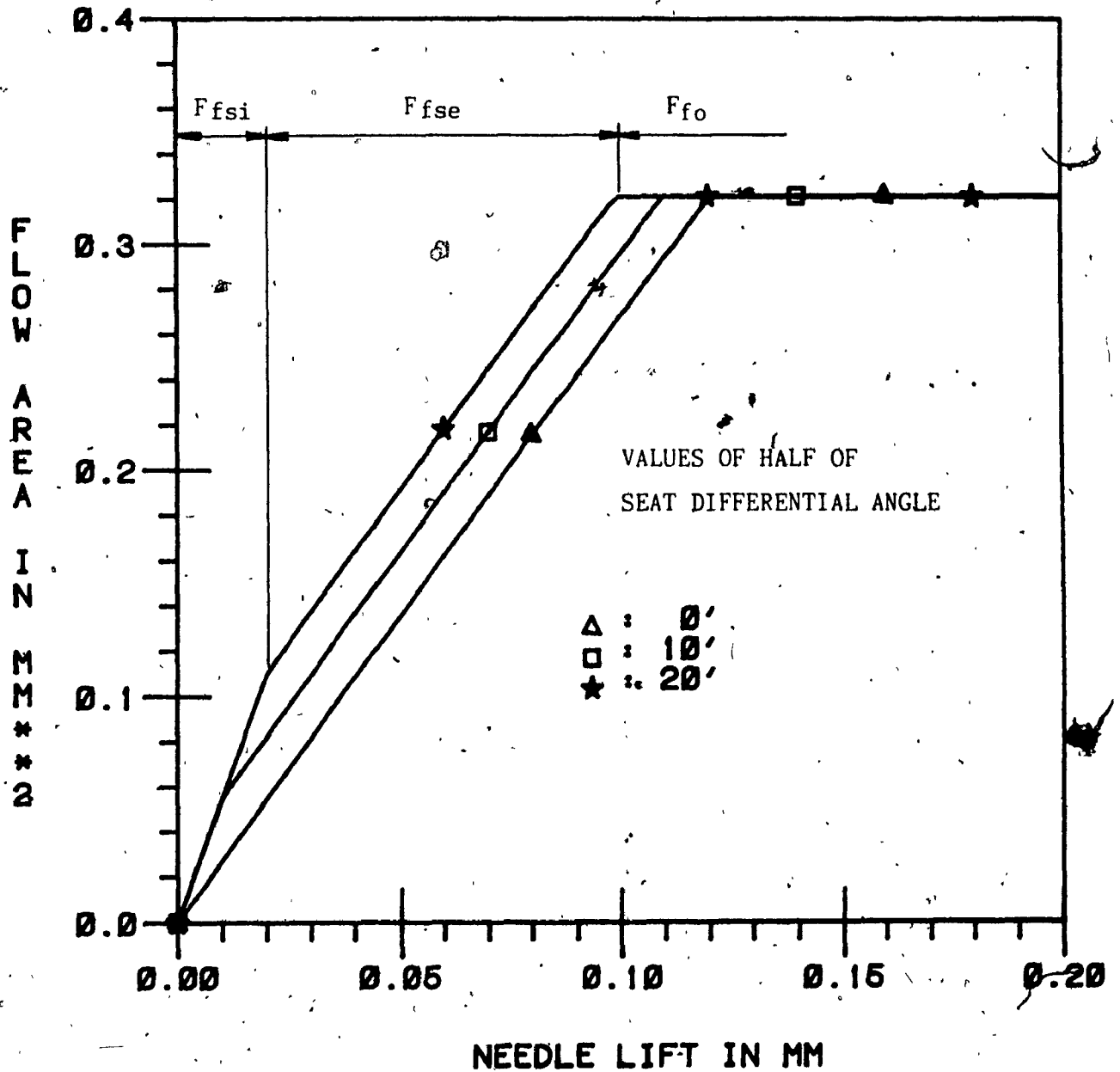
Fig.4.2. Flow Areas at Nozzle Seat Inlet, and Exit Section
and at Orifices versus Needle Lift for different
Values of Seat Differential Angle
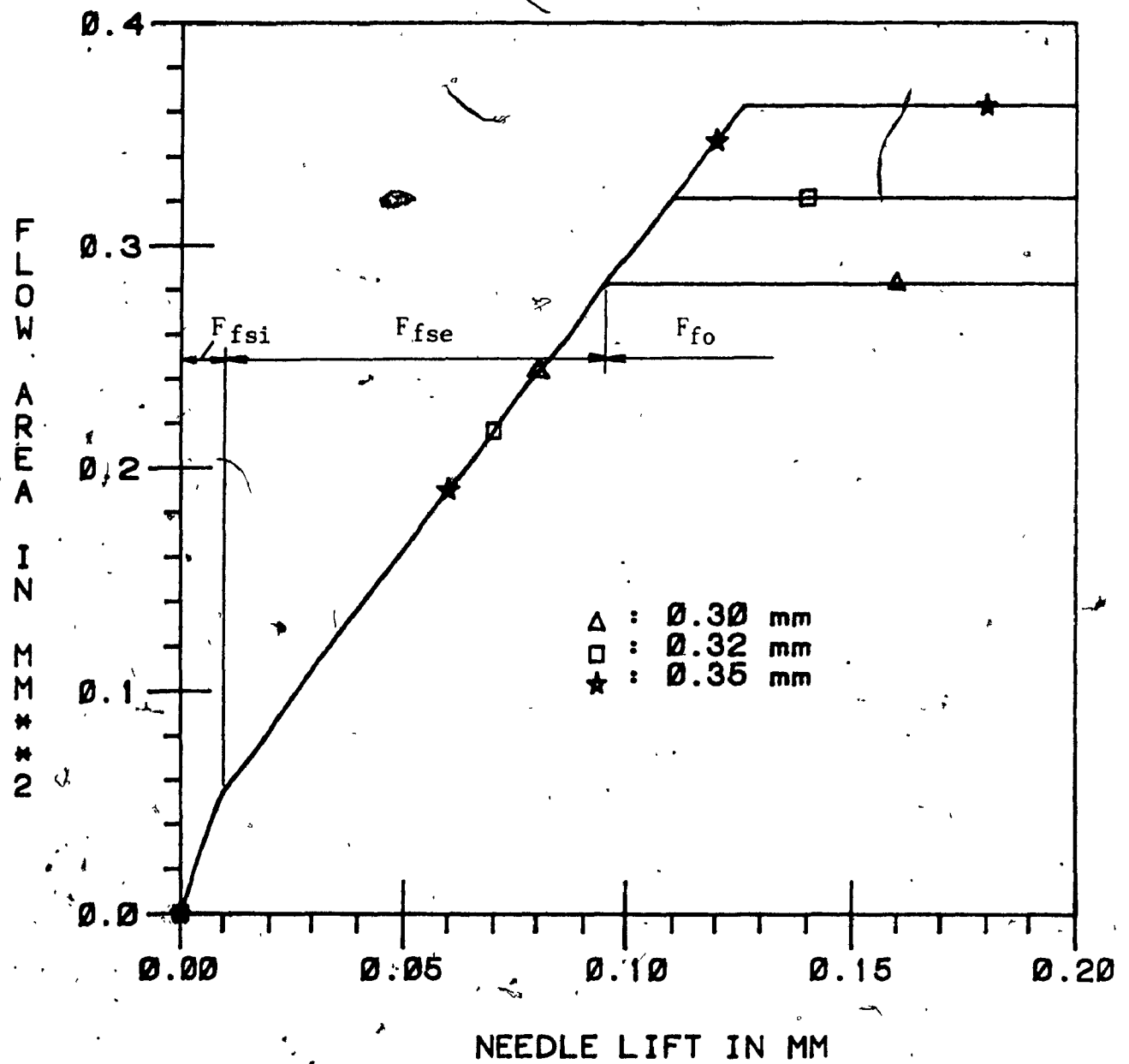
Fig.4.3. Flow Areas at Nozzle Seat Inlet, and Exit Sections and at Orifices versus Needle Lift for different Values of Orifices Diameter
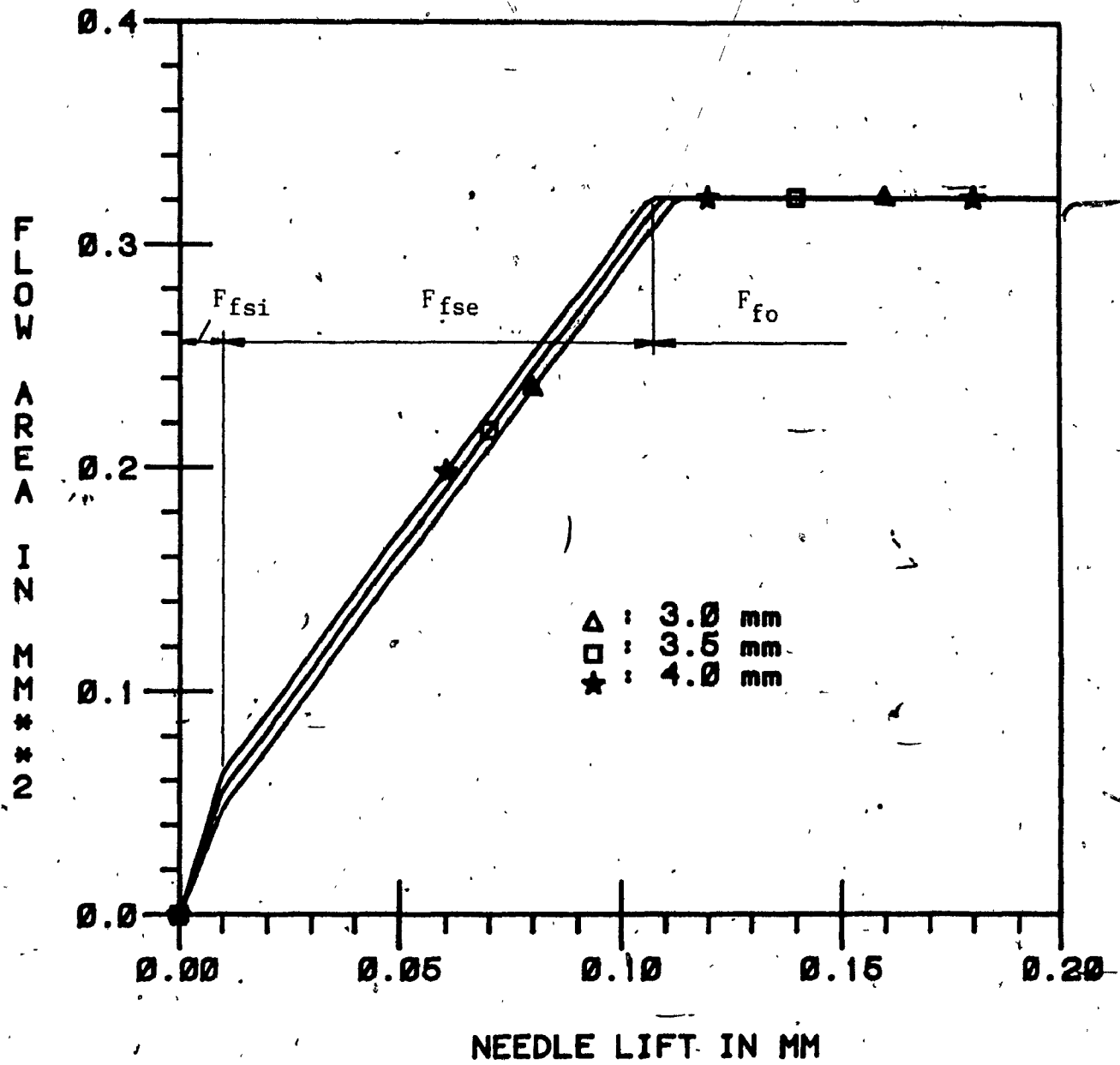
Fig.4.4. Flow Areas at Nozzle Seat Inlet, and Exit Sections
and at Orifices versus Needle Lift for different
Values of Seat Outer Diameter
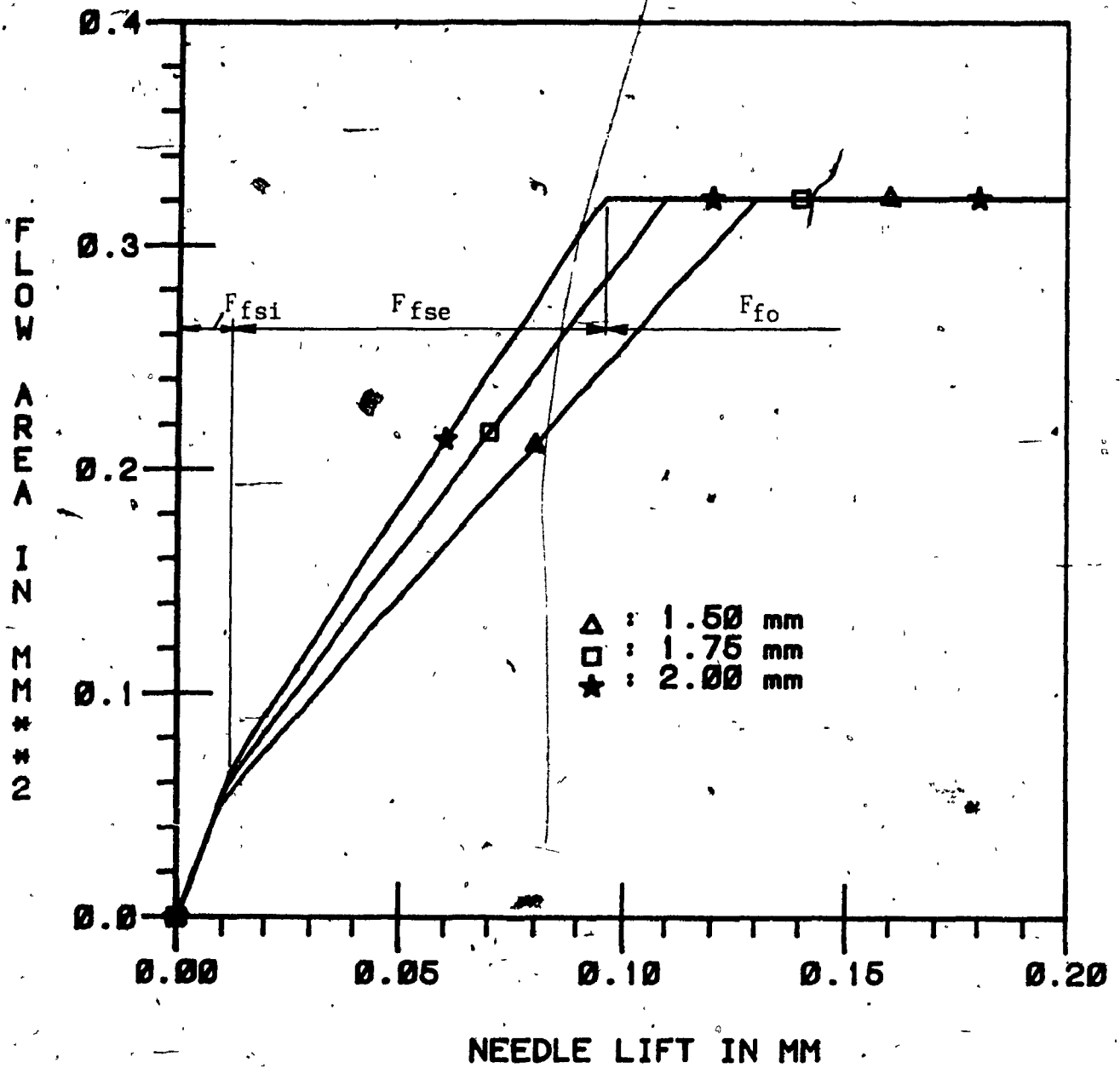
Fig.4.5. Flow Areas at Nozzle Seat Inlet, and Exit Sections
and at Orifices versus Needle Lift for different
Values of Seat Inner Diameter

4.3. Methodology for Evaluation of Seat Flow Conditions

4.3.1. Pressure in the Seat Chamber

The model of the force system acting on the injector needle can be described as shown in figure 4.6.

The motion equation for the injector needle is then written as:

$$m_i \frac{dv_i}{dt} + \delta_i v_i + k_{is} h_i + P_{is} \pm R_i = p_i (F_i - F_{so}) + p_s (F_{so} - F_{sl}) + p_b (F_{sl}) \tag{4.1}$$

To find the seat pressure from that equation, the force terms on the left side of equation (4.1) should be measured during a transient process what would be difficult. Therefore, the seat pressure in this investigation will be established at steady flow conditions. Then, the total force of the terms on the right side of equation (4.1) can be measured using a force transducer. This means that the dynamic motion equation for the injector needle is replaced by a static equilibrium equation. To produce such configuration, the injector holder should be redesigned to make the injector needle stationary at a desired distance from the nozzle seat. Then, the first two terms on the left side of equation (4.1) become zero, and the mechanical friction R_i is also ignored. To eliminate the spring force $(P_{is} + k_{is} h_i)$, the spring can be replaced by a cylindrical spacer. There are two reasons in using a cylindrical spacer instead of a spring. First, the injector needle does not tend to move. Second, the maximum lift of the injector can be adjusted for any desired value, and between the spacer and the injector needle a force transducer can be installed to
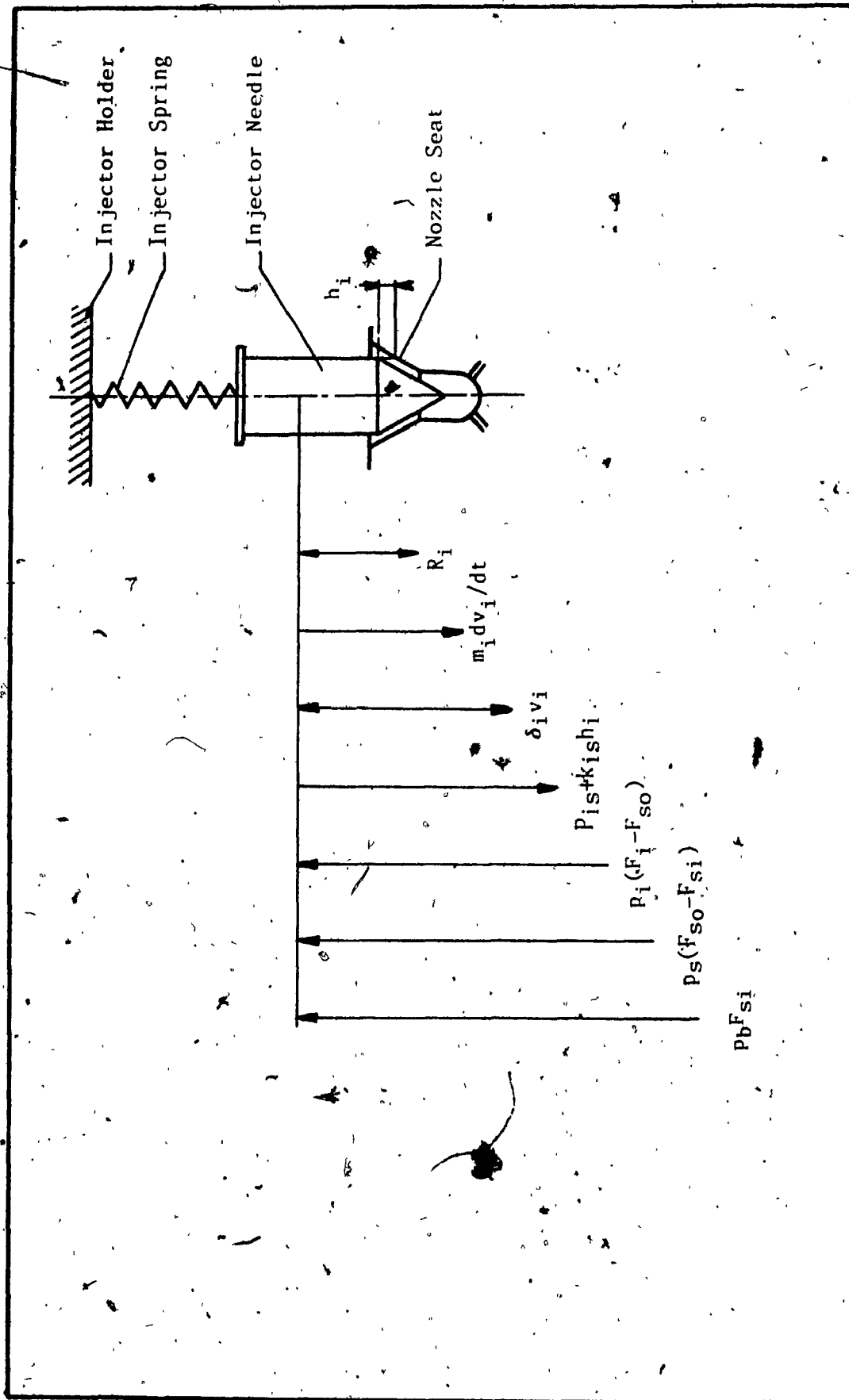
Fig. 4.6. Force System Acting on Injector Needle

record the net static force acting on the needle.

The schematic of this modification is shown in figure 4.7, and the detailed drawing of redesigned injector holder is given in figure 4.8.

Referring to figure 4.7, one can see that there are only pressure forces acting on the injector needle which are balanced by the load cell. These pressure forces come from the injector chamber, seat chamber, and bag chamber. If P is denoted for the summation of these forces, then,

$$P = p_i(F_i - F_{so}) + p_s(F_{so} - F_{si}) + p_b(F_{si}) \qquad (4.2)$$

If the total force P, the injector pressure p_i, and the bag pressure p_b can be measured, the seat pressure can be determined from equation:

$$P_s = \frac{P - p_i(F_i - F_{so}) - p_b(F_{si})}{F_{so} - F_{si}} \qquad (4.3)$$

There is no problem in measuring the total force P and the injector pressure p_i. However, the bag pressure is difficult to measure because of the bag chamber configuration and its small dimensions. An indirect method of measuring the bag pressure is, therefore, proposed. There is a relationship between the flow rate of fuel discharged from the injector orifices and the bag pressure:

$$q_{fo} = I\mu_o F_{fo}\sqrt{\frac{2}{\rho}(p_b - p_a)} \qquad (4.4)$$
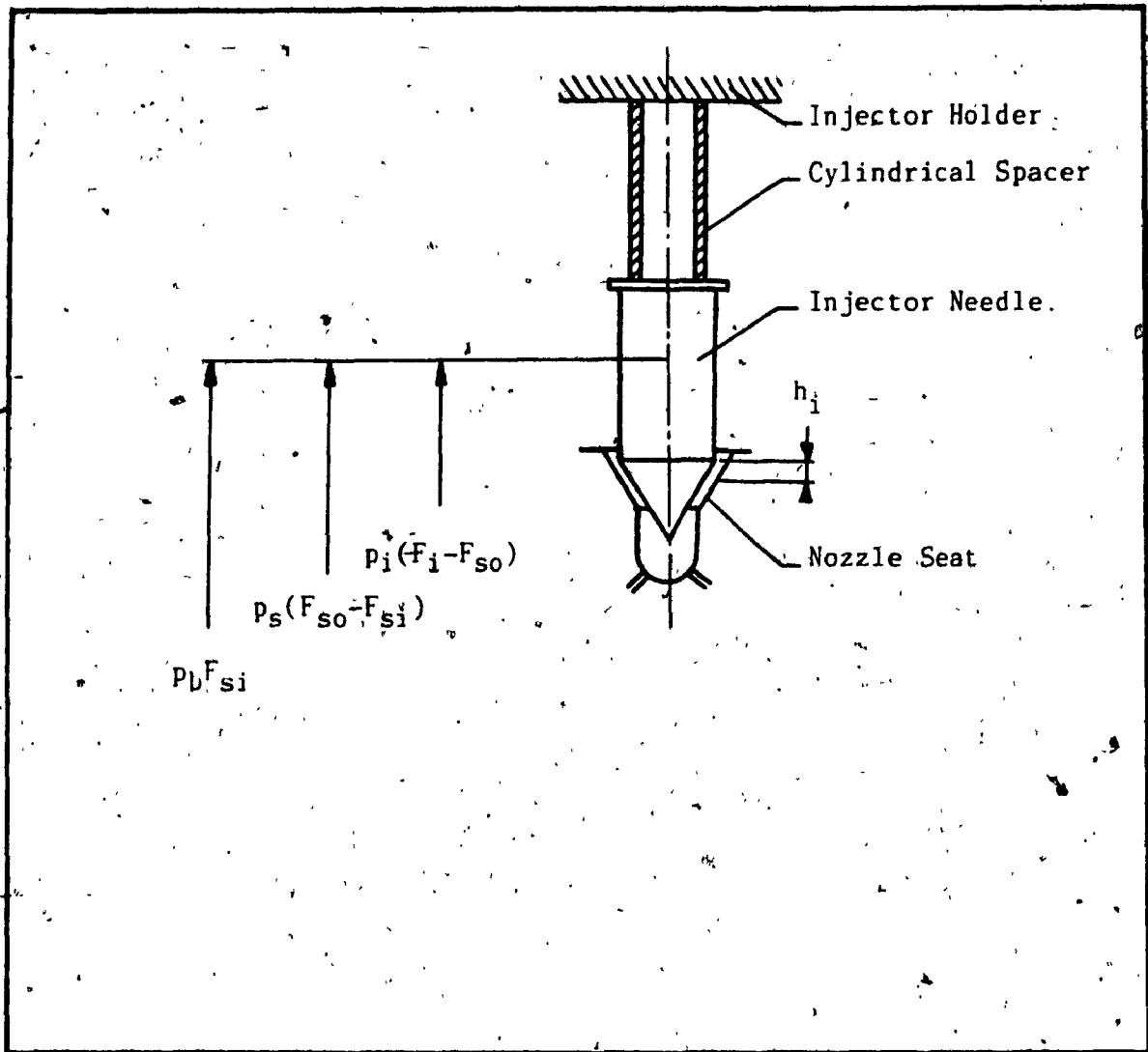
Fig.4.7. Force System Acting on the Needle of Modified Injector

1. Lift Transducer
2. Retainer
3. Cylindrical Spacer
4. Force Transducer
5. Injector Holder
6. Needle Rod
7. Injector Needle
8. Injector Nozzle
9. Pressure Transducer
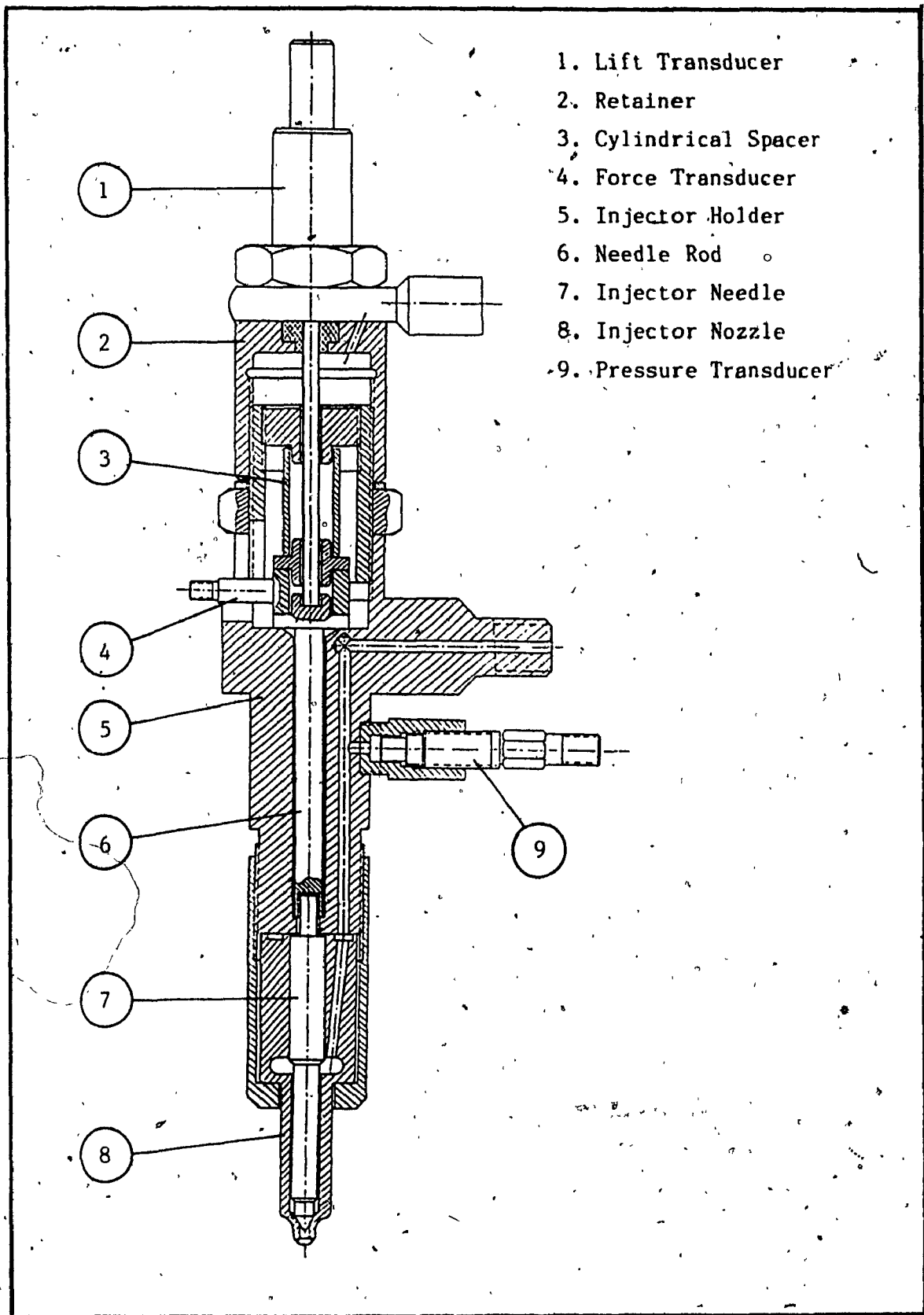
Fig.4.8. Drawing of Modified Injector Holder

If the fuel flow rate is known, the bag pressure can be determined from formula:

$$p_b = \frac{\rho}{2}\left(\frac{q_{fo}}{I\mu_o F_{fo}}\right)^2 + p_a \qquad (4.5)$$
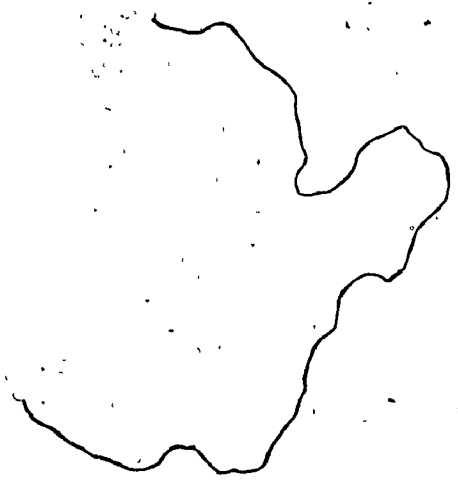
4.3.2. Flow Coefficients in the Seat Chamber
of Injector Nozzle

Assuming that the flow through the injector is at steady-state conditions, three flow restrictions can be established with the flow areas as follows:

a. Flow through Seat Inlet Area:

$$q_{fsi} = \mu_{si} F_{fsi} \sqrt{\frac{2}{\rho}(P_i - P_s)} \qquad (4.6)$$

b. Flow through Seat Exit Area:

$$q_{fse} = \mu_{se} F_{fse} \sqrt{\frac{2}{\rho}(P_s - P_b)} \qquad (4.7)$$

c. Flow through Orifices:

$$q_{fo} = I \mu_o F_{fo} \sqrt{\frac{2}{\rho}(P_b - P_a)} \qquad (4.8)$$

The flows through those restrictions are equal:

$$q_{fsi} = q_{fse} = q_{fo} = q \qquad (4.9)$$

Then, the flow coefficients can be determined from those flow equations:

a. At Seat Inlet:

$$\mu_{si} = \frac{q}{F_{fsi}\sqrt{\frac{2}{\rho}(P_i - P_s)}} \qquad (4.10)$$

b. At Seat Exit:

$$\mu_{se} = \frac{q}{F_{fse}\sqrt{\frac{2}{\rho}(P_s - P_b)}} \qquad (4.11)$$

c. At Orifices:

$$\mu_o = \frac{q}{IF_{fo}\sqrt{\frac{2}{\rho}(P_b - P_a)}} \qquad (4.12)$$

The flow areas F_{fsi} and F_{fse} are functions of needle lift h_i, and they are given by equations (3.41) and (3.45). The total flow area through the orifices (IF_{fo}) is calculated from the orifices diameter.

It should be noted that the above equations are valid for the turbulent flow. Therefore, the flow conditions should be analyzed to justify such assumption.

4.4. Test Set-Up Description

A schematic of the test set-up for seat pressure measurement is shown in figure 4.9. Description and calibration of the instruments used in the experiments are described in appendix E.

In this test set-up, two fuel pumps, in series, supply fuel from a reservoir to the injector. The low pressure pump from the Bosch test bench creates the boost pressure for a high pressure variable displacement pump. This arrangement of pumps is capable of producing over 200 bars of pressure at a flow rate over 3.6 litre per minute. However, there is a heat dissipation problem while the test requires a steady temperature of fuel. For that reason, a water cooler is used as indicated in figure 4.9. The fuel supplied to the tested injector is passing through a distributor connected to a bladder accumulator which is used to reduce the pressure fluctuation and to improve steady-state conditions for the test. A pressure gage is installed, as shown, to record the pressure in the injector. Inside the injector holder, one pressure transducer, one needle lift transducer, and one force transducer are installed. To accomodate these transducers, the injector holder has been redesigned as presented in figure 4.8. Either a turbine flowmeter, a rotameter, or a cylinder with a scale can be used to measure the fuel flow rate. Since, the fuel flow occurs at steady-state condition, the latter device is chosen for simplicity and accuracy, using the test bench automatized flow measuring system. Finally, the fuel should be filtered after leaving the main fuel tank. For that reason, a filter is used, and it is located in the test bench, as indicated in figure 4.9.

1. Fuel Tank
2. Low Pressure Pump.
3. High Pressure Pump
4. Water Cooler
5. Low Flow Turbine Flowmeter
6. Pressure Gage

7. Distributor
8. Bladder Accumulator
9. Tested Injector
10. Oscilloscope
11. Indicator Container
12. Filter
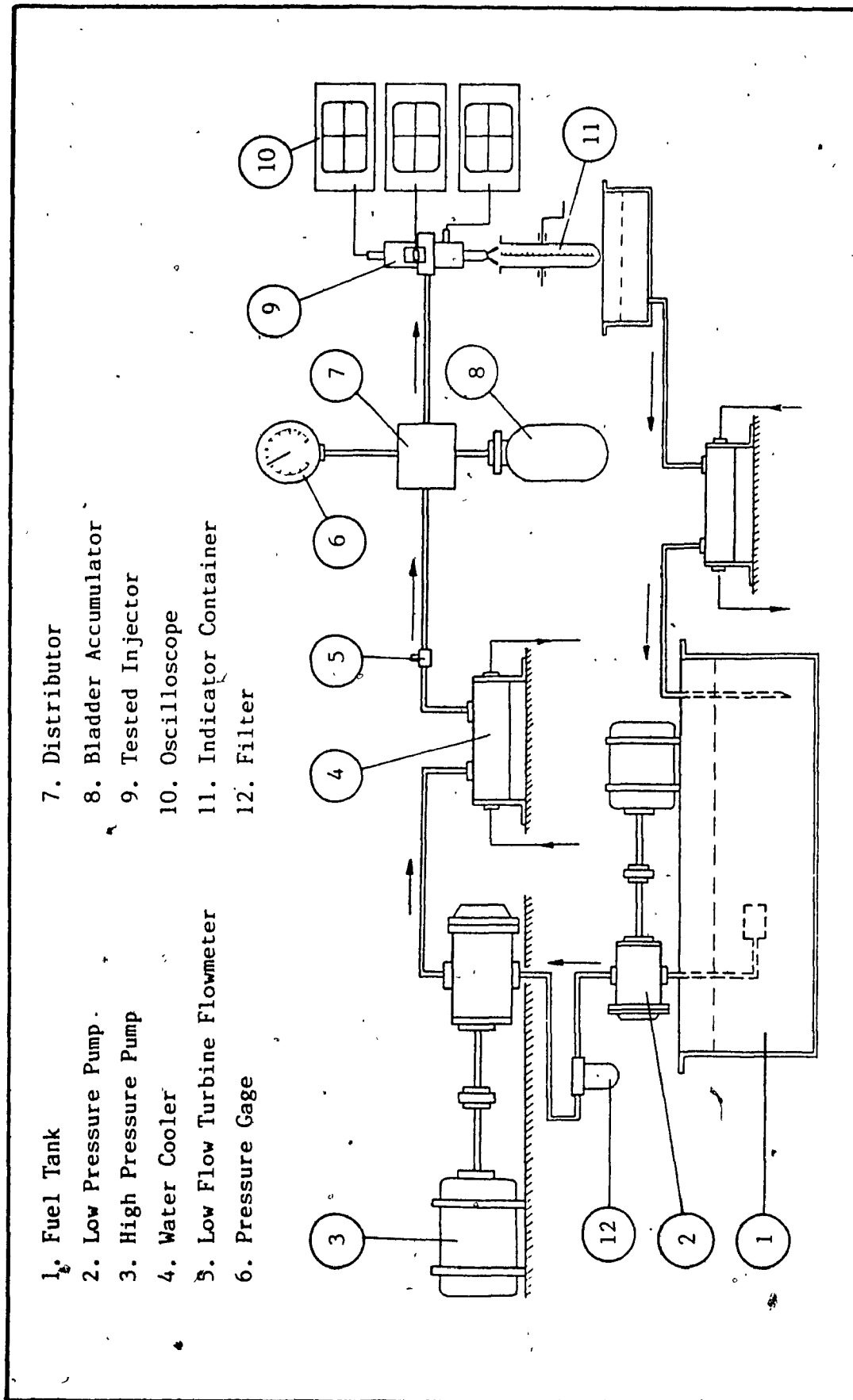
Fig.4.9. Schematic of Seat Pressure Measurement Set-up

4.5. Test Procedure

Before starting the experiments to measure the seat pressure, tests were performed with the fully opened injector to determine the flow coefficient at the orifices. With fully open seat flow area, the injector nozzle is so designed that there is no significant throttling effect and, therefore, almost no pressure drop across the seat. This means that the injector pressure and the bag pressure are almost identical. With that assumption, the experiment was carried out to measure the fuel flow rate q at the scheduled injector pressures p_i which are considered to be equal to the bag pressures p_b. According to equation (4.12), with full opening of seat flow area:

$$q = I\mu_o F_{fo}\sqrt{\frac{2}{\rho}(p_b - p_a)} = I\mu_o F_{fo}\sqrt{\frac{2}{\rho}(p_i - p_a)} \qquad (4.13)$$

From that equation, knowing the fuel flow rate, either the flow coefficient at the orifices or the orifices diameter could be confirmed using the formulae:

– For Orifice Flow Coefficient:

$$\mu_o = \frac{q}{I F_{fo}\sqrt{\frac{2}{\rho}(p_i - p_a)}} \qquad (4.14)$$

- For Orifice Flow Area:

$$F_{fo} = \frac{q}{I\mu_o\sqrt{\frac{2}{\rho}(p_1 - p_a)}} \qquad , \quad (4.15)$$

After the flow rate at maximum needle lift was determined, the tests were performed to measure the flow rate at various needle lifts as follows. The needle lift was readjusted to a desired value which was recorded by a displacement-transducer (LVDT) connected to a voltmeter. Then, the high pressure pump displacement was controlled in such a way that the injector pressure p_1 reached the particular required value and remained constant during the test. For each position of the injector needle, the fuel flow rate, the injector pressure, and the total force acting on the needle were recorded. The same procedure was repeated for different values of injector pressure. It should be emphasized that the test terminated when the lift of the injector needle reached a position at which the throttling effect across the seat was not visible, i.e. the injector pressure, the seat pressure, and the bag pressure were similar.

Tests were performed at three different levels of injector pressure: 80 bars, 124 bars, and 165 bars.

4.6. Test Results

4.6.1. Flow Coefficients at Orifices

As mentioned previously, tests were first performed at the full opening of the seat flow area to determine the flow coefficient for the orifices. Table 4.1 presents the results of measuring the fuel flow rates for three different values of injector pressure. The orifice flow coefficients were calculated using equation (4.14) for the injector with four orifices having diameter of 0.32 milimeter each.

Injector Pressure [bar]	80.0	124.0	165.0
Fuel Flow Rate [cm^3/s]	30.0	37.0	43.3
Orifices Flow Area x 10^6 [m^2]	.3217	.3217	.3217
Fuel Density [kg/m^3] —	820.0	820.0	820.0
Fuel Temperature [^oC]	38.0	38.0	38.0
Orifice Flow Coefficient μ_o	.6655	.6614	.6699
Percentage of Deviation from the Average Value of μ_o	−.0150	−.6300	+.6460

Table 4.1. Test Data and Calculated Orifice Flow Coefficient

Observation of the results in table 4.1 reveals that the orifice flow coefficients are different by less than one percent as compared with the average flow coefficient. Based on these test results, one can conclude that the average flow coefficient at the orifices is of 0.6656. Referring to literature [17] and [18], the flow coefficient at the orifices ranges from 0.65 to 0.75 depending on Reynolds number.

Hence, the flow coefficient value for the orifices which was determined in this test is within the expected range.

4.6.2. Seat Pressure

The needle lift, fuel flow rate and force acting on the injector needle at steady-state flow condition for the three injector pressures of 80 bars, 124 bars, and 165 bars are presented in table 4.2.

The conversions of the needle lift from volt [V] to milimeter [mm], and of the load from milivolt [mV] to Newton [N] using the gain factors derived in appendix E are given in tables 4.3, 4.4, and 4.5 for different values of injector pressure. It should be mentioned that the needle rod elastic deflection caused by the high pressure force affected the readings obtained by the lift transducer due to the installation and arrangement as seen in figure 4.8. This deflection has been calculated separately and added to the needle lift recorded by the lift transducer to obtain the actual displacement of the needle. The elastic deflection of the needle rod was calculated from:

$$\Delta h_i = \frac{PL_r}{F_r G_r} \tag{4.16}$$

Other measured quantities such as seat pressure, bag pressure, and flow coefficients at the seat inlet and exit are also presented in these tables.

The graphs of the injector pressure, seat pressure and bag pressure versus the needle lift for different values of injector pressure are given in figures 4.10, 4.11, and 4.12. The plots of flow coefficients at the seat inlet and exit flow areas versus the needle lift are shown in figures 4.13 and 4.14 respectively. In these plots, the flow

coefficients which are not relevant due to the very low needle lift, are not being shown for the reasons explained in the section 4.7.

$p_i = 80.0$ bars			$p_i = 124.0$ bars			$p_i = 165.0$ bars		
h_i	q	P	h_i	q	P	h_i	q	P
V	cm^3/s	mV	V	cm^3/s	mV	V	cm^3/s	mV
1.82	3.67	130.0	1.89	12.80	212.0	1.86	14.00	280.0
1.86	7.20	137.0	1.93	15.47	221.0	1.92	19.33	302.0
1.98	14.27	161.0	2.03	22.40	258.0	1.96	23.47	323.0
2.04	18.27	173.0	2.08	24.93	270.0	1.98	25.07	341.0
2.15	22.13	178.0	2.12	27.60	274.0	2.01	27.33	347.0
2.18	23.87	180.0	2.20	30.93	282.0	2.07	29.33	354.0
2.33	26.13	185.5	2.30	32.27	286.0	2.11	31.47	364.0
2.54	28.27	190.0	2.34	33.33	288.0	2.13	33.33	369.0
2.79	29.60	193.0	2.41	33.87	290.0	2.25	37.73	381.5
			2.51	34.93	292.0	2.43	40.00	390.0
			2.62	35.60	294.0	2.68	42.13	395.0
			2.69	36.00	295.0			
			2.82	36.40	296.0			

Table 4.2. Test Data Recorded for Injector Pressure

p_i = 80, 124, and 165 bars

h_1 [mm]	P [N]	p_s [bar]	p_b [bar]	μ_{si}	μ_{se}
.0099	153.4	3.35	1.23	0.486	1.455
.0205	161.7	13.63	4.73	0.498	1.109
.0520	190.0	48.27	18.55	0.556	0.747
.0678	204.1	63.94	30.41	0.758	0.758
.0964	210.0	67.37	44.65	0.721	0.870
.1043	212.4	69.05	49.42	0.768	0.952
.1433	218.9	73.10	59.75	0.753	0.990
.1979	224.2	78.10	66.83	0.991	0.899
.2628	227.7	78.66	73.86	0.872	1.142

Table 4.3. Experimental and Calculated Results for
Injector Pressure p_i = 80 bars

h_i [mm]	P [N]	p_s [bar]	p_b [bar]	μ_{sd}	μ_{se}
.0295	250.2	21.0	14.9	0.496	2.026
.0401	260.8	33.5	21.8	0.470	1.509
.0666	304.4	85.9	45.7	0.629	0.858
.0798	318.6	102.2	56.7	0.766	0.795
.0903	323.3	104.2	69.4	0.791	0.919
.1112	332.8	110.1	83.7	0.855	1.015
.1372	337.5	114.0	91.4	0.852	0.971
.1476	339.8	115.0	95.3	0.860	1.014
.1658	342.2	117.2	98.5	0.891	0.965
.1918	344.6	118.2	105.2	0.860	1.060
.2204	346.9	120.1	109.5	0.920	1.070
.2386	348.1	120.9	112.2	0.955	1.116
.2723	349.3	121.6	114.8	0.964	1.142

Table 4.4. Experimental and Calculated Results for
Injector Pressure $p_i = 124$ bars

h_i [mm]	P [N]	p_s [bar]	p_b [bar]	μ_{si}	μ_{se}
.0229	303.4	24.0	17.9	0.597	2.478
.0388	356.4	54.6	34.1	0.548	1.446
.0496	381.1	83.6	50.2	0.605	1.194
.0551	402.4	110.6	57.3	0.711	0.945
.0629	409.5	116.8	68.1	0.719	0.989
.0787	417.7	124.8	78.4	0.674	0.934
.0892	429.5	137.3	90.3	0.764	0.910
.0945	435.4	141.8	101.3	0.833	0.996
.1258	450.2	151.4	121.8	0.913	1.062
.1727	460.2	159.9	137.8	1.113	1.015
.2377	466.1	162.1	149.8	1.081	1.104

Table 4.5. Experimental and Calculated Results for
Injector Pressure p_i — 165 bars
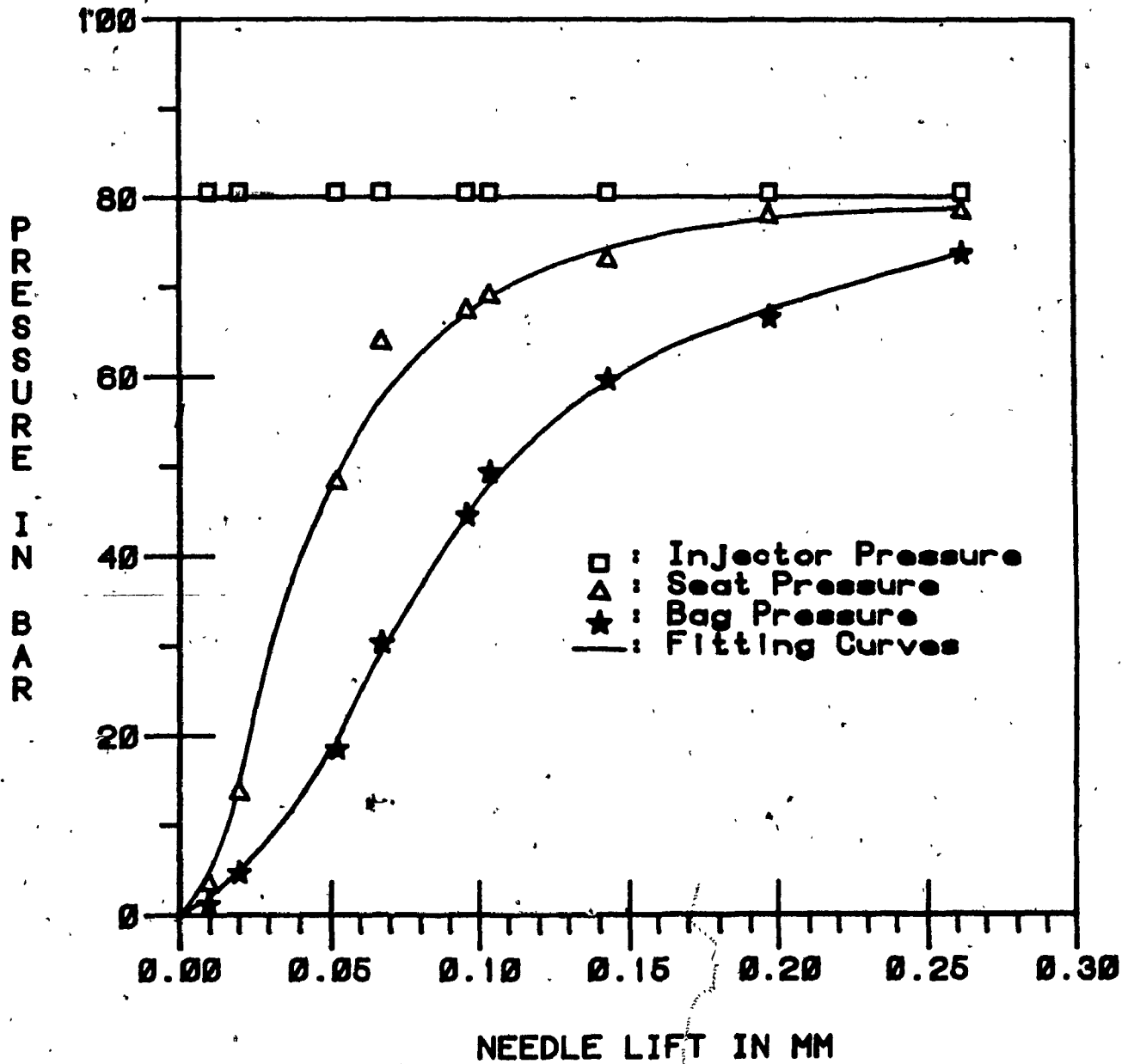
Fig.4.10. Seat and Bag Pressures versus Needle Lift Measured
for Injector Pressure p_i = 80 bars
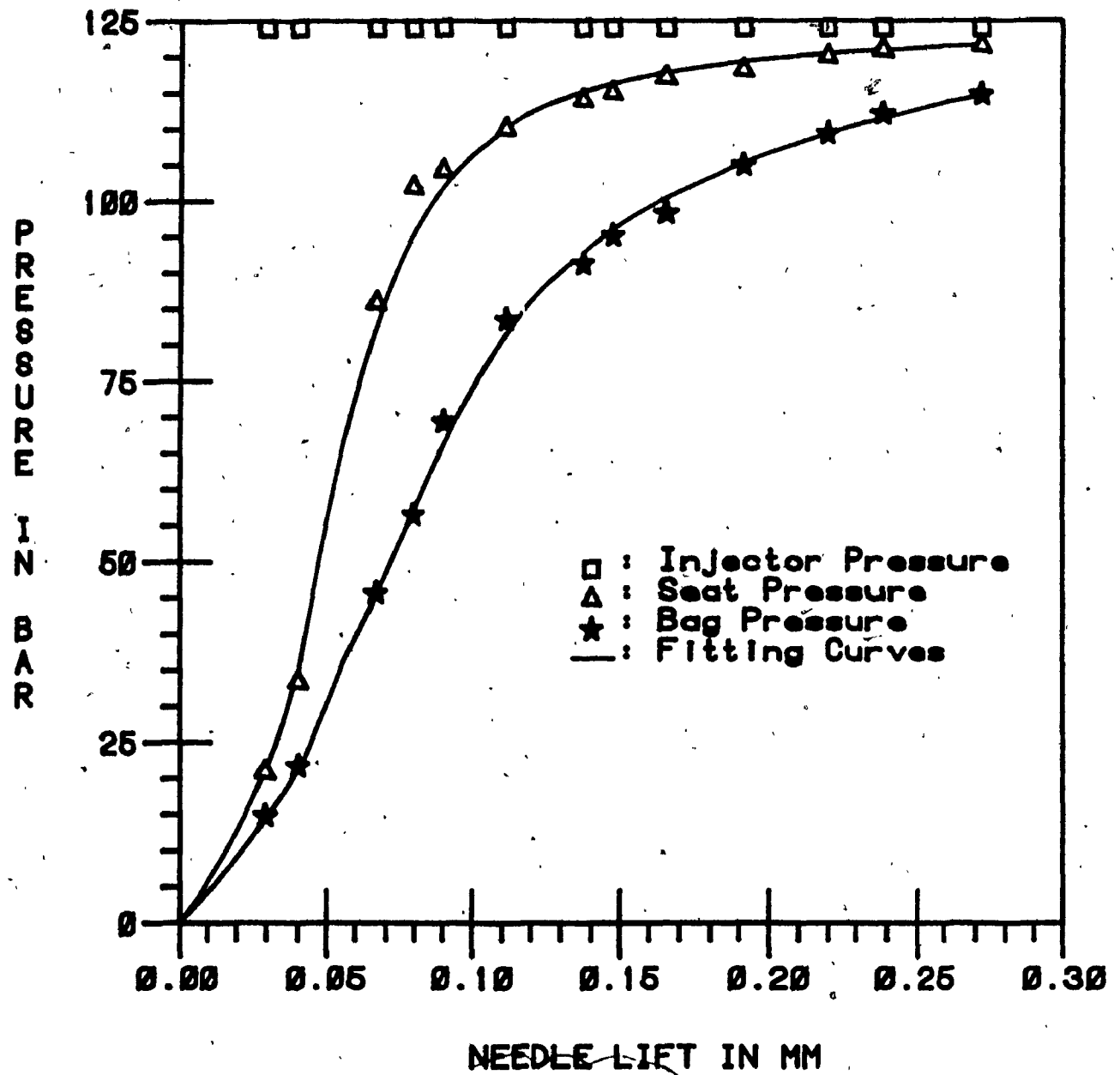
Fig.4.11. Seat and Bag Pressures versus Needle Lift Measured
for Injector Pressure p_i = 124 bars
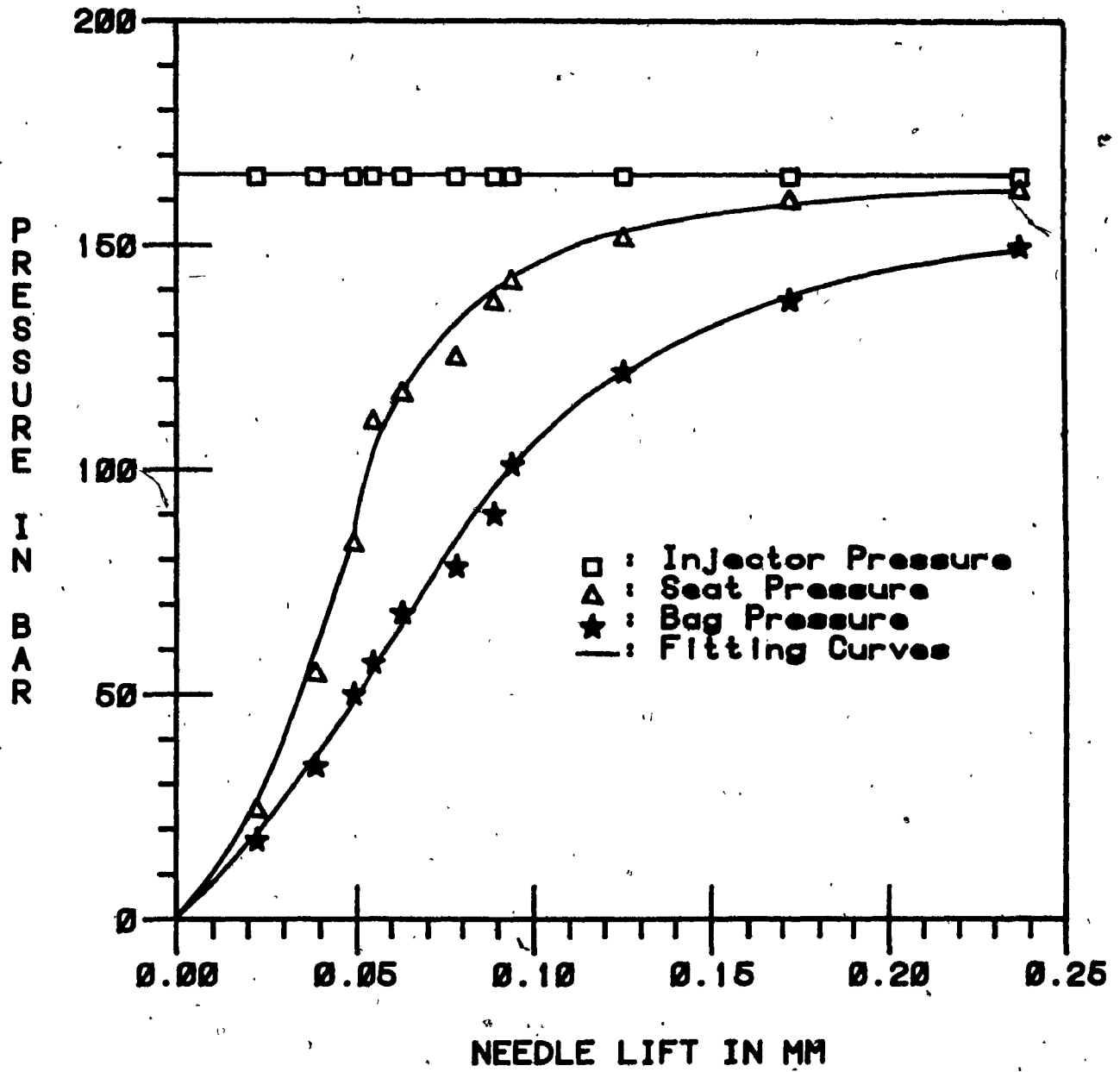
Fig.4.12. Seat and Bag Pressures versus Needle Lift Measured
for Injector Pressure $p_i = 165$ bars
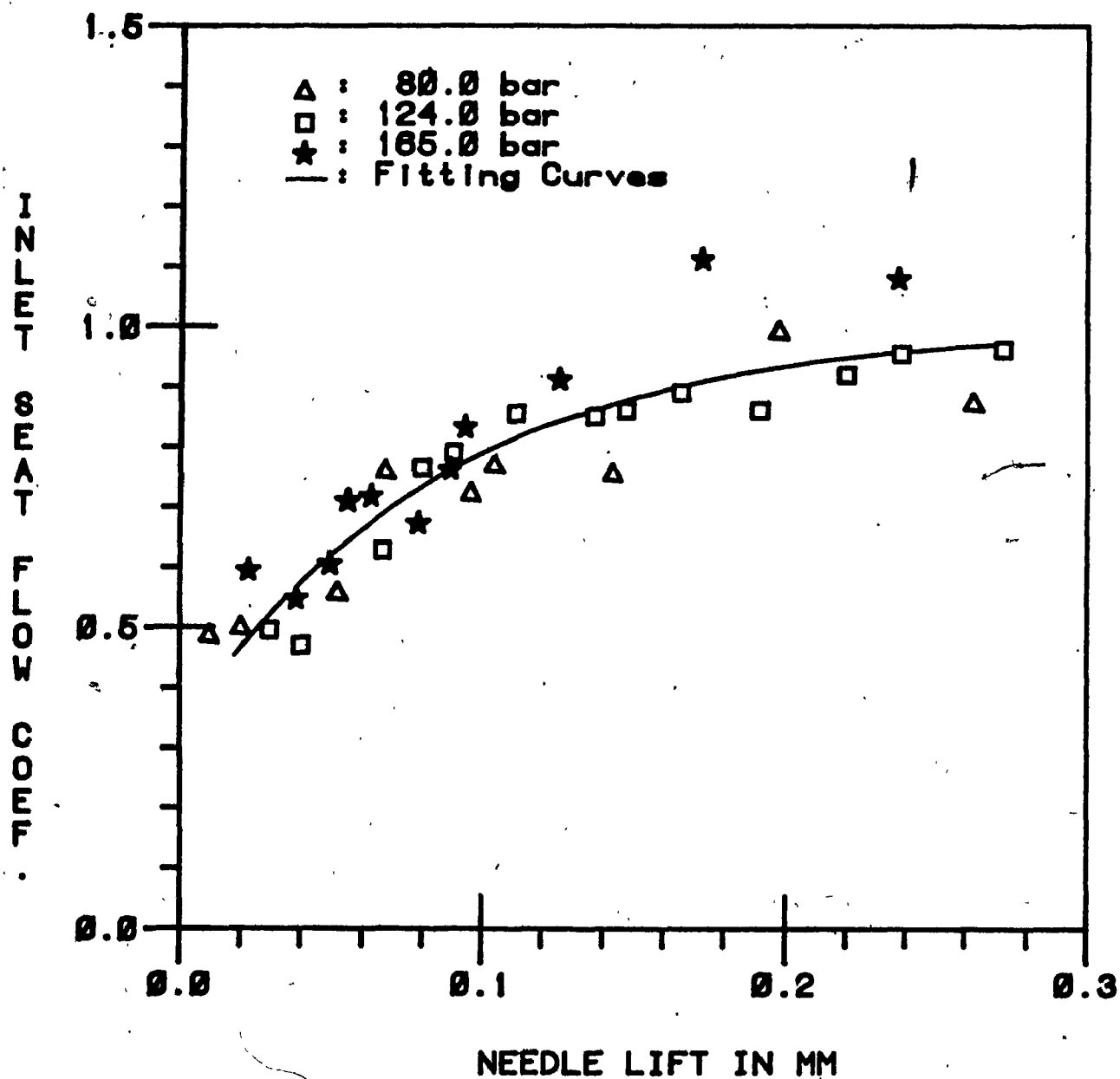
Fig. 4.13. Flow Coefficient at Nozzle Seat Inlet Section versus Needle Lift Obtained Experimentally
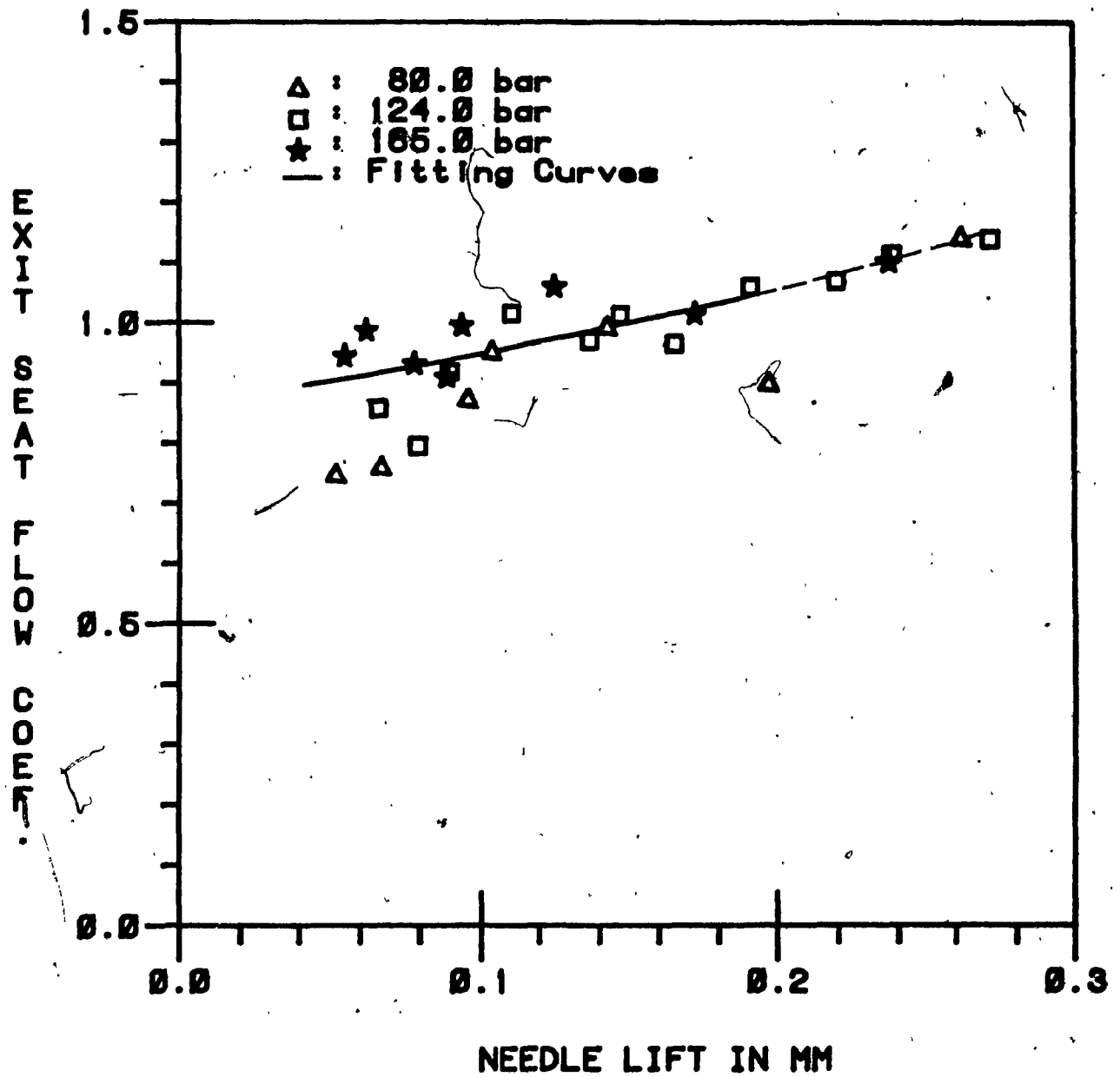
Fig. 4.14. Flow Coefficient at Nozzle Seat Exit Section
versus Needle Lift Obtained Experimentally

4.6.3. Forces Acting on the Injector Needle

From the pressure measurement experiments, the pressure forces acting on the injector needle can be calculated according to the following formulae:

— Injector Pressure Force:

$$P_i = p_i(F_i - F_{so}) \tag{4.17}$$

— Seat Pressure Force:

$$P_s = p_s(F_{so} - F_{si}) \tag{4.18}$$

— Bag Pressure Force:

$$P_b = p_b(F_{si}) \tag{4.19}$$

— Spring Force:

$$P_{sp} = P_{is} + k_{is}h_i \tag{4.20}$$

The plot of these forces is given in figure 4.15 for the injector pressure $p_i = 165$ bars.
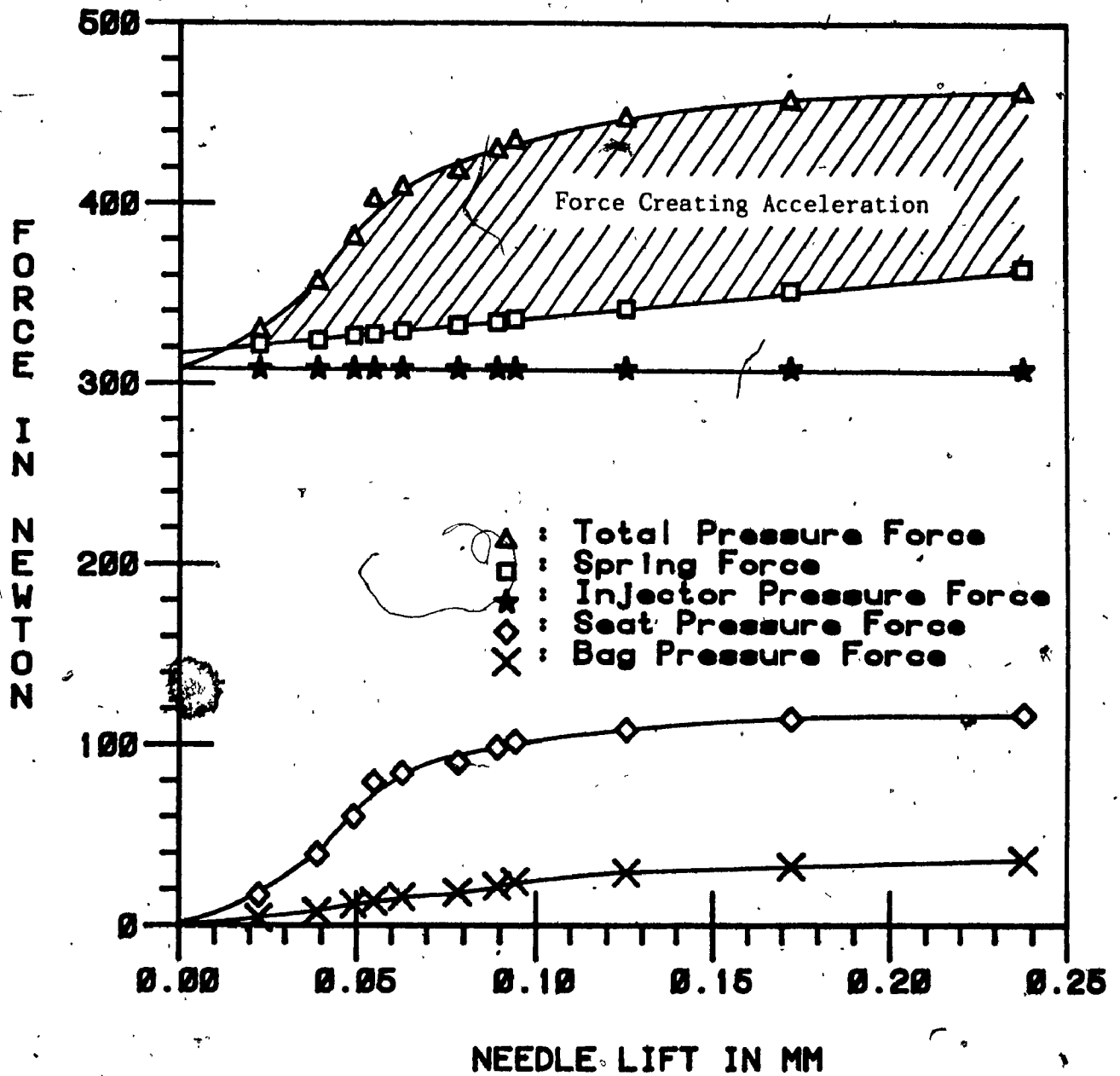
Fig.4.15. Pressure Forces versus Needle Lift

for Injector Pressure p_i = 165 bars

4.7. Discussion of Experimental Results and Conclusions

From the above experiments and from the test results, there are several remarks that can be drawn.

Firstly, the tests are performed for the three selected injector pressure values of 80 bars, 124 bars, and 165 bars because of the following reasons. At the beginning of the injector needle movement, or in other words, at the low lift range of the injector needle movement, the injector pressure p_i falls down from the opening pressure, point a, to the pressure at point b as seen in figure 4.16. This is due to the escape of fuel from the injector chamber and due to the accumulation of fuel under the accelerating needle. There is a throttling effect across the seat, and a significant pressure drop between the injector chamber and the bag chamber occurs. During this period, the seat pressure value is of very importance because it plays big role in accelerating the needle. When the injector pressure starts to increase at point b as indicated in figure 4.16, the needle is already at the maximum lift position. Then, the seat pressure is equal to the injector pressure due to almost no pressure drop across the seat. Similar situation occurs at the injector closing pressure, point c as shown in figure 4.16. At this point, the seat pressure value can decide about the combustion gases penetration through the injector orifices, which can cause corrosion and carbon deposits in the nozzle. From the above discussion, it is of interest to know what is the pressure developed in the seat chamber only when the injector pressure is within the range of nozzle opening and closing which are of 170 bars and 110 bars, respectively, for the type of the injector
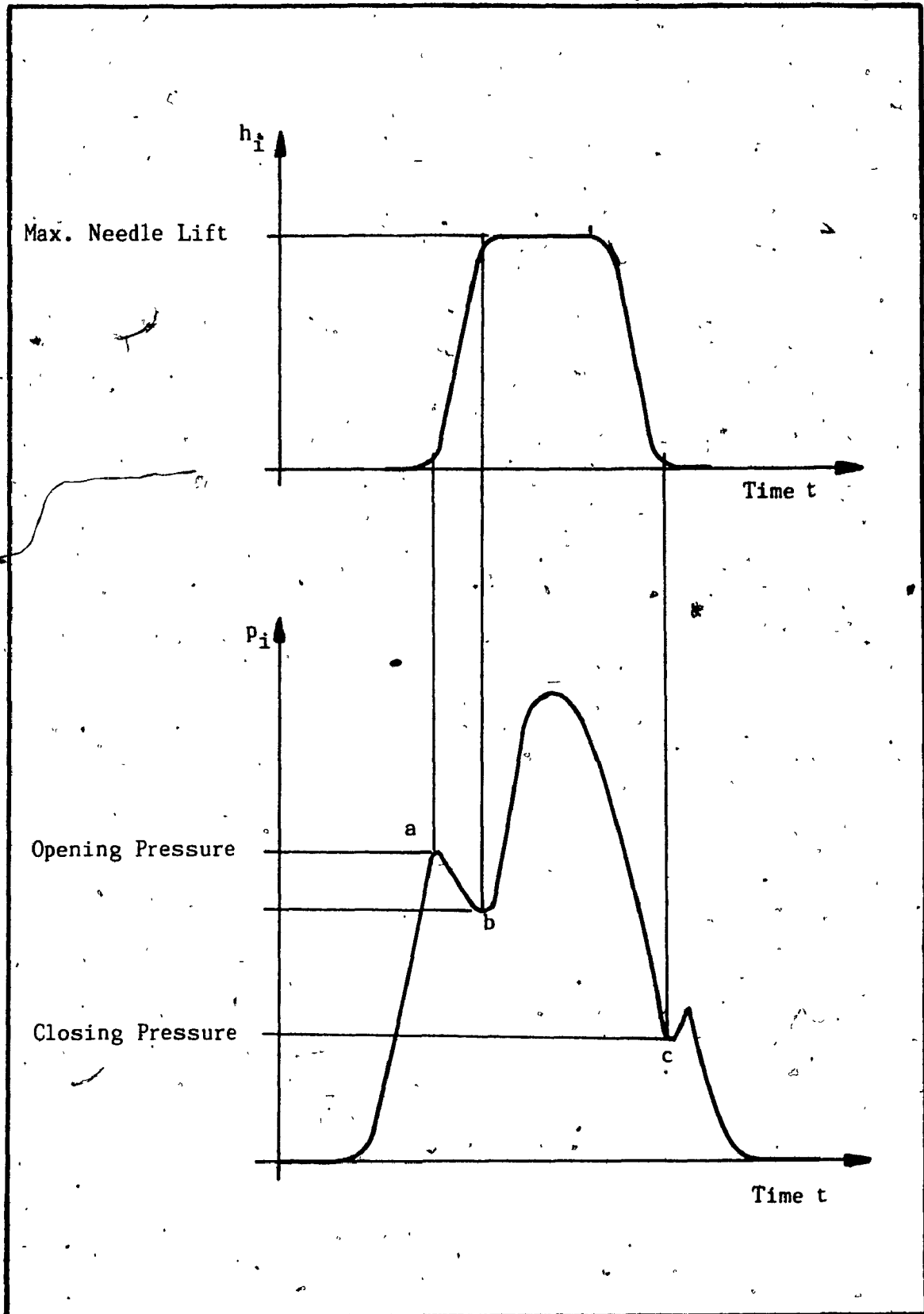
Fig.4.16. Injector Pressure and Needle Lift versus Time
(Typical Diagram)

tested. These are the reasons why the tests were performed for the injector pressure varying from 80 bars to 165 bars, taking into account that there are also injectors in use with only 120 bars opening pressure. The investigation of the seat pressure for the injector pressure higher than the opening pressure is not needed.

Secondly, referring to figures 4.10, 4.11 and 4.12 one can see that the seat pressure at very low needle lift is close to the bag pressure, and at high needle lift it approaches the injector pressure, as it was predicted.

Thirdly, observing the numerical values found for the seat exit flow coefficients in tables 4.3, 4.4 and 4.5, one can see that at the beginning of nozzle opening they are greater than one which is, of course, impossible. The explanation for this fact could be that at low needle lift the flow through the seat exit area is not turbulent but laminar. In that case, equation (4.11) derived to calculate the flow coefficient for the seat exit area would not be valid any more. To investigate this possibility, the plot of Reynolds number versus needle lift has been made and presented in figure 4.17. From this graph, it can be recognized that the fuel flow through the seat gap could be considered laminar for low needle lift and smaller injection pressures. At higher needle lift and greater injection pressure, the flow has to be considered as turbulent. However, a conclusion can be drawn that for unsteady flow process when the needle is moving, the flow is turbulent even at the low needle lifts due to the lack of time to stabilize the flow in the seat and also due to the disruptive effect of the gap increase following the fast needle movement which will
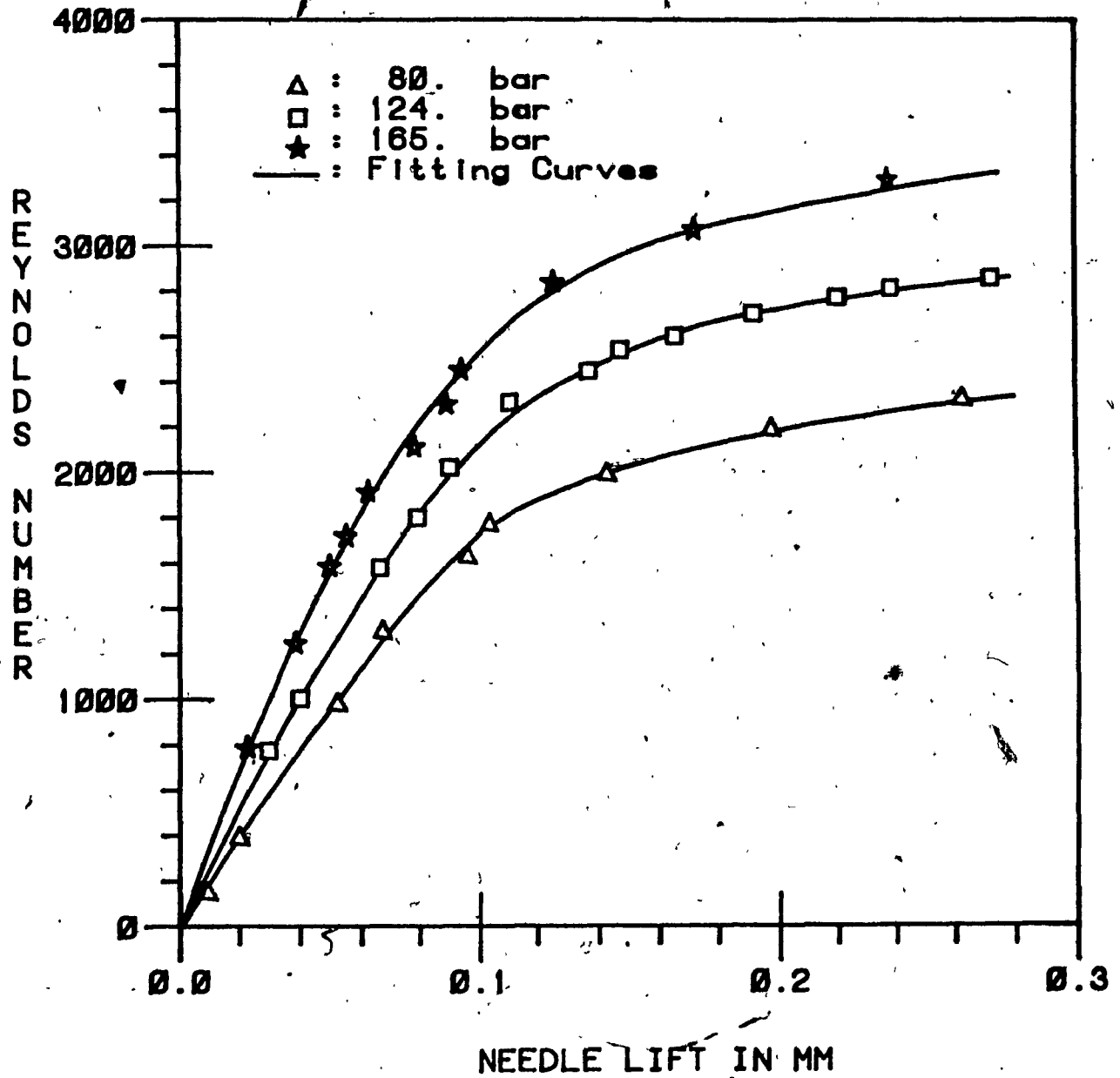
Fig.4.17. Reynolds Number in the middle of the Nozzle Seat versus Needle Lift

disorganize the streamline of the laminar flow. With these conclusions, it is really not known at what lift level the flow is becoming turbulent. It can be only recognized that at the beginning of the lift movement it starts as laminar and this could explain the strange results obtained for the flow coefficients at low needle lift.

Finally, at high needle lift both seat inlet and exit flow coefficients are exceeding the value of one. The reason can be that at the high needle lift the pressures in the injector chamber, seat chamber and bag chamber differ by a very small amount, while there is not enough sensitivity in the equipment used in the experiments to correctly record these small differences in pressure. Taking the above analysis into account, only the middle part of the experimentally obtained flow coefficient curves should be considered for practical use. There is no need for calculation of the flow through the seat at very low needle lift (almost no flow) and at high needle lift (flow almost the same through three restrictions). Assuming that the derived values of the flow coefficients in the middle part of the needle movement are correct, the average flow coefficients for the seat inlet and exit could be proposed as follows:

- At the Seat Inlet: $\mu_{si} = 0.75$

- At the Seat Exit: $\mu_{se} = 0.95$

These values are comparing well with those given for the poppet valves by Von Mises [18].

A pictorial view of the test set-up for the seat pressure measurement is shown in figure 4.18.
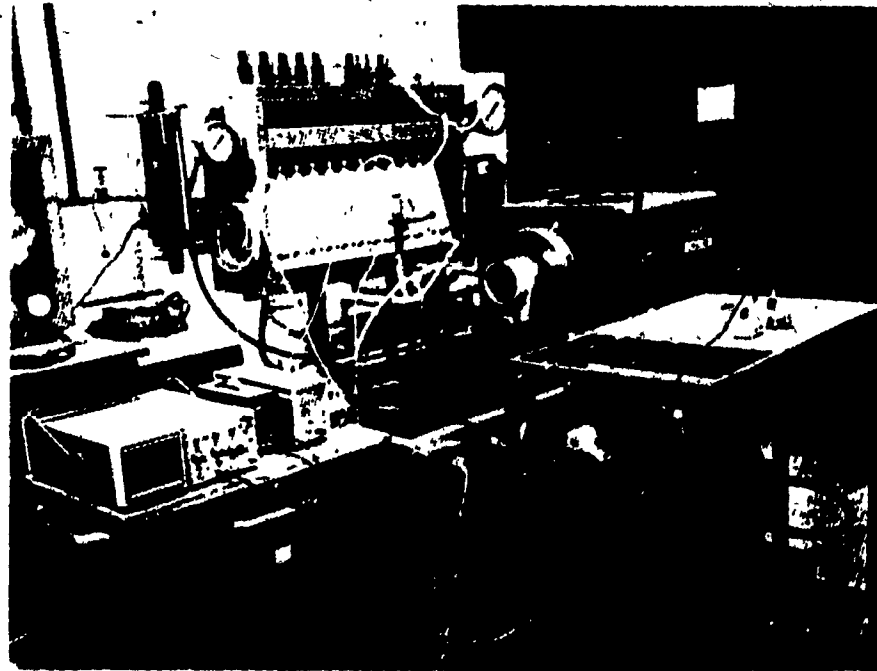
Fig.4.18. Pictorial View of the Test Set-up for
Seat Pressure Measurement

Chapter 5
EVALUATION OF DYNAMIC RESPONSE OF
DIESEL INJECTORS

5.1. Introduction

As discussed before, a diesel injector should deliver fuel into the combustion chamber of a diesel engine through the nozzle orifices with high flow rate to obtain a good fuel atomization and distribution in the compressed air. This condition is easier to fulfill at high engine speed and fuel dose, i.e. at high engine power than at idling or starting conditions. In the latter cases, the dynamic response of the injector becomes very important because it affects the time of the injector's opening and closing. When the injector is opening, it is required to open quickly to provide the high pressure differential across the injector orifices. When the pressure inside the injector drops, the injector should close quickly so that it will not allow the fuel to be injected through orifices with a low discharge rate.

It is important for the diesel injector manufacturers and users to be able to evaluate the dynamic response of the diesel injectors in the conditions similar to those on the diesel engine. For that reason, the test-rigs are used where some specific conditions are created simulating the engine conditions in which the dynamic response of the injector could be exactly recorded and compared to that obtained by mathematical simulation. Then, it would be possible to determine the effect of changes of particular design and operational parameters on the dynamic response of a diesel injector, and to optimize these

parameters. Such method would also provide the investigator with an opportunity to determine the criteria for allowable changes of particular design and operational parameters of the injector in case of wear or manufacturing deviations.

It has to be mentioned here that the design parameters for an injector such as orifices diameter, needle and seat diameters, volume inside the injector, spring constant, nozzle opening pressure, etc. are usually chosen by the fuel injection system designer at the time when the injector is adapted to a diesel engine, from the point of view of the engine performance. While the proposed investigation of the dynamic response of an injector would provide the designer with a proper measure of the effects of the design parameters, these parameters could not be arbitrarily selected to improve the dynamic response of the injector only because this could worsen the engine performance. Therefore, the proposed evaluation method has more significance in investigating the impact of the deviations from the design and operational parameters resulting from some assignable causes occuring during the manufacturing process (for new injector), as well as during the engine operation (for used injector). Hence, the proposed evaluation method based on the injector dynamic response could be rather considered as an evaluation of the quality of the diesel injectors. However, it could be also used for the adaptation of the fuel injectors to the diesel engine, as discussed in further chapters.

5.2. Dynamic Response of Diesel Injector as a Nozzle Quality Measure

This chapter will show how the dynamic response of a diesel injector can be affected by the various operational parameters related either to the manufacturing quality of the new injectors or to the service deterioration of the used injectors. For that reason, a schematic representation of a diesel injector can be used as shown in figure 3.7, and following factors affecting the forces acting on the injector needle can be distinguished:

1. Mechanical friction of the needle in the nozzle can vary from zero for an ideal injector to high values when there is a deformation of the nozzle hole due to the clamping force of the nut attaching the nozzle to the injector, and when contamination in form of a particle or in form of carbon deposit enters the gap between the needle and the nozzle body.

2. Damping force acting on the needle, which can vary due to the changes in gap between the needle and the nozzle body as the result of manufacturing accuracy or from the wear.

3. Force from the pressure acting on the needle in the bag chamber, which depends on the flow area of the orifices. The orifice flow area can be affected by the burrs left after drilling or by the carbon deposits resulting from the service on the engine.

4. Force acting on the needle from the pressure in the seat, which depends on the seat geometry (seat chamber differential angle), and on the seat inlet and exit flow coefficients which can be affected

by the manufacturing accuracy and by the wear of the seat surfaces due to the service of the injector on the engine.

5. Force from the spring acting on the needle, which can be affected by the inaccuracy in adjusting of the opening pressure and by the wear of the injector components between the spring and the needle.

All these factors which decide about the quality of an injector will be taken into account in developing a mathematical model for calculation of the dynamic response of an injector.

5.2. Model for Investigation of the Dynamic Response of an Injector

The set-up for investigation of the dynamic response of a diesel injector is shown in figure 5.1. It represents a mechanical system of second order with mass, spring, damper and friction which responds to the forcing input action of an hydraulic system represented by a chamber accumulating a volume of fuel under high pressure and connected with the test-rig pump by a restriction.

To make the dynamic response of the injector more relevant to the outlined objectives, it is assumed that the model will simulate the fuel injection process corresponding to idling conditions of the diesel engines, i.e. with small dose of fuel being injected and with the injector needle lift being smaller than the maximum stroke. Such conditions produce a single "jump" of the needle with fuel discharge through the orifices. Since, the needle moves at low lift level and the critical flow area remains within the restricted seat flow area, the seat flow conditions which decide about the needle acceleration can be, therefore, well recognized.

For experimental purposes, the proposed model can be realized practically using a simple injector tester to feed a hydraulic accumulator through a metering valve with restricted flow area, as shown in figure 5.2. If the accumulator is supplied at a constant pressure, the injection process will occur as shown in figure 5.3. The pictorial view of the test set-up is shown in figure 5.4.
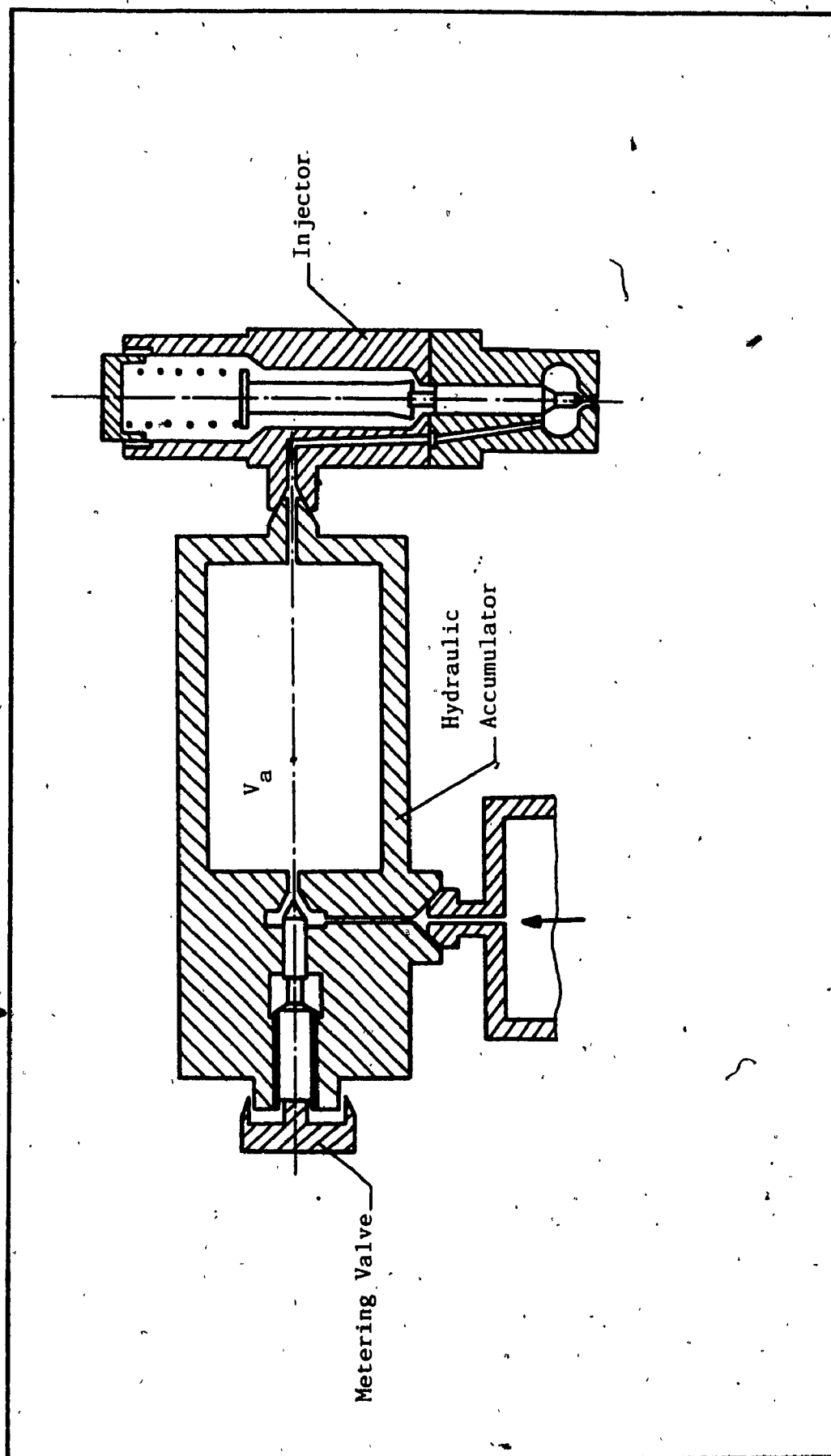
Fig.5.1. Set-up for Investigation of Injector Dynamic Response
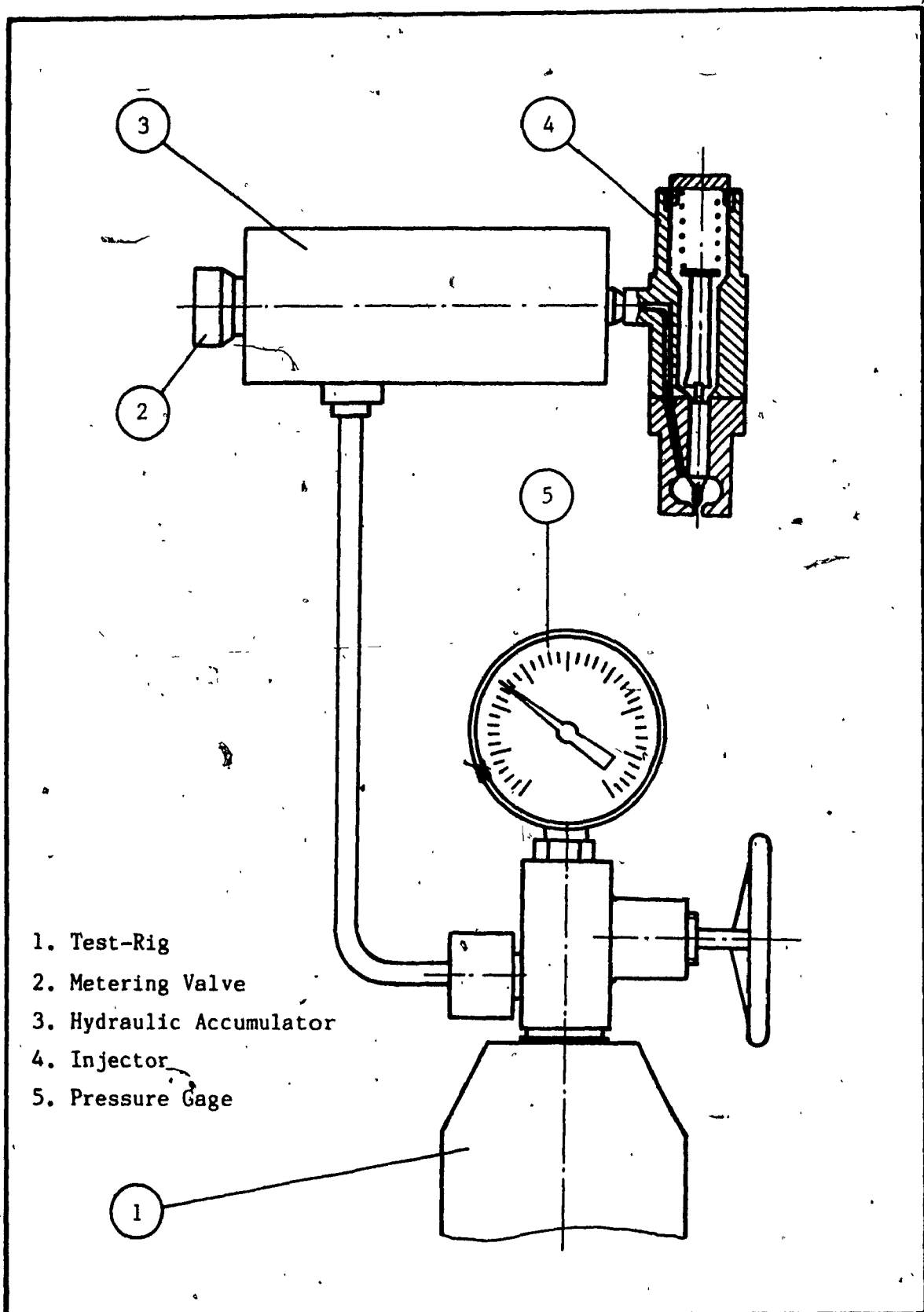
Fig.5.2. Injector Test-Rig for Injector Dynamic Response Investigation

1. Test-Rig
2. Metering Valve
3. Hydraulic Accumulator
4. Injector
5. Pressure Gage

Needle
Lift

Injector
Pressure

Fig.5.3. Fuel Injection Process
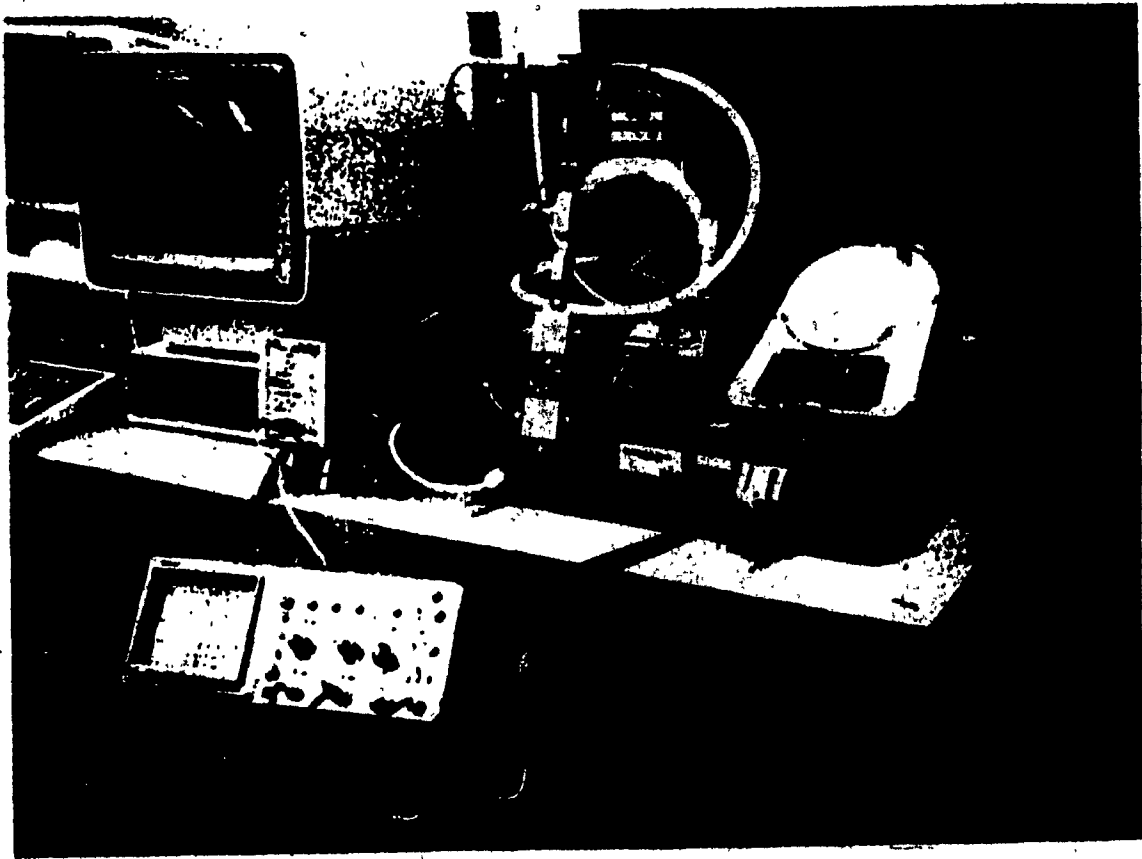
Fig.5.4. Pictorial View of the Test Set-up
on the Test-Rig

5.4. Mathematical Simulation of Injector Dynamic Response

For mathematical simulation, it is assumed that the impact of pressure wave can be neglected because of proximity of all components of the model. A second assumption can be made that during the short injection period no fuel is passing from the reservoir to the accumulator. This is almost true when the fuel flow rate through the metering valve is very low; i.e. the metering orifice flow area is very small; it affects the injection frequency but not the injection process.

Besides these assumptions, the procedures of calculation are carried out for the system which is simplified by making some more assumptions. They are:

1. The sealing between mechanical components is considered perfect. That is the fuel leakage is not taken into account.

2. All elastic deformation of solid parts of the system due to pressure changes is neglected.

3. The fuel is discharged at atmospheric pressure, but not into the engine cylinder.

With these assumptions, the fuel injection process can be calculated using the formulae:

1. Continuity Equations

    a. For Injector Chamber with Accumulator:

$$\frac{V_i + V_a}{E} \frac{dp_i}{dt} + (F_i - F_{so})v_i + q_{fsi} = 0 \qquad (5.1)$$

    b. For Seat Chamber:

$$(F_{so} - F_{si})v_i + q_{fse} = q_{fsi} \qquad (5.2)$$

    c. For Bag Chamber:

$$\frac{V_b}{E} \frac{dp_b}{dt} + F_{si}v_i + q_{fo} = q_{fse} \qquad (5.3)$$

2. Motion Equation for Injector Needle

$$p_i(F_i - F_{so}) + p_s(F_{so} - F_{si}) + p_b F_{si} = m_i \frac{dv_i}{dt} + \delta_i v_i + k_{is} h_i +$$

$$+ P_{is} \pm R_i \qquad (5.4)$$

and,

$$\frac{dh_i}{dt} = v_i \qquad (5.5)$$

3. Equations for Fuel Discharge

a. For the Flows through the Seat:

— At Seat Inlet:

$$q_{fsi} = \mu_{si} F_{fsi} \sqrt{\frac{2}{\rho}(p_1 - p_s)} \qquad (5.6)$$

— At Seat Exit:

$$q_{fse} = \mu_{se} F_{fse} \sqrt{\frac{2}{\rho}(p_s - p_b)} \qquad (5.7)$$

The seat flow areas F_{fsi} and F_{fse} are functions of the needle lift h_1, and given by equations (3.41) and (3.45) respectively.

b. For the Flow through the Orifices:

$$q_{fo} = I \mu_o F_{fo} \sqrt{\frac{2}{\rho}(p_b - p_a)} \qquad (5.8)$$

The dynamic response of a diesel injector fitted with a multi-hole nozzle as specified in chapter 3 was calculated for various differential angles γ between nozzle seat and needle tip cones. Then, the calculations were repeated by changing those nozzle parameters which can vary as the result of manufacturing deviations, nozzle contamination or wear. Calculations were also made for various volumes of accumulator V_a, included into the test set-up as shown in figure 5.1. The results of calculations are presented in figure 5.5 where the maximum needle lift obtained during a single injection is plotted versus different nozzle parameters.
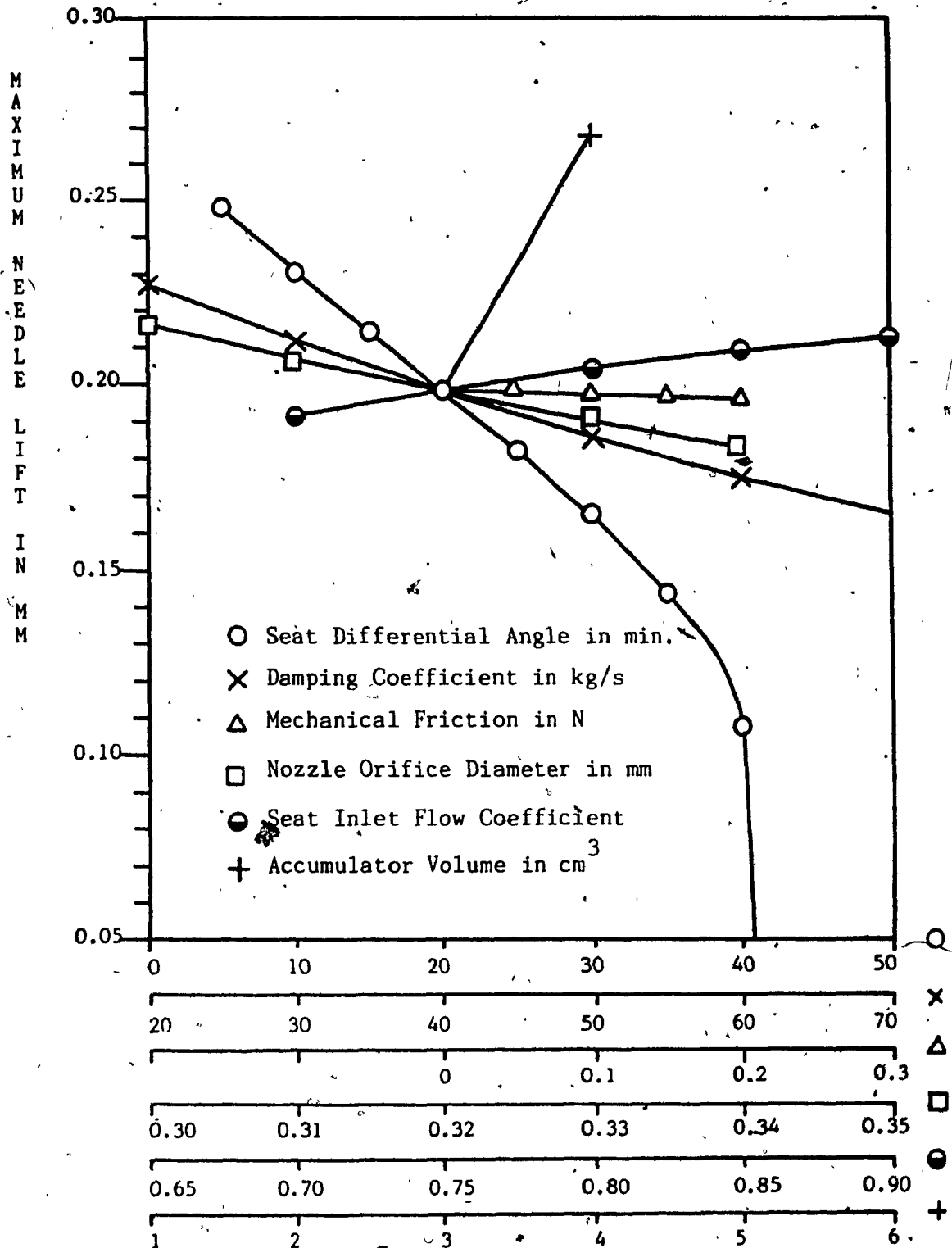
Fig.5.5. Maximum Needle Lift Calculated versus
Various Injector Parameters

Some experiments have been conducted using a data acquisition system built at Concordia University in the Centre for Industrial Control. The schematic of the test set-up with the data acquisition system is shown in figure 5.6. The lift of the needle was recorded by the computer, shown on the screen and printed. Figure 5.7 shows the needle lift characteristic obtained from the injector for which the calculations of dynamic response have been made. The comparison of the needle lift travel is made under assumption that the needle seat differential angle in that injector is at the range of 20' which is a typical value for diesel injectors.
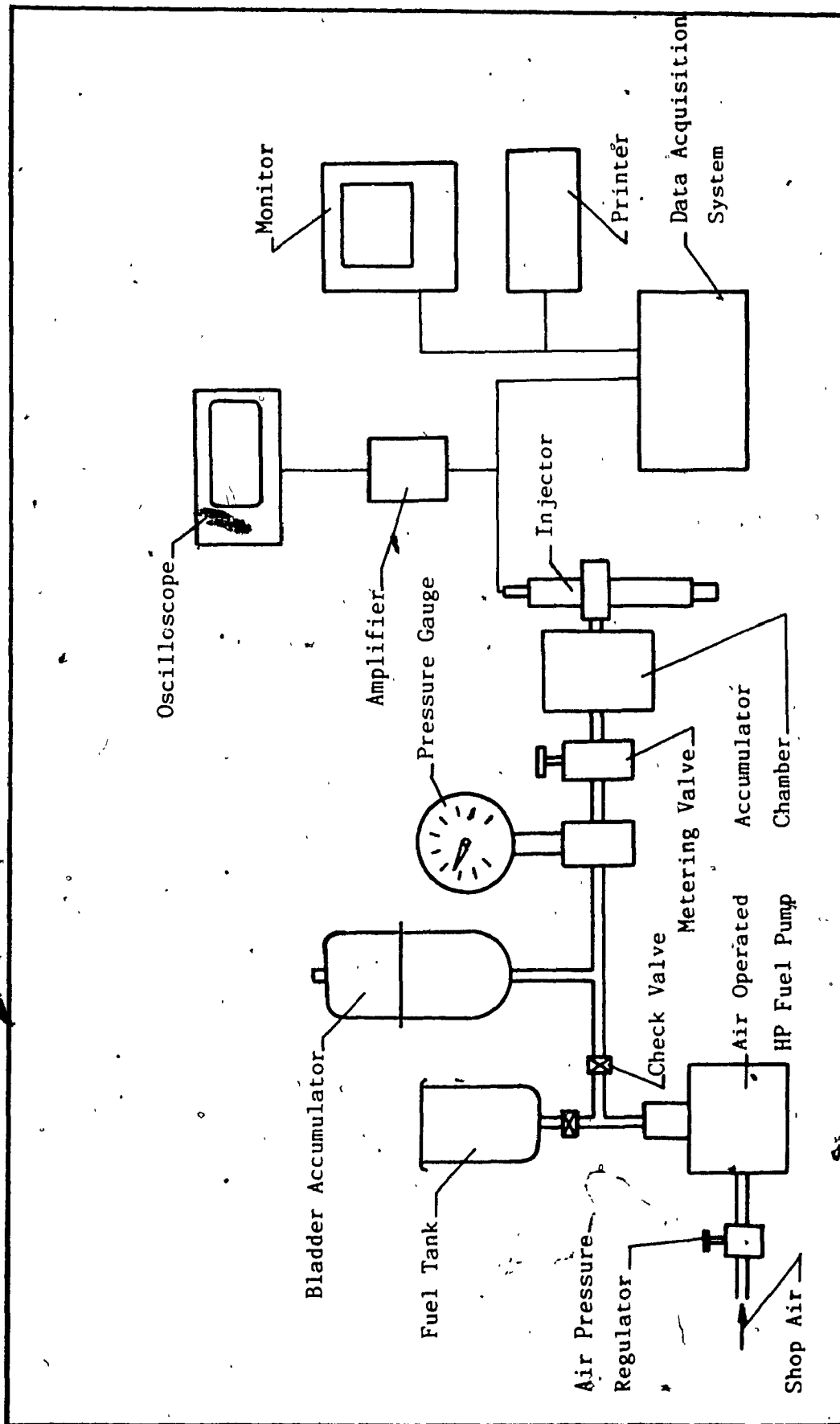
Fig.5.6. Schematic of the Test Set-up with the Data Acquisition System
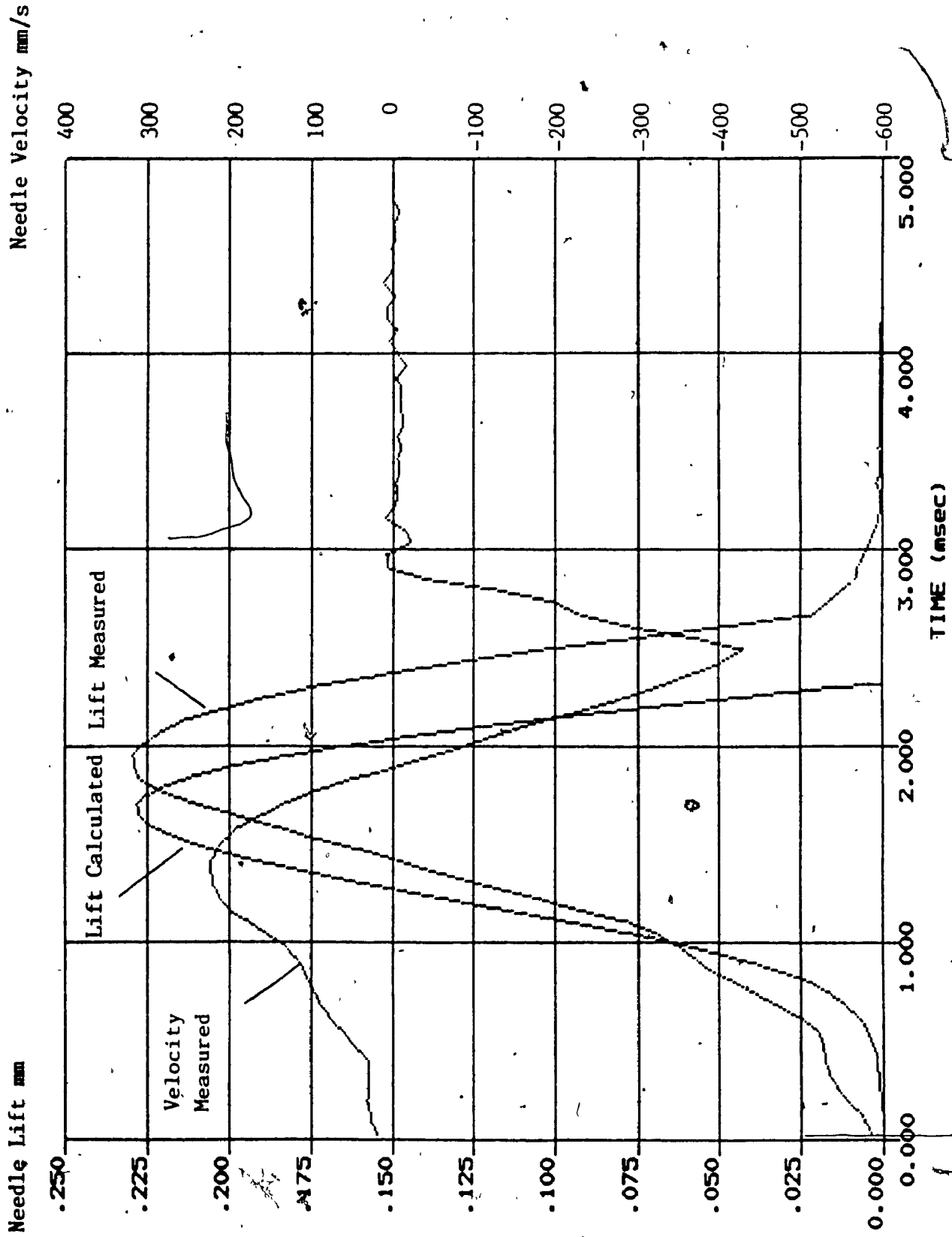
Fig.5.7. Calculated and Measured Needle Lift and Velocity versus Time
(Obtained from Computer Controlled Data Acquisition System)

5.5. Discussion of Calculated Results

Analysis of graph in figure 5.5 is showing a significant impact of variations in seat differential angle and in accumulator volume V_a on the maximum lift of the injector needle.

To better analyze the effect of particular factors, the graph from figure 5.5 was extended to show the maximum needle lift changes versus seat differential angle for several nozzle parameters and for various accumulator volume V_a, figure 5.8.

Conclusions can be drawn that for accumulator volume of 3 cm^3, corresponding to engine fuel dose at idling about 15 mm^3, the maximum differential angle should be around 40' to maintain the unstable operation of injector resulting in high seat flow area openings. Variations in needle damping coefficient δ_1, mechanical friction R_1, and in orifice flow area F_{fo} do not show such deciding effect, unless they overpass the typical deviation limits.

From the above analysis, it might be concluded that a very small seat differential angle should be desired. However, the minimum value of that angle is limited by the sealing ability of the needle-valve which requires a distinct contact line between the seat and the needle. Based on disponible manufacturing accuracy, it can be recommended that the seat differential angle should not be smaller than 20'. Therefore, the required tolerance for that angle, for manufacturing purposes, should be 20' to 40' approximately.
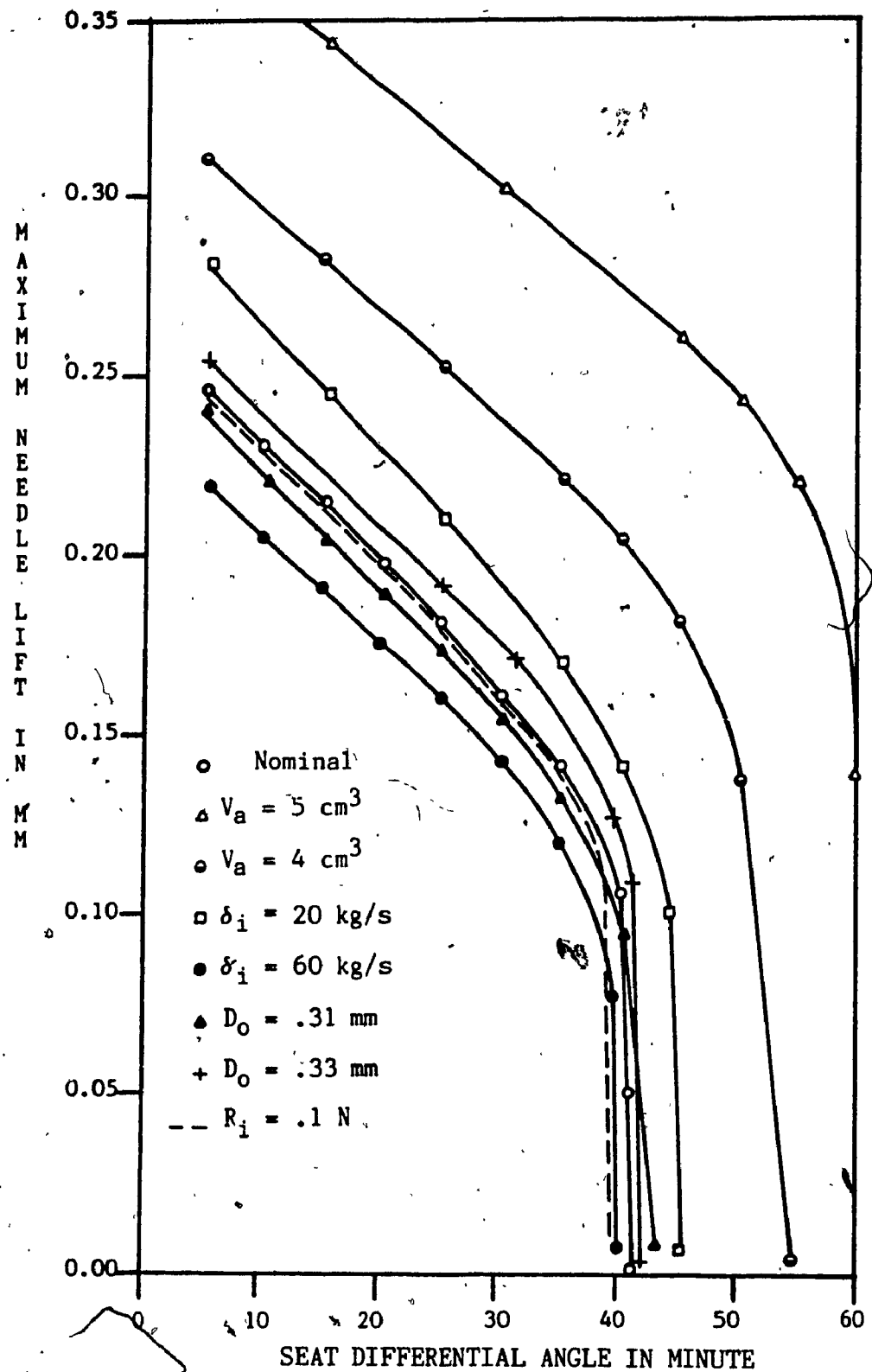
Fig.5.8. Maximum Needle Lift versus Seat Differential Angle
for different Values of Injector Parameters

It would be interesting to note that the informations given in the literature from recognized manufacturers, such as American Bosch Corporation [12], mention the value of the seat differential angle as 25' to 45' regarding the correct "chatter" behaviour on a test-rig. This, however, was found from the manufacturing experience, not as a result of analytical investigation.

The developed method of investigating the dynamic response of the diesel injector can be used for different types of injectors to determine the criteria for the evaluation of quality of injector nozzle for both new injectors and those after some service time on the engine. By changing the accumulator volume according to the type of injector, the test-rig equipped with an LVDT sensor and a peak voltage indicator with digital read-out can be very useful in evaluation of injector nozzle quality.

The application of a computer controlled data acquisition system creates new possibilities in evaluation of diesel injectors. It cannot only evaluate the maximum needle lift in a fast manner, but it can be also used as an injector analyser to better determine the reasons of malfunction of injectors by comparing the needle lift characteristics with that calculated for different values of operational parameters. This is not the main objective of this thesis, however in figure 5.7 an example of such comparison is given; the needle velocity, calculated and displayed easily by the computer as a derivative of needle lift, can make such comparison even more accurate.

Chapter 6

EFFECT OF DYNAMIC RESPONSE
OF A CLOSED INJECTOR ON FUEL ATOMIZATION
IN A DIESEL ENGINE AT LOW SPEED

6.1. Introduction

In this chapter, an attempt is made to show the possibility of improvement in atomization of fuel injected by a closed hole-injector in a diesel engine at idling and starting conditions through optimization of the injector design parameters.

As it was already mentioned in introduction, in a modern high speed diesel engine with direct injection of fuel through multi-hole injectors, there are difficulties in determining the size of orifices in the nozzle because of the need to compromise between two opposing requirements:

a. To allow the injection of a large fuel dose during a short time period without excessive pressure when the engine delivers full power. This requires larger size orifices in the nozzle.

b. To produce a good atomization of small fuel dose injected at low engine speed during starting or idling. This requires smaller size orifices in the nozzle.

This problem is becoming particularly accute for highly rated turbocharged automotive engines in which the fuel dose at maximum power output can be by 50% higher than that injected in atmospheric engines.

When that problem arised several years ago, it was partly solved by introducing closed multi-hole injectors acting as differential pressure valves; i.e. being unstable at low fuel flow rate, and therefore providing fast opening and closing of the injector when the discharge flow rate was not high. This resulted in cutting off the flow of fuel from the injector if high differential pressure across the nozzle orifices was not available. Consequently, at low engine speed, the injector opened for only a short period of time so that it did not allow the pressure in the injector to drop to a low level due to large flow area of orifices which were being made to accomodate the high fuel flow rate at maximum engine power. The situation experienced with injector's pressure at high power, at idling and at starting conditions is well shown in figure 6.1, [7].

There is also another factor making the fuel atomization at low engine speed more difficult. It is the presence of a seat under the needle which throttles the fuel flow at low needle position. Therefore, the differential pressure across the nozzle orifices is reduced. The answer to this undesired throttling effect of the seat could be found in the improvement of the dynamic response of the injector which should provide the injector needle with high acceleration during opening and closing of the injector, particularly at low engine speed. As discussed previously, the opening and closing processes at high engine power are so fast, due to high fuel flow and pressure change rates, that the effect of the seat presence can be neglected. Therefore, the needle seat geometry can be left free for optimization to improve the fuel atomization at low engine speed.
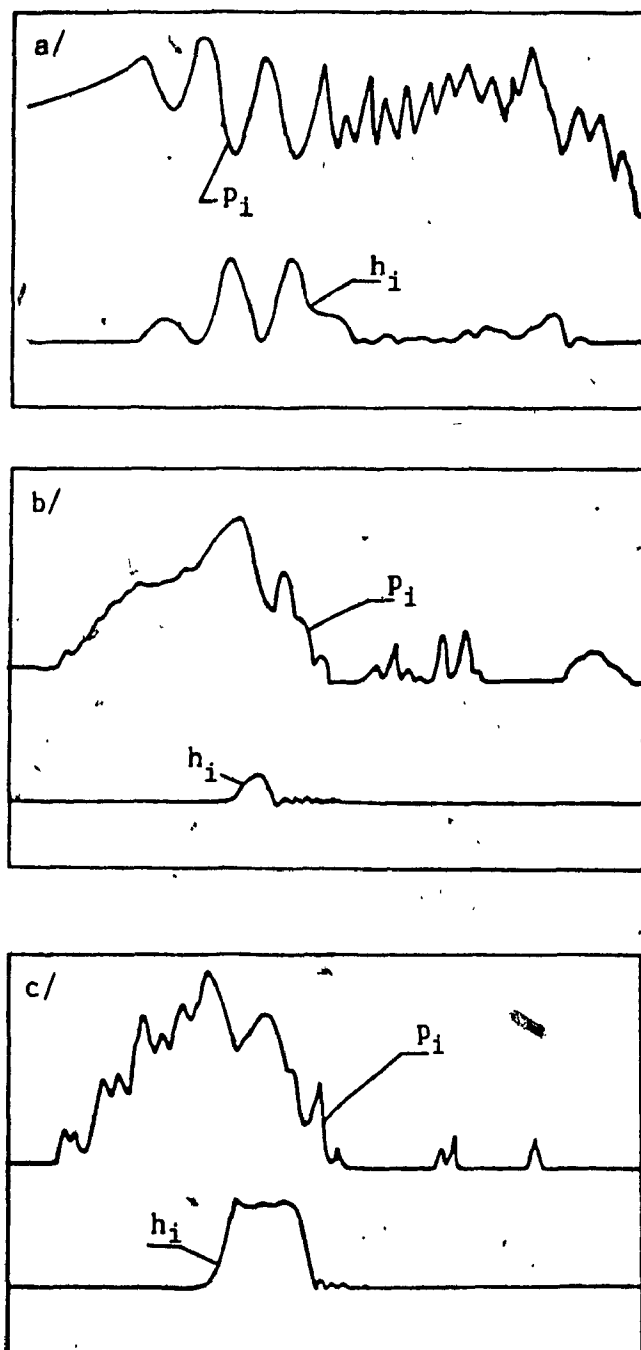
Fig.6.1. Injector Pressure and Needle Lift versus Time

a/ at Starting Conditions

b/ at Idling Conditions

c/ at Maximum Power

(Reproduced from Ref.[7])

6.2. Optimization of Injector Design Parameters
for Low Engine Speed

The objective of optimization of injector design parameters is to obtain such values of these parameters that the fuel injection period is minimized for a particular fuel dose injected at low engine speed. In order to assess the variations of injection duration with respect to the injector parameters, the fuel discharge rate was calculated for the injector specified in chapter 3, by using the mathematical model described in chapter 5.

To obtain the optimization curves, several calculations of fuel discharge rate were made for different values of injector design parameters. The following parameters were selected to be optimized.

1. Differential angle γ between conical surfaces of injector needle tip and nozzle seat.

2. Injector needle mass m_i.

3. Damping coefficient δ_i for needle movement.

As the result of discharge rate computing, a graph is produced showing the variations of the fuel injection duration versus the values of involved parameters, as shown in figure 6.2.

From figure 6.2, one can see that as the values of those three parameters increase, the fuel injection duration also increases. The quantitative evaluation of the impact of design parameters on the time of injection of the fuel dose, allows to select the values of the design parameters in order to obtain the best atomization of injected fuel at low speed of the engine.
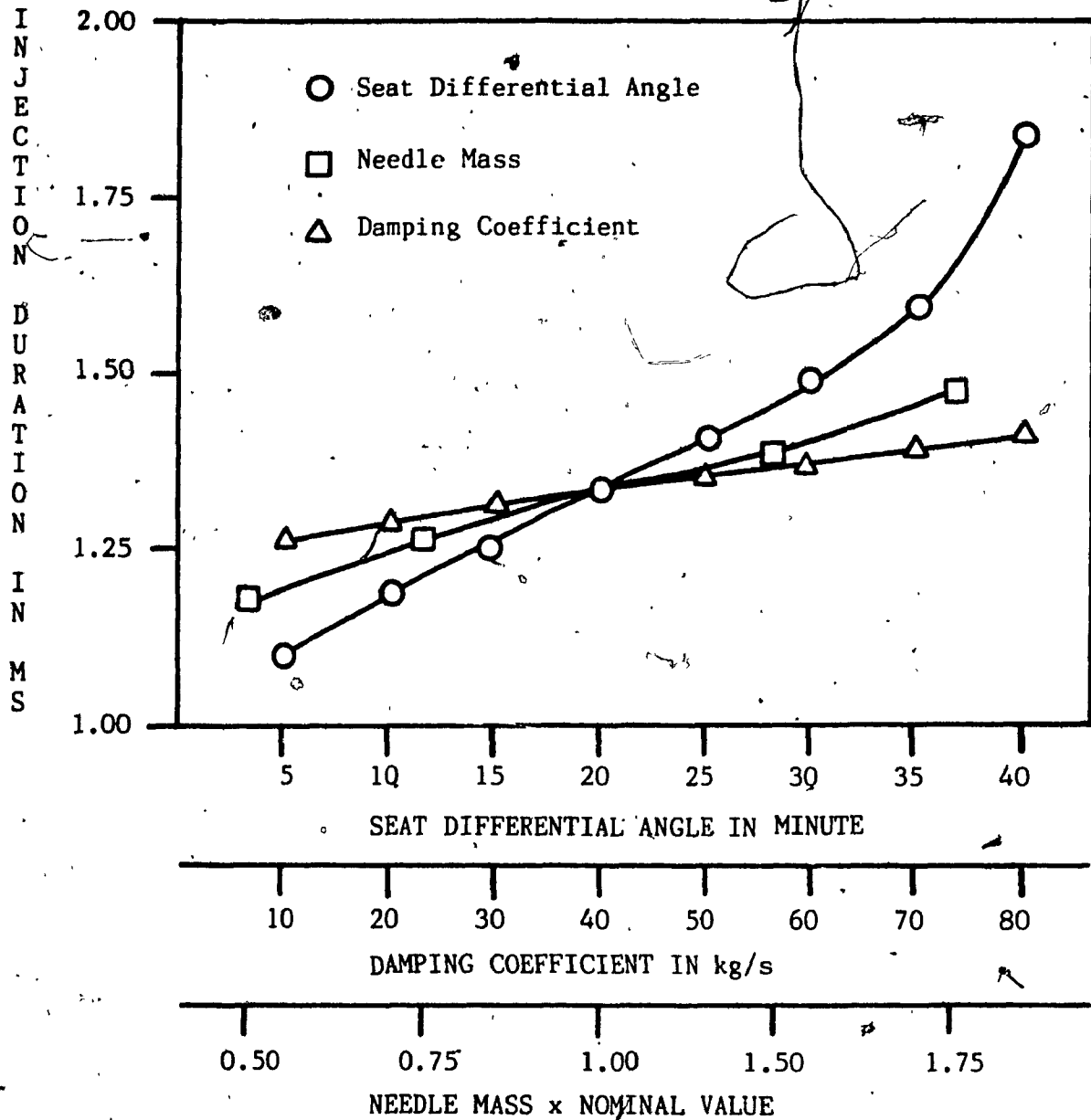
Fig.6.2. Fuel Injection Duration versus
different Values of Injector Parameters

6.3. Calculation of Fuel Discharge Rate at Low Speed
to Assess the Improvement in Fuel Atomisation

To confirm the results obtained from the optimisation procedure performed in section 6.2, the entire mathematical model for full fuel discharge rate calculation developed in chapter 3 was used for comparison of behaviour of two injectors at injection pump idling and starting speeds of 400 RPM and 150 RPM respectively, with following parameters:

Parameter	Injector No.1	Injector No.2
Differential angle [minute]	5	40
Injector needle mass [g]	Nominal	1.5 Nominal
Damping coefficient [kg/s]	10	80

The other parameters were kept constant with values as specified in chapter 3.

As found from the injector dynamic response calculation, it can be predicted that injector No.1 should provide better fuel atomization than injector No.2 at low engine speed.

In this chapter, the characteristic method [16] was chosen to solve the continuity and motion equations (3.1) and (3.3) for the unsteady fuel flow in the injection pipe for following reasons:

The calculation method described and used in chapter 3 can be only applied to solve the pipe flow equations which are simplified by neglecting the convective terms $v\frac{\partial p}{\partial x}$ and $v\frac{\partial v}{\partial x}$ and the friction term $f\frac{v|v|}{2D}$. However, to obtain more accurate results [11], [19], those terms can be taken into account by seeking another method, such as finite difference method or characteristic method, rather than the one described in chapter 3, which is named "Element Storage Method".

Comparison between the characteristic method and the element storage method reveals that each of them has some advantages and disadvantages. The latter method takes less time for computing as compared with the former one because it does not need to calculate the quantities p and v at every section of the pipe as the characteristic method does. However, as described in chapter 3, the element storage method would take more computer memories to store the calculated forward and backward pressure amplitude values at the pipe ends for every calculation time interval. Also, the computer program developed for the element storage method is more complex. This is because the program should provide a mean to retrieve the forward and backward pressure wave amplitude values at proper time to calculate the processes in the pump and in the injector. Whereas, the characteristic method can give more accurate results due to the terms which are not neglected, as mentioned above. Furthermore, because the characteristic method can determine the pressure p and velocity v at different sections of the pipe, the phenomena in the pipe such as occurence of vapor cavities can be examined.

The results of calculations for the pump speed of 400 RPM are presented in figures 6.3, 6.4, 6.5, 6.6, and 6.7 where the variations of pressures in the injector chamber, seat chamber, bag chamber, the needle lift and the fuel discharge rate versus time are being shown. Figure 6.8 shows the variations of the needle lift versus time for pump starting speed of 150 RPM.

From those figures, one can see that at pump speed of 400 RPM injector No.1 has the fuel injection duration of 0.931 ms at the fuel dose of 17 mm^3 which is 7.9% less than the injection duration of 1.011 ms for injector No.2, at the fuel dose of 16.25 mm^3. Also, the mean fuel flow rate for injector No.1 as seen in figure 6.7 is considerably higher than that for injector No.2. For pump starting speed of 150 RPM, the total fuel injection duration for injector No.1 is 4.89 ms which is 15.4% less than the injection duration of 5.78 ms for injector No.2, at fuel dose of 110 mm^3. These results confirm that an injector with low values of seat differential angle, injector needle mass and damping coefficient will provide better fuel atomization than an injector having these design parameters with high values.

The presented injector optimization procedure, together with a full calculation of the fuel discharge process by varying three selected design parameters, is showing the possibilities for diesel injector design improvement at engine idling and starting conditions. This procedure can be extended to other design parameters, if required. Then, the short calculations of injector dynamic response can be performed to draw the conclusions towards the direction of changes for each design parameter to obtain the desired improvement.
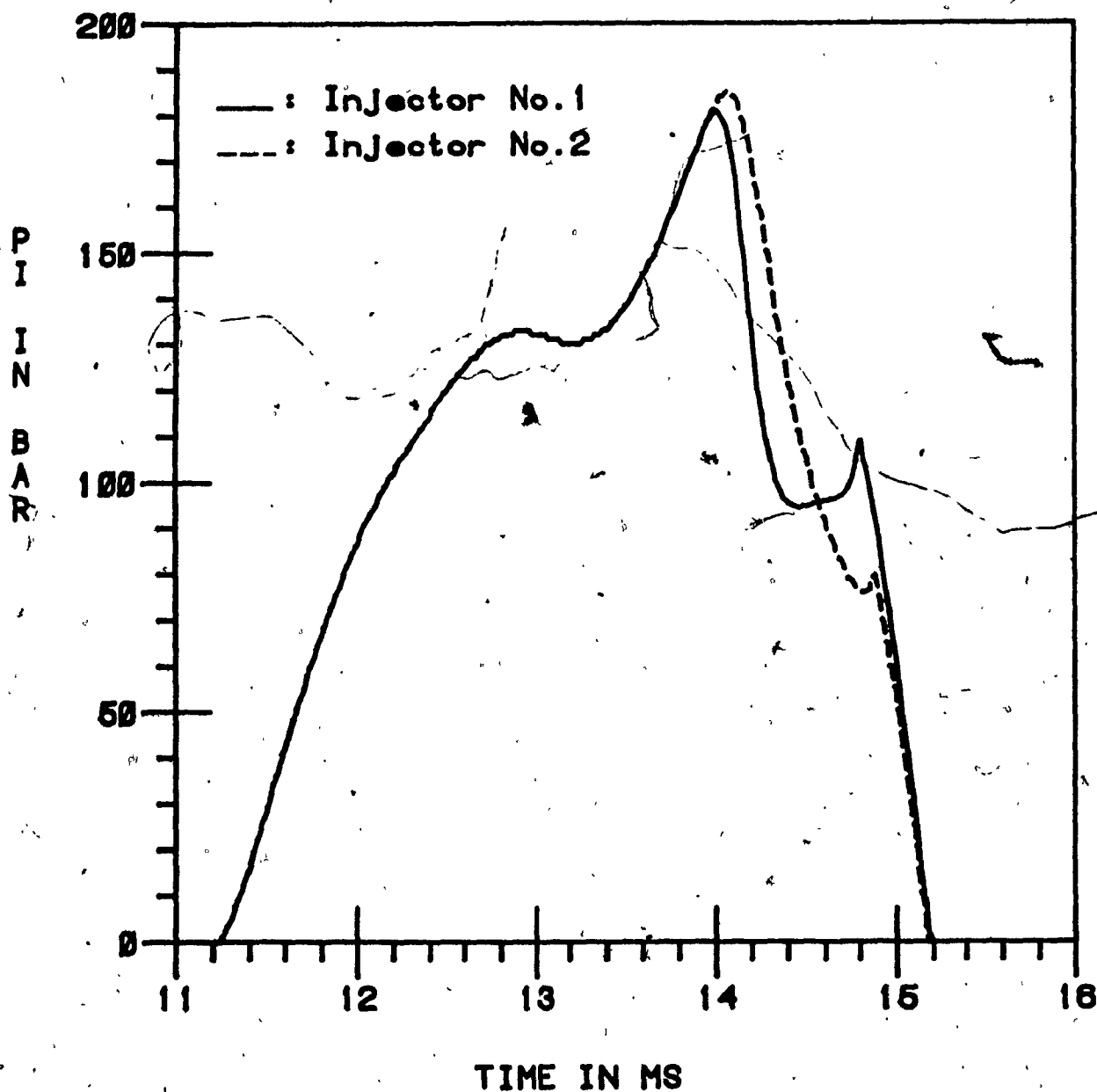
Fig.6.3. Injector Pressure versus Time
at Pump Speed of 400 RPM
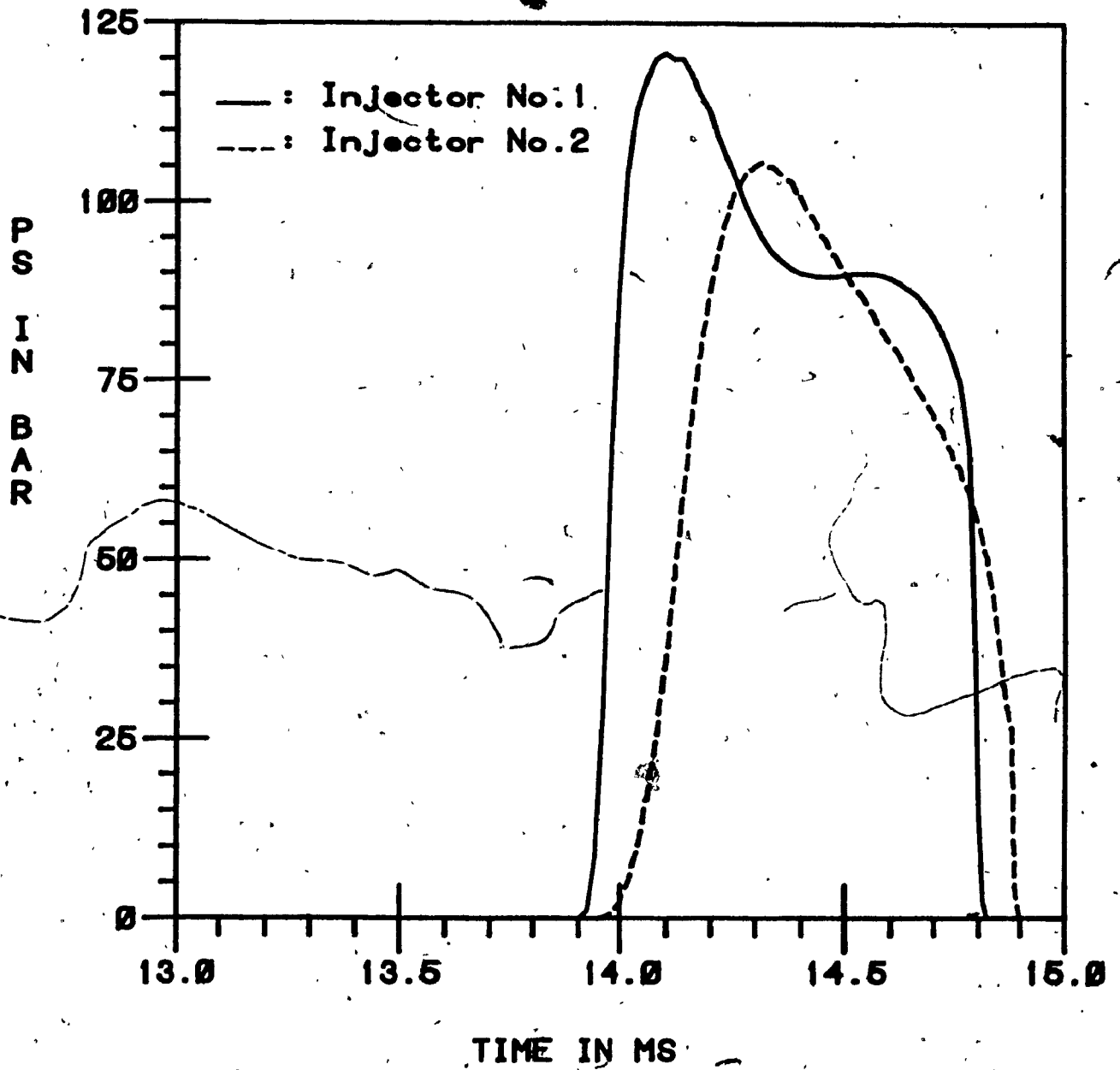
Fig.6.4. Seat Pressure versus Time
at Pump Speed of 400 RPM
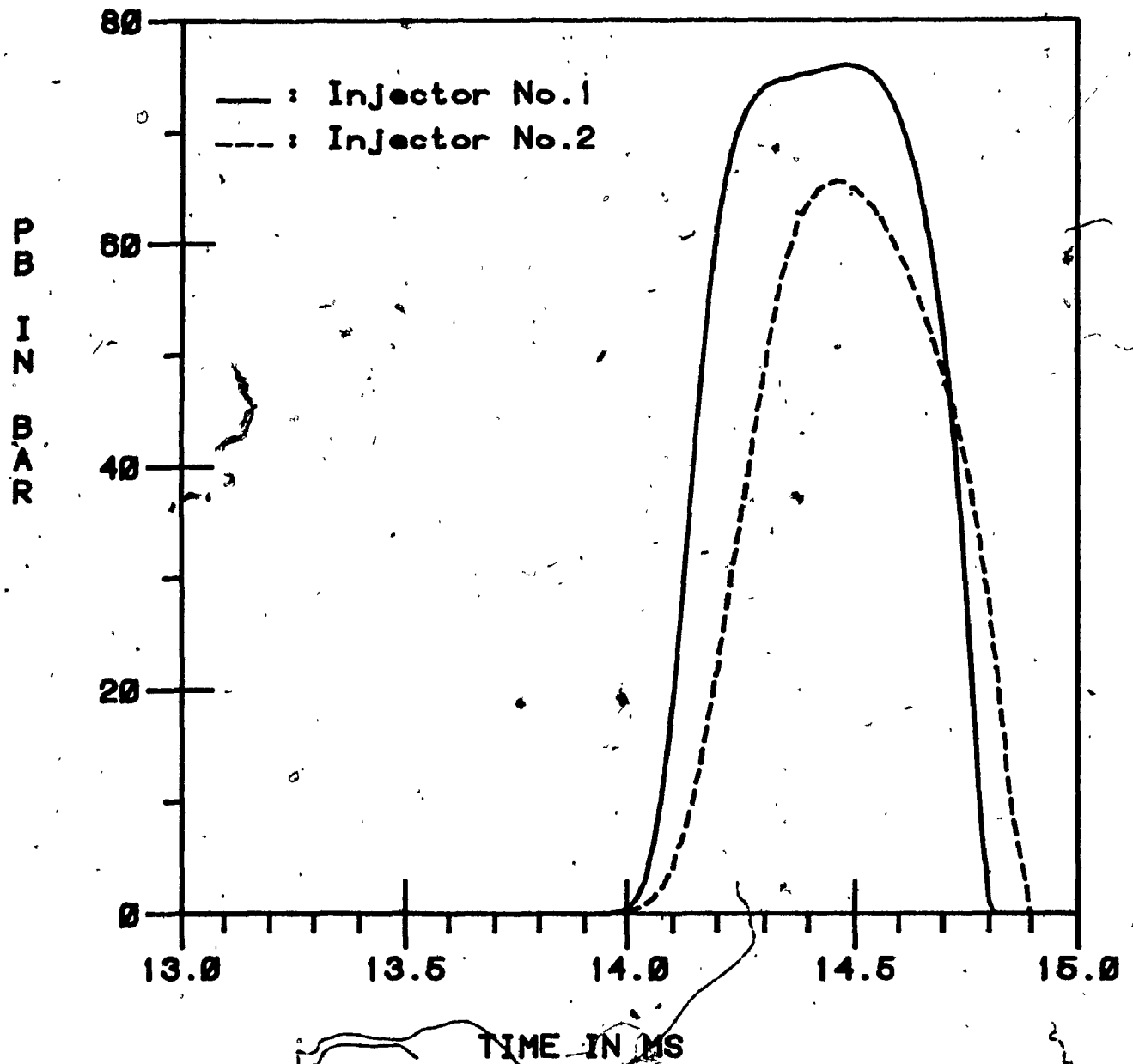
Fig.6.5. Bag Pressure versus Time
at Pump Speed of 400 RPM
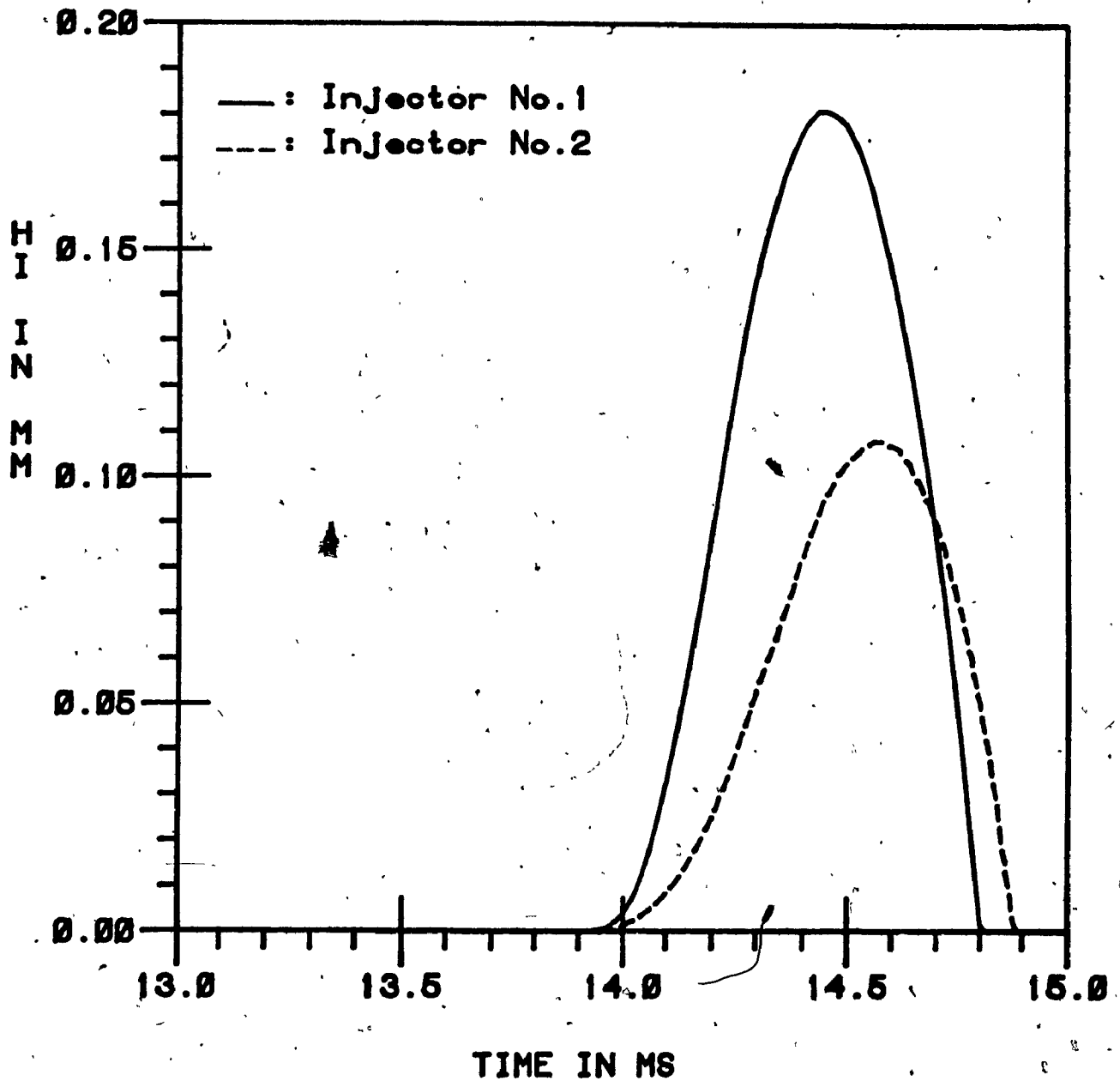
Fig.6.6. Needle Lift versus Time
at Pump Speed of 400 RPM
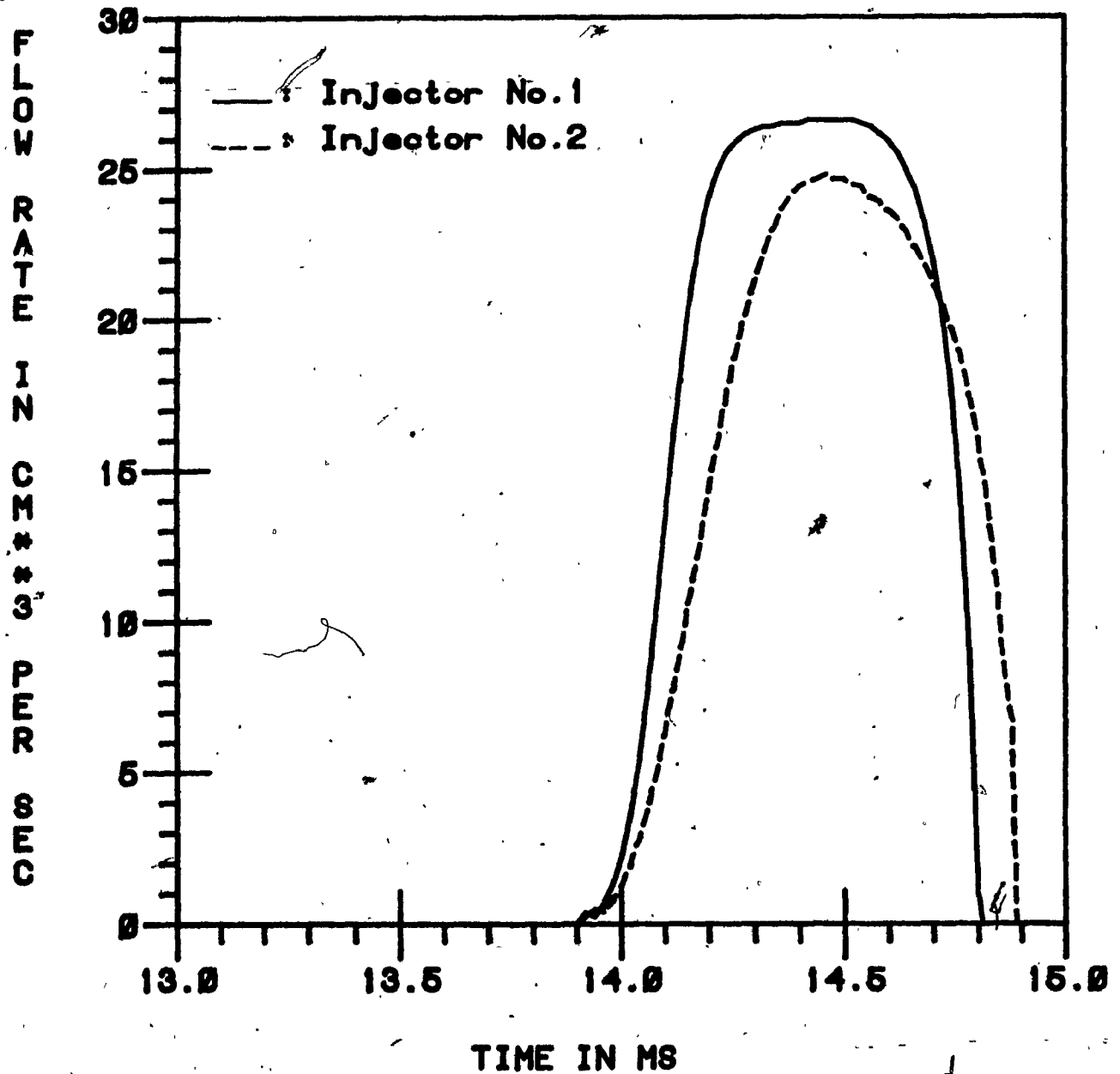
Fig.6.7., Fuel Discharge Rate versus Time
at Pump Speed of 400 RPM
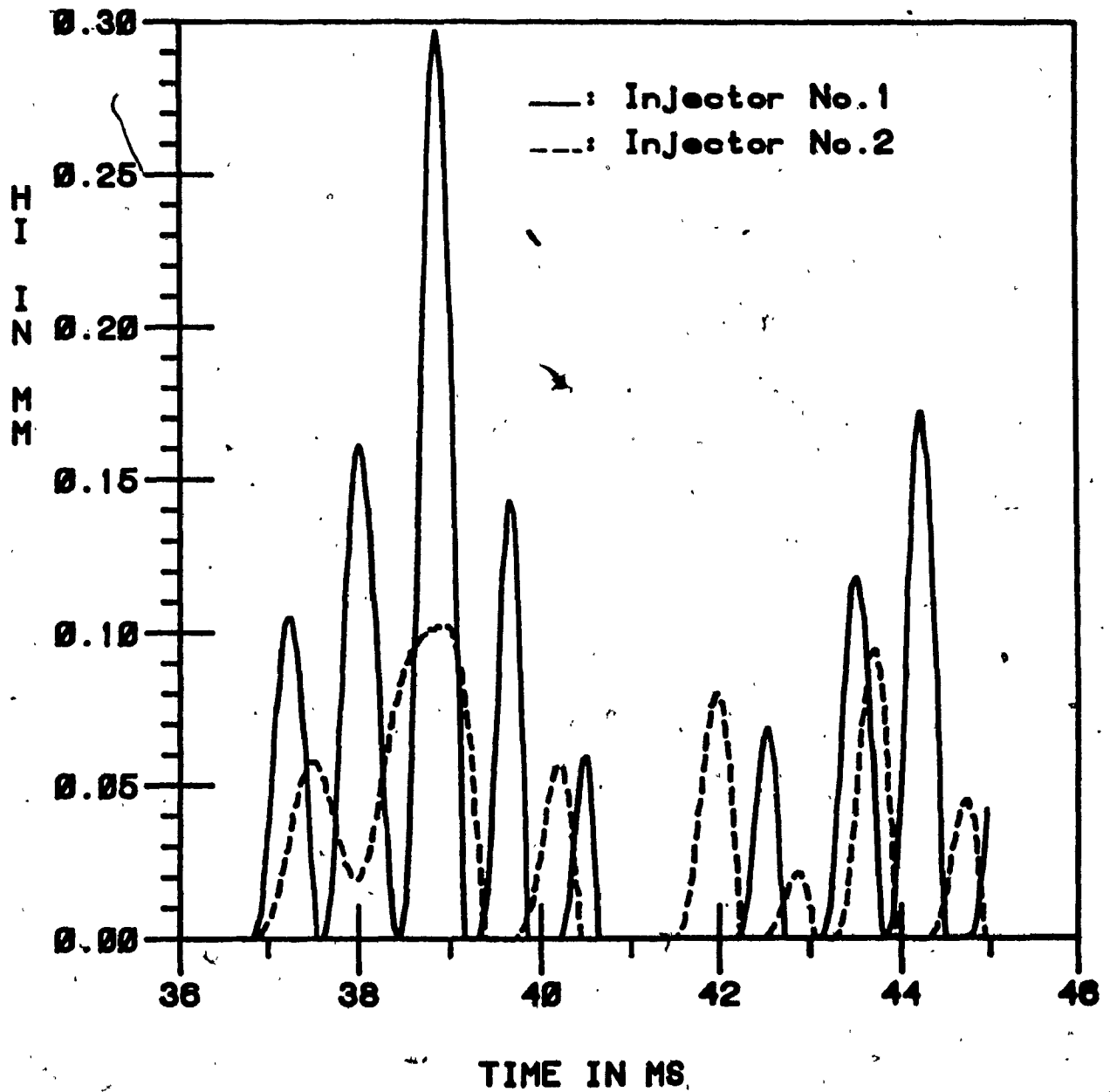
Fig.6.8. Needle Lift versus Time
at Pump Speed of 150 RPM

Chapter 7

OPTIMIZATION OF

DIESEL INJECTOR DESIGN FOR HIGH ENGINE POWER
BASED ON CALCULATION OF FUEL INJECTION RATE
FROM MEASURED PUMP DELIVERY RATE

7.1. Introduction

The optimization of a diesel fuel injection system is considered to be one of the most difficult engineering tasks. This is because the problem must deal with complex high speed, high pressure compressible transient flow process occurring in a sophisticated hydraulic system to provide the engine combustion chamber with precisely metered fuel discharge rate characteristic.

Before 1955, when the computers were not used, the optimization of a diesel fuel injection system was done in a conventional manner by an experienced engineer relying mainly on his feeling being supported by coarse calculations. The main reason for this approach was the large amount of time required to perform detailed fuel discharge rate calculations. Theoretical background for a mathematical model of the fuel injection process has already been developed and solved graphically by Pischinger [4] in 1939 based on the waterhammer theory published by Alliévi [20]. However, even the more convenient graphical method could not encourage professional practitioners to apply a more analytical approach in adapting the fuel injection system to a diesel engine.

After 1955, with spread of computers and with the development of numerical calculation methods [6], [9], [10], engineers started to use these tools in optimization of fuel injection systems. However, a new problem arose due to the overabundance of computation results and time lost for their analysis and evaluation. The use of mathematical optimization methods seemed to be a logical help. However, it proved that those methods are not very effective due to the great number of interrelated factors affecting the outcome of modelling. As a result, project engineers developing diesel engines were not very eager to use computing in development of the fuel injection systems. They still preferred to rely on their professional feelings. It became evident that more work has to be done to provide diesel engine developers with more effective analytical tool.

In searching for a better solution, as computer technology developed, one would conclude that some improvement could be made by extending computer use in the optimization procedure. This means the application of computers not only in calculations but also in data acquisition, in graphics, etc. An example of such application will be described in this chapter related to a case of analysis and optimization of a diesel injector design.

7.2. Methodology

To calculate the full fuel injection rate characteristic in the regular manner, the pumping process should be calculated first [21], as described in chapter 3, based on the design parameters of the fuel injection pump. Then, having the shape of the forward propagating pressure wave, the dynamic response of the injector would be calculated together with the resulting fuel discharge process. However, this procedure takes a lot of computing time, and might be considered unnecessary for the case of optimization of the injector design only; i.e. when the fuel injection pump is being left without changes. Such situation happens very often, for example when the diesel engine producer wants to replace the supplier of injectors without changing the type of injection pump being used.

In that case, if the forward propagating pressure wave produced by the pump could be first precisely measured, instead of being calculated from the pump design parameters, and then the recorded data would be loaded into the computer program to calculate the injector response. The total computing procedure would be considerably shortened saving the time required to determine the pump design parameters, and also giving more accurate results. This would be the task for a computer controlled data acquisition system to insure a convenient and accurate recording of fuel pressure transient process in the fuel injection pump, and then for a computer graphic system to show these records on the screen, to print them or to draw them using a computer controlled plotter. Finally, a transfer of the recorded pump output data into the calculation program of a

main frame computer would be made to facilitate the fast computing of fuel discharge rate characteristics.

One of the main difficulties in this procedure would be the acquisition of the forward propagating pressure wave produced by the pump, which should not be distorted by the backward propagating pressure wave reflected from the injector. To achieve that aim, a specially made three meter long injection pipe was introduced between the fuel injection pump and the injector, as shown in figure 7.1. At control surfaces I-I and II-II, two pressure transducers were installed and connected to the data acquisition system to record the pressures at these injection system sections.

The length of the pipe was selected in such a way that the pressure wave, produced by the pump and then reflected from the injector, could not return to the pump before the end of the pumping process. This condition can be expressed as follows:

$$L > \frac{\bar{a}\Delta t_{inj}}{2} \qquad (7.1)$$

where the time for injection is given by:

$$\Delta t_{inj} = \frac{\varphi_{inj}}{360} \frac{60}{N} \qquad (7.2)$$

and φ_{inj} is the cam rotation angle during injection.

There was another problem that had to be overcome when using a long injection pipe, which was related to the residual pressure existing within the system after the end of injection period. In a regular injection system which is equipped with a relatively short
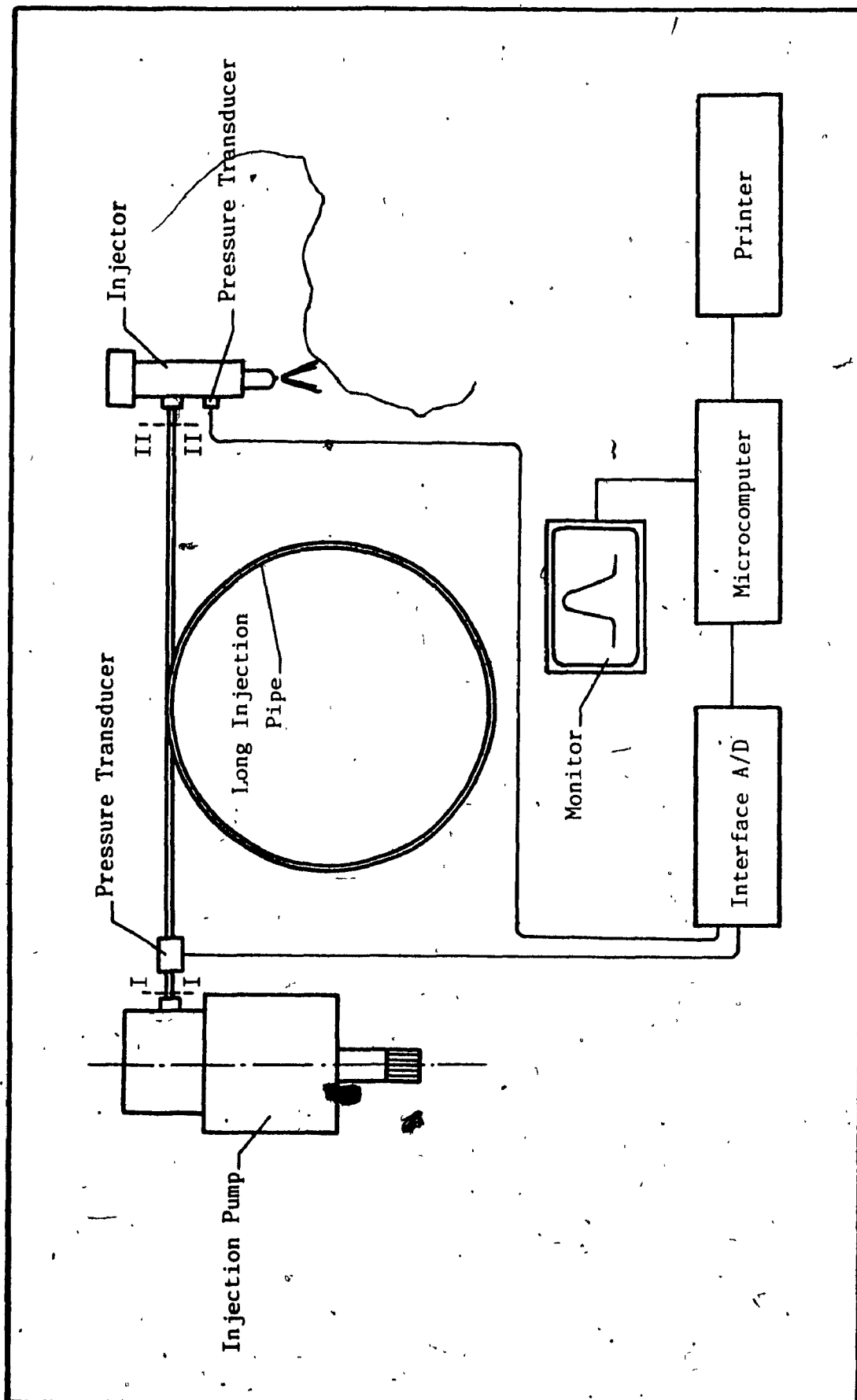
Fig.7.1. Test Set-up with Data Acquisition System

injection pipe, the pressure within the system drops to sub-atmospheric pressure at the end of injection process because of small expansion volume of fuel compressed inside the system. However, with the long injection pipe the volume of compressed fuel is greater and the residual pressure stays at higher level.

The in-line pump is equipped with a delivery valve which creates a retraction volume at the end of fuel delivery period and causes the residual pressure to drop to the sub-atmospheric value in a regular fuel injection system. If this retraction volume is smaller than the expansion volume of compressed fuel, as it is with long pipe, then a residual pressure higher than atmospheric pressure will exist in the system. To reduce the residual pressure in the system to the sub-atmospheric level after the end of injection process, the injector opening pressure could be reduced as required when the forward propagating pressure wave is recorded by the data acquisition system.

To determine at what level the residual pressure, or the fuel vapor filled volume, is produced in the fuel injection system after the end of injection period, the injector closing pressure and the expansion volume of fuel compressed inside the injection system should be calculated according to the following formulae:

— Injector closing pressure:

$$P_{cl} = \frac{P_{is}}{F_i} \qquad\qquad (7.3)$$

– Expansion volume of compressed fuel:

$$V_{exp} = \frac{V_{sys}}{E} (p_{cl} - p_a) \qquad (7.4)$$

The expansion volume for the system with long injection pipe, together with the opening pressure should provide the injection system with the same vapor filled volume or residual pressure as that found for the regular injection system. This is the necessary condition to obtain the forward pressure wave identical to that obtained from the pump fitted with the regular injection pipe.

In the case described in this research, a rotary distributor fuel injection pump is used, which equalizes the residual fuel pressure in the system with the pump supply pressure after every injection process. In that case, the residual pressure cannot vary and does not affect the pumping process.

7.3. Data Acquisition System

In order to monitor the forward propagating pressure wave in the pump, a strain gage based AVL pressure transducer specially designed not to increase the volume of the injection system, has been installed just at the exit of the pumping section, i.e. at control surface I-I, and connected to the data acquisition system, as shown in figure 7.1. This data acquisition system consists of a Northstar Horizon microcomputer with an A/D interface unit developed in the Centre for Industrial Control at Concordia University. It allows to acquire the short transient processes of about 3 ms duration time with a sampling rate of approximately 9000 Hz. The forward propagating pressure wave which was recorded with the help of a Vectrix graphics system and printed with a dot-matrix Epson printer, is shown in figure 7.2.

In figure 7.3, the test set-up installed on the test bench is shown including the data acquisition system described above.
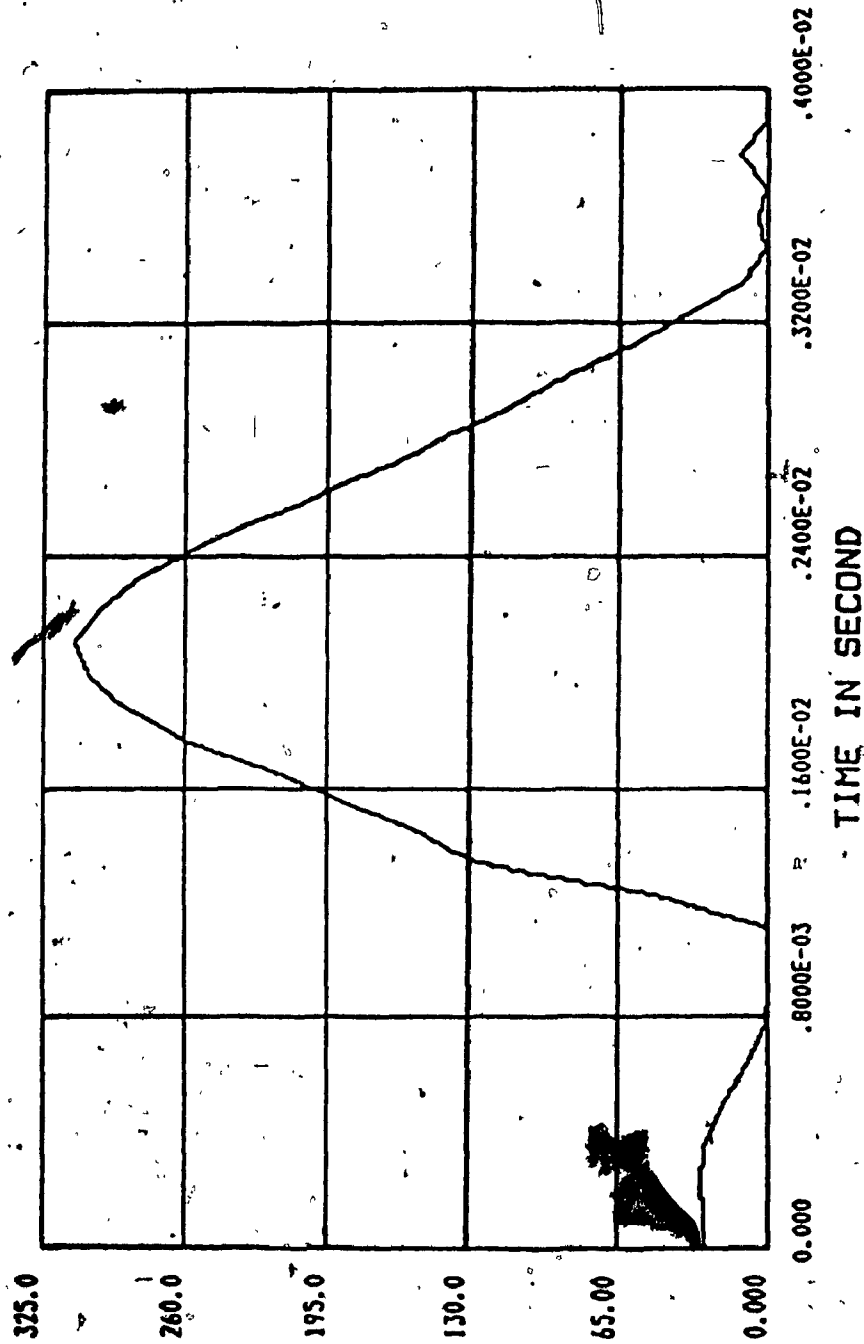
Fig.7.2: Forward Propagating Pressure Wave Recorded by
Data Acquisition System at Pump Speed of 900 RPM
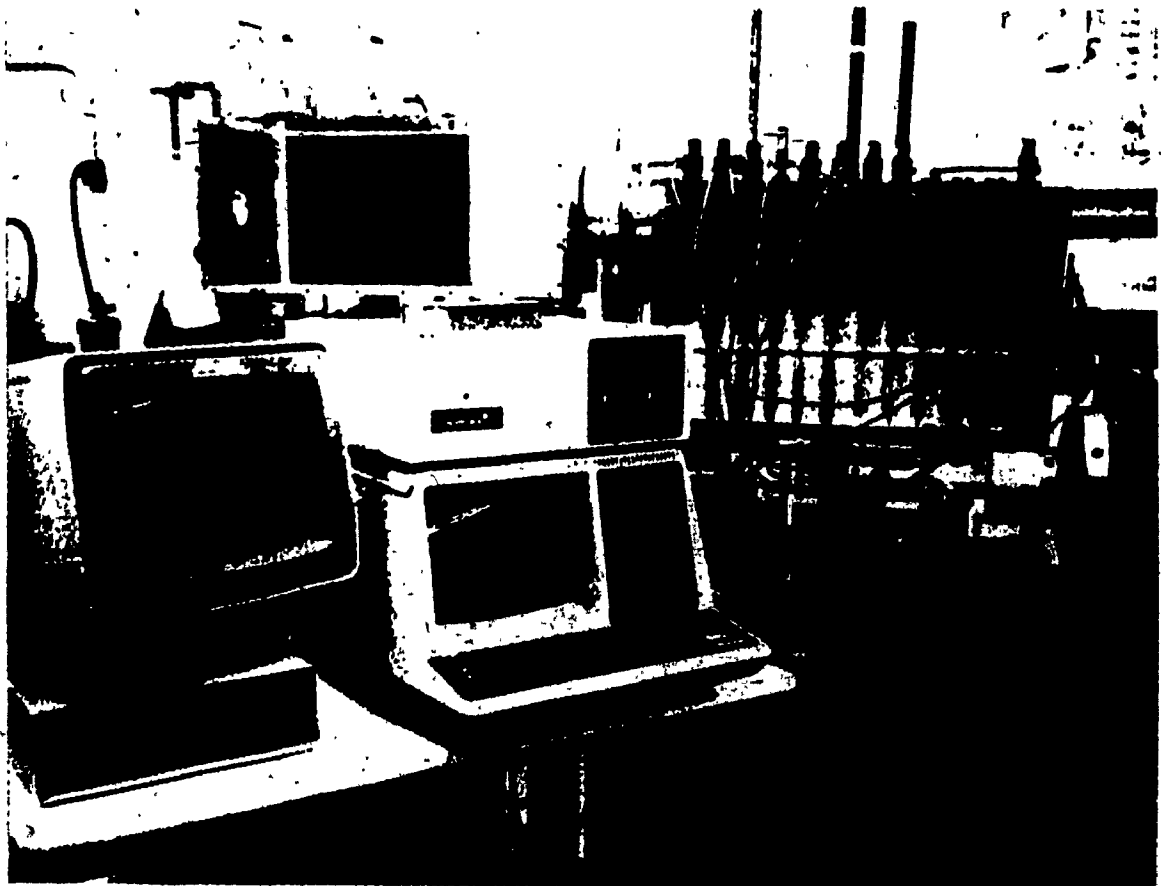
Fig. 7.3. Pictorial View of the Test Set-up

7.4. Mathematical Model

A set of differential equations describing the continuity and force equilibrium conditions for the fuel injection system was developed in chapter 3. For the case of optimization of diesel injector design parameters, only equations for the injector side of the system are used. The dynamic response of the injector is then calculated using the forward propagating pressure wave data acquired, instead of being calculated. Since the injection pipe in a real injection system is short, the backward propagating pressure wave would come to the injection pump before the end of pumping process. Therefore, the calculation should include the modification of the pump produced pressure wave arriving at the injector after the time $t = \frac{2L}{a}$; i.e. after being affected by the pressure wave reflected at the injector.

The following equations are used to calculate the fuel discharge rate characteristics:

1. Injector chamber continuity equation:

$$\frac{dp_i}{dt} = \frac{E}{V_\gamma}\left[F_{II}K(2p_{if} - p_i + p_{io}) - (F_i - F_{so})v_i - \right.$$

$$\left. - \zeta_{si}\mu_{si}F_{fsi}\sqrt{\frac{2}{\rho}|p_i - p_s|}\right] \qquad (7.5)$$

where,

$$\zeta_{si} = 1 \qquad \text{if } p_i > p_s$$

$$\varsigma_{si} = -1 \quad \text{if } p_i < p_s$$

2. Seat chamber continuity equation:

$$\varsigma_{si}\mu_{si}F_{fsi}\sqrt{\frac{2}{\rho}|p_i - p_s|} = \varsigma_{se}\mu_{se}F_{fse}\sqrt{\frac{2}{\rho}|p_s - p_b|} +$$

$$+ (F_{so} - F_{si})v_1 \qquad (7.6)$$

where,

$$\varsigma_{se} = 1 \quad \text{if } p_s > p_b$$

$$\varsigma_{se} = -1 \quad \text{if } p_s < p_b$$

3. Bag chamber continuity equation:

$$\frac{dp_b}{dt} = \frac{E}{V_b}\left(\varsigma_{se}\mu_{se}F_{fse}\sqrt{\frac{2}{\rho}|p_s - p_b|} - F_{si}v_1 - \right.$$

$$\left. - I\varsigma_o\mu_oF_{fo}\sqrt{\frac{2}{\rho}|p_b - p_a|}\right) \qquad (7.7)$$

where,

$$\varsigma_o = 1 \quad \text{if } p_b > p_a$$

$$\varsigma_o = 0 \quad \text{if } p_b < p_a$$

4. Injector needle motion equation:

$$\frac{dv_i}{dt} = \frac{1}{m_i}\left[p_i(F_i - F_{so}) + p_s(F_{so} - F_{si}) + p_bF_{si} - \right.$$

$$\left. - P_{is} \pm R_i - k_{is}h_i - \delta_1v_1\right] \qquad (7.8)$$

and

$$\frac{dh_i}{dt} = v_i \tag{7.9}$$

and

$$p_{ib} = p_i - p_{if} - p_{io} \tag{7.10}$$

5. Fuel discharge rate from injector to atmosphere:

$$q_{fo} = I\mu_o F_{fo}\sqrt{\frac{2}{\rho}(p_b - p_a)} \tag{7.11}$$

The above differential equations are utilized to produce the solutions for q_{fo} and for the optimization of the injector design parameters. A computer program is developed based on the four-step Runge Kutta approximation. The program should include the case where the forward propagating pressure wave is distorted by the backward propagating pressure wave as occurs in a real system with a short injection pipe.

Calculation is performed at the injector control surface II-II for consecutive time intervals. For the time period from $t=0$ to $t=\frac{2L}{a}$, the forward propagating pressure wave p_{if} is used as recorded at the pump control surface I-I with long injection pipe, i.e. without any impact of the backward pressure wave reflected from the injector. After the time period $t=\frac{2L}{a}$, the calculation is continued using the forward pressure wave already distorted by the reflected pressure wave. This modified forward propagating pressure wave has been determined by superimposing of the reflected pressure wave on the pressure wave recorded previously with the long injection pipe.

It should be mentioned that the forward propagating pressure wave measured with long injection pipe and modified by the backward pressure wave is a little different from that measured with short injection pipe, and the difference is mainly related to the impact of the volume in the delivery chamber which is small. This difference, though might affect to very small extend the absolute value of the injector discharge rate, dose not have any impact on the value of the optimization procedure of the injector which is based on the comparison of results obtained when varying the design parameters of the injector.

7.5. Optimisation of Diesel Injector Design Parameters

One of the objectives in-optimization of diesel injector design is to obtain such values of design parameters that the injection time duration is minimized, for a particular injected fuel dose. There are some mathematical optimization techniques which could be used. However, they are difficult and ineffective when being used in a complex system. Therefore, the procedure proposed in this chapter is based on the so-called logical approach. This approach is described as follows:

1. The fuel discharge process is simulated mathematically for the nominal design parameters of the injector, i.e. according to its design specification.

2. Several calculations of the fuel discharge process are made varying the value of only one design parameter.

3. Calculations are repeated varying the values of the other design parameters.

4. The results are plotted versus the varying values of each design parameter.

In this calculation, the injector specified in chapter 3 was used and the following parameters were selected to be optimized:

- Injector needle mass
- Injector spring constant
- Injector needle seat outer diameter
- Injector opening pressure

As a result of computing, a graph was produced showing the variations of the fuel injection time duration versus the values of the involved parameters, as shown in figure 7.4.

Referring to figure 7.4, one can see that as the injector opening pressure and injector spring constant increase, the injection time duration tends to decrease. In contrast, as the injector seat outer diameter and injector needle mass increase, the duration of the injection time also increases.
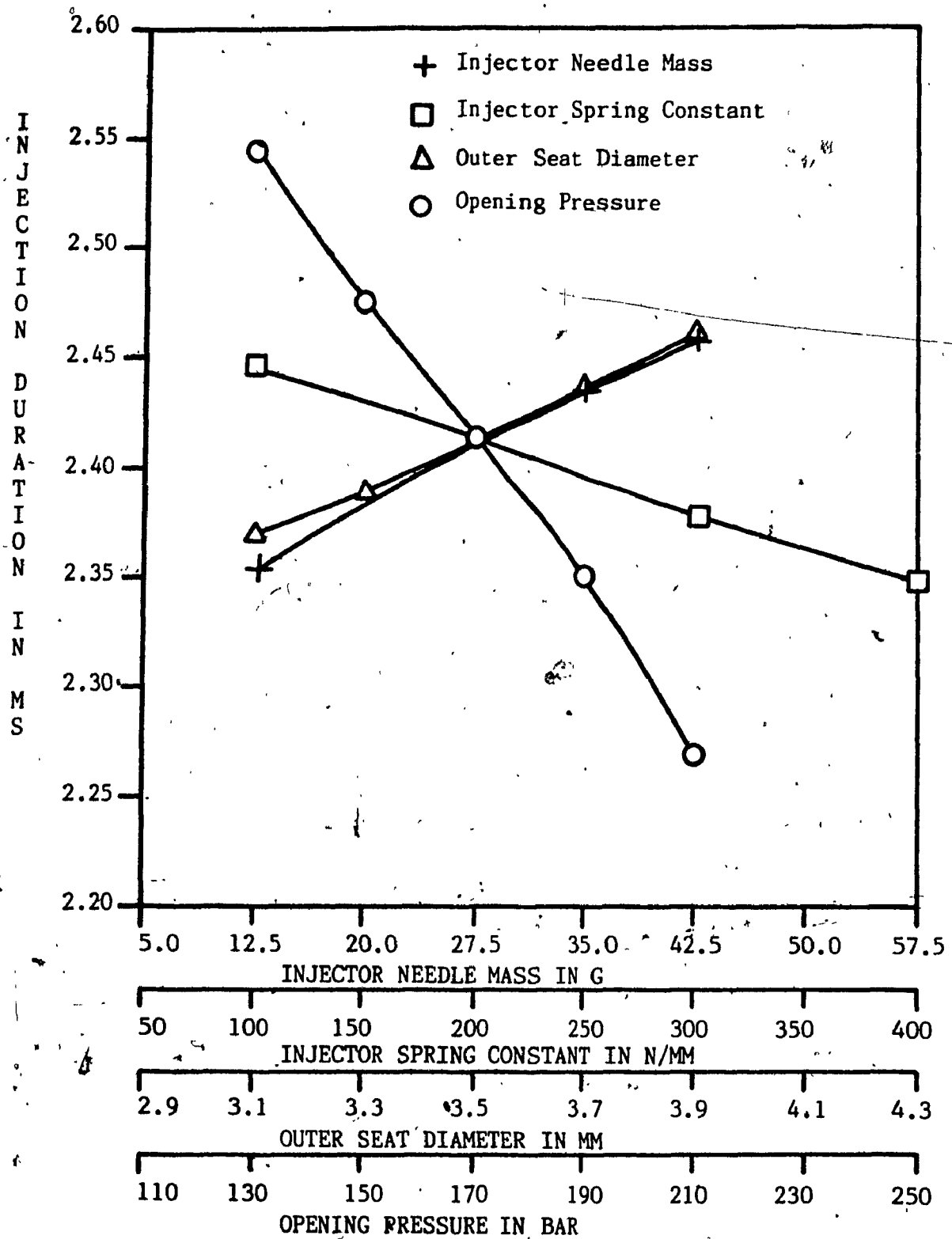
Fig.7.4. Fuel Injection Duration versus
varying Values of Injector Design Parameters

7.6. Discussion of Calculated Results

Based on the graph shown in figure 7.4, a conclusion could be drawn by an engine developer regarding the options he has in the modification of an injector, in order to achieve the required change in the shape of the fuel discharge rate characteristic.

As an example of more complete optimization work, to improve the injector design some criteria are proposed as follows:

1. Fuel discharge duration should be as short as possible at full engine speed and power, i.e. at nominal fuel dose, without significant pressure increase and without increase of the nozzle orifices diameter.

2. Fuel injection duration should be as short as possible at engine idling, i.e. at idling fuel dose, providing that the nozzle orifices are not changed.

3. The injector should be unstable at low engine speed.

4. No secondary fuel injection should occur at engine utility power range.

5. There should be no gas penetration through the orifices into the nozzle, i.e. fuel pressure in the nozzle should be always higher than the gas pressure in the engine cylinder, when the nozzle remains open.

It is obvious that only the first three of these criteria are quantitative and can be fulfilled using the described optimization technique and the injector stability analysis described in the next chapter. The remaining two must be considered as qualitative and,

therefore, could be investigated only by performing the flow rate characteristic calculations or measurements for every configuration of the injector and for all operational conditions.

Computing the fuel injection rate for different design parameters of the injector leads to an optimization graph which is shown in figure 7.4 for the injection time period at full engine power (first criterium). Based on this graph, a researcher cannot only predict the effect of variation of a single design parameter of injector on the fuel discharge rate characteristic, but he can also calculate the combined effect of variations of several parameters when knowing in which direction he should change them. Together with similar graphs made for other criteria, he can fully optimize the design parameters of the injector.

Chapter 8
STABILITY STUDY OF DIESEL INJECTOR

8.1. Introduction

Diesel injector is built as a differential pressure valve, i.e. its opening pressure is higher than its closing pressure. This injector's feature is leading to the instability of the injector when it is supplied with low fuel flow rate as is the case at some engine operational conditions like starting or idling speed. At those conditions, the instability of the injector is beneficial to the engine operation because it leads to fast opening and closing of the injector, thus limiting the fuel injection at low discharge rate and at poor atomization. When fuel flow rate increases, the injector does not need to control the injection pressure, the needle is reaching the higher lift, and it is becoming stable. The critical fuel flow rate at which injector is becoming stable, is an important factor in evaluation of the injector's ability to control the fuel atomization. It can also provide information about the injector's quality.

The discussed phenomenon leads to the investigation of the "chatter" behaviour of the injector needle in term of its instability. According to the industrial experience, the injector needle is said to be stable if it is lifted off the nozzle seat to a determined height by a starting fuel flow, and then becomes stationary at that level if this flow rate continues. If the injector needle is lifted, and then it returns immediately to the nozzle seat when the flow continues, it is said to be unstable. For low flow rate, the injector behaviour can be seen as

shown in figure 5.3.

In this chapter, the stability of the injector needle is studied and stability criteria are established. From these criteria, the effects of the injector design and operational parameters on the "chatter" behaviour of the injector are investigated.

The injector's stability was studied by Höfken [14], as described in chapter 2. However, Höfken did not include the correct needle seat parameters in his analysis. Because, as discussed in chapter 4, the seat geometry is a deciding factor in the dynamic response of an injector, the simplified mathematical model for injector stability study proposed by Höfken cannot be considered acceptable. Therefore, new mathematical model was developed and used for simulation in order to optimize the fuel injector design from the point of view of injector stability requirements, as shown in the next sections.

8.2. Injector Stability Criteria

Considering the model described in figure 3.7, the following assumptions are made in developing the stability criteria for the injector needle.

1. Firstly, the seat pressure is assumed to be equal to the pressure in the bag chamber. This assumption is made to simplify the solution. Otherwise, the analysis would become very complex. However, the flow restrictions at the seat inlet and exit are combined according to the following analysis.

Referring to figure 3.7, the pressure drop between the injector and bag chambers $(p_i - p_b)$ can be written as:

$$p_i - p_b = (p_i - p_s) + (p_s - p_b) \tag{8.1}$$

Since the flow rate q for turbulent flow is related to pressure drop Δp by:

$$\Delta p = \frac{\varrho}{2}\left(\frac{q}{\mu F}\right)^2$$

If $\mu_{sf} F_{sf}$ is denoted as an effective flow area, a product of flow coefficient and geometric flow area, between the injector and bag chambers, the equation (8.1) can be rewritten as:

$$\frac{\varrho}{2}\left(\frac{q}{\mu_{sf} F_{sf}}\right)^2 = \frac{\varrho}{2}\left(\frac{q}{\mu_{si} F_{fsi}}\right)^2 + \frac{\varrho}{2}\left(\frac{q}{\mu_{se} F_{fse}}\right)^2$$

or,

$$\left(\frac{1}{\mu_{sf}F_{sf}}\right)^2 = \left(\frac{1}{\mu_{si}F_{fsi}}\right)^2 + \left(\frac{1}{\mu_{se}F_{fse}}\right)^2$$

or,

$$\mu_{sf}F_{sf} = \left[(\mu_{si}F_{fsi})^{-2} + (\mu_{se}F_{fse})^{-2}\right]^{-\frac{1}{2}}$$

where F_{fsi} and F_{fse} are functions of needle lift h_1 and given by equations (3.41) and (3.45). Therefore, $\mu_{sf}F_{sf}$ is also a function of h_1. Let $F(h_1)$ denote this function, i.e.

$$F(h_1) = \mu_{sf}F_{sf} = \left[(\mu_{si}F_{fsi})^{-2} + (\mu_{se}F_{fse})^{-2}\right]^{-\frac{1}{2}} \qquad (8.2)$$

2. Secondly, the forward propagating wave v_{fII} coming from the pump to the injector at control surface II-II, as indicated in figure 3.7, is assumed to have a step shape, i.e. its amplitude is constant. Together with backward propagating wave reflected in the injector, the total velocity wave amplitude is:

$$v_{II} = v_{fII} + v_{bII}$$

3. Thirdly, the injection pipe is assumed to be so long that the forward propagating wave modified by the backward wave after being reflected at the pump, could not arrive to the injector.

With these assumptions, the continuity and motion equations are written in the next section

8.2.1. Continuity Equations

8.2.1.1. For Injector Chamber

Considering figure 3.7 with the first assumption, the continuity equation written for the injector chamber is:

$$F_{II}v_{II} = \frac{V_i}{E}\frac{dp_i}{dt} + (F_i - F_{so})\frac{dh_i}{dt} + F(h_i)\sqrt{\frac{2}{\rho}(p_i - p_b)} \qquad (8.3)$$

It is assumed that a disturbance is applied to the system remaining at steady-state conditions. Then due to the disturbance, the injector needle displacement, and the injector and bag pressures will change. Two subscripts "s" and "d" are used in combination with other notations to indicate the values at steady-state conditions and the small changes of those values from the steady-state values due to the disturbance, respectively. Then, at any instant:

$$h_i = h_{is} + h_{id} \qquad (8.4)$$

$$p_i = p_{is} + p_{id} \qquad (8.5)$$

$$p_b = p_{bs} + p_{bd} \qquad (8.6)$$

$$\frac{dh_i}{dt} = \frac{dh_{id}}{dt} \qquad (8.7)$$

$$\frac{dp_i}{dt} = \frac{dp_{id}}{dt} \qquad (8.8)$$

$$\frac{dp_b}{dt} = \frac{dp_{bd}}{dt} \qquad (8.9)$$

The fluid velocity, from equations (3.8), (3.9), (3.14), (3.15) and (3.16):

$$v_{II} = \frac{1}{\rho \bar{a}}(2p_{if} + p_{io} - p_i)$$

With a disturbance, substituting equation (8.5) into the equation above, one gets:

$$v_{II} = \frac{1}{\rho \bar{a}}(2p_{if} + p_{io} - p_{is}) - \frac{p_{id}}{\rho \bar{a}}$$

Let,

$$v_{IIs} = \frac{1}{\rho \bar{a}}(2p_{if} + p_{io} - p_{is}) \tag{8.10}$$

and,

$$v_{IId} = -\frac{1}{\rho \bar{a}} p_{id} \tag{8.11}$$

Then,

$$v_{II} = v_{IIs} + v_{IId} \tag{8.12}$$

In this equation, v_{IIs} is the fluid velocity at steady-state conditions whereas v_{IId} is the change in fluid velocity due to a disturbance.

a. Steady-State Analysis

At steady-state conditions, the continuity equation (8.3) can be written as:

$$F_{II}v_{IIs} = F(h_{is})\sqrt{\frac{2}{\rho}(p_{is} - p_{bs})}$$

Let,

$$\Delta p_{ibs} = p_{is} - p_{bs}$$

Then,

$$F_{II} v_{IIs} = F(h_{is})\sqrt{\frac{2}{\rho}\Delta p_{ibs}} \qquad (8.13)$$

b. **With Disturbance**

Substituting equations from (8.4) to (8.12) into equation (8.3),

$$F_{II}(v_{IIs} + v_{IId}) = \frac{V_i}{E}\frac{dp_{id}}{dt} + (F_i - F_{so})\frac{dh_{id}}{dt} +$$
$$+ F(h_{is}+h_{id})\sqrt{\frac{2}{\rho}(p_{is} + p_{id} - p_{bs} - p_{bd})}$$

Let,

$$\Delta p_{ibd} = p_{id} - p_{bd}$$

Then,

$$F_{II}(v_{IIs} + v_{IId}) = \frac{V_i}{E}\frac{dp_{id}}{dt} + (F_i - F_{so})\frac{dh_{id}}{dt} +$$
$$+ F(h_{is}+h_{id})\sqrt{\frac{2}{\rho}(\Delta p_{ibs} + \Delta p_{ibd})}$$

or,

$$F_{II}(v_{IIs} + v_{IId}) = \frac{V_i}{E}\frac{dp_{id}}{dt} + (F_i - F_{so})\frac{dh_{id}}{dt} +$$
$$+ F(h_{is}+h_{id})\sqrt{\frac{2}{\rho}\Delta p_{ibs}\left(1 + \frac{\Delta p_{ibd}}{\Delta p_{ibs}}\right)} \qquad (8.14)$$

Considering the last term in the right side of equation (8.14):

$$F(h_{is}+h_{id})\sqrt{\frac{2}{\rho}\Delta p_{ibs}\left(1 + \frac{\Delta p_{ibd}}{\Delta p_{ibs}}\right)}$$

Since,

$$\frac{\Delta p_{ibd}}{\Delta p_{ibs}} < 1$$

Therefore,

$$\sqrt{\left(1 + \frac{\Delta p_{ibd}}{\Delta p_{ibs}}\right)} \simeq 1 + \frac{\Delta p_{ibd}}{2\Delta p_{ibs}}$$

and $F(h_{is}+h_{id})$ can be written in terms of $F(h_{is})$ and its derivatives by using Taylor series expansion as follows:

$$F(h_{is}+h_{id}) = F(h_{is}) + h_{id}F'(h_i)\Big|_{h_{is}} + \frac{1}{2}h_{id}^2 F''(h_i)\Big|_{h_{is}} + \dots$$

Neglecting the terms with high order derivative,

$$F(h_{is}+h_{id}) = F(h_{is}) + h_{id}F'(h_i)\Big|_{h_{is}}$$

From equations (8.2) and (3.41), (3.45)

$$F'(h_i)\Big|_{h_{is}} = CF(h_{is})$$

where,

$$C = \text{Constant}$$

and,

$$C = (B + D)\left[(\mu_{si}F_{fsi})^{-2} + (\mu_{se}F_{fse})^{-2}\right]^{-1}$$

with,

$$B = \mu_{si}^{-2}(A_{fsi}h_{is}^2 + B_{fsi}h_{is})^{-3}(2A_{fsi}h_{is} + B_{fsi})$$

$$D = \mu_{se}^{-2}(A_{fse}h_{is}^2 + B_{fse}h_{is} + C_{fse})^{-3}(2A_{fse}h_{is} + B_{fse})$$

Therefore,

$$F(h_{is}+h_{id}) = F(h_{is}) + CF(h_{is})h_{id}$$

$$F(h_{is}+h_{id}) = F(h_{is})(1 + Ch_{id})$$

Hence, the last term in the right side of equation (8.14) becomes:

$$F(h_{is}+h_{id})\sqrt{\frac{2}{\rho}\Delta p_{ibs}\left(1 + \frac{\Delta p_{ibd}}{\Delta p_{ibs}}\right)} =$$

$$F(h_{is})(1 + Ch_{id})\left(1 + \frac{\Delta p_{ibd}}{2\Delta p_{ibs}}\right)\sqrt{\frac{2}{\rho}\Delta p_{ibs}} \tag{8.15}$$

Thus, equation (8.14) becomes:

$$F_{II}(v_{IIs} + v_{IId}) = \frac{V_i}{E}\frac{dp_{id}}{dt} + (F_i - F_{so})\frac{dh_{id}}{dt} +$$

$$+ F(h_{is})(1 + Ch_{id})\left(1 + \frac{\Delta p_{ibd}}{2\Delta p_{ibs}}\right)\sqrt{\frac{2}{\rho}\Delta p_{ibs}} \tag{8.16}$$

Substracting equation (8.13) from equation (8.16),

$$F_{II}v_{IId} = \frac{V_i}{E}\frac{dp_{id}}{dt} + (F_i - F_{so})\frac{dh_{id}}{dt} +$$
$$+ F(h_{is})\sqrt{\frac{2}{\rho}\Delta p_{ibs}}\left[\left(1 + \frac{\Delta p_{ibd}}{2\Delta p_{ibs}}\right)(1 + Ch_{id}) - 1\right]$$

or,

$$F_{II}v_{IId} = \frac{V_i}{E}\frac{dp_{id}}{dt} + (F_i - F_{so})\frac{dh_{id}}{dt} +$$
$$+ F(h_{is})\sqrt{\frac{2}{\rho}\Delta p_{ibs}}\left(Ch_{id} + \frac{\Delta p_{ibd}}{2\Delta p_{ibs}} + C\frac{\Delta p_{ibd}}{2\Delta p_{ibs}}h_{id}\right)$$

Neglecting the third term in the brackets since it is small as compared with other terms, and using equations (8.11) and (8.13), one obtains:

$$F_{II}\frac{P_{id}}{\rho\bar{a}} + \frac{V_i}{E}\frac{dp_{id}}{dt} + (F_i - F_{so})\frac{dh_{id}}{dt} +$$
$$+ F_{II}v_{IIs}\left(Ch_{id} + \frac{\Delta p_{ibd}}{2\Delta p_{ibs}}\right) = 0$$

or,

$$\left(F_{II}v_{IIs}C\right)h_{id} + \left(\frac{F_{II}v_{IIs}}{2\Delta p_{ibs}} + \frac{F_{II}}{\rho\bar{a}}\right)P_{id} - \left(\frac{F_{II}v_{IIs}}{2\Delta p_{ibs}}\right)P_{bd} +$$
$$+ \left(\frac{V_i}{E}\right)\frac{dp_{id}}{dt} + (F_i - F_{so})\frac{dh_{id}}{dt} = 0 \qquad (8.17)$$

8.2.1.2. For Bag Chamber

The continuity equation for the bag chamber is:

$$F(h_l)\sqrt{\frac{2}{\rho}(p_l - p_b)} = \frac{V_b}{E}\frac{dp_b}{dt} + F_{so}\frac{dh_l}{dt} + \mu_o IF_{fo}\sqrt{\frac{2}{\rho}(p_b - p_a)} \quad (8.18)$$

a. Steady-State Analysis

At steady-state conditions, equation (8.18) becomes:

$$F(h_{ls})\sqrt{\frac{2}{\rho}(p_{ls} - p_{bs})} = \mu_o IF_{fo}\sqrt{\frac{2}{\rho}(p_{bs} - p_a)}$$

Let,

$$\Delta p_{bas} = p_{bs} - p_a$$

Then,

$$F(h_{ls})\sqrt{\frac{2}{\rho}\Delta p_{lbs}} = \mu_o IF_{fo}\sqrt{\frac{2}{\rho}\Delta p_{bas}}$$

Comparing this equation and equation (8.13), one has:

$$F_{II}v_{IIs} = F(h_{ls})\sqrt{\frac{2}{\rho}\Delta p_{lbs}} = \mu_o IF_{fo}\sqrt{\frac{2}{\rho}\Delta p_{bas}} \quad (8.19)$$

b. With Disturbance

Substituting equations from (8.4) to (8.9) into equation (8.18),

$$F(h_{ls}+h_{ld})\sqrt{\frac{2}{\rho}(\Delta p_{lbs} + \Delta p_{lbd})} = \frac{V_b}{E}\frac{dp_{bd}}{dt} + F_{so}\frac{dh_{ld}}{dt} +$$

$$+ \mu_o IF_{fo}\sqrt{\frac{2}{\rho}(p_{bd} + \Delta p_{bas})}$$

Using equation (8.15) and approximating,

$$\mu_o IF_{fo}\sqrt{\frac{2}{\rho}(p_{bd} + \Delta p_{bas})} \simeq \mu_o IF_{fo}\sqrt{\frac{2}{\rho}\Delta p_{bas}}\left(1 + \frac{p_{bd}}{2\Delta p_{bas}}\right)$$

one obtains:

$$F(h_{is})(1 + Ch_{id})\left(1 + \frac{\Delta p_{ibd}}{2\Delta p_{ibs}}\right)\sqrt{\frac{2}{\rho}\Delta p_{ibs}} = \frac{V_b}{E}\frac{dp_{bd}}{dt} + F_{so}\frac{dh_{id}}{dt} +$$

$$+ \mu_o IF_{fo}\sqrt{\frac{2}{\rho}\Delta p_{bas}}\left(1 + \frac{p_{bd}}{2\Delta p_{bas}}\right) \qquad (8.20)$$

Substracting equation (8.19) from equation (8.20),

$$F(h_{is})\sqrt{\frac{2}{\rho}\Delta p_{ibs}}\left(Ch_{id} + \frac{\Delta p_{ibd}}{2\Delta p_{ibs}} + C\frac{\Delta p_{ibd}}{2\Delta p_{ibs}}h_{id}\right) = \frac{V_b}{E}\frac{dp_{bd}}{dt} +$$

$$+ F_{so}\frac{dh_{id}}{dt} + \mu_o IF_{fo}\sqrt{\frac{2}{\rho}\Delta p_{bas}}\left(\frac{p_{bd}}{2\Delta p_{bas}}\right)$$

Neglecting the small terms and using equation (8.19),

$$F_{II^\nabla IIs}\left(Ch_{id} + \frac{\Delta p_{ibd}}{2\Delta p_{ibs}}\right) = \frac{V_b}{E}\frac{dp_{bd}}{dt} + F_{so}\frac{dh_{id}}{dt} + F_{II^\nabla IIs}\frac{p_{bd}}{2\Delta p_{bas}}$$

or,

$$\left(F_{II^\nabla IIs}C\right)h_{id} + \left(\frac{F_{II^\nabla IIs}}{2\Delta p_{ibs}}\right)p_{id} - \left(\frac{F_{II^\nabla IIs}}{2\Delta p_{ibs}} + \frac{F_{II^\nabla IIs}}{2\Delta p_{bas}}\right)p_{bd} -$$

$$- \left(\frac{V_b}{E}\right)\frac{dp_{bd}}{dt} - (F_{so})\frac{dh_{id}}{dt} = 0 \qquad (8.21)$$

8.2.2. Motion Equation

The motion equation for the injector needle without mechanical friction is as follows:

$$m_i \frac{d^2 h_i}{dt^2} + \delta_i \frac{dh_i}{dt} + k_{is} h_i + P_{is} = p_i(F_i - F_{so}) + p_b F_{so} \qquad (8.22)$$

a. Steady-State Analysis

At steady-state conditions, equation (8.22) becoms:

$$k_{is} h_{is} + P_{is} = p_{is}(F_i - F_{so}) + P_{bs} F_{so} \qquad (8.23)$$

b. With Disturbance

Substituting equations from (8.4) to (8.9) into equation (8.22),

$$m_i \frac{d^2 h_{id}}{dt^2} + \delta_i \frac{dh_{id}}{dt} + k_{is}(h_{is} + h_{id}) + P_{is} = (p_{is} + p_{id})(F_i - F_{so}) + (p_{bs} + p_{bd})F_{so} \qquad (8.24)$$

Substracting equation (8.23) from equation (8.24) and rearranging,

$$m_i \frac{d^2 h_{id}}{dt^2} + \delta_i \frac{dh_{id}}{dt} + k_{is} h_{id} - p_{id}(F_i - F_{so}) - p_{bd} F_{so} = 0 \qquad (8.25)$$

8.2.3. Stability Criteria

In order to establish the stability criteria for the injector, the continuity and motion equations (8.17), (8.21) and (8.25) should be reduced to one equation consisting of only the quantity h_{id}.

In the following derivation, for simplification, let:

$$a = F_{II} v_{IIs} C$$

$$b = \frac{F_{II} v_{IIs}}{2\Delta p_{ibs}}$$

$$c = \frac{F_{II}}{\rho \bar{a}}$$

$$e = \frac{V_i}{E}$$

$$f = F_i - F_{so}$$

$$g = -\left(\frac{F_{II} v_{IIs}}{2\Delta p_{bas}}\right)$$

$$j = -\left(\frac{V_b}{E}\right)$$

$$l = -(F_{so})$$

Then, equations (8.17), (8.21) and (8.25) become:

$$ah_{id} + (b + c)p_{id} - bp_{bd} + e\frac{dp_{id}}{dt} + f\frac{dh_{id}}{dt} = 0 \tag{8.26}$$

$$ah_{id} + bp_{id} - (b - g)p_{bd} + j\frac{dp_{bd}}{dt} + l\frac{dh_{id}}{dt} = 0 \tag{8.27}$$

$$m_i \frac{d^2 h_{id}}{dt^2} + \delta_i \frac{dh_{id}}{dt} + k_{is} h_{id} - fp_{id} + lp_{bd} = 0 \tag{8.28}$$

An easy way to eliminate P_{id}, P_{bd} and their derivatives in these three equations is to use Laplace transformation.

Let H_{id}, P_{id} and P_{bd} be Laplace transforms of h_{id}, P_{id} and P_{bd} respectively. Then, after rearranging, one has:

$$(a + fs)H_{id} + (b + c + es)P_{id} - bP_{bd} = 0 \tag{8.29}$$

$$(a + ls)H_{id} + bP_{id} + (-b + g + js)P_{bd} = 0 \tag{8.30}$$

$$(m_i s^2 + \delta_i s + k_{is})H_{id} - fP_{id} + lP_{bd} = 0 \tag{8.31}$$

Eliminating P_{id} and P_{bd} in these three equations:

$$\left\{ \left[(a+fs)(-b+g+js)+b(a+ls) \right]\left[(b+c+es)l-bf \right] - \right.$$
$$\left. - \left[(a+fs)l+b(m_i s^2+\delta_i s+k_{is}) \right]\left[(b+c+es)(-b+g+js)+b^2 \right] \right\}H_{id} = 0 \tag{8.32}$$

Expanding and rearranging equation (8.32), one obtains:

$$(A_4 s^4 + A_3 s^3 + A_2 s^2 + A_1 s + A_0)H_{id} = 0 \tag{8.33}$$

where,

$$A_0 = ag(bl+cl-bf)-(al+bk_{is})(bg-bc+cg) \tag{8.34}$$

$$A_1 = agel+(aj-bf+fg+bl)(bl+cl-bf) -$$
$$- (al+bk_{is})(bj+cj-be+eg)-(fl+b\delta_i)(bg-bc+cg) \tag{8.35}$$

$$A_2 = el(aj-bf+fg+bl)+fj(bl+cl-bf)-ej(al+bk_{is}) -$$
$$- (fl+b\delta_i)(bj+cj-be+eg)-bm_i(bg-bc+cg) \tag{8.36}$$

$$A_3 = efjl-ej(fl+b\delta_i)-bm_i(bj+cj-be+eg) \tag{8.37}$$

$$A_4 = -bejm_i \tag{8.38}$$

and the characteristic equation is:

$$A_4 s^4 + A_3 s^3 + A_2 s^2 + A_1 s + A_0 = 0 \qquad (8.39)$$

There are several methods which can be used to study the stability of the injector. Routh-Hurwitz test has been selected to establish the stability criteria for the injector in this chapter. The method involves a "Routh-Hurwitz array" as follows:

	First column	Second column	Third column
s^4	A_4	A_2	A_0
s^3	A_3	A_1	0
s^2	$\dfrac{A_2 A_3 - A_1 A_4}{A_3}$	A_0	0
s^1	$\dfrac{A_1(A_2 A_3 - A_1 A_4) - A_0 A_3^2}{A_2 A_3 - A_1 A_4}$	0	
s^0	A_0		

The Routh-Hurwitz criterion states that the system is stable if all of the terms in the first column of the array are different from zero and have the same sign [22].

With the coefficients A_0, A_1, A_2, A_3 and A_4 given by equations from (8.34) to (8.38), it is found that all terms in the first column of the Routh array are different from zero and positive except the term:

$$\frac{A_1(A_2A_3 - A_1A_4) - A_0A_3^2}{A_2A_3 - A_1A_4}$$

which could be positive or negative.

Let $T(h_{is})$ represent that term. Thus, the injector needle is stable if:

$$T(h_{is}) = \frac{A_1(A_2A_3 - A_1A_4) - A_0A_3^2}{A_2A_3 - A_1A_4} > 0 \qquad (8.40)$$

At the lift h_{is} of the needle where $T(h_{is}) = 0$, the stability limit of the needle could be found.

Depending on the design and operational parameters of the injector, the term $T(h_{is})$ can be either positive or negative or even zero. The effects of the injector design and operational parameters on the injector's stability will be analyzed in the following sections.

8.3. Effect of Injector Design and Operational Parameters on the Injector Stability

In studying the effects of the injector design and operational parameters on the injector stability criteria, the injector with data specified in chapter 3 is used as an example.

The injector design and operational parameters selected to study their effects on the injector stability are: needle damping factor δ_i, differential angle between the needle and the nozzle body seat cones γ, and outer seat diameter D_{so}.

The criterion term $T(h_{is})$ in inequation (8.40) is plotted versus the steady-state needle lift h_{is} for each set of values of the selected parameters. The plots are shown in figures 8.1, 8.2 and 8.3 for different values of damping factor δ_i, seat differential angle γ, and outer seat diameter D_{so} respectively.

As mentioned before, the stability of the injector needle is considered as an undesirable behaviour at low needle lifts. Referring to figures 8.1, 8.2 and 8.3, one can see that as the damping factor δ_i, seat differential angle γ, and outer seat diameter D_{so} increase, all the curves are shifted upward. Consequently, the stability limit for the needle lift h_{is} becomes smaller. This means that in order to have the injector more unstable, the injector should be designed to have the values of the above parameters smaller. However, the instability of the injector is not the only optimization requirement. Usually, the design parameters are selected as the result of a compromise to fulfill all the criteria requirements for a diesel injector, as dicussed in the section 7.8.
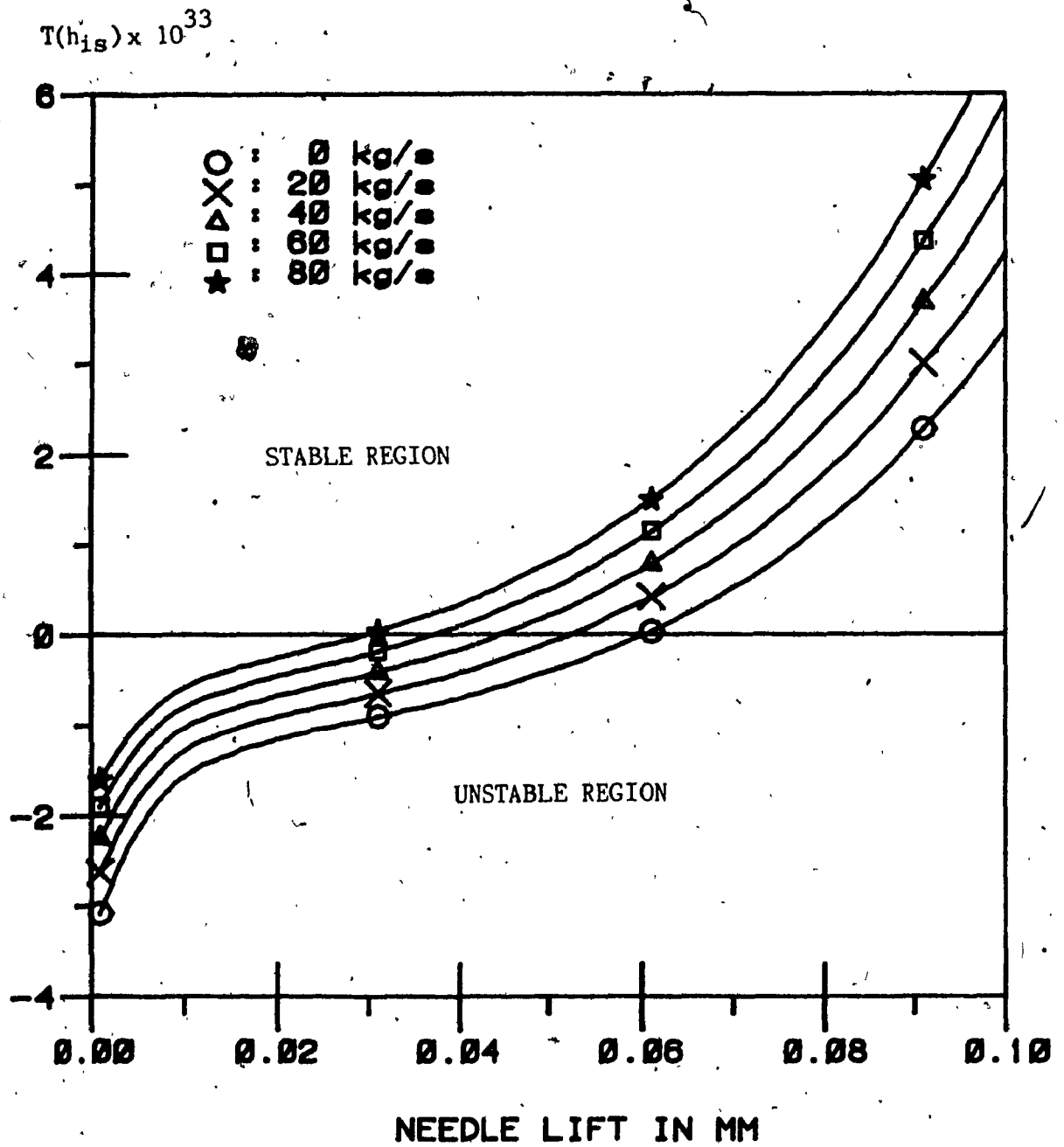
Fig.8.1. $T(h_{is})$ versus Needle Lift for different Values of Damping Coefficient
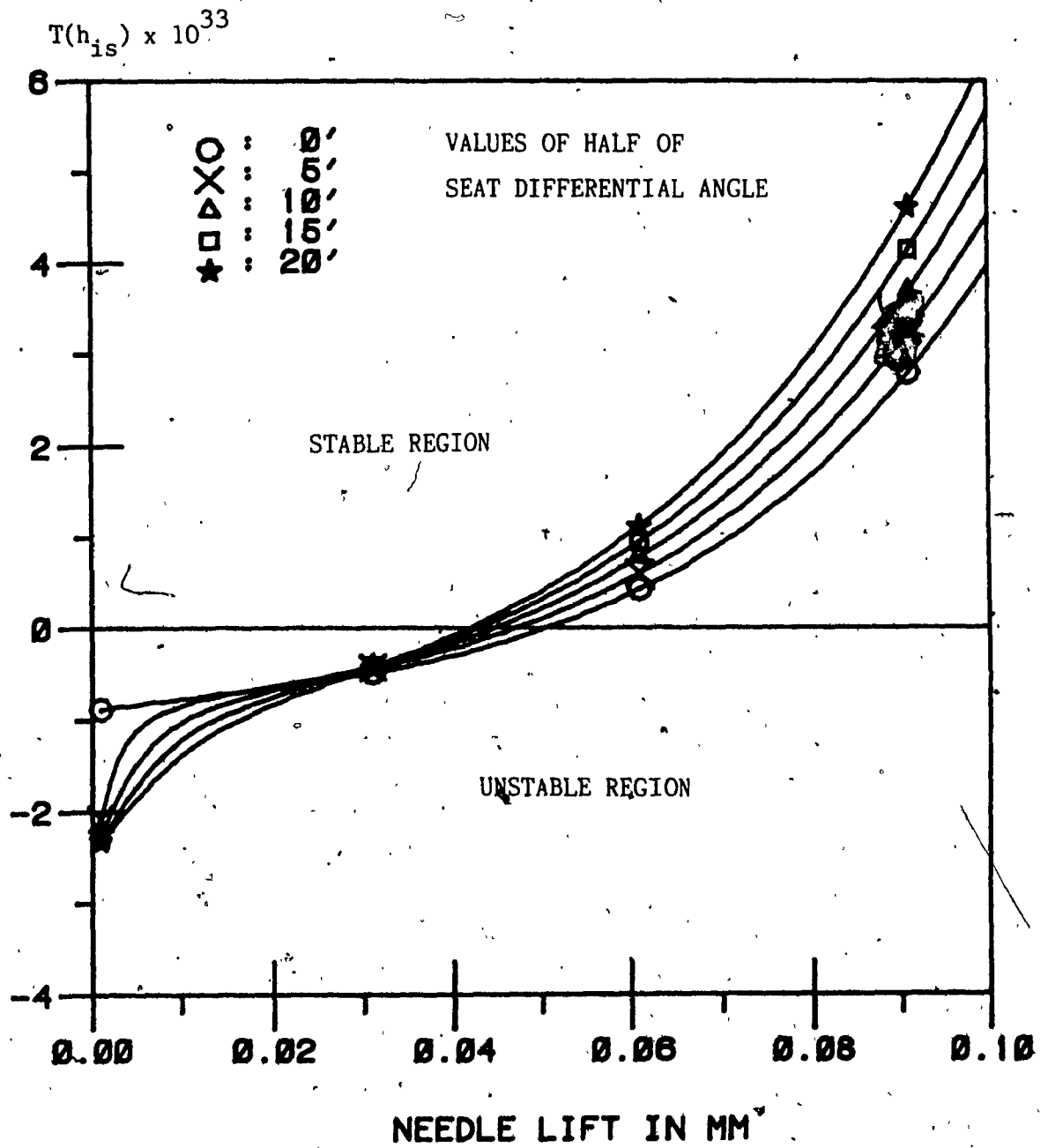
Fig. 8.2. $T(h_{is})$ versus Needle Lift for different Values of Seat Differential Angle

$T(h_{is}) \times 10^{33}$
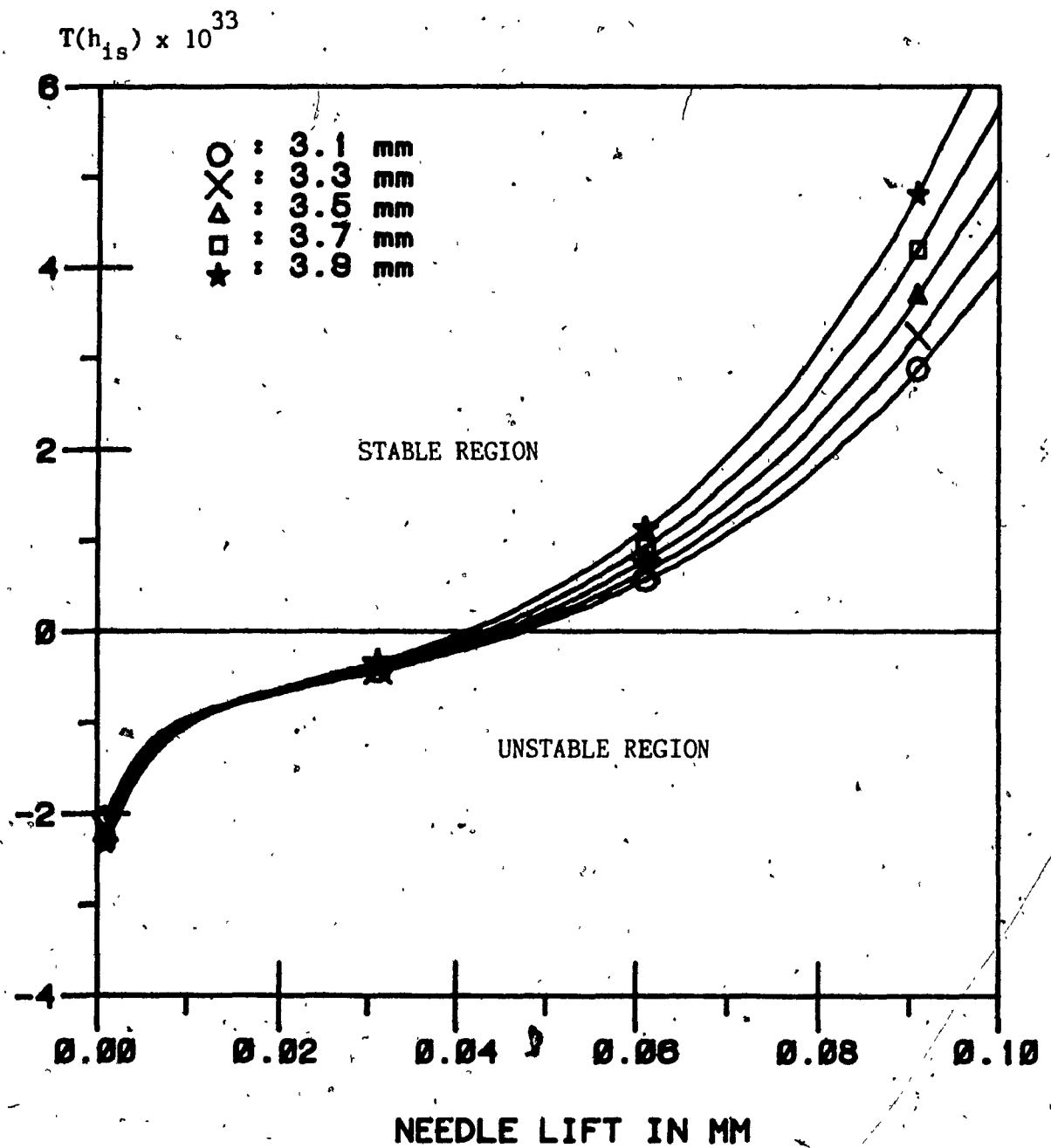
Fig.8.3. $T(h_{is})$ versus Needle Lift for
different Values of Seat Outer Diameter

The three injector design parameters were selected for this study to serve only as an example. However, the inequality (8.40) established in this chapter can be also used for design improvement of an injector by changing the values of other parameters to find out how the stability limit h_{is} changes, and where it is located.

It should be noted that in the above calculations, the quantities $F_{II}V_{IIs}$, Δp_{ibs} and Δp_{bas} should be derived in terms of h_{is}, because their values are unknown, according to the following analysis.

From equation (8.23), one can write:

$$
\begin{aligned}
k_{is} h_{is} + P_{is} \ &= p_{is}(F_i - F_{so}) + p_{bs}F_{so} \\
&= (p_{is} - p_{bs} + p_{bs})(F_i - F_{so}) + p_{bs}F_{so} \\
&= \Delta p_{ibs}(F_i - F_{so}) + p_{bs}(F_i - F_{so} + F_{so}) \\
&= \Delta p_{ibs}(F_i - F_{so}) + (p_{bs} - p_a + p_a)F_i \\
&= \Delta p_{ibs}(F_i - F_{so}) + \Delta p_{bas}F_i + p_a F_i
\end{aligned}
\tag{8.41}
$$

But from steady-state flow rate given by equation (8.19),

$$
F_{II}V_{IIs} = F(h_{is})\sqrt{\frac{2}{\rho}\Delta p_{ibs}} = \mu_o \mathbb{F}_{fo}\sqrt{\frac{2}{\rho}\Delta p_{bas}}
\tag{8.19}
$$

or,

$$
\Delta p_{ibs} = \left[\frac{\mu_o \mathbb{F}_{fo}}{F(h_{is})}\right]^2 \Delta p_{bas}.
\tag{8.42}
$$

Subsituting equation (8.42) into equation (8.41), and rearranging,

$$\Delta p_{bss} = \frac{k_{is}h_{is} + P_{is} - p_a F_1}{F_i + (F_i - F_{so})\left[\dfrac{\mu_o IF_{fo}}{F(h_{is})}\right]^2}$$

(8.43)

Therefore,

$$\Delta p_{1bs} = \frac{k_{is}h_{is} + P_{is} - p_a F_i}{(F_i - F_{so}) + F_i\left[\dfrac{F(h_{is})}{\mu_o IF_{fo}}\right]^2}$$

(8.44)

and,

$$F_{II}v_{IIs} = \mu_o IF_{fo}\sqrt{\frac{2}{\rho}\frac{k_{is}h_{is} + P_{is} - p_a F_i}{F_i + (F_i - F_{so})\left[\dfrac{\mu_o IF_{fo}}{F(h_{is})}\right]^2}}$$

(8.45)

Using the above relationship between the fuel flow rate $F_{II}v_{IIs}$ and needle lift at steady-state h_{is}, the plots of the term $T(h_{is})$ in inequation (8.40) versus steady-state fuel flow rate are made and given in figures 8.4, 8.5, and 8.6.

The transient response of the injector as the needle displacement to the fuel flow rate step input is also calculated for the nominal design and operational parameters in this analysis. Using the basic continuity and motion equations (8.3), (8.18), and (8.22) derived previously, a computer program was written to solve them simultaneously for h_i, p_i, and p_b with a fuel flow rate step function as an input. The plot of the needle lift h_i versus time for two
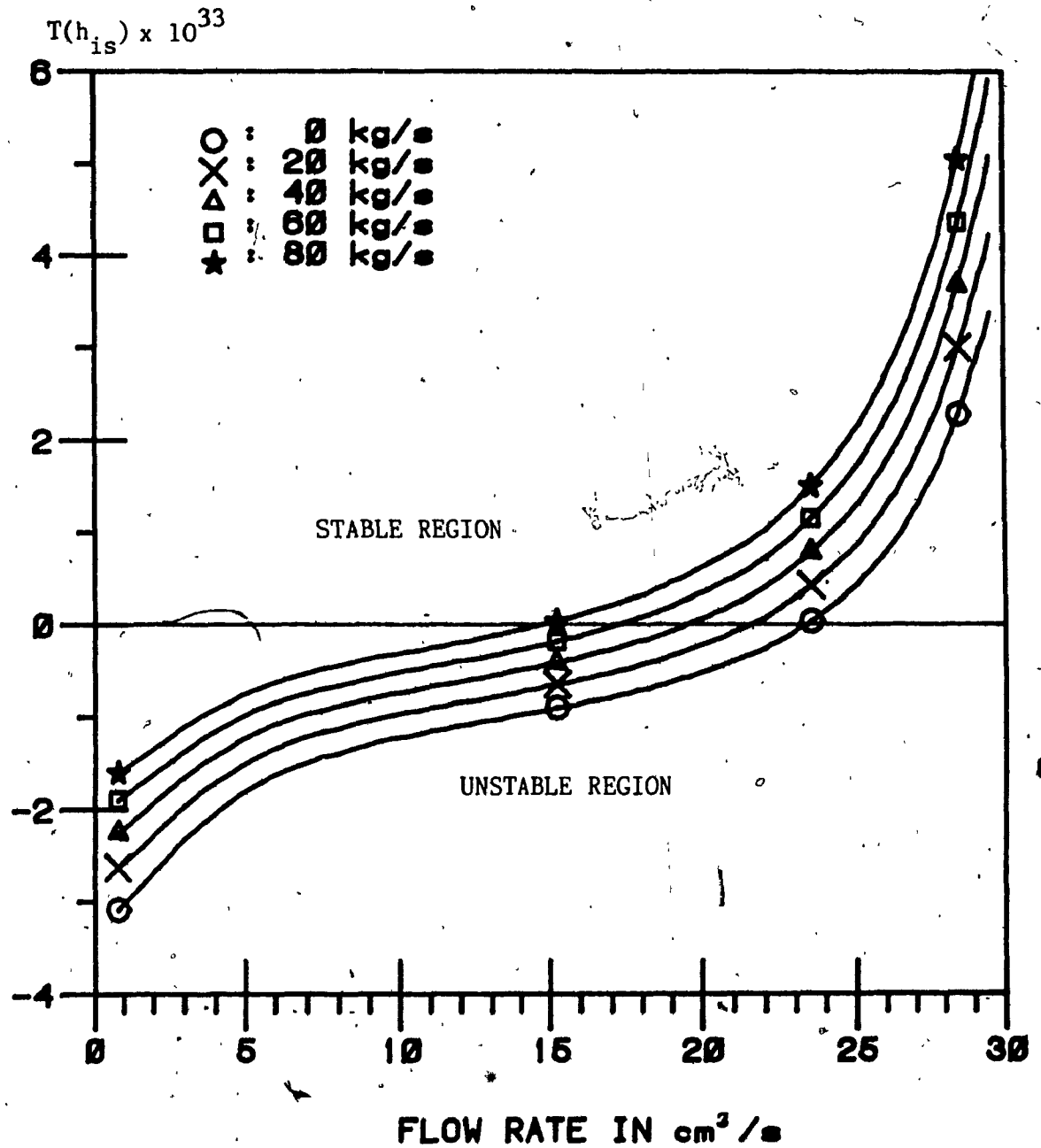
Fig.8.4. $T(h_{is})$ versus Fuel Flow Rate for different Values of Damping Coefficient
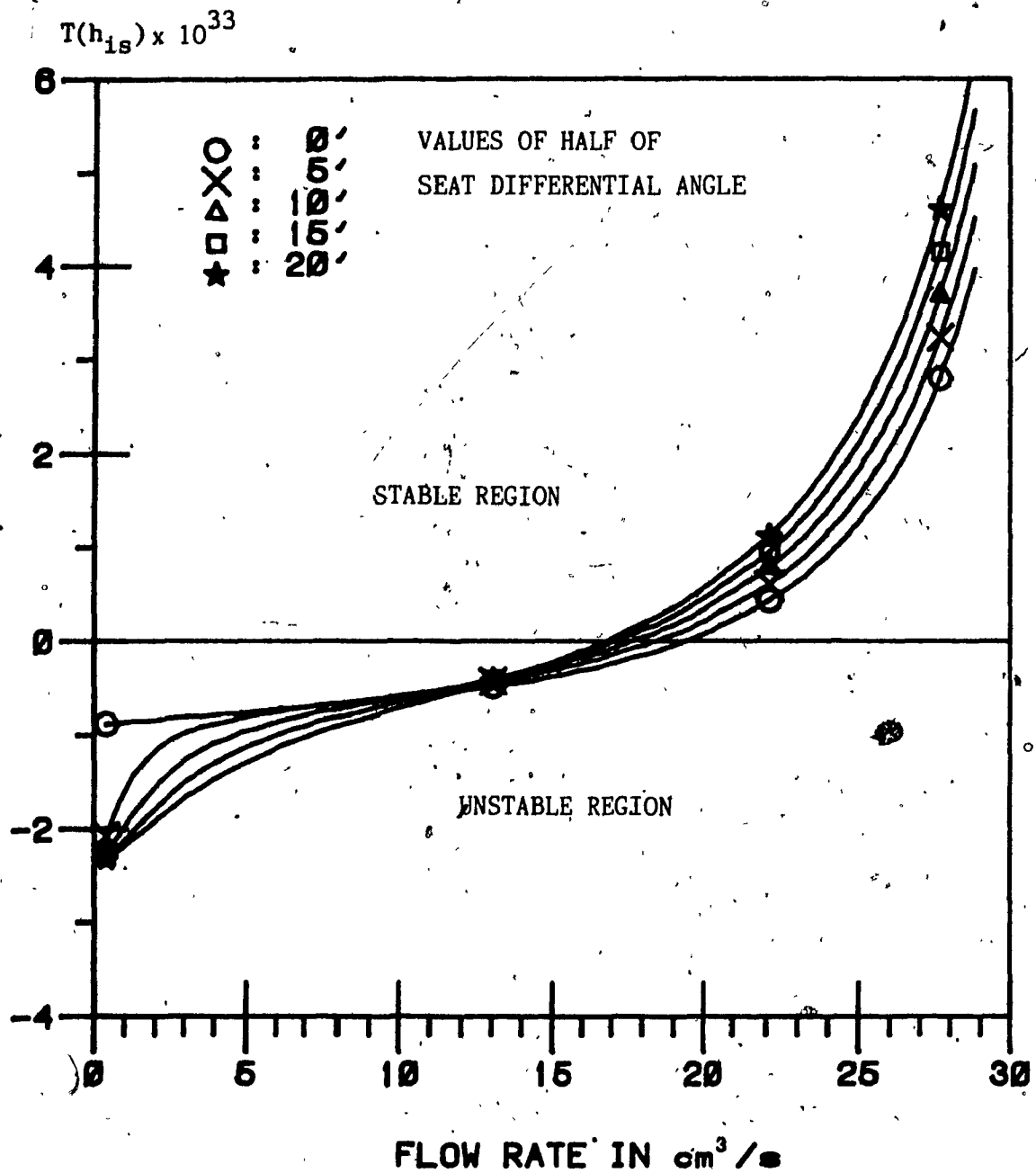
Fig.8.5. $T(h_{is})$ versus Fuel Flow Rate for different Values of Seat Differential Angle
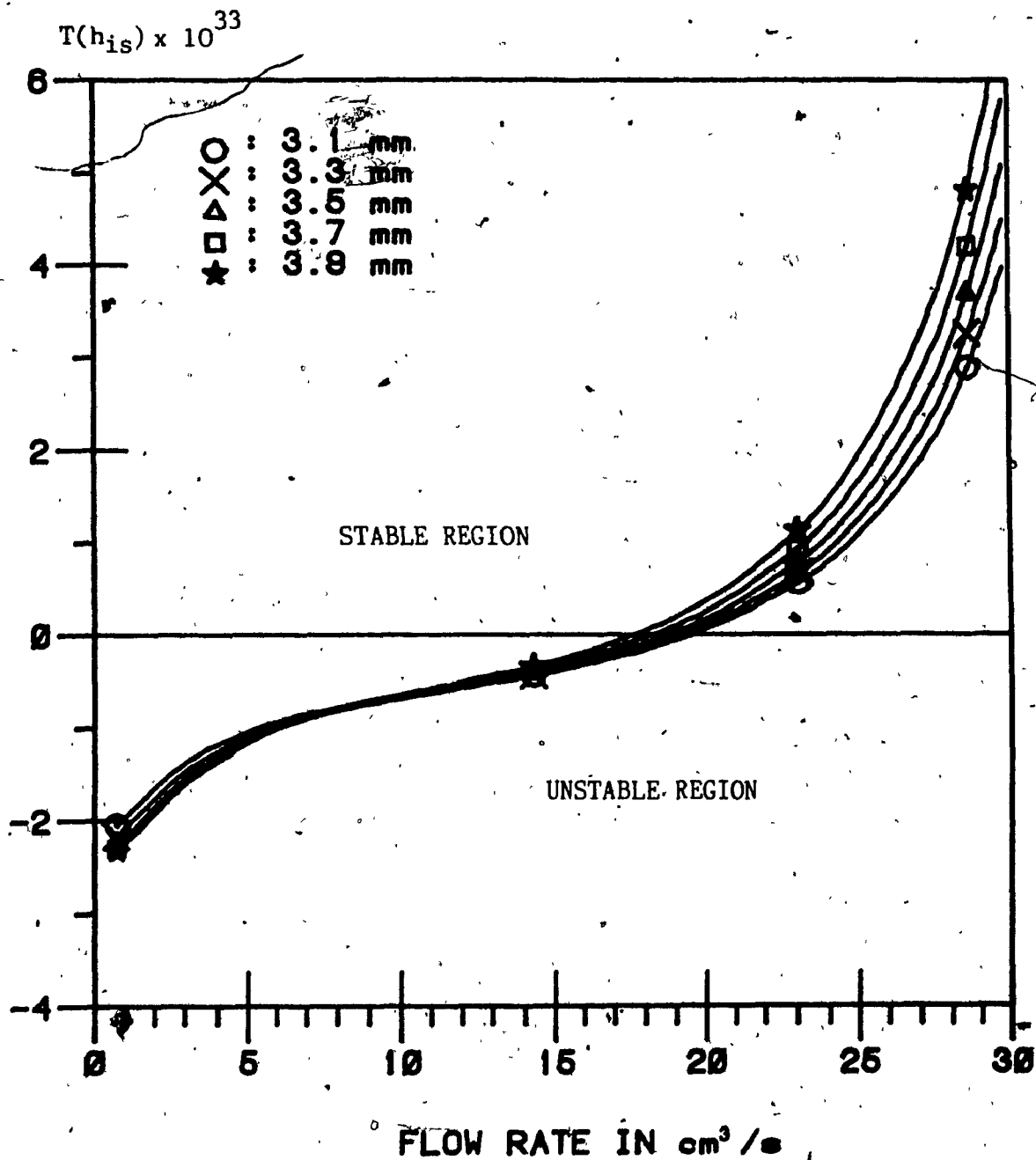
Fig.8.6. $T(h_{is})$ versus Fuel Flow Rate for
different Values of Seat Outer Diameter

selected steady-state fuel flow rates $q_s = 10$ cm^3/s, and 38 cm^3/s are shown in figures 8.7 and 8.8 respectively.

In figure 8.7, one can see that the injector needle is lifted at a distance from its seat, then it returns to the nozzle seat, where it waits for a little while until the pressure in the injector increases again. Then, a jump of needle is repeated as long as the fuel is supplied to the injector. This provides a proof of the instability of the injector needle and this phenomenon occurs because the fuel flow rate $q_s = 10$ cm^3/s is selected in the range of needle instability according to figure 8.4, 8.5, and 8.6.

Whereas, figure 8.8 shows that the injector needle is first lifted off the nozzle seat and reaches some distance, then oscillates during a short time before it stabilizes at a steady-state level. This is a proof of the stability of the injector needle because the fuel flow rate $q_s = 38$ cm^3/s is in the stable range of the injector needle.

The discussed stability calculation of a diesel injector can be considered as a next tool for a project engineer developing a diesel engine. This allows him to ensure that the injector which he is selecting will have unstable operation at the range of the injection pump flow rate which does not provide high enough injector pressure at continuous fuel discharge. And also that, when the high enough discharge rate will be reached, the injector will operate at stable mode, thus assuring the required fuel atomization inside the combustion chamber of a diesel engine.
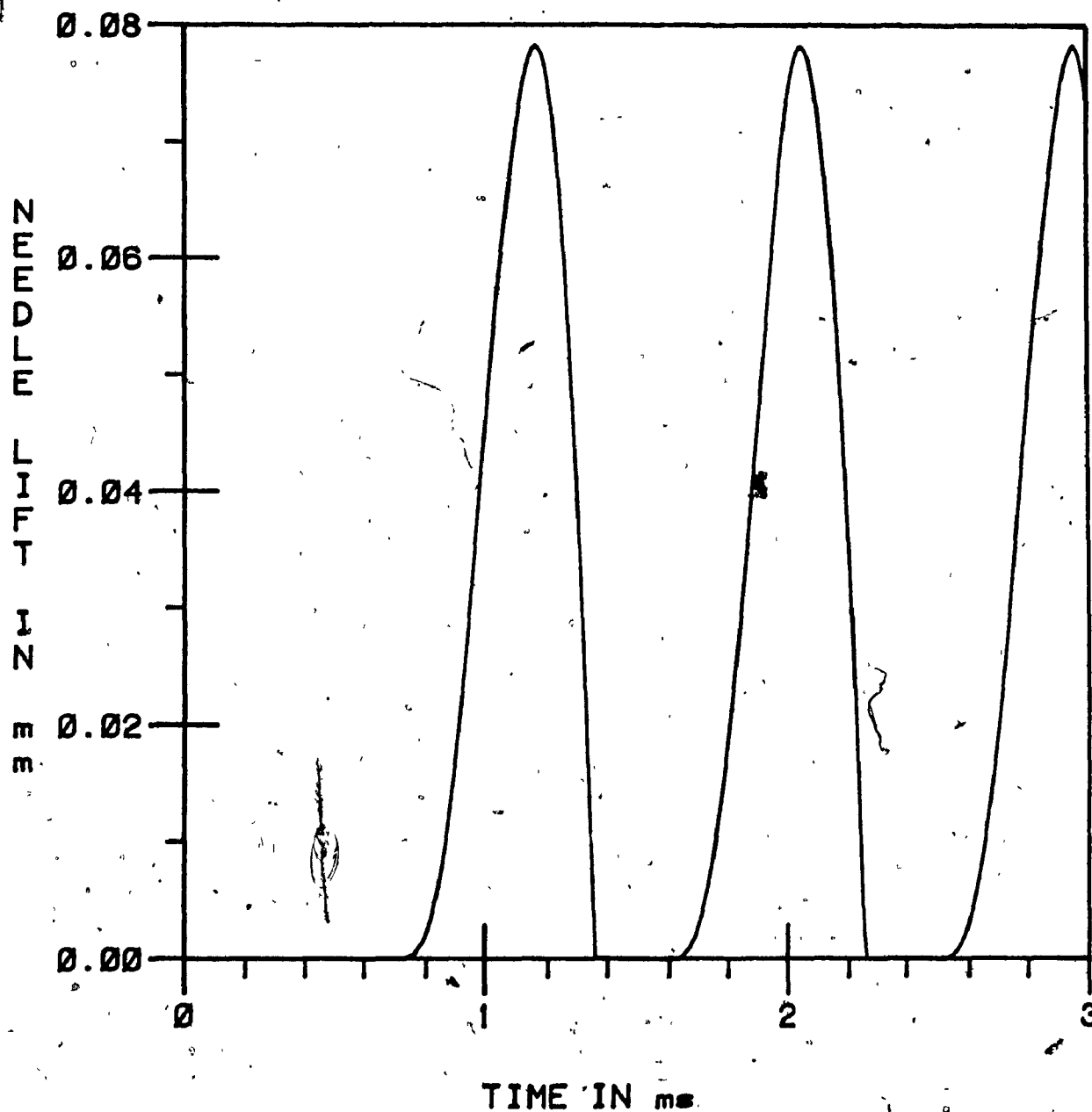
Fig.8.7. Needle Lift versus Time for Unstable Conditions
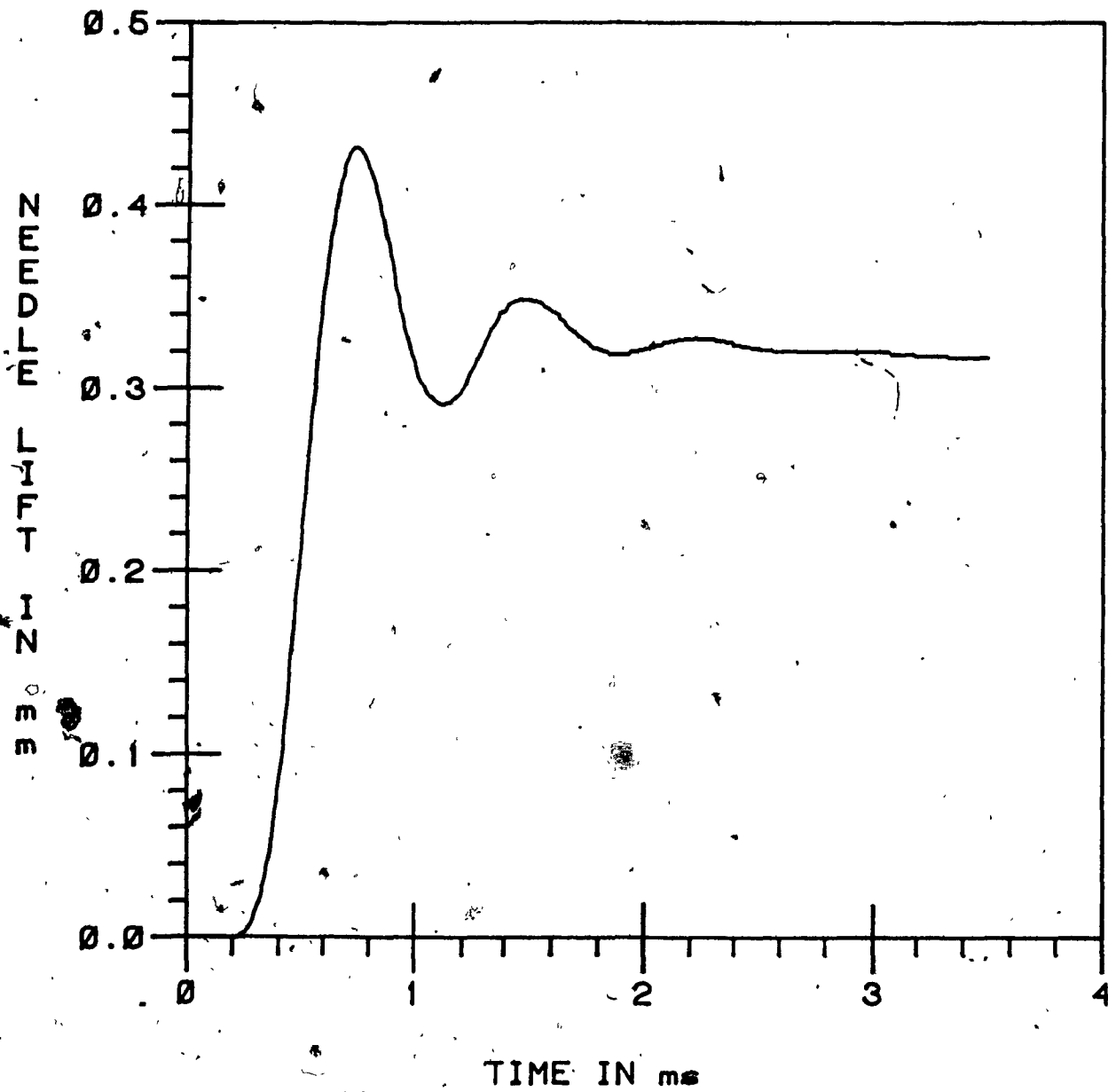
Fig.8.8. Needle Lift versus Time for Stable Conditions

Chapter 9
CONCLUSIONS AND RECOMMENDATIONS
FOR FUTURE WORK

9.1. Conclusions

The objective of this thesis was to optimize the design of
multi-hole fuel injectors used for high speed diesel engines with direct
injection. For that purpose, an improved mathematical model for the
fuel injection system was first developed, and the calculation methods
for fuel discharge rate were analyzed. The proposed mathematical
model specified the beginning of calculation procedure and also added
the seat chamber which was relevant for calculations with low fuel
flow rate. This mathematical model was checked to be consistent with
experimental results.

To establish the fuel flow conditions in the seat chamber,
experiments were made to measure the seat pressure from which the
numerical values of the flow coefficients at the inlet and at the exit
sections of the seat chamber were derived. These flow coefficients were
used in the proposed model for calculation of the fuel flow rate
characteristic.

A method was developed to calculate the dynamic response of
the diesel injector using a simplified model which could be easily
simulated on an injector test-rig. Using this method, as well as the
seat chamber approach, the injector dynamic response was calculated
and the impact of the design and operational parameters on the
injector dynamic response was established. This method was considered

to be useful in evaluation of the injector nozzles quality, particularly when using a computer controlled data acquisition system.

The simplified calculation method for the injector dynamic response based on the seat chamber approach, was also used to optimize the design parameters of the injector to obtain the best fuel atomization at idling and starting conditions. This was confirmed by the full calculation of the fuel injection process at low engine speeds with the use of characteristic method for computation purpose.

An attempt was also made to optimize the design parameters of the injector at the high engine speed using a shorten calculation method. This method was based on the pressure wave characteristic created by the injection pump and recorded by a computer controlled data acquisition system. The obtained results showed that the proposed approach reduced significantly the computing time required for optimization procedure.

Finally, the stability of the injector was analyzed to determine the criteria for its unstable operation depending on the fuel flow rate discharged towards an injector by an injection pump. Using the optimization results from the dynamic response calculation, the engine developer can select the critical flow rate for an injector according to the requirements of the diesel engine.

The above research, though not complete, is considered helpful to the diesel engines developers and manufacturers in regard to the fuel injectors design and their adaptation to the diesel engines. It should also improve the understanding of the phenomena related to the fuel injection systems for high speed engines.

9.2. Recommendations for Future Work

For future investigation towards improvement in the diesel injector performance, the following suggestions are made:

1. As mentioned in chapter 5 related to the evaluation of injector dynamic response, the seat differential angle contributes significantly to the dynamic response of the injector. However, the variation of maximum needle lift with respect to the seat differential angle has not yet been confirmed experimentally. This is due to the lack of a seat angle measuring device which should be developed for the nondestructive measurements of the nozzles.

2. The multi-hole type nozzle with the seat located above the bag chamber and orifices, creates a significant bag volume between the nozzle seat and orifices. This leads to the penetration of unburnt fuel into the cylinder of the engine increasing the hydrocarbons emission. To overcome this disadvantage of the hole-type nozzle, a nozzle with the orifices drilled directly into the nozzle seat was developed under the name of the Valve Covers Orifice (VCO) nozzle. The VCO nozzle certainly isolates the bag volume from orifices during non-injection period, thus preventing fuel from entering the combustion chamber once the valve is closed. In this thesis, the study of this type of nozzle has not been made. It is recommended to use the calculation and testing methods presented in this thesis for the analysis of this new type of nozzle. An optimization of the VCO nozzle could also improve the fuel injection characteristic at low engine speed.

3. Canada can easily produce a great amount of alternative liquid fuels such as ammonia, propane, methanol, etc., which are presently not much in use in automotive combustion engines. Those fuels can be quite easily used in spark ignition engines, but with low thermal efficiency. In diesel engines, however, the use of those fuels is presently restricted due to the difficult ignition after injection to the combustion chamber. The adaptation of the diesel engine to those alternative liquid fuels could be an interesting subject of future investigations. The mathematical model with computer supported simulation developed in this thesis can be utilized in investigations of the injection, vaporization and ignition processes of those fuels with some modifications related to the properties of particular fuel.

REFERENCES AND BIBLIOGRAPHY

1. A. Neitz, and N. D'Alfonso, "The M.A.N. Combustion System with Controlled Direct Injection for Passenger Car Diesel Engines", SAE paper No. 810479, 1981.

2. K.L. Hulsing, "Diesel Engine Concepts for the 1980's", SAE paper No. 790807, 1979

3. S.J. Davis, and E. Giffen, "Injection, Ignition, and Combustion in High Speed Heavy Oil Engines", Proc. Instn. of Automobile Engrs, 1931, p.399.

4. A. Pischinger, "Gemischbildung und Verbrennung im Dieselmotor", Springer-Verlag, Wien, 1957.

5. E. Blaum, "Das Einspritzgesetz des Schnellaufenden Dieselmotors", VDI-Verlag, Berlin, 1942.

6. B.E. Knight, "Fuel Injection System Calculations", Proc. Instn. of Mech. Engrs. (A.D.), No.1, 1960-1961.

7. T. Krepec, "Sposob Obliczania Przebiegu Utrysku Paliwa w Silniku Wysokopreznym", Silniki Spalinowe, No.1, 1968.

8. J. Kijewski, "Wplyw Odksztalcen Sprezystych Walka Krzywkowego Pompy Wtryskowej na Thrzenia Paliwa", Praca Doktorska Litechnika Warszawska, 1967.

9. G.A. Becchi, "Analytical Simulation of Fuel Injection in Diesel Engines", SAE paper No. 710568, 1971.

10. E.B. Wylie, J.A. Bold, and M.F. El-Erian, "Diesel Fuel Injection System Simulation and Experimental Correlation", SAE paper No. 710569, 1971.

11. K. Kumar, R.R. Gaur, R.D. Garg, and M.K. Gajendra Babu, "A Finite Difference Scheme for the Simulation of a Fuel Injection System", SAE paper No. 831337, 1983.

12. P.G. Burman, and F. Deluca, "Fuel Injection and Controls for Internal Combustion Engines", The Technical Press, London, 1962, pp. 248-250.

13. H.F. Woodward, "Factors Affecting Nozzle Chatter", BICERA, London, 1963.

14. W. Höfken, "Die Bestimmung der Schnarrfrequenzen von Einspritzventilen", MTZ, No.8, 1967.

15. T. Krepec, "New Possibilities of Evaluation of Injectors for Diesel Engines", Proceedings of Aviation Institude, No.51, Warsaw, 1972.

16. E.B. Wylie, and V.L. Streeter, "Fluid Transients", McGraw-Hill Book Co., Inc., New-York, 1978.

17. D. McCloy, and H.R. Martin, "The Control of Fluid Power", Longman, London, 1973.

18. R. Von Mises, "The Calculation of Flow Coefficients for Nozzle and Orifice", V.D.A. 61, No.21, 22, 23, May-July 1917.

19. S. Matsuoka, K. Yakota, and T. Kamimoto, "A Study of Fuel Injection Systems in Diesel Engines", SAE paper No.760551, 1976.

20. A. Alliévi, "Allgemeine Theorie über die Veränder Liche Bewegung des Wassers in Leitungen", Julius Springer, Berlin, 1909.

21. C.H. To, and T. Krepec, "Fuel Discharge Rate in Diesel Engine. Computer Simulation", Technical Report, Concordia University, Montreal, 1982.

22. R.C. Dorf, "Modern Control Systems", Addison-Wesley Publishing Co., Inc., Reading, California, 1981.

23. V.L. Streeter, and E.B. Wylie, "Fluid Mechanics", McGraw-Hill Book Co., Inc., New York, 1979.

24. H.E. Merrit, "Hydraulic Control Systems", John Wiley and Sons, Inc., New York, 1967.

25. R.L. Burden, J.D. Fairs, and A.C. Reynolds, "Numerical Analysis", Prindle, Weber and Schmidt Book Co., Inc., Boston, 1981.

26. M.L. James, G.M. Smith, and J.C. Wolford, "Applied Numerical Methods for Digital Computations with Fortran and CSMP", Harper and Row Book Co., Inc., New York, 1977.

27. J.T. King, "Introduction to Numerical Computation", McGraw-Hill Book Co., Inc., New York, 1984.

28. E. Kreyszig, "Advanced Engineering Mathematics", John Wiley and Sons, Inc., New York, 1979.

29. C.H. To, and T. Krepec, "Evaluation of Diesel Injector Dynamic Response as the Nozzle Quality Measure", the 9th. CANCAM, Saskatoon, Saskatchewan, 1983, Proceedings pp. 529-530.

30. T. Krepec, C.H. To, and M. Krepec, "Evaluation of Diesel Injector Dynamic Properties", the 6th. IFTOM Congress, New Delhi, India, 1983, Proceedings pp. 693-696.

31. C.H. To, and T. Krepec, "Use of Computer in Optimization of Diesel Injector Design", the 2nd. Canadian Universities Conference on CAD/CAM, 1985, Proceedings pp. 23-32.

Appendix A

SOLUTIONS OF SIMPLIFIED MOTION AND CONTINUITY EQUATIONS FOR FLUID FLOW IN A PIPE

Motion equation:

$$\frac{\partial v}{\partial t} = -\frac{1}{\rho}\frac{\partial p}{\partial x} \tag{A.1}$$

Continuity equation:

$$\frac{\partial v}{\partial x} = -\frac{1}{\rho \bar{a}^2}\frac{\partial p}{\partial t} \tag{A.2}$$

A.1. Solution for v

Assuming that the sound velocity in fluid $\bar{a}$ is constant. Then, differentiating both sides of equation (A.1) with respect to t, one obtains:

$$\frac{\partial^2 v}{\partial t^2} = -\frac{1}{\rho}\frac{\partial^2 p}{\partial x \partial t} \tag{A.3}$$

From equation (A.2), differentiating both sides with respect to x:

$$\frac{\partial^2 v}{\partial x^2} = -\frac{1}{\rho \bar{a}^2}\frac{\partial^2 p}{\partial x \partial t} \tag{A.4}$$

Comparing equation (A.3) and (A.4):

$$\frac{\partial^2 v}{\partial t^2} = \bar{a}^2 \frac{\partial^2 v}{\partial x^2} \tag{A.5}$$

To obtain the solution of this equation, let:

$$u = t + \frac{x}{a}$$

and,

$$z = t - \frac{x}{a}$$

Then,

$$\frac{\partial u}{\partial t} = 1$$

$$\frac{\partial z}{\partial t} = 1$$

and,

$$\frac{\partial u}{\partial x} = \frac{1}{a}$$

$$\frac{\partial z}{\partial x} = -\frac{1}{a}$$

The fluid velocity v then becomes a function of u and z. Using the chain rule to obtain:

$$\frac{\partial v}{\partial t} = \frac{\partial v}{\partial u}\frac{\partial u}{\partial t} + \frac{\partial v}{\partial z}\frac{\partial z}{\partial t}$$

$$\frac{\partial v}{\partial t} = \frac{\partial v}{\partial u} + \frac{\partial v}{\partial z}$$

and,

$$\frac{\partial^2 v}{\partial t^2} = \frac{\partial}{\partial u}\left(\frac{\partial v}{\partial u} + \frac{\partial v}{\partial z}\right)\frac{\partial u}{\partial t} + \frac{\partial}{\partial z}\left(\frac{\partial v}{\partial u} + \frac{\partial v}{\partial z}\right)\frac{\partial z}{\partial t}$$

$$\frac{\partial^2 v}{\partial t^2} = \frac{\partial^2 v}{\partial u^2} + 2\frac{\partial^2 v}{\partial u \partial z} + \frac{\partial^2 v}{\partial z^2} \tag{A.6}$$

Similarly,

$$\frac{\partial v}{\partial x} = \frac{\partial v}{\partial u}\frac{\partial u}{\partial x} + \frac{\partial v}{\partial z}\frac{\partial z}{\partial x}$$

$$\frac{\partial v}{\partial x} = \frac{1}{a}\left(\frac{\partial v}{\partial u} - \frac{\partial v}{\partial z}\right)$$

and,

$$\frac{\partial^2 v}{\partial x^2} = \frac{1}{a}\left[\frac{\partial}{\partial u}\left(\frac{\partial v}{\partial u} - \frac{\partial v}{\partial z}\right)\frac{\partial u}{\partial x} + \frac{\partial}{\partial z}\left(\frac{\partial v}{\partial u} - \frac{\partial v}{\partial z}\right)\frac{\partial z}{\partial x}\right]$$

$$\frac{\partial^2 v}{\partial x^2} = \frac{1}{a^2}\left(\frac{\partial^2 v}{\partial u^2} - 2\frac{\partial^2 v}{\partial u \partial z} + \frac{\partial^2 v}{\partial z^2}\right) \tag{A.7}$$

Substituting equations (A.6) and (A.7) into equation (A.5):

$$\frac{\partial^2 v}{\partial u^2} + 2\frac{\partial^2 v}{\partial u \partial z} + \frac{\partial^2 v}{\partial z^2} = \frac{\partial^2 v}{\partial u^2} - 2\frac{\partial^2 v}{\partial u \partial z} + \frac{\partial^2 v}{\partial z^2}$$

or,

$$\frac{\partial^2 v}{\partial u \partial z} = 0$$

or,

$$\frac{\partial}{\partial u}\left(\frac{\partial v}{\partial z}\right) = 0$$

i.e.

$$\frac{\partial v}{\partial z} = h(z)$$

which is a function of z only.

Integrating this equation with respect to z.

$$v = \int h(z)dz + b_1 \Psi(u) + v_o$$

where $\Psi(u)$ is a function of u only and v_o, b_1 are constants.

Since $\int h(z)dz$ is a function of z only, one can write:

$$v = a_1 \Phi(z) + b_1 \Psi(u) + v_0$$

Substituting z, u in terms of t and $\frac{x}{a}$ into the above equation:

$$v = v_0 + a_1 \Phi\left(t - \frac{x}{a}\right) + b_1 \Psi\left(t + \frac{x}{a}\right) \tag{A.8}$$

A.2. Solution for p

From equation (A.1), differentiating both sides with respect to x:

$$\frac{\partial^2 v}{\partial t \partial x} = -\frac{1}{\rho} \frac{\partial^2 p}{\partial x^2} \tag{A.9}$$

From equation (A.2), differentiating both sides with respect to t:

$$\frac{\partial^2 v}{\partial t \partial x} = -\frac{1}{\rho \bar{a}^2} \frac{\partial^2 p}{\partial t^2} \tag{A.10}$$

Comparing two equations (A.9) and (A.10):

$$\frac{\partial^2 p}{\partial t^2} = \bar{a}^2 \frac{\partial^2 p}{\partial x^2} \tag{A.11}$$

Equation (A.11) has the same form as equation (A.5). Therefore, similar procedure is applied to obtain the solution of equation (A.11); i.e.

$$p = P_0 + a_2 \Phi\left(t - \frac{x}{a}\right) + b_2 \Psi\left(t + \frac{x}{a}\right) \tag{A.12}$$

Since two solutions given by equations (A.8) and (A.12) must satisfy the motion and continuity equations (A.1) and (A.2) simultaneously, there are relationships between the constants a_1, a_2, b_1, b_2 in equations (A.8) and (A.12).

From equation (A.8), differentiating both sides with respect to t:

$$\frac{\partial v}{\partial t} = a_1 \frac{\partial \Phi(t - \frac{x}{a})}{\partial(t - \frac{x}{a})} + b_1 \frac{\partial \Psi(t + \frac{x}{a})}{\partial(t + \frac{x}{a})} \qquad (A.13)$$

From equation (A.12), differentiating both sides with respect to x:

$$\frac{\partial p}{\partial x} = -\frac{a_2}{\bar{a}} \frac{\partial \Phi(t - \frac{x}{a})}{\partial(t - \frac{x}{a})} + \frac{b_2}{\bar{a}} \frac{\partial \Psi(t + \frac{x}{a})}{\partial(t + \frac{x}{a})} \qquad (A.14)$$

Substituting equations (A.13) and (A.14) into equation (A.1):

$$a_1 \frac{\partial \Phi(t - \frac{x}{a})}{\partial(t - \frac{x}{a})} + b_1 \frac{\partial \Psi(t + \frac{x}{a})}{\partial(t + \frac{x}{a})} = \frac{1}{\rho \bar{a}}\left[a_2 \frac{\partial \Phi(t - \frac{x}{a})}{\partial(t - \frac{x}{a})} - b_2 \frac{\partial \Psi(t + \frac{x}{a})}{\partial(t + \frac{x}{a})}\right]$$

Comparing the coefficients of both sides:

$$a_1 = \frac{1}{\rho \bar{a}} a_2$$

$$b_1 = -\frac{1}{\rho \bar{a}} b_2$$

Choosing:

$$a_1 = b_1 = \frac{g}{a}$$

Then,

$$a_2 = \rho g$$

$$b_2 = -\rho g$$

Thus, the general solutions of the simplified motion and continuity equations for fluid flow in a pipe (A.1) and (A.2) are:

$$v = v_o + \frac{g}{a}\left[\Phi\left(t - \frac{x}{a}\right) + \Psi\left(t + \frac{x}{a}\right)\right]$$

$$p = p_o + \rho g\left[\Phi\left(t - \frac{x}{a}\right) - \Psi\left(t + \frac{x}{a}\right)\right].$$

Appendix B

SPILL PORT OPENING AREA

The sequence of derivation of equation for the spill port opening area F_{sp} consists of three main steps depending on the displacement of the pump plunger.

1. The first step:

In this step, the opening area of the spill port becomes smaller and smaller as the pump plunger is moving up. This step ends when the spill port is completely covered by the pump plunger.

Assuming that at the beginning of the pump plunger movement, the spill port is covered partly as shown in figure 3.5.a.

Let h_{po} be the distance between the lower spill port tangent line and the upper edge of the pump plunger at the position where it starts to move. Then, in this step the pump plunger displacement varies from $h_p=0$ to $h_p=h_{p1}$, where h_{p1} is the distance between the upper edge of the pump plunger at the beginning of plunger movement and the upper spill port tangent line, figure 3.5.b.

The opening area of the spill port F_{sp} for this step is derived based on:

$$F_{sp} = \pi(r_{sp})^2 - \left[(r_{sp})^2 \varphi_1 - 2 \frac{1}{2}(r_{sp} - x_1)r_{sp}\sin\varphi_1\right] \quad (B.1)$$

where,

$$x_1 = (h_p + h_{po})\cos\alpha_{spu} \qquad (B.2)$$

$$\cos\varphi_1 = \frac{r_{sp} - x_1}{r_{sp}} \qquad (B.3)$$

$$\sin\varphi_1 = \sqrt{1 - \cos^2\varphi_1}$$

Substituting $\cos\varphi_1$ from (B.3):

$$\sin\varphi_1 = \sqrt{1 - \left[\frac{r_{sp} - x_1}{r_{sp}}\right]^2}$$

or,

$$\sin\varphi_1 = \frac{1}{r_{sp}}\sqrt{(r_{sp})^2 - (r_{sp} - x_1)^2} \qquad (B.4)$$

Substituting equations (B.2), (B.3), and (B.4) into equation (B.1), one obtains:

$$F_{sp} = \pi(r_{sp})^2 - \left\{(r_{sp})^2\cos^{-1}\left[\frac{r_{sp} - (h_p + h_{po})\cos\alpha_{spu}}{r_{sp}}\right]\right.$$

$$\left. - \left[r_{sp} - (h_p + h_{po})\cos\alpha_{spu}\right]\sqrt{(r_{sp})^2 - \left[r_{sp} - (h_p + h_{po})\cos\alpha_{spu}\right]^2}\right\} \qquad (B.5)$$

2. The second step:

In this step, the displacement of the plunger varies from $h_p = h_{p1}$ to $h_p = (h_{p1} + ES)$, figure 3.5.b.

Where,

$$h_{p1} = \frac{2r_{sp}}{\cos\alpha_{spu}} - h_{po} \tag{B.6}$$

The spill port is completely closed in this step, i.e.

$$F_{sp} = 0 \tag{B.7}$$

When the plunger keeps on moving upwards with $h_p > (h_{p1} + ES)$, the spill port is opened again, and the third step of calculation of F_{sp} begins.

8. The third step:

For the third step, the lift of the plunger is $h_p > (h_{p1} + ES)$; figure 3.5.c

The opening area of the spill port is derived from:

$$F_{sp} = (r_{sp})^2 \varphi_2 - 2\frac{1}{2}(r_{sp} - x_2)r_{sp}\sin\varphi_2 \tag{B.8}$$

where,

$$x_2 = \left[h_p - (h_{p1} + ES)\right]\cos\alpha_{spl} \tag{B.9}$$

$$\cos\varphi_2 = \frac{r_{sp} - x_2}{r_{sp}} \tag{B.10}$$

$$\sin\varphi_2 = \sqrt{1 - \cos^2\varphi_2}$$

Substituting $\cos\varphi_2$ in equation (B.10):

$$\sin\varphi_2 = \sqrt{1 - \left[\frac{r_{sp} - x_2}{r_{sp}}\right]^2}$$

or,

$$\sin\varphi_2 = \frac{1}{r_{sp}}\sqrt{(r_{sp})^2 - (r_{sp} - x_2)^2} \qquad (B.11)$$

Substituting equations (B.9), (B.10), and (B.11) into equation (B.8):

$$F_{sp} = r_{sp}^{\ 2}\cos^{-1}\left[\frac{r_{sp} - [h_p - (h_{p1} + ES)]\cos\alpha_{spl}}{r_{sp}}\right] -$$

$$-\left[r_{sp} - [h_p - (h_{p1} + ES)]\cos\alpha_{spl}\right]\sqrt{r_{sp}^{\ 2} - \left[r_{sp} - [h_p - (h_{p1} + ES)]\cos\alpha_{spl}\right]^2}$$

$$(B.12)$$

Appendix C
FLOW AREA
BETWEEN DELIVERY VALVE AND SEAT

The schematic view of the delivery valve is shown in figure 3.6.

Referring to figure 3.6, the flow area F_{fdv} between the delivery valve and seat is obtained by:

$$F_{fdv} = (\pi D_{dva})y \qquad (C.1)$$

where,

$$y = (h_{dv} - S_r)\sin\alpha_{dv} \qquad (C.2)$$

and,

$$D_{dva} = D_{dv} + 2\,\frac{y}{2}\cos\alpha_{dv} \qquad (C.3)$$

Substituting y in equation (C.2) into equation (C.3):

$$D_{dva} = D_{dv} + (h_{dv} - S_r)\sin\alpha_{dv}\cos\alpha_{dv} \qquad (C.4)$$

Substituting equations (C.2) and (C.4) into equation (C.1), one gets the flow area F_{fdv} between the delivery valve and seat as follows:

$$F_{fdv} = \pi\left[D_{dv} + (h_{dv} - S_r)\sin\alpha_{dv}\cos\alpha_{dv}\right](h_{dv} - S_r)\sin\alpha_{dv} \qquad (C.5)$$

Appendix D

NOZZLE SEAT INLET AND EXIT FLOW AREAS

Figure 3.8 shows the schematic view of the nozzle seat configuration. It includes the effect of the difference in angles of the cones on the needle and in the nozzle seat. Two critical flow areas (ab) and (gj) are indicated in the figure.

D.1. Seat Inlet Flow Area

The seat inlet flow area F_{fsi} between the injector chamber and the seat chamber is obtained from:

$$F_{fsi} = \pi D_{avri}(ab) \tag{D.1}$$

where,

$$D_{avri} = D_{so} + 2(dc) \tag{D.2}$$

and the length:

$$\begin{aligned}(dc) &= (cb)\\ &= \frac{(ab)}{2}\cos\beta\end{aligned} \tag{D.3}$$

Considering the triangle (abe), one has the relationship:

$$\frac{\sin\alpha}{(ab)} = \frac{\sin(90^\circ + \gamma)}{(ae)}$$

or,

- 218 -

$$(ab) \quad \frac{\sin\alpha}{\sin(90^0 + \gamma)} \quad (ae) \tag{D.4}$$

but,

$$(ae) = h_1$$

and,

$$\sin(90^0 + \gamma) = \cos\gamma$$

Thus, equation (D.4) becomes:

$$(ab) = \frac{\sin\alpha}{\cos\gamma} h_1 \tag{D.5}$$

Substituting equations (D.3) and (D.5) into equation (D.2):

$$D_{avri} = D_{so} + \frac{\sin\alpha}{\cos\gamma} \cos\beta \ h_1 \tag{D.6}$$

Substituting equations (D.5) and (D.6) into equation (D.1), one obtains the seat inlet flow area F_{fsi} as follows:

$$F_{fsi} = \pi\left(D_{so} + \frac{\sin\alpha}{\cos\gamma} \cos\beta \ h_1\right) \frac{\sin\alpha}{\cos\gamma} h_1$$

or,

$$F_{fsi} = \left[\pi\left(\frac{\sin\alpha}{\cos\gamma}\right)^2 \cos\beta\right](h_1)^2 + \left[\pi D_{so} \frac{\sin\alpha}{\cos\gamma}\right](h_1) \tag{D.7}$$

Hence, the seat inlet flow area F_{fsi} has the form:

$$F_{fsi} = A_{fsi}(h_1)^2 + B_{fsi}(h_1) \tag{D.8}$$

where,

$$A_{fsi} = \pi \left(\frac{\sin\alpha}{\cos\gamma}\right)^2 \cos\beta \qquad (D.9)$$

and,

$$B_{fsi} = \pi D_{so} \frac{\sin\alpha}{\cos\gamma} \qquad (D.10)$$

D.2. Seat Exit Flow Area

The same consideration is made to derive the equation for the seat exit flow area F_{fse} between the seat chamber and the bag chamber. This flow area is calculated from:

$$F_{fse} = \pi D_{avre}(gj) \qquad (D.11)$$

where,

$$(gj) = (gi) + (ij) \qquad (D.12)$$

but,

$$(gi) = (ef)$$

$$= (ae)\sin\beta$$

$$= h_i \sin\beta \qquad (D.13)$$

and,

$$(ij) = (ej)\sin\gamma \qquad (D.14)$$

Considering the right triangle (ejk), one has:

$$(ej) = \frac{D_{so} - D_{si}}{2\sin\alpha}$$

Thus, equation (D.14) becomes:

$$(ij) = \frac{D_{so} - D_{si}}{2\sin\alpha} \sin\gamma \qquad (D.15)$$

Substituting equations (D.13) and (D.15) into equation (D.12):

$$(gj) = h_i\sin\beta + \frac{D_{so} - D_{si}}{2\sin\alpha} \sin\gamma \qquad (D.16)$$

The average diameter D_{avre} is calculated from:

$$D_{avre} = D_{si} - 2(jl) \qquad (D.17)$$

where,

$$(jl) = \frac{(gj)}{2} \cos\beta$$

From equation (D.16):

$$(jl) = \frac{1}{2}\left(h_i\sin\beta + \frac{D_{so} - D_{si}}{2\sin\alpha} \sin\gamma\right)\cos\beta \qquad (D.18)$$

Substituting equation (D.18) into equation (D.17):

$$D_{avre} = D_{si} - \left(h_i\sin\beta + \frac{D_{so} - D_{si}}{2\sin\alpha} \sin\gamma\right)\cos\beta \qquad (D.19)$$

Finally, the seat exit flow area F_{fse} is obtained by substituting equations (D.16) and (D.19) into equation (D.11):

$$F_{fse} = \pi\left[D_{si} - \left(h_i\sin\beta + \frac{D_{so} - D_{si}}{2\sin\alpha}\sin\gamma\right)\cos\beta\right]\left(h_i\sin\beta + \right.$$

$$\left. + \frac{D_{so} - D_{si}}{2\sin\alpha}\sin\gamma\right) \tag{D.20}$$

or,

$$F_{fse} = A_{fse}(h_i)^2 + B_{fse}(h_i) + C_{fse} \tag{D.21}$$

where,

$$A_{fse} = -\pi(\sin\beta)^2\cos\beta \tag{D.22}$$

$$B_{fse} = \pi\left(D_{si} - \frac{D_{so} - D_{si}}{\sin\alpha}\sin\gamma\cos\beta\right)\sin\beta \tag{D.23}$$

$$C_{fse} = \pi\left(D_{si} - \frac{D_{so} - D_{si}}{2\sin\alpha}\sin\gamma\cos\beta\right)\frac{D_{so} - D_{si}}{2\sin\alpha}\sin\gamma \tag{D.24}$$

Appendix E
DESCRIPTION AND CALIBRATION OF ELECTRONIC TRANSDUCERS

E.1. Force Transducer

In the experiments made for measuring the seat pressure and flow coefficients at the orifices, seat inlet and exit, a piezo-electric load cell was used as a force measuring device. The load cell used in the experiment is produced by KISTLER, type 9001, and the specifications are:

Range   : from 0 to 7500 N
Sensitivity   : −4.2 pC/N
Operating Temperature Range   : −196 to 200°C

The converter used is the Charge Amplifier produced by KISTLER, model 504E.

In the calibration of the force transducer, a material tensil testing machine was used. By gradually applying a load from 0 to 760 N to the load cell, the electrical output from the force transducer was recorded. Table E.1 presents the calibration data. The calibration curve plotted according to those data is shown in figure E.1.

Load in N	Voltage Output in mV
000.	000.0
20.	17.4
310.	260.0
370.	314.0
410.	345.0
525.	445.0
705.	600.0
760.	645.0

Table E.1. Force Transducer Calibration Data

The static gain K_f was found to be:

$$K_f = 1.18 \frac{N}{mV} \tag{E.1}$$
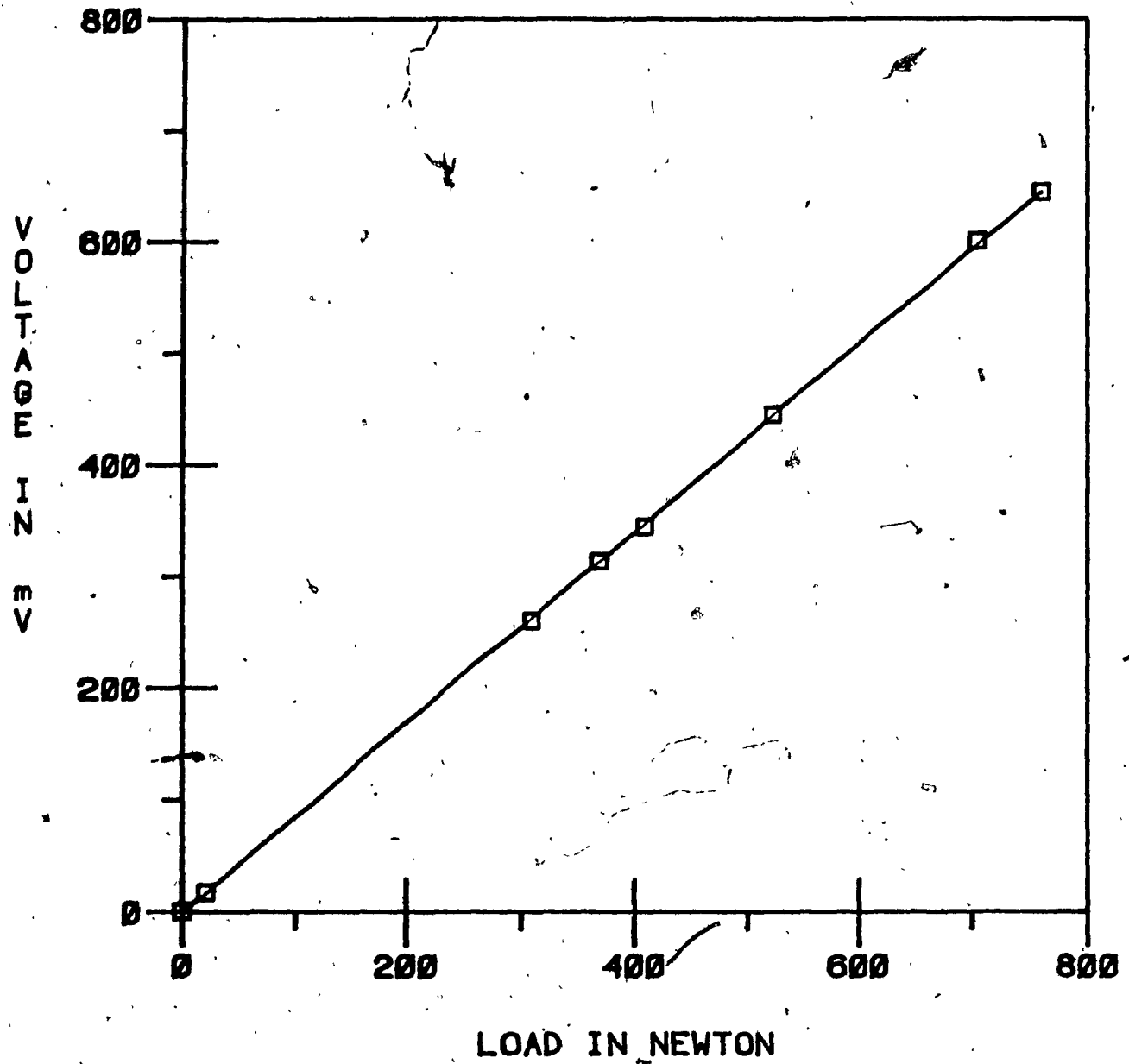
Fig.E.1. Force Transducer Calibration Curve

E.2. Inductive Nozzle Needle Lift Transducer

An AVL nozzle needle lift transducer, type 420, was used to measure the injector needle displacement. This transducer has the following specifications:

Principle	: Inductive lift transducer, half-bridge circuit
Inductance	: 2 x 160 μH nominal
Sensitivity	: Approximate 0.9 V/0.1 mm lift
Permissible Temperature at Connector	: +80°C
Maximum Lift	: ±1 mm

The converter used is the AVL Carrier Amplifier, model 3075.A02.

In calibration of the displacement transducer, the injector needle position was first recorded when it was resting on the nozzle seat, i.e. at zero lift. The voltage output from the transducer was then read. The injector needle was next readjusted to the stop at maximum lift of 0.34 milimeter, and again, the electrical output from the transducer was recorded. The results of calibration are shown in table E.2.

Lift in mm	Voltage in V
0.00	1.79
0.34	3.10

Table E.2. Nozzle Needle Lift Transducer Calibration Data

Assuming linear relationship between the lift and voltage output from the transducer, one has the following expression for the injector needle lift as a function of voltage output from the inductive nozzle needle lift transducer.

$$h_i = 0.25595(\text{Voltage}) - 0.46458 \tag{E.2}$$

In this expression, lift h_i and Voltage are in milimeter [mm] and in volt [V] respectively.

E.3. Pressure Transducers

E.3.1. Piezo-Electric Pressure Transducer

A piezo-electric transducer was used as a pressure measuring device. The pressure transducer used is manufactured by KISTLER, model 603A, and the specifications are:

Pressure Range, Full Scale	: 0 to 3000 psi
Sensitivity (nominal)	: 0.35 pC/psi
Operating Temperature Range	: −450 to 500 $^\circ$F

The converter used is the Charge Amplifier produced by KISTLER, model 504E.

To calibrate this pressure transducer, a hand-operated injector tester was used. An injector was installed and connected to the calibration system. Without any pressure supplied to the calibration system, a zero voltage reference was recorded. Then, the injector opening pressure was adjusted to a desired value. This opening pressure was examined by a previously calibrated pressure gage. At the same time, voltage output from the transducer was read by different types of indicating instruments such as oscilloscope or voltmeter.

The results of this calibration are presented in table E.3.

Gage Pressure in bar	Voltage in mV
000.	000.0
170.	603.5

Table E.3. Piezo-Electric Pressure Transducer Calibration Data

From these results, the gain factor for this transducer was found to be:

$$K_p = 0.2817 \frac{bar}{mV} \qquad (E.3)$$

E.3.2. Strain-Gage Pressure Transducer

A strain-gage pressure transducer was used in measuring the pressure in the pump delivery chamber. This transducer is manufactured by AVL, type 31DP 500E-2.0, and the specifications are:

Pressure Range : 0 to 500 bar

Operating Temperature Range : $-10^{\circ}C$ to $90^{\circ}C$

The converter used is produced by VISHAY INSTRUMENTS, model VE 11K. The calibration procedure for this transducer is the same as for the piezo-electric transducer. The calibration results are presented in table E.4.

Gage Pressure in bar	Voltage in mV
000.0	000.0
100.0	275.0

Table E.4. Strain-Gage Pressure Transducer Calibration Data

The gain factor for this transducer was found to be:

$$K_{ps} = 0.3636 \ \frac{bar}{mV} \tag{E.4}$$

Appendix F
COMPUTER PROGRAM LISTING

```
      PROGRAM INJSYS(INPUT,OUTPUT,TAPE1)
C--------------------------------------------------------------C
C                                                              C
C                   CONCORDIA UNIVERSITY                       C
C                                                              C
C            MECHANICAL ENGINEERING DEPARTMENT                 C
C                                                              C
C       ================================================      C
C                                                              C
C            WRITTEN BY:   TO, CONG HIEP                       C
C                 I.D.#:   8864357                             C
C                   FOR:   MASTER DEGREE THESIS                C
C      UNDER SUPERVISION OF:   DR. T. KREPEC                   C
C                  DATE:   JUNE 20, 1985                       C
C                                                              C
C--------------------------------------------------------------C
C                                                              C
C       THIS PROGRAM IS WRITTEN TO CALCULATE THE FUEL          C
C   DISCHARGE RATE OF A FUEL INJECTION SYSTEM FOR A DIESEL      C
C   ENGINE.                                                    C
C       THE INJECTION SYSTEM CONSISTS OF:                      C
C           1. AN INJECTION PUMP.                              C
C           2. AN INJECTION PIPE.                              C
C           3. A DIESEL INJECTOR.                              C
C--------------------------------------------------------------C
C                                                              C
C                       L E G E N D                            C
C                       =============                          C
C                                                              C
C                                                              C
C     1. IN PUMP:                                              C
C        =======                                               C
C                                                              C
C            N: PUMP SPEED (RPM)                               C
C        EFFSTR: MAXIMUM LIFT OF PUMP PLUNGER                  C
C           VOP: VOLUME OF PUMPING CHAMBER                     C
C           VOD: VOLUME OF DELIVERY CHAMBER                    C
C            DP: DIAMETER OF PUMP PLUNGER                      C
C           NUO: FLOW COEFFICIENT AT SPILL PORT                C
C          NUDV: FLOW COEFFICIENT AT DELIVERY VALVE            C
C            PF: PRESSURE IN THE FEEDING CHAMBER               C
C            DV: DIAMETER OF DELIVERY VALVE                    C
C            D1: DIAMETER OF THE PIPE END ADJACENT TO THE PUMP C
C          MDVN: MASS OF DELIVERY VALVE NEEDLE                 C
C          MDVS: MASS OF DELIVERY VALVE SPRING                 C
C           KDV: DELIVERY VALVE SPRING CONSTANT                C
C          OPDV: OPENING PRESSURE OF DELIVERY VALVE            C
C          RTVL: RETRACTION VOLUME OF DELIVERY VALVE           C
C           RDV: FRICTION FORCE ACTING ON DELIVERY VALVE       C
C         DELDV: DAMPING COEFFICIENT ACTING ON DELIVERY VALVE  C
C            FP: CROSS AREA OF PUMP PLUNGER                    C
C            FV: CROSS AREA OF DELIVERY VALVE                  C
C            F1: CROSS AREA OF PIPE END ADJACENT TO PUMP       C
C           MDV: TOTAL MASS OF DELIVERY VALVE MOVING PARTS     C
```

```
C          PDV: PRELOAD ON DELIVERY VALVE                              C
C           PP: PRESSURE IN PUMPING CHAMBER                            C
C           PD: PRESSURE IN DELIVERY CHAMBER                           C
C           VP: PUMP PLUNGER VELOCITY                                  C
C           HP: PUMP PLUNGER LIFT                                      C
C            V: PUMP PLUNGER VELOCITY TAKEN FROM GRAPH                 C
C            H: PUMP PLUNGER LIFT TAKEN FROM GRAPH                     C
C          VDV: VELOCITY OF DELIVERY VALVE                             C
C          HDV: LIFT OF DELIVERY VALVE                                 C
C           FO: FLOW AREA OF SPILL PORT                                C
C          SIO: FACTOR USED TO CONTROL FLOW AT SPILL PORT              C
C         SIDV: FACTOR USED TO CONTROL FLOW AT DELIVERY VALVE  C
C          PDB: BACKWARD PRESSURE AT PUMP                              C
C          PDF: FORWARD PRESSURE AT PUMP                               C
C          FDV: FLOW AREA THROUGH DELIVERY VALVE                       C
C                                                                      C
C       2. IN INJECTOR:                                                C
C          ============                                                C
C                                                                      C
C           DI: DIAMETER OF INJECTOR NEEDLE                            C
C          DSO: NOZZLE SEAT OUTER DIAMETER                             C
C          DSI: NOZZLE SEAT INNER DIAMETER                             C
C           D2: DIAMETER OF PIPE END ADJACENT TO INJECTOR             C
C          ALP: HALF OF NOZZLE SEAT CONE ANGLE                         C
C         BETA: HALF OF NEEDLE TIP CONE ANGLE                          C
C         GAMA: HALF OF SEAT DIFFERENTIAL ANGLE (IN RADIAN)           C
C       DIFANG: HALF OF SEAT DIFFERENTIAL ANGLE (IN MINUTES)          C
C           DC: DIAMETER OF INJECTOR ORIFICE                           C
C           MN: MASS OF INJECTOR NEEDLE                                C
C          MSN: MASS OF INJECTOR SPRING                                C
C           MR: MASS OF INJECTOR NEEDLE ROD                            C
C           KI: INJECTOR SPRING CONSTANT                               C
C           RI: FRICTION FORCE ACTING ON INJECTOR NEEDLE              C
C         DELI: DAMPING FACTOR ACTING ON INJECTOR NEEDLE              C
C          OPI: INJECTOR OPENING PRESSURE                              C
C        HIMAX: MAXIMUM LIFT OF INJECTOR NEEDLE                        C
C          VON: VOLUME OF INJECTOR CHAMBER                             C
C          VOB: VOLUME OF BAG CHAMBER                                  C
C         NUIS: FLOW COEFFICIENT AT NOZZLE SEAT INLET                 C
C         NUES: FLOW COEFFICIENT AT NOZZLE SEAT EXIT                  C
C          NUC: FLOW COEFFICIENT AT ORIFICES                          C
C           FI: CROSS AREA OF INJECTOR NEEDLE                          C
C          FSO: CROSS AREA OF OUTER NOZZLE SEAT                        C
C          FSI: CROSS AREA OF INNER NOZZLE SEAT                        C
C           F2: CROSS AREA OF PIPE END ADJACENT TO INJECTOR          C
C           MI: TOTAL MASS OF INJECTOR MOVING PARTS                   C
C          PLI: PRELOAD ON INJECTOR NEEDLE                             C
C           PN: PRESSURE IN INJECTOR CHAMBER                           C
C          PNB: BACKWARD PRESSURE AT INJECTOR                          C
C          PNF: FORWARD PRESSURE AT INJECTOR                           C
C           PS: PRESSURE IN THE SEAT CHAMBER                           C
C           PB: PRESSURE IN THE BAG CHAMBER                            C
C           VI: VELOCITY OF INJECTOR NEEDLE                            C
```

```
C               HI: LIFT OF INJECTOR NEEDLE                          C
C             SIIS: FACTOR USED TO CONTROL THE FLOW AT NOZZLE        C
C                   SEAT INLET SECTION                               C
C             SIES: FACTOR USED TO CONTROL THE FLOW AT NOZZLE        C
C                   SEAT EXIT SECTION                                C
C              SIC: FACTOR TO CONTROL THE FLOW AT ORIFICE            C
C                                                                    C
C          3. FLUID:                                                 C
C             =====                                                  C
C                                                                    C
C             RO: FLUID DENSITY                                      C
C              E: FUEL MODULUS OF ELASTICITY                         C
C                                                                    C
C          4. PIPELINE:                                              C
C             ========                                               C
C                                                                    C
C      LENGTH: LENGTH OF PIPELINE                                    C
C                                                                    C
C          5. MISCELLANEOUS:                                         C
C             =============                                          C
C                                                                    C
C             PA: ATMOSPHERIC PRESSURE                               C
C            ESP: VOLUME OF EMPTY SPACE                              C
C           PCLO: INJECTOR CLOSING PRESSURE                          C
C           VEXP: EXPANSION VOLUME OF FLUID IN THE SYSTEM            C
C                 AFTER INJECTION PROCESS                            C
C           VSYS: VOLUME OF INJECTION PIPE, DELIVERY CHAMBER,        C
C                 AND INJECTOR CHAMBER                               C
C             SV: SOUND VELOCITY IN FLUID                            C
C         TIM1WAY: TIME FOR PRESSURE WAVE TO TRAVEL 1 WAY IN         C
C                 PIPELINE                                           C
C         TIM2WAY: TIME FOR PRESSURE WAVE TO TRAVEL 2 WAYS IN        C
C                 PIPELINE                                           C
C           TIME: INSTANT TIME                                       C
C           DELT: TIME STEP SIZE                                     C
C            TPR: TIME TO PRINT OUT                                  C
C           DTPR: PRINT TIME STEP SIZE                               C
C        TIMEMAX: MAXIMUM TIME USED TO SIMULATE THE SYSTEM           C
C           DCSE: TOTAL FUEL INJECTED                                C
C            QPS: FUEL FLOW RATE                                     C
C                                                                    C
C--------------------------------------------------------------------C
       DIMENSION TIMERF(16),TIMERS(16),V(16),H(16)
       DIMENSION Q(2),PDF(10000),PNB(10000)
       REAL N
       REAL NUO,NUDV,NUIS,NUES,NUC
       REAL MDVN,MDVS,MDV
       REAL MN,MSN,MR,MI
       REAL KDV,KI,LENGTH
C--------------------------------------------------------------------C
C-----FUNCTIONS FOR PUMP---------------------------------------------C
C--------------------------------------------------------------------C
C
```

```
C------CONTINUITY EQUATION WRITTEN FOR PUMPING CHAMBER-------C
C
      FPP(PP,PD,VP,HP,VDV,FO,FDV,SIO,SIDV)
     *    = (E/(VOP-FP*HP))*(FP*VP-
     *       SIO*NUO*FO*SQRT((2./RO)*ABS(PP-PF))-
     *       FV*VDV-SIDV*NUDV*FDV*SQRT((2./RO)*ABS(PP-PD)))
C
C------CONTINUITY EQUATION WRITTEN FOR DELIVERY CHAMBER-----C
C
      FPD(PP,PD,PDB,VDV,FDV,SIDV)
     *    = (E/VOD)*(FV*VDV+SIDV*NUDV*FDV*
     *       SQRT((2./RO)*ABS(PP-PD))-(F1/SQRT(E*RO))*
     *       (PD-2.*PDB))
C
C------MOTION EQUATION WRITTEN FOR DELIVERY VALVE----------C
C
      FVDV(PP,PD,VDV,HDV)
     *    = (1./MDV)*(FV*(PP-PD)-PDV-KDV*HDV-
     *       RDV-DELDV*VDV)
C
      FHDV(VDV) = VDV
C------------------------------------------------------------C
C------FUNCTIONS FOR INJECTOR--------------------------------C
C------------------------------------------------------------C
C
C------CONTINUITY EQUATION WRITTEN FOR INJECTOR CHAMBER-----C
C
C------BEFORE THE NOZZLE IS OPENED--------------------------C
C
      FPNB(PN,PNF)
     *    = (E/VON)*(F2/SQRT(E*RO))*(2.*PNF-PN)
C
C------AFTER THE NOZZLE IS OPENED---------------------------C
C
      FPN(PN,PS,PNF,VI,HI,SIIS)
     *    = (E/VON)*((F2/SQRT(E*RO))*
     *       (2.*PNF-PN)-(FI-FSO)*VI-(SIIS*NUIS*
     *       (COEFI1*HI**2+COEFI2*HI)*
     *       SQRT((2./RO)*ABS(PN-PS))))
C
C------CONTINUITY EQUATION WRITTEN FOR BAG CHAMBER---------C
C
      FPB(PS,PB,VI,HI,SIES,SIC)
     *    = (E/VOB)*(SIES*NUES*
     *       (COEFE1*HI**2+COEFE2*HI+COEFE3)*
     *       SQRT((2./RO)*ABS(PS-PB))-
     *       FSI*VI-SIC*NUC*FC*SQRT((2./RO)*ABS(PB-PA)))
C
C------MOTION EQUATION WRITTEN FOR INJECTOR NEEDLE---------C
C
      FVI(PN,PB,PS,VI,HI)
     *    = (1./MI)*((FI-FSO)*PN+(FSO-FSI)*PS+FSI*PB-
     *       PLI-KI*HI-RI-DELI*VI)
```

```
C
      FHI(VI) = VI
C
C-----------------------------------------------------------------C
C-----DATA FOR THE SIMULATED SYSTEM--------------------------------C
C-----------------------------------------------------------------C
C
         PI = 2.*ATAN2(1.,0.)
C
C-----FOR FLUID---------------------------------------------------C
C
         E = 14400.E5
         RO = .82E3
C
C-----FOR PUMP----------------------------------------------------C
C
          N = 1000.
     EFFSTR = 4.24E-3
        VOP = 585.E-9
         DP = 7.5E-3
        NUO = NUDV = 0.65
         PF = 1.E5
         DV = 6.E-3
        VOD = 1850.E-9
         D1 = 2.E-3
       MDVN = 3.1347E-3
       MDVS = 3.2246E-3
        KDV = 6.6456E3
        RDV = DELDV = 0.
       OPDV = 14.337E5
       PCLO = 90.E5
       RTVL = 50.E-9
C
C-----FOR PIPE LINE-----------------------------------------------C
C
      LENGTH = 950.E-3
C
C-----FOR INJECTOR-----------------------------------------------C
C
         DI = 6.E-3
         D2 = 2.E-3
     DIFANG = 10.
       GAMA = DIFANG*PI/180.
        ALP = 30.*PI/180.
       BETA = ALP+GAMA
        DSI = 1.75E-3
        DSO = 3.5E-3
         DC = 0.32E-3
         MN = 9.027E-3
        MSN = 22.3875E-3
         MR = 11.067E-3
         KI = 200.E3
         RI = 0.
```

```
              DELI = 40.
               OPI = 170.E5
               VON = 600.E-9
               VOB = 4.E-9
              NUIS = 0.75
              NUES = 0.95
               NUC = 0.65
             HIMAX = 0.35E-3
C-------------------------------------------------------------------C
C-----CALCULATION OF PARAMETERS------------------------------------C
C-------------------------------------------------------------------C
C
C-----FOR PUMP-----------------------------------------------------C
C
               FP = PI*(DP**2)/4.
               FV = PI*(DV**2)/4.
               F1 = PI*(D1**2)/4.
              MDV = MDVN + MDVS/3.
              PDV = OPDV * FV
C
C------FOR INJECTOR------------------------------------------------C
C
               FI = PI*(DI**2)/4.
               F2 = PI*(D2**2)/4.
              FSI = PI*(DSI**2)/4.
              FSO = PI*(DSO**2)/4.
               FC = 4.*PI*(DC**2)/4.
               MI = MN + MR + MSN/3.
              PLI = OPI*(FI-FSO)
C
C-----FOR EMPTY SPACE----------------------------------------------C
C
             VSYS = VOD + F1*LENGTH + VON
             VEXP = VSYS*PCLO/E
              ESP = RTVL - VEXP
C-------------------------------------------------------------------C
C-----CALCULATION OF COEFFICIENTS FOR SEAT FLOW AREAS--------------C
C-------------------------------------------------------------------C
           COEFI1 = PI*(SIN(ALP)/COS(GAMA))**2*COS(BETA)
           COEFI2 = PI*DSO*SIN(ALP)/COS(GAMA)
           COEFE1 = -PI*SIN(BETA)**2*COS(BETA)
           COEFE2 = PI*(DSI-(DSO-DSI)*SIN(GAMA)*COS(BETA)/
          *          SIN(ALP))*SIN(BETA)
           COEFE3 = PI*(DSO-DSI)*SIN(GAMA)/(2.*SIN(ALP))*
          *          (DSI-(DSO-DSI)*SIN(GAMA)*COS(BETA)/
          *          (2.*SIN(ALP)))
C-------------------------------------------------------------------C
C-----TIME FOR PRESSURE WAVE TO TRAVEL IN THE PIPE----------------C
C-------------------------------------------------------------------C
               SV = SQRT(E/RO)
          TIM1WAY = LENGTH/SV
          TIM2WAY = 2.*TIM1WAY
C-------------------------------------------------------------------C
```

```
C-----INITIALIZATION------------------------------------------------C
C------------------------------------------------------------------C
C        (
C-----FOR PUMP-----------------------------------------------------C
C                         (
                 PP  =  0.E5
                 PD  =  0.E5
                HDV  =  0.0
                VDV  =  0.0
                PDB  =  0.E5
C
C-----FOR INJECTOR-------------------------------------------------C
C
                 PN  =  0.E5
                 PS  =  0.E5
                 PB  =  0.E5
                 PA  =  0.E5
                 HI  =  VI  =  0.
C
C-----FOR TIME, PRINT OUT, AND CONTROLLING-------------------------C
C
               TIME  =  0.0
               DELT  =  1.E-7
               DTPR  =  0.02E-3
            TIMEMAX  =  9.E-3
                TPR  =  DTPR + TIME
               LOOP  =  J4 = I = J = L = 0
               DOSE  =  Q(1) = 0.
C------------------------------------------------------------------C
C-----PUMP PLUNGER VELOCITY AND LIFT READ IN-----------------------C
C------------------------------------------------------------------C
       DO 10, KK = 1,16
10     READ(1,20)TIMERF(KK),TIMERS(KK),H(KK),V(KK)
20     FORMAT(1X,4E10.4)
C------------------------------------------------------------------C
C-----SOLVING THE DIFFERENTIAL EQUATIONS BY RUNGE-KUTTA------------C
C------------------------------------------------------------------C
C-----AT PUMP------------------------------------------------------C
C      =======                                                     C
C
3000   TIME  =  TIME + DELT
        SIO  =  1.
       IF (PP.LT.PF) SIO = -1.
       CALL SUBVPHP(VP,HP,TIME,V,H,TIMERF,TIMERS,N)
       CALL SUBFO(FO,HP,EFFSTR)
       CALL SUBFDV(FDV,HDV,RTVL,FV,DV)
C
       IF ((HDV*FV).GE.ESP.OR.LOOP.EQ.1) GO TO 100
C
C-----DELIVERY VALVE IS STILL CLOSED-------------------------------C
C
       SIDV  =  0.
         TK  =  TIME
```

```
C .
C------RUNGE-KUTTA---------------------------------------------------C
C
      AK1=DELT*FPP(PP,PD,VP,HP,VDV,FO,FDV,SIO,SIDV)
      AL1=DELT*FVDV(PP,PD,VDV,HDV)
      AM1=DELT*FHDV(VDV)
C
      AK2=DELT*FPP(PP+AK1/2,PD,VP,HP,VDV+AL1/2,FO,FDV,SIO,
     *     SIDV)
      AL2=DELT*FVDV(PP+AK1/2,PD,VDV+AL1/2,HDV+AM1/2)
      AM2=DELT*FHDV(VDV+AL1/2)
C
      AK3=DELT*FPP(PP+AK2/2,RD,VP,HP,VDV+AL2/2,FO,FDV,SIO,
     *     SIDV)
      AL3=DELT*FVDV(PP+AK2/2,PD,VDV+AL2/2,HDV+AM2/2)
      AM3=DELT*FHDV(VDV+AL2/2)
C
      AK4=DELT*FPP(PP+AK3,PD,VP,HP,VDV+AL3,FO,FDV,SIO,
     *     SIDV)
      AL4=DELT*FVDV(PP+AK3,PD,VDV+AL3,HDV+AM3)
      AM4=DELT*FHDV(VDV+AL3)
C
      PP = PP+(AK1+2*AK2+2*AK3+AK4)/6.
      VDV=VDV+(AL1+2*AL2+2*AL3+AL4)/6.
      HDV=HDV+(AM1+2*AM2+2*AM3+AM4)/6.
C
      IF (PP.LE.0.)                    PP = 0.
      IF (HDV.LE.0.)                   HDV = 0.
      IF (VDV.LE.0..AND.HDV.LE.0.) VDV = 0.
      GO TO 200
C
C------DELIVERY VALVE IS OPENED-------------------------------------C
C
100   LOOP = 1
      SIDV = 1.
      IF (PP.LT.PD) SIDV = -1.
      IF (HDV*FDV.LT.RTVL) SIDV = 0.
C
C------RUNGE-KUTTA---------------------------------------------------C
C
      AK1=DELT*FPP(PP,PD,VP,HP,VDV,FO,FDV,SIO,SIDV)
      AL1=DELT*FVDV(PP,PD,VDV,HDV)
      AM1=DELT*FHDV(VDV)
      AN1=DELT*FPD(PP,PD,PDB,VDV,FDV,SIDV)
C
      AK2=DELT*FPP(PP+AK1/2,PD+AN1/2,VP,HP,VDV+AL1/2,
     *              FO,FDV,SIO,SIDV)
      AL2=DELT*FVDV(PP+AK1/2,PD+AN1/2,VDV+AL1/2,HDV+AM1/2)
      AM2=DELT*FHDV(VDV+AL1/2)
      AN2=DELT*FPD(PP+AK1/2,PD+AN1/2,PDB,VDV+AL1/2,FDV,
     *              SIDV)
C
      AK3=DELT*FPP(PP+AK2/2,PD+AN2/2,VP,HP,VDV+AL2/2,
```

```
     *                   FO,FDV,SIO,SIDV)
       AL3=DELT*FVDV(PP+AK2/2,PD+AN2/2,VDV+AL2/2,HDV+AM2/2)
       AM3=DELT*FHDV(VDV+AL2/2)
       AN3=DELT*FPD (PP+AK2/2,PD+AN2/2,PDB,VDV+AL2/2,FDV,
     *                   SIDV)
C

       AK4=DELT*FPP(PP+AK3,PD+AN3,VP,HP,VDV+AL3,FO,FDV,SIO,
     *                   SIDV)
       AL4=DELT*FVDV(PP+AK3,PD+AN3,VDV+AL3,HDV+AM3)
       AM4=DELT*FHDV(VDV+AL3)
       AN4=DELT*FPD (PP+AK3,PD+AN3,PDB,VDV+AL3,FDV,SIDV)
C

       PP = PP+(AK1+2*AK2+2*AK3+AK4)/6.
       VDV=VDV+(AL1+2*AL2+2*AL3+AL4)/6.
       HDV=HDV+(AM1+2*AM2+2*AM3+AM4)/6.
       PD = PD+(AN1+2*AN2+2*AN3+AN4)/6.

       IF (PP.LE.0.)                        PP = 0.
       IF (PD.LE.0.)                        PD = 0.
       IF (HDV.LE.0.)                       HDV = 0.
       IF (VDV.LE.0..AND.HDV.LE.0.) VDV = 0.
C
C-----STORE FORWARD PRESSUE AT PUMP--------------------------------C
C
       I = I + 1
       IF (I.GT.8000) I = I - 8000
       PDF(I) = PD - PDB
C
       IF (TIME.LT.(TK+TIM1WAY)) GO TO 200
C
C-----CALCULATION OF FORWARD PRESSURE AT INJECTOR-----------C
C
       J = J + 1
       IF (J.GT.8000) J = J - 8000
       PNF = PDF(J)
C
C-----CALCULATION OF BACKWARD PRESSURE AT PUMP--------------C
C
       IF (TIME.GE.(TK+TIM2WAY)) THEN
       L = L + 1
       PDB = PNB(L)
       ELSE
       PDB = PA
       END IF
C
C-----AT INJECTOR----------------------+----------------------C
C     ============                                            C
C
       IF (PN.GE.OPI.OR.J4.EQ.1) GO TO 400
C
C-----INJECTOR IS CLOSED---------------------------------------C
C
C-----RUNGE-KUTTA---------------------------------------------C
```

```
  C
        AK1=DELT*FPNB(PN,PNF)
        AK2=DELT*FPNB(PN+AK1/2,PNF)
        AK3=DELT*FPNB(PN+AK2/2,PNF)
        AK4=DELT*FPNB(PN+AK3,PNF)
  C
        PN = PN+(AK1+2.*AK2+2.*AK3+AK4)/6.
  C
        IF (PN.LT.0.) PN = 0.
        GO TO 900
  C
  C-----INJECTOR IS OPENED--------------------------------------------C
  C
  400   J4 = 1
        SIIS = SIES = SIC = 1.
        IF (HI.LE.0.) THEN
        SIIS = 0.
        ELSE
        IF (PN.LT.PS) SIIS = -1.
        END IF
        IF (PS.LT.PB) SIES = -1.
        IF (PB.LE.PA)  SIC = 0.
  C
  C-----RUNGE-KUTTA-------------------------------------------------C
  C
        AK1=DELT*FPN(PN,PS,PNF,VI,HI,SIIS)
        AL1=DELT*FPB(PS,PB,VI,HI,SIES,SIC)
        AM1=DELT*FVI(PN,PB,PS,VI,HI)
        AN1=DELT*FHI(VI)
  C
        AK2=DELT*FPN(PN+AK1/2,PS,PNF,VI+AM1/2,HI+AN1/2,SIIS)
        AL2=DELT*FPB(PS,PB+AL1/2,VI+AM1/2,HI+AN1/2,SIES,SIC)
        AM2=DELT*FVI(PN+AK1/2,PB+AL1/2,PS,VI+AM1/2,HI+AN1/2)
        AN2=DELT*FHI(VI+AM1/2)
  C
        AK3=DELT*FPN(PN+AK2/2,PS,PNF,VI+AM2/2,HI+AN2/2,SIIS)
        AL3=DELT*FPB(PS,PB+AL2/2,VI+AM2/2,HI+AN2/2,SIES,SIC)
        AM3=DELT*FVI(PN+AK2/2,PB+AL2/2,PS,VI+AM2/2,HI+AN2/2)
        AN3=DELT*FHI(VI+AM2/2)
  C
        AK4=DELT*FPN(PN+AK3,PS,PNF,VI+AM3,HI+AN3,SIIS)
        AL4=DELT*FPB(PS,PB+AL3,VI+AM3,HI+AN3,SIES,SIC)
        AM4=DELT*FVI(PN+AK3,PB+AL3,PS,VI+AM3,HI+AN3)
        AN4=DELT*FHI(VI+AM3)
  C
        PN=PN+(AK1+2.*AK2+2.*AK3+AK4)/6.
        PB=PB+(AL1+2.*AL2+2.*AL3+AL4)/6.
        VI=VI+(AM1+2.*AM2+2.*AM3+AM4)/6.
        HI=HI+(AN1+2.*AN2+2.*AN3+AN4)/6.
  C
        IF (PN.LE.0.)                          PN = 0.
        IF (PB.LE.0.)                          PB = 0.
        IF (HI.LE.0.)                          HI = 0.
```

```
      IF (HI.GE.HIMAX) THEN
      HI = HIMAX
      VI = 0.
      ELSE
      END IF
      IF (VI.LE.0..AND.HI.LE.0.)          VI = 0.
C
C-----CALCULATION OF SEAT PRESSURE-------------------------------C
C
      IF (HI.LE.0.) THEN
      PS = PB
      ELSE
      X = NUES*(COEFE1*HI**2+COEFE2*HI+COEFE3)*SQRT(2./RO)
      Y = (FSO-FSI)*VI
      Z = NUIS*(COEFI1*HI**2+COEFI*HI)*SQRT(2./RO)
      XX= (SIES*X**2+SIIS*Z**2)**2
      YY= (SIES*X**2+SIIS*Z**2)*(SIES*X**2*PB+SIIS*Z**2*PN)+
     *   (Y**2)*(SIES*X**2-SIIS*Z**2)
      ZZ= (SIES*X**2*PB+SIIS*Z**2*PN)**2+(Y**4)-
     *   2.*(Y**2)*(SIIS*Z**2*PN-SIES*X**2*PB)
      DELTA = YY**2-XX*ZZ
      IF (DELTA.GE.0.) THEN
      SQDELTA = SQRT(DELTA)
      PS = (YY+SQDELTA)/XX
      ELSE
      END IF
      END IF
      IF (PS.LT.0.) PS = 0.
C
C-----STORE BACKWARD PRESSURE AT INJECTOR-----------------------C
C
900   PNB(J) = PN - PNF
C
C-----CALCULATION OF FLOW RATE AND INJECTED FUEL DOSE-----C
C
      IF (PB.GE.PA.AND.HI.NE.0.) THEN
      QPS  = NUC*FC*SQRT((2./RO)*(PB-PA))
      Q(2) = QPS
      DOSE = DOSE+(Q(1)+Q(2))*DELT/2.
      Q(1) = Q(2)
      ELSE
      Q(2) = QPS = 0.
      Q(1) = Q(2)
      END IF
C-------------------------------------------------------------C
C-----PRINT OUT THE RESULTS-----------------------------------C
C-------------------------------------------------------------C
200   IF (ABS(TIME-TPR)-DELT/10.) 1000,1000,2000
1000  TPR = TPR + DTPR
      PRINT 17,TIME,PP,VDV,HDV,PD,PN,PS,PB,VI,HI,QPS,DOSE
2000  IF (TIME-TIMEMAX) 3000,3000,4000
17    FORMAT(E11.4,11E9.3)
4000  STOP
      END
```

```fortran
      SUBROUTINE SUBVPHP(VP,HP,TIME,V,H,TIMERF,TIMERS,N)
C-----------------------------------------------------------------C
C                                                                 C
C     THIS SUBROUTINE IS USED TO CALCULATE THE PUMP               C
C  PLUNGER VELOCITY AND LIFT.                                      C
C                                                                 C
C-----------------------------------------------------------------C
      DIMENSION TIMERF(16),TIMERS(16),V(16),H(16)
      REAL N
      I = 1
  10  IF (TIME.GE.TIMERF(I)) THEN
      I = I + 1
      GO TO 10
      ELSE
      END IF
      I = I - 1
C
      VP= (V(I)+(TIME-TIMERF(I))*(V(I+1)-V(I))/
     *    (TIMERF(I+1)-TIMERF(I)))*N/1000.
      J = 1
  20  IF (TIME.GE.TIMERS(J)) THEN
      J = J + 1
      GO TO 20
      ELSE
      END IF
      J = J - 1
      HP = H(J)+(TIME-TIMERS(J))*(H(J+1)-H(J))/
     *     (TIMERS(J+1)-TIMERS(J))
      RETURN
      END
```

```fortran
      SUBROUTINE SUBFO(FO,HP,EFFSTR)
C-------------------------------------------------------------C
C                                                             C
C     THIS SUBROUTINE IS USED TO CALCULATE FLOW AREA          C
C  OF THE SPILL PORT.                                         C
C                                                             C
C-------------------------------------------------------------C
      PI = 2.*ATAN2(1.,0.)
      RF = 1.5E-3
      CC = 1.75E-3
       Z = 2.*RF - CC
   ALPSA = 26.*PI/180.
   IF (HP.LE.CC) THEN
   X = Z + HP
   PHI = ACOS((RF - X)/RF)
   FO = PI*RF**2 - (RF**2*PHI-(RF-X)*RF*SIN(PHI))
   GO TO 10
   ELSE
   IF (HP.LE.EFFSTR) THEN
      FO = 0.
      GO TO 10
   ELSE
   X = HP - EFFSTR
   PHI = ACOS((RF-X*COS(ALPSA))/RF)
    FO = RF**2*PHI - (RF - X*COS(ALPSA))*RF*SIN(PHI)
   END IF
   END IF
10   RETURN
   END
```

```fortran
      SUBROUTINE SUBFDV(FDV,HDV,RTVL,FV,DV)
C----------------------------------------------------------------C
C                                                                C
C      THIS SUBROUTINE IS USED TO CALCULATE THE FLOW AREA        C
C   THROUGH DELIVERY VALVE                                       C
C                                                                C
C----------------------------------------------------------------C
      PI = 2.*ATAN2(1.,0.)
   ALPDV = 45.*PI/180.
      CA = RTVL/FV
   IF (HDV.LE.CA) THEN
     FDV = 0.
   GO TO 10
   ELSE
     FDV = PI*(DV+(HDV-CA)*SIN(ALPDV)*COS(ALPDV))*
     *          (HDV-CA)*SIN(ALPDV)
   END IF
10    RETURN
      END
```